STUDY OF OPTIMUM SIMULATION TECHNIQUES FOR THE DESIGN AND EVALUATION OF ANTI-JAM COMMUNICATION SYSTEMS

SIGNATRON, INCORPORATED

PREPARED FOR
AIR FORCE AVIONICS LABORATORY

MARCH 1976

AFAL-TR-75-186

194094

STUDY OF OPTIMUM SIMULATION TECHNIQUES
FOR THE DESIGN AND EVALUATION
OF ANTI-JAM COMMUNICATION SYSTEMS

Signatron, Inc.
27 Hartwell Avenue
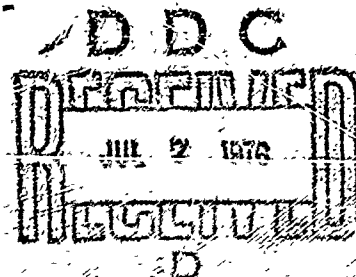Lexington, Massachusetts 02173

March 1976

TECHNICAL REPORT AFAL-TR-75-186
Final Report for Period 1 February 1974 to 30 June 1975

Approved for public release; distribution unlimited

AIR FORCE AVIONICS LABORATORY/AAI
AIR FORCE WRIGHT AERONAUTICAL LABORATORIES
Air Force Systems Command
Wright-Patterson Air Force Base, Ohio 45433

DDC

JUL 2 1976

D
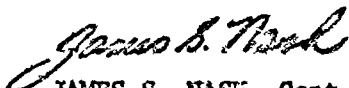
REPORT DOCUMENTATION PAGE		READ INSTRUCTIONS BEFORE COMPLETING FORM
1. REPORT NUMBER AFAL-TR-75-186	2. GOVT ACCESSION NO.	3. RECIPIENT'S CATALOG NUMBER
4. TITLE (and Subtitle) STUDY OF OPTIMUM SIMULATION TECHNIQUES FOR THE DESIGN AND EVALUATION OF ANTI-JAM COMMUNICATION SYSTEMS		5. TYPE OF REPORT & PERIOD COVERED Final Report; 1 February 1974 to 30 June 1975
		6. PERFORMING ORG. REPORT NUMBER A-167-F
7. AUTHOR(s) Leonard Ehrman Steen Parl John N. Pierce Steven H. Richman		8. CONTRACT OR GRANT NUMBER(s) F33615-74-C-4065
9. PERFORMING ORGANIZATION NAME AND ADDRESS Signatron, Inc. 27 Hartwell Avenue Lexington, Massachusetts 02173		10. PROGRAM ELEMENT, PROJECT, TASK AREA & WORK UNIT NUMBERS Project 1227 Task 12
11. CONTROLLING OFFICE NAME AND ADDRESS Air Force Avionics Laboratory Wright-Patterson Air Force Base Ohio 45433		12. REPORT DATE March 1976
		13. NUMBER OF PAGES 289
14. MONITORING AGENCY NAME & ADDRESS(If different from Controlling Office) SAME		15. SECURITY CLASS. (of this report) UNCLASSIFIED
		15a. DECLASSIFICATION/DOWNGRADING SCHEDULE N/A

16. DISTRIBUTION STATEMENT (of this Report)

Approved for Public Release; Distribution Unlimited.

17. DISTRIBUTION STATEMENT (of the abstract entered in Block 20, if different from Report)

SAME

18. SUPPLEMENTARY NOTES

NONE

19. KEY WORDS (Continue on reverse side if necessary and identify by block number)

RADIO CHANNEL SIMULATION
ANTI-JAM COMMUNICATIONS
SATELLITE SIMULATION

20. ABSTRACT (Continue on reverse side if necessary and identify by block number)

The Communication Systems Evaluation Laboratory (CSEL), located at the Air Force Avionics Laboratory, is a real-time satellite simulation facility. This report investigates the application of CSEL to the LES 8/9 and GPS satellite programs. In addition, a new analysis of the effects of soft and hard limiters on frequency-hopped signals is presented.

DD FORM 1473 EDITION OF 1 NOV 65 IS OBSOLETE

JAMES S. NASH, Capt, USAF
Program Monitor

ALLEN L. JOHNSON
Project Engineer

GEORGE F. CUDAHY, Colonel, USAF
Chief, System Avionics Division
AF Avionics Laboratory

ii

FOREWORD

This technical report covers work performed by SIGNATRON, Inc.
Lexington, Massachusetts, under Contract F33615-74-C-4065, Project
1227, Task 12, over the period 1 February 1974 to 30 June 1975.
The draft of this report was submitted 29 July 1975. The Project
Engineer at SIGNATRON was Dr. Leonard Ehrman, who was also
responsible for the sections on Doppler simulation, system
validation, and propagation effects. Mr. John N. Pierce per-
formed the analyses of the hard and soft limiters, assisted
by Dr. Steen Parl. Dr. Parl also performed the NAVSTAR GPS
analysis. Dr. Steven H. Richman performed the repeater jamming
analysis. Computer programming for the soft limiter analysis
was performed by Mrs. Linda Vears.

The authors wish to acknowledge the valuable assistance
of the AFAL/AAI Project Engineer, Capt. James Nash, whose sug-
gestions were of great benefit to the study.

D D C

JUL 7 1976

D

iii

TABLE OF CONTENTS

TABLE OF CONTENTS (cont'd)

TABLE OF CONTENTS(cont'd)

LIST OF ILLUSTRATIONS

LIST OF ILLUSTRATIONS (cont'd)

LIST OF TABLES

LIST OF TABLES (cont'd)

SECTION 1

INTRODUCTION

This document constitutes the final report prepared by
SIGNATRON, Inc., Lexington, Massachusetts, for the Air Force
Avionics Laboratory, Wright-Patterson Air Force Base, Ohio,
under Contract F33615-74-C-4065, entitled Optimum Simulation
Techniques for Communication System Design.

1.1 Objectives of the Program

The Air Force Avionics Laboratory has developed the Com-
munication Systems Evaluation Laboratory (CSEL) to investigate
and analyze, through simulation, a variety of communication
problems. The laboratory utilizes three solutions to the prob-
lems:

(1) building and testing special purpose hardware;

(2) developing computer software programs to simulate
     the problems on a digital, analog, or hybrid com-
     puter; or

(3) developing some combination of the two methods.

In addition to the above, over-the-air tests can be performed
using CSEL's rooftop facility.

The objective of the present program was to perform a study
of simulation techniques for anti-jam communications systems
design and evaluation, and provide recommendations which utilize
the capabilities of CSEL in testing these systems. The emphasis
in the study was placed on two satellite systems: The Lincoln
Experimental Satellites 8 and 9 (LES 8/9) and the NAVSTAR Global

Positioning System (GPS). The LES 8/9 effort included studies
of hard and soft limiting, repeater jamming, simulation hardware/
software validation experiments, and Doppler simulation. The
GPS effort was limited to a study of the requirements for GPS
simulation, and the interfacing of the GPS simulator with the
proposed AFAL Generalized Development Model (GDM) system. In
addition to the studies oriented towards the LES 8/9 and GPS systems,
specifically, studies were also performed in the fields of satel-
lite signal properties and the simulation of desired scintillation
statistics.

1.2 Brief Summary of Results

Analytic results have been obtained for the suppression of
a frequency-hopped signal with CW jamming in a hard limiter.
The soft limiter which was examined was modeled as a linear
amplifier for input levels less than a specific threshold value,
and clipper for input levels above the threshold. Calculations
were made of signal suppression; for J/S < 0 dB, the hard limiter
has less suppression, while for J/S > 0 dB, the soft limiter has less.

The repeater jammer was studied for a frequency-hopped system
which utilized error correcting coded transmission and hard limit-
ing at the receiver. The signal detection statistic took into
account the effects of matched filtering, limiting, and random
frequency and phase errors, as well as partial chip jamming.
The analyses demonstrated that for this class of signal, repeater
jamming is in general more efficient than either random noise or
multitone jamming.

When CSEL is first to be used in LES 8/9 simulations, it is
important to have a systematic procedure for validating the simu-
lation. Three experiments are considered, the first being
a validation of the programmed signal processor

2

(PSP) model of the satellite, the second being the downlink simu-lation, and the third being jamming on the forward uplink. Ex-perimental procedures and predicted results are given.

The final LES 8/9 study is concerned with Doppler simulation. The simulation of Doppler shift on a wideband signal is compli-cated by the linear increase in Doppler shift across the signal band, resulting in a differential Doppler shift across the band. This can be ignored in a narrow-band signal, but must be included in the simulation of wideband signals. A hybrid method of simu-lating both the Doppler and the differential Doppler for the LES 8/9 system is described.

The NAVSTAR Global Positioning System (GPS) will enable both civilian and military users to accurately locate their po-sition in three-dimensional space. Many classes of users are envisioned for GPS. Depending on their accuracy requirements, they may receive satellite data at either one or two frequencies, with or without A/J protection. AFAL is supporting the GPS Joint Program Office to provide performance trade-offs related to high-anti-jam techniques for GPS, as well as to expand the technology base for GPS user equipment. As part of this program, AFAL is procuring the AFAL Generalized Development Model (GDM) of the GPS user equipment, which includes the hardware and soft-ware necessary to receive and process GPS navigation signals, along with inertial and auxiliary sensor data in some modes, and determine optimum estimates of the three dimensional position, velocity, and system time. In our study of GPS we have summarized the GPS system and sources of errors, investigated ionospheric modeling techniques, and proposed means of integrating the GDM into CSEL, thus allowing GPS system concepts to be validly tested through a hybrid simulation. Among the items considered are:

3

expected GDM receiver structure; integration of the GDM simulator into CSEL; the use of the Draper Laboratory's CSDL/4 - SV satellite simulator; new techniques for constructing variable delay lines; antenna simulation; stabilization of time delays; and hardware and software requirements.

The final part of the study deals with some features of satellite signal propagation. It consists of two separate but complementary parts. The first is a summary of the properties of satellite signals. The second is concerned with means of simulating, on a digital computer, signal distributions which would be the same as measured on a scintillating signal. Algorithms are derived for generating signals with the distribution of either envelope alone, or both the envelope and phase.

1.3 Contents of the Report

The report is divided into four main sections. Section 2 contains the material related to LES 8/9, Section 3 the material related to GPS, and Section 4 the material related to satellite signal propagation. Conclusions and recommendations are given in Section 5.

SECTION 2

LES 8/9 STUDIES

2.1 Introduction

The Lincoln Experimental Satellites LES 8/9 are experimental satellites, operating at VHF and K-band. They are designed to accept signals which are frequency-hopped over a wide bandwidth for A/J purposes, process them, and reformat, remodulate, and re-transmit their data to other users. Thus the satellites are con-siderably more sophisticated than the conventional repeater-type satellite, which simply heterodyne incoming signals to another band and then retransmit them with no further processing.

In this section we discuss four aspects of the LES 8/9 system and their application to the CSEL facility. In Section 2.2 we describe the effects of limiters on frequency-hopped signals. The simulation of Doppler and differential Doppler shifts, which is an important effect in wideband A/J systems, is considered in Section 2.3. Repeater jamming of frequency-hopped signals is analyzed in Section 2.4. Section 2 ends with a discussion of systematic tests to be run using CSEL with the LES 8/9 simulator.

2.2 Effects of Limiters on Frequency-Hopped Signals

A frequency-hopped (FH) signal is often processed through a limiter, as this provides a means of reducing the effect of a jammer on a coded system. In this section we consider the sup-pression which FH signals undergo in both hard and soft limiters, when combined with CW or FH jamming signals.

5

2.2.1 CW Jamming Suppression of FH Signals in a Hard Limiter

Suppose that two CW signals are present at the input to a hard limiter: one of them arising from a frequency-hopped (FH) desired signal, and the other from either a CW or FH jammer. If the desired signal is at frequency f_o, and the undesired signal at f_1, then the output of the limiter contains an infinite number of spectral lines spaced at multiples of the difference frequency $(f_1 - f_o)$. The bulk of the limiter output energy appears in the lines at f_o and f_1; however, as much as 19% of the limiter output can appear in other lines when the signal and jamming are equal.

If S and J are the signal and jamming powers, respectively, the fraction of the total output power that would appear at the desired frequency when using a linear amplifier would be $S/(S+J)$.

Beside wasting power in spurious spectral lines, the hard limiter increases the disparity between the power in the spectral lines at f_o and f_1; this is the well known weak-signal suppression effect.

This combination of weak-signal suppression and power in spurious lines causes the power in the desired component to be some number

$$\psi(J/S) \cdot \frac{S}{S+J} \qquad (1)$$

rather than S/(S+J). We call ψ(J/S) the "suppression factor" and we have plotted ψ in Fig. 1. The details of calculating ψ are given in the Appendix. Although ψ is indeed a suppression factor in the important situation where the jamming/signal ratio is greater than unity, it is apparent from the figure that ψ is actually an improvement factor when the signal is more than 0.9 dB stronger than the jamming.

In an actual hard limiting repeater the power amplifier that follows the repeater will have a bandwidth approximately equal to the input bandwidth and only a finite number of the spurious spectral lines will be passed by the amplifier. Whether or not the power that would have been in these lines will appear in the remaining lines depends on the exact characteristics of the power amplifier. Any slight improvement that results from this effect is likely to be counterbalanced by incidental AM to PM conversion.

In any event changes from the signal-suppression effect shown in the figure are negligible if the separation between the two frequencies is small compared to the bandwidth, and we may take the curve as shown to be both the worst-case and a good approximation to all of the other cases. The derivation of ψ is given next.

2.2.1.1 Calculation of Hard Limiter Suppression Factor

Using complex notation, let
$$\text{signal} = \exp(j\omega_o t), \tag{2}$$

$$\text{jamming} = A \exp(j\omega_1 t), \tag{3}$$

so that the jamming/signal ratio is A^2. The total input to the limiter is then
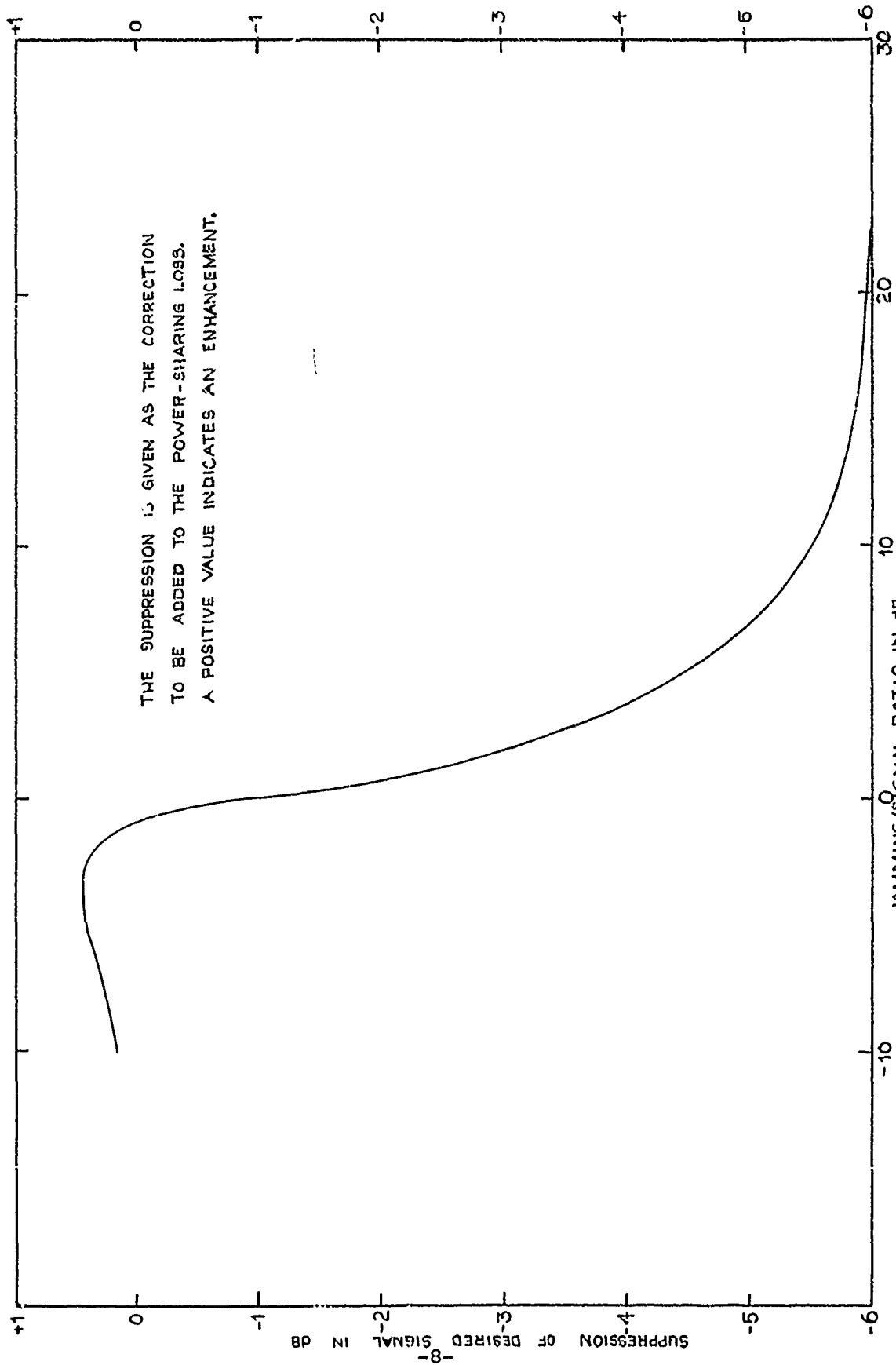
THE SUPPRESSION IS GIVEN AS THE CORRECTION
TO BE ADDED TO THE POWER-SHARING LOSS.
A POSITIVE VALUE INDICATES AN ENHANCEMENT.

JAMMING/SIGNAL RATIO IN dB

SUPPRESSION OF DESIRED SIGNAL IN dB

Figure 1   Hard Limiter Suppression Factor

-8-

$$v(t) = \exp(j\omega_o t) + A \exp(j\omega_1 t), \qquad (4)$$

and the hard-limited output (with unity peak voltage) is

$$w(t) = v(t)/|v(t)|. \qquad (5)$$

Since

$$|v(t)|^2 = 1 + A^2 + 2A\cos[\omega_1 - \omega_o)t], \qquad (6)$$

we have

$$w(t) = [1 + A^2 + 2A\cos[(\omega_1 - \omega_o)t]^{-\frac{1}{2}} v(t). \qquad (7)$$

The amplitude of the desired component at the limiter output is

$$v_o = \lim_{T\to\infty}(1/T) \int_0^T \exp(-j\omega_o t)\, w(t)\, dt$$

$$= \lim_{T\to\infty}(1/T) \int_0^T \frac{1+A\exp[j(\omega_1-\omega_o)t]}{[1+A^2+2A\cos(\omega_1-\omega_o)t]^{\frac{1}{2}}}\, dt. \qquad (8)$$

It is easily verified that this is equal to the average over a whole period of the difference frequency:

$$v_o = (1/2\pi) \int_{-\pi}^{\pi} d\theta\, \frac{1+A\exp(j\theta)}{[1+A^2+2A\cos\theta]^{\frac{1}{2}}} \qquad (9)$$

Since the integral of the odd part of the integrand vanishes, we have

$$v_o = (1/2\pi) \int_{-\pi}^{\pi} d\theta\, \frac{1+A\cos\theta}{(1+A^2+2A\cos\theta)^{\frac{1}{2}}}$$

$$= (1/\pi) \int_0^{\pi} d\theta\, \frac{1+A\cos\theta}{(1+A^2+2A\cos\theta)^{\frac{1}{2}}}. \qquad (10)$$

(The latter expression follows from the even symmetry of the integrand.)

9

It is convenient to write the numerator in this integrand as

$$1+A\cos\theta = (1/2)(2+2A\cos\theta)$$

$$= (1/2)(1+A^2+2A\cos\theta + 1-A^2), \qquad (11)$$

so that

$$v_0 = (1/2\pi) \int_0^\pi d\theta \ (1+A^2+2A\cos\theta)^{\frac{1}{2}}$$

$$+ [(1-A^2)/(2\pi)]\int_0^\pi d\theta \ (1+A^2+2A\cos\theta)^{-\frac{1}{2}}. \qquad (12)$$

The change of variable $\theta = 2\varphi$ combined with application of the trigonometric identity

$$\cos 2\varphi = 1-2 \sin^2\varphi \qquad (13)$$

leads to

$$v_0 = (1/\pi) \int_0^{\pi/2} d\varphi \ (1+2A+A^2-4A \sin^2\varphi)^{\frac{1}{2}}$$

$$+ [(1-A)^2/\pi] \int_0^{\pi/2} d\varphi \ (1+2A+A^2-4A \sin^2\varphi)^{-\frac{1}{2}}. \qquad (14)$$

Let us now introduce the parameter m defined by
$$m = 4A/(1+A)^2. \qquad (15)$$

We then have

$$v_0 = [(1+A)/\pi] \int_0^{\pi/2} d\varphi \ (1-m\sin^2\varphi)^{\frac{1}{2}}$$

$$+ [(1-A)/\pi \int_0^{\pi/2} d\varphi \ (1-m\sin^2\varphi)^{-\frac{1}{2}}. \qquad (16)$$

10

This final expression is in the form of complete elliptic integrals. (See, for instance, Eqs. 17.3.1 and 17.3.3 of $\underline{\text{Handbook of Mathematical Functions}}$ by Abramowitz and Stegun.) We thus can write

$$v_o = (1+A) \; E(m)/\pi + (1-A) \; K(m)/\pi. \tag{17}$$

The value of v_o can be calculated using Eqs. 17.3.34 and 17.3.36 of the cited reference; we can then write

$$p_o = v_o^2 \tag{18}$$

as the power in the desired component. Noting that if the unity power output of the limiter had been divided proportionally between just the ω_o and ω_1 components we would have had a power level in the desired component of

$$P_o = (1+A^2)^{-1}, \tag{19}$$

we can define a signal suppression effect

$$\psi = p_o/P_o. \tag{20}$$

This suppression effect in dB is given in Table 1. It is useful to include in the table some extreme cases outside of the calculation range. For $m \approx 0$, (corresponding to $A \to 0$ or $A \to \infty$), it is conveninent to work directly with one of the earlier expressions for v_o which we repeat here:

$$v_o = (1/\pi) \int_o^\pi d\theta \; \frac{1+A \cos\theta}{(1+2A\cos\theta + A^2)^{\frac{1}{2}}} \; .$$

For $A \to \infty$, this can be written as

TABLE 1.   SUPPRESSION EFFECT

J/S, DB	Suppression,DB
$-\infty$	0.00
$-$ 10.0	0.18
$-$ 8.0	0.27
$-$ 6.0	0.37
$-$ 4.0	0.45
$-$ 2.0	0.35
$-$ 1.0	0.07
$-$ 0.8	$-$ 0.04
$-$ 0.6	$-$ 0.16
$-$ 0.4	$-$ 0.33
$-$ 0.2	$-$ 0.55
0.0	$-$ 0.91
0.2	$-$ 1.32
0.4	$-$ 1.60
0.6	$-$ 1.83
0.8	$-$ 2.04
1.0	$-$ 2.23
2.0	$-$ 3.01
4.0	$-$ 4.07
6.0	$-$ 4.76
8.0	$-$ 5.21
10.0	$-$ 5.50
15.0	$-$ 5.86
20.0	$-$ 5.97
25.0	$-$ 6.01
30.0	$-$ 6.02
∞	$-$ 6.02

$$v_o = (1/\pi) \int d\theta \; \frac{\cos\theta + A^{-1}}{(1+2A^{-1}\cos\theta + A^{-2})^{\frac{1}{2}}}. \tag{21}$$

The denominator in this expression can be expanded in powers of A^{-1} using two terms of the negative binomial expansion to obtain

$$(1+2A^{-1}\cos\theta + A^{-2})^{-\frac{1}{2}} \approx 1-A^{-1}\cos\theta. \tag{22}$$

Multiplication of this by the numerator then gives

$$v_o \approx (1/\pi) \int_o^\pi d\theta \; [\cos\theta + A^{-1}\sin^2\theta]$$

$$= 1/2A. \tag{23}$$

The corresponding power is

$$p_o \approx 1/4A^2 \tag{24}$$

yielding the well known 6 dB signal suppression effect:

$$\psi \approx (1/4A^2)/(1/A^2) = 1/4 \text{ as } A\to\infty. \tag{25}$$

At the other extreme of $A\to 0$, we evaluate the integrals by inspection to verify that

$$\psi\to 1 \text{ as } A\to 0. \tag{26}$$

The one significant case remaining is that of equal jamming and signal power. In that case $A=1$ and the expression for v_o becomes

$$v_O = (1/\pi) \int_0^\pi d\theta \; \frac{1+\cos\theta}{(2+2\cos\theta)^{\frac{1}{2}}}$$

$$= 2^{-\frac{1}{2}} \pi^{-1} \int_0^\pi d\theta \; (1+\cos\theta)^{\frac{1}{2}}$$

$$= 2^{\frac{1}{2}} \pi^{-1} \int_0^{\pi/2} d\varphi \; (1+\cos 2\varphi)^{\frac{1}{2}}$$

$$= 2^{\frac{1}{2}} \pi^{-1} \int_0^{\pi/2} d\varphi \; (2\cos^2\varphi)^{\frac{1}{2}}$$

$$= (2/\pi) \int_0^{\pi/2} \cos\varphi \; d\varphi$$

$$= 2/\pi. \tag{27}$$

We thus have

$$P_O = 4/\pi^2, \tag{28}$$

and, since $P_O = 1/2$,

$$\psi = 8/\pi^2 = -0.91 \text{ dB} \quad \text{if } A = 1. \tag{29}$$

2.2.2 CW Jamming Suppression of FH Signals in a Soft Limiter

In Section 2.2.1 we analyzed the suppression of signal energy that occurs when a frequency-hopped (FH) signal and CW or FH jamming are simultaneously present at the input of a hard-limiting repeater. It was suggested by Capt. James Nash of the Air Force Avionics Laboratory that we extend that analysis to the soft-limiting repeater. This section is the result of that suggestion. We first summarize some aspects of the problem, and then present the detailed analysis.

14

2.2.2.1 Summary of Soft Limiter Results

(1) The use of a soft-limiter presupposes use of an ampli-
fier that is operating part of the time in the linear
region and part of the time in a saturation region.
In the most general situation, the phase-shift through
such a device will be a function of the amplitude of
the input. We have made the simplifying assumption
that only the gain depends on drive level and not the
phase shift. It must be recognized that there will be
some practical applications for which the results here
represent an incomplete solution.

(2) In most applications both the input signal power and
input jamming power are variables so that some form
of automatic gain control (AGC) must be used if the
soft-limiting repeater is to depend only on relative
jamming and signal power and not on the absolute
levels. We have shown in the main body of the text
that if the performance is to be invariant to scaling
of the total input, then the voltage gain preceding
the soft limiter should be inversely proportional to
the L_p-norm of the waveform. We have used the L_2-norm
of the total input waveform which corresponds to making
the voltage gain of the preamplifier inversely propor-
tional to the rms input envelope. Correspondingly,
the average power at the input to the soft limiter will
be constant.

(3) The exact performance depends on the specific form of
the nonlinear output/input characteristic. However,
an excellent approximation to the performance can be
obtained by treating the soft-limiter as a device that
acts as a linear amplifier for input envelopes less than
a specified constant times the rms envelope, and clips
the output above this level as shown in Fig. 2.   We
refer to this as a saturating amplifier characteristic.

As in the hard limiter we compare the power in the signal com-
ponent of the output with the signal power out of an ideal amplifier
constrained by an average power limitation rather than a peak power
limitation; the ratio of these signal powers we refer to as the
signal suppression.

15
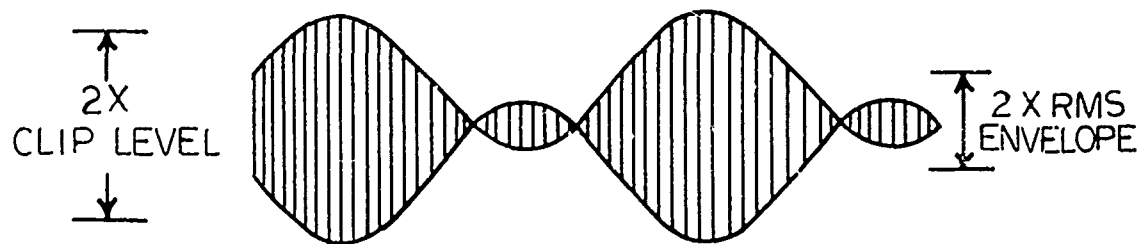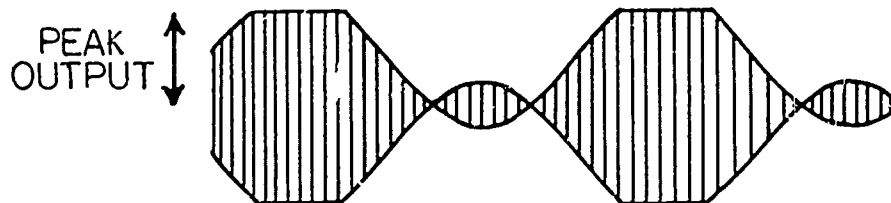
Figure 2. Saturating Amplifier Characteristic

16

The results of the computer calculations of signal suppression vs. J/S ratio show that for each J/S ratio there is an optimum clipping level. Table 2 gives this optimum clipping level for several values of J/S. The optimum clip level exhibits an interesting pattern:

(a) For J/S $\leq$ 0 dB the hard limiter is optimum.

(b) For J/S > 0 dB a soft limiter is optimum but the clip level is always less than 1.3 dB above the rms envelope.

(c) As J/S $\rightarrow \infty$ the optimum clip level is slightly above but not equal to the rms envelope.

Since any operational system would undoubtedly have to work at a fixed clipping level, it is also of interest to determine the worst case suppression for each clipping level. Table 3 gives these numbers for several clipping levels. The minimax value in this table occurs with a clipping level of 0.7 dB above the rms envelope.

The choice of clipping level clearly depends on which range of J/S values is most likely to occur on the operational link. As an aid to possible system design we include Tables 4 to 11 which give the signal suppression vs. J/S for clip levels of 0.1 to 1.3 dB above rms signal level, and for the hard limiter. In addition, some of these data points are plotted in Fig. 3 to show graphically the type of tradeoff involved. We have specifically chosen for graphing the clipping levels of

(a) 1.3 dB, which is the largest clip level that would ever be considered

(b) 0.7 dB, which minimizes the maximum suppression

(c) 0.1 dB, which nearly minimizes the suppression at arbitrarily large J/S ratios

(d) $-\infty$ dB, which is the hard limiter.

17

TABLE 2 OPTIMUM CLIP LEVEL VS J/S

J/S	Optimum Clip Level RMS Envelope (20 $\log_{10}$ voltage ratio)	Signal Suppression (positive values = enhancement)
$-\infty$ dB	$-\infty$ dB	0.00 dB
-10	$-\infty$	0.18
- 9	$-\infty$	0.23
- 8	$-\infty$	0.27
- 7	$-\infty$	0.32
- 6	$-\infty$	0.37
- 5	$-\infty$	0.44
- 4	$-\infty$	0.45
- 3	$-\infty$	0.44
- 2	$-\infty$	0.35
- 1	$-\infty$	0.07
0	$-\infty$	-0.91
1	-5.	-1.51
2	-2.	-1.80
3	-1.	-1.98
4	0.6	-2.09
5	0.9	-2.12
6	1.2	-2.11
7	1.3	-2.06
8	1.3	-1.99
9	1.3	-1.91
10	1.3	-1.81
11	1.3	-1.70
12	1.3	-1.58
13	1.3	-1.47
14	1.2	-1.35
15	1.2	-1.25
16	1.1	-1.14
17	1.0	-1.04
18	0.9	-0.94
19	0.8	-0.86
20	0.7	-0.79
21	0.7	-0.70
22	0.6	-0.64
23	0.6	-0.60
24	0.5	-0.51
25	0.5	-0.50
26	0.4	-0.42
27	0.4	-0.40
28	0.3	-0.38
29	0.3	-0.30
30	0.3	-0.30
∞	0^+	≈ 0

TABLE 3.   WORST SUPPRESSION AT EACH CLIPPING LEVEL

Clip Level	Worst Case Signal Suppression	J/S Value at Which Worst Case Occurs
1.3 dB	− 2.18 dB	3 dB
1.2	− 2.16	3
1.1	− 2.14	3
1.0	− 2.13	4
0.9	− 2.12	4
0.8	− 2.12	5
0.7	− 2.11	5
0.6	− 2.12	6
0.5	− 2.13	6
0.4	− 2.15	7
0.3	− 2.18	8
0.2	− 2.23	9
0.1	− 2.31	12
0.0	− 2.50	∞
< 0	− 6.01	∞

TABLE 4.   SIGNAL SUPPRESSION IN HARD-LIMITING REPEATER

J/S, dB	Suppression, dB
-10	0.18
- 9	0.28
- 8	0.27
- 7	0.32
- 6	0.37
- 5	0.42
- 4	0.45
- 3	0.44
- 2	0.35
- 1	0.07
0	-0.92
1	-2.23
2	-3.01
3	-3.60
4	-4.07
5	-4.45
6	-4.76
7	-5.00
8	-5.21
9	-5.37
10	-5.50
11	-5.61
12	-5.69
13	-5.76
14	-5.81
15	-5.86
16	-5.89
17	-5.92
18	-5.94
19	-5.96
20	-5.97
21	-5.98
22	-5.99
23	-6.00
24	-6.00
25	-6.01
26	-6.01
27	-6.01
28	-6.02
29	-6.02
30	-6.02

TABLE 5.   SOFT-LIMITING REPEATER CLIPPING LEVEL IN DB 0.1

J/S IN DB	PSI-SUB-S/N,DB
-10	-0.83
-9	91
-8	-0 . ?
-7	-1.08
-6	-1.17
-5	-1.27
-4	-1.37
-3	-1.47
-2	-1.57
-1	-1.67
0	-1.77
1	-1.85
2	-1.93
3	-2.01
4	-2.08
5	-2.13
6	-2.18
7	-2.22
8	-2.25
9	-2.28
10	-2.29
11	-2.30
12	-2.31
13	-2.30
14	-2.30
15	-2.28
16	-2.26
17	-2.24
18	-2.21
19	-2.18
20	-2.14
21	-2.09
22	-2.04
23	-1.98
24	-1.92
25	-1.84
26	-1.76
27	-1.67
28	-1.57
29	-1.47
30	-1.35

TABLE 6.   SOFT–LIMITING REPEATER CLIPPING LEVEL IN DB 0.3

J/S IN DB	PSI-SUB-S/N,DB
-10	-0.92
-9	-1.00
-8	-1.08
-7	-1.16
-6	-1.25
-5	-1.35
-4	-1.44
-3	-1.54
-2	-1.63
-1	-1.73
0	-1.81
1	-1.89
2	-1.96
3	-2.03
4	-2.08
5	-2.12
6	-2.15
7	-2.17
8	-2.18
9	-2.18
10	-2.17
11	-2.15
12	-2.12
13	-2.08
14	-2.03
15	-1.98
16	-1.91
17	-1.83
18	-1.74
19	-1.64
20	-1.53
21	-1.41
22	-1.28
23	-1.14
24	-0.99
25	-0.83
26	-0.67
27	-0.52
28	-0.38
29	-0.30
30	-0.30

TABLE 7. SOFT-LIMITING REPEATER CLIPPING LEVEL IN DB 0.5

J/S IN DB	PSI-SUB-S/N,DB
-10	-1.02
-9	-1.09
-8	-1.17
-7	-1.25
-6	-1.34
-5	-1.43
-4	-1.52
-3	-1.61
-2	-1.70
-1	-1.78
0	-1.86
1	-1.93
2	-2.00
3	-2.05
4	-2.09
5	-2.11
6	-2.13
7	-2.13
8	-2.12
9	-2.10
10	-2.07
11	-2.02
12	-1.96
13	-1.89
14	-1.80
15	-1.71
16	-1.60
17	-1.48
18	-1.35
19	-1.21
20	-1.07
21	-0.91
22	-0.76
23	-0.62
24	-0.51
25	-0.50
26	-0.50
27	-0.50
28	-0.50
29	-0.50
30	-0.50

TABLE 8.   SOFT-LIMITING REPEATER CLIPPING LEVEL IN DB 0.7

J/S IN DB	PSI-SUB-S/N,DB
-10	-1.12
-9	-1.19
-8	-1.26
-7	-1.34
-6	-1.43
-5	-1.51
-4	-1.60
-3	-1.68
-2	-1.77
-1	-1.84
0	-1.92
1	-1.98
2	-2.03
3	-2.07
4	-2.10
5	-2.11
6	-2.11
7	-2.10
8	-2.07
9	-2.03
10	-1.97
11	-1.90
12	-1.82
13	-1.72
14	-1.61
15	-1.49
16	-1.36
17	-1.22
18	-1.07
19	-0.93
20	-0.79
21	-0.70
22	-0.70
23	-0.70
24	-0.70
25	-0.70
26	-0.70
27	-0.70
28	-0.70
29	-0.70
30	-0.70

TABLE 9.   SOFT-LIMITING REPEATER CLIPPING LEVEL IN DB 0.9

J/S IN DB	PSI-SUB-S/N,DB
-10	-1.23
-9	-1.29
-8	-1.36
-7	-1.44
-6	-1.52
-5	-1.60
-4	-1.68
-3	-1.76
-2	-1.84
-1	-1.91
0	-1.97
1	-2.03
2	-2.07
3	-2.10
4	-2.12
5	-2.12
6	-2.11
7	-2.08
8	-2.03
9	-1.97
10	-1.90
11	-1.81
12	-1.71
13	-1.59
14	-1.47
15	-1.33
16	-1.19
17	-1.06
18	-0.94
19	-0.90
20	-0.90
21	-0.90
22	-0.90
23	-0.90
24	-0.90
25	-0.90
26	-0.90
27	-0.90
28	-0.90
29	-0.90
30	-0.90

TABLE 10.   SOFT-LIMITING REPEATER CLIPPING LEVEL IN DB 1.1

J/S IN DB	PSI-SUB-S/N,DB
-10	-1.34
-9	-1.40
-8	-1.47
-7	-1.54
-6	-1.62
-5	-1.69
-4	-1.77
-3	-1.84
-2	-1.91
-1	-1.98
0	-2.04
1	-2.08
2	-2.12
3	-2.14
4	-2.14
5	-2.13
6	-2.11
7	-2.07
8	-2.01
9	-1.93
10	-1.84
11	-1.74
12	-1.63
13	-1.50
14	-1.37
15	-1.25
16	-1.14
17	-1.10
18	-1.10
19	-1.10
20	-1.10
21	-1.10
22	-1.10
23	-1.10
24	-1.10
25	-1.10
26	-1.10
27	-1.10
28	-1.10
29	-1.10
30	-1.10

TABLE 11.   SOFT-LIMITING REPEATER CLIPPING LEVEL IN DB 1.3

J/S IN DB	PSI-SUB-S/N,DB
-10	-1.47
-9	-1.52
-8	-1.58
-7	-1.65
-6	-1.72
-5	-1.79
-4	-1.86
-3	-1.93
-2	-1.99
-1	-2.05
0	-2.10
1	-2.14
2	-2.17
3	-2.18
4	-2.17
5	-2.15
6	-2.12
7	-2.06
8	-1.99
9	-1.91
10	-1.81
11	-1.70
12	-1.58
13	-1.47
14	-1.36
15	-1.30
16	-1.30
17	-1.30
18	-1.30
19	-1.30
20	-1.30
21	-1.30
22	-1.30
23	-1.30
24	-1.30
25	-1.30
26	-1.30
27	-1.30
28	-1.30
29	-1.30
30	-1.30

27
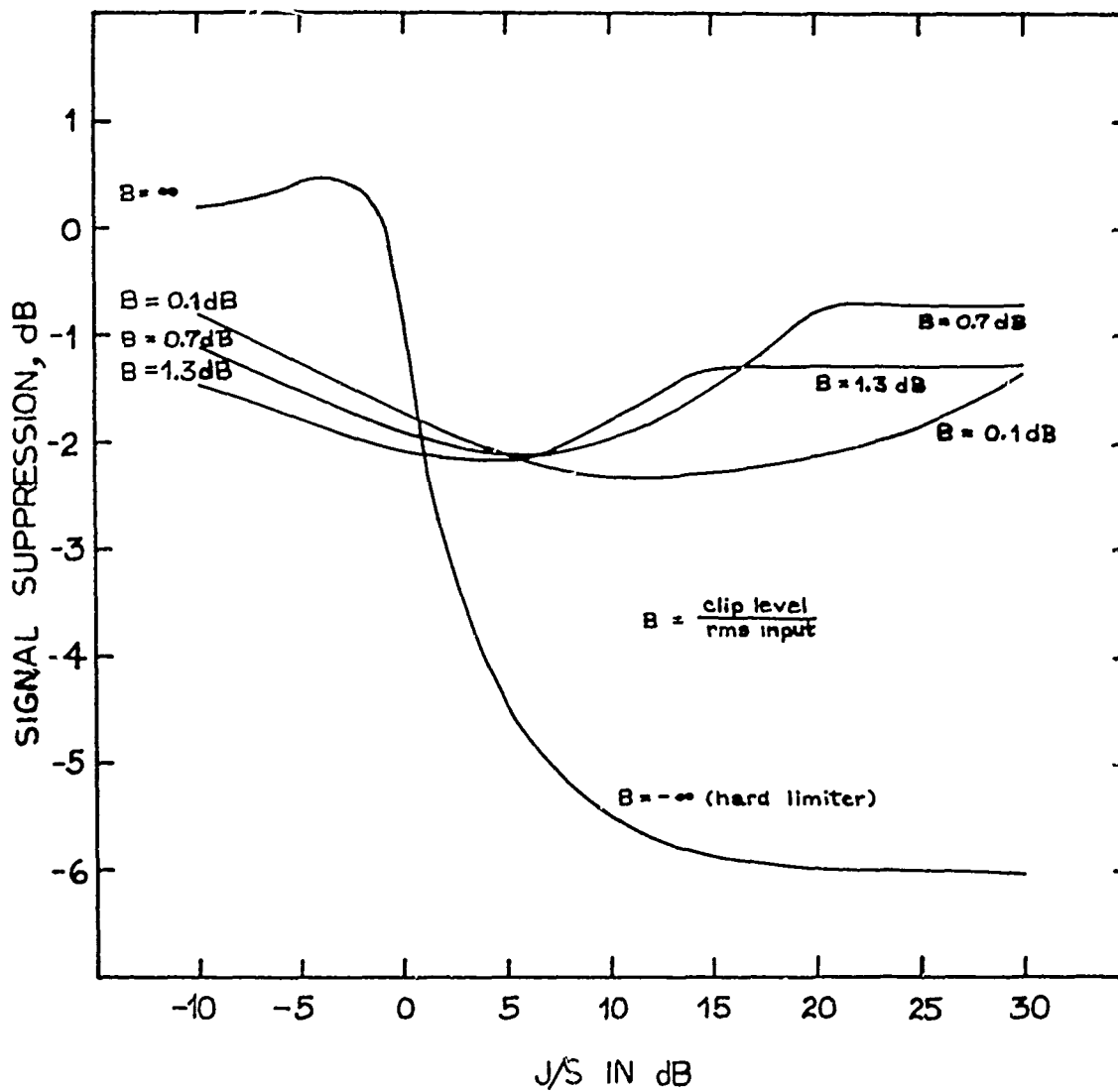
Figure 3. Signal Suppression in Soft-Limiting Repeater.

In addition to the obvious application of soft-limiting in satellite or RPV repeaters, there are certain MFSK receivers that use limiting prior to the multiple filters. A typical situation is one involving a coded 8-FSK or 16-FSK signal, where the 8 or 16 possible tones are hopped as a group, and where the receiver consists of a dehopper followed by a narrow-band limiter followed by a filter bank, followed by decoding circuitry. Because soft-limiting appeared to be such a desirable tool in the satellite-repeater framework, we felt that it might also prove to be useful as a receiver preclipper in place of the hard limiter. Furthermore, it was easy to extend the numerical programming to include this case.

For the receiver preclipper, it is again necessary to assume some form of automatic gain control so that the clipping level is referred to input power or rms envelope. This is not the place for a detailed discussion of demodulation of coded FH transmissions; however, a brief analysis suggests that the gain control should not be set in terms of the average total input power, but rather should be referred to the rms envelope of the desired signal. We base our analysis on this assumption.

When the satellite repeater was analyzed, it was sufficient to consider the signal suppression alone because the dominant cause of link failure in that situation is the downlink noise. This is no longer true in the case of the receiver preclipper where the source of errors is the jamming power at the output of the non-linearity. One is thus led to considering the suppression of both signal and jamming power below the peak output of the non-linearity.

Figure 4 presents curves of both suppression effects at three clipping levels. The results are inconclusive as to whether use of a soft limiter in this application would be beneficial or not. Basically what is needed is an analysis paralleling that in the repeater study, Section 2.4 of this report. Such an analysis would determine the optimum operating point for the jammer for each clipping level and establish the improvement or degradation that accompanies soft limiting.

2.2.2.2 Analytical Development of the Soft Limiter

In Section 2.2.1 we analyzed the suppression of frequency-hopped signals by constant amplitude jamming in a hard limiter amplifier. In this section we extend that analysis to other non-linear amplifiers, including AGC effects.

2.2.2.2.1 Description of the Input Signal

Let

$$S = \text{signal power at input to nonlinearity} \tag{30a}$$

$$J = \text{jamming power at input to nonlinearity} \tag{30b}$$

$$\omega_S = \text{signal frequency, radians/sec} \tag{30c}$$

$$\omega_J = \text{jamming frequency, radians/sec .} \tag{30d}$$

If we refer the power levels to a ½-ohm impedance level (the actual impedance level is obviously irrelevant), the voltage waveform at the input can be written as

$$V(t) = S^{\frac{1}{2}} \cos(\omega_S t) + J^{\frac{1}{2}} \cos(\omega_J t). \tag{31}$$

With reference to any frequency in the signal band, this waveform has a slowly-varying envelope, and slowly-varying phase.

30
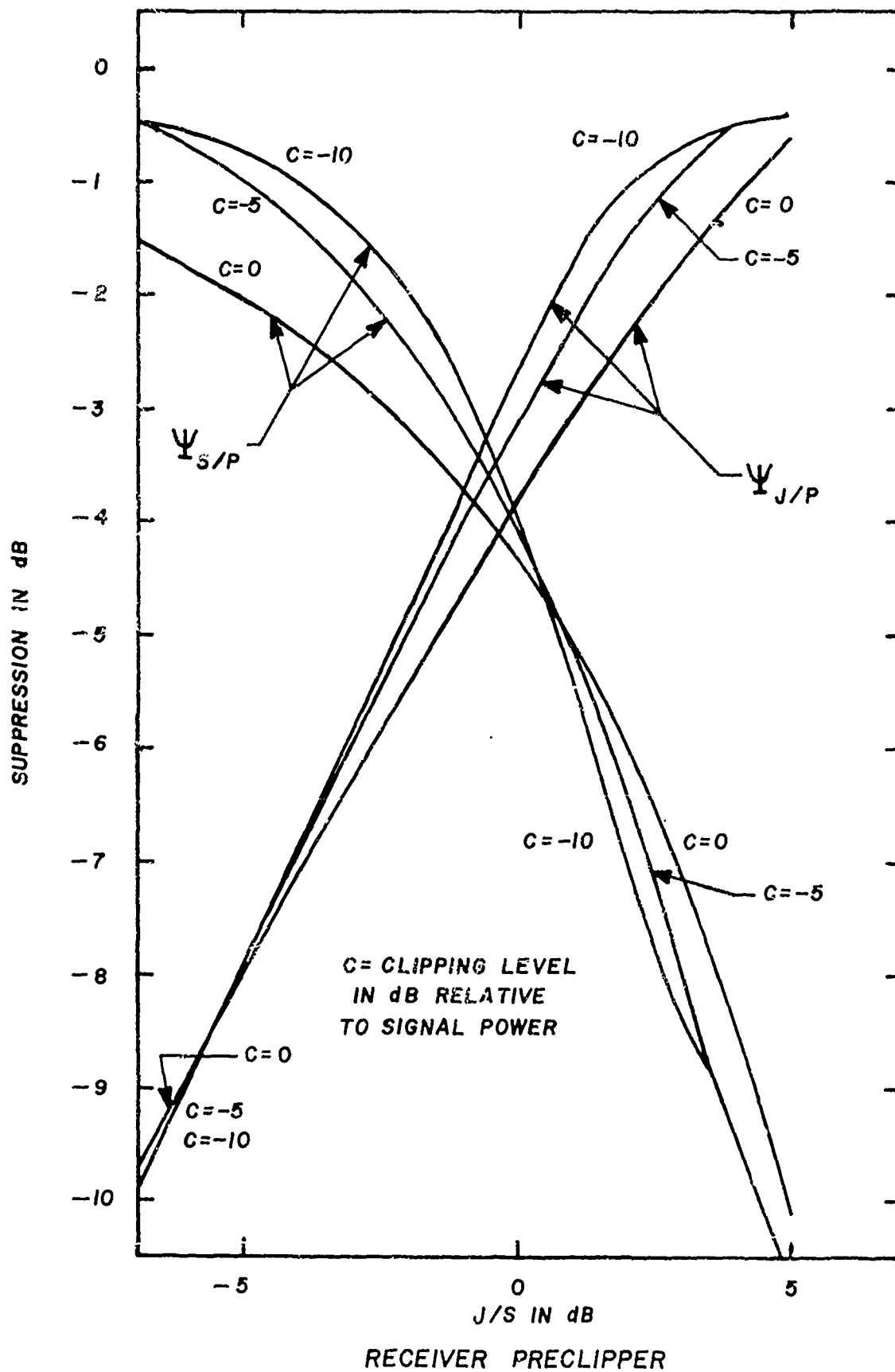
Figure 4. $\Psi_{S/P}$ and $\Psi_{J/P}$ vs J/S.

31

For example, if we select the signal frequency itself as a reference, we can rewrite Eq. (31) as

$$V(t) = R(t) \cos[\omega_s t + \varphi(t)],$$ (32)

where the fluctuations of both $R(t)$ and $\varphi(t)$ are very slow compared to those of $\cos(\omega_s t)$.

Before evaluating $R(t)$ and $\varphi(t)$ it is helpful to make a few notational simplifications to make the ensuing mathematics shorter. Specifically we write

$$a = S^{\frac{1}{2}},$$ (33a)

$$b = J^{\frac{1}{2}},$$ (33b)

and

$$\omega = \omega_J - \omega_s .$$ (34)

In terms of these quantities Eq. (31) can be rewritten as

$$V(t) = a \cos(\omega_s t) + b \cos(\omega_s t + \omega t),$$ (35)

or, upon expanding the second term using routine trigonometric identities,

$$V(t) = [a + b\cos(\omega t)] \cos(\omega_s t)$$

$$- b \sin(\omega t) \sin(\omega_s t).$$ (36)

If we use a similar expansion of Eq. (32) we find the alternate expression for $V(t)$:

$$V(t) = R(t) \cos[\varphi(t)] \cos(\omega_s t)$$

$$- R(t) \sin[\varphi(t)] \sin(\omega_s t).$$ (37)

The coefficients of $\cos(\omega_s t)$ in Eqs. (36) and (37) must be equal to each other, as must the coefficients of $\sin(\omega_s t)$. We therefore have

$$R(t) \cos[\varphi(t)] = a + b \cos(\omega t), \tag{38a}$$

$$R(t) \sin[\varphi(t)] = b \sin(\omega t). \tag{38b}$$

The ratio of these two equations yields

$$\tan[\varphi(t)] = \frac{b \sin(\omega t)}{a + b \cos(\omega t)}, \tag{39}$$

while the sums of squares of the two equations yields

$$R^2(t) = a^2 + 2 a b \cos(\omega t) + b^2. \tag{40}$$

2.2.2.2.2 Description of the Nonlinearity

If we passed $V(t)$ through an ideal linear amplifier, the output would be

$$W(t) = KV(t) = KR(t) \cos[\omega_s t + \varphi(t)]. \tag{41}$$

The type of nonlinear amplifier we are concerned with can be thought of as an amplifier with drive-dependent gain followed by a bandpass filter which only permits transmission of frequencies near the nominal carrier frequency. Let us write the output of this device as

$$W(t) = Q(t) \cos[\omega_s t + A(t)]. \tag{42}$$

We now need to examine the relation of $Q(t)$ and $A(t)$ to $R(t)$ and $\varphi(t)$.

Since $R(t)$ and $\varphi(t)$ are slowly-varying let us look at the values of $Q(t)$ and $A(t)$ when $R(t)$ and $\varphi(t)$ are constant for some small interval of time. In this situation $V(t)$ is a constant amplitude sinusoid:

$$V(t) = R \cos[\omega_s t + \varphi] \quad \text{if } R(t) = R \text{ and } \varphi(t) = \varphi. \tag{43}$$

Clearly, the output of the nonlinear device must also be a constant amplitude sinusoid,

$$W(t) = Q \cos[\omega_s t + \theta]. \qquad (44)$$

Furthermore, since we can write

$$\cos[\omega_s t + \varphi] = \cos[\omega_s(t + \varphi/\omega_s)], \qquad (45)$$

the phase shift ω is completely equivalent to a shift in time. Since the behavior of the nonlinearity must not be a function of the time origin, we then have

$$W(t) = Q \cos[\omega_s(t + \omega/\omega_s) + \theta_o]$$

$$= Q \cos[\omega_s t + \omega + \theta_o] \qquad \cdot \qquad (46a)$$

where θ_o is the equivalent phase shift of the device viewed as a linear amplifier:

$$\theta = \theta_o \text{ when } \varphi = 0. \qquad (46b)$$

Since neither θ_o nor Q depends on φ, the most general form that we can assume for the device is

$$Q = H(R) \qquad \cdot \qquad (47a)$$
$$\theta_o = h(R) \qquad (47b)$$

or

$$W(t) = H(R) \cos[\omega_s t + \omega + h(R)]$$

$$\text{when } R(t) = R \text{ and } \omega(t) = \varphi. \qquad (48)$$

We can now generalize to the actual case. As long as the variations of R(t) are sufficiently slow compared to the time

34

constants of the circuits in the nonlinear device, Eqs.(47) and (48) generalizes immediately to

$$Q(t) = H[R(t)], \tag{49a}$$

$$\theta_o(t) = h[R(t)], \tag{49b}$$

and

$$W(t) = H[R(t)] \cos\{\omega_s t + \varphi + h[R(t)]\}. \tag{50}$$

The form of the output give by Eq.(50) is the most general form of distortion we reasonably need to consider in analyzing the effect of nonlinearities, and there are, in fact, many types of amplifiers (beam power devices like travelling-wave tubes, for example) that require the full generality of this expression. It is virtually impossible, however, to achieve any useful analytic results when we include the drive-dependent phase shift $h[R(t)]$ except with a case-by-case numerical analysis. Let us therefore consider a more restricted model.

2.2.2.2.2.1 A Restrictive Assumption

Suppose we model the nonlinear amplifier as a memoryless nonlinearity followed by a band-limitation. Let us consider first the effects of the memoryless nonlinearity by itself without including the effect of the subsequent band-limitation.

We will write the output of the nonlinearity as

$$U(t) = f[V(t)]. \tag{51}$$

Now it is certainly possible to assume that $V(t)$ is bounded in magnitude by some large number L,

$$|V(t)| \leq L, \tag{52}$$

35

and on the range $|v| \leq L$ we can always find a polynomial approximation to $f(v)$:

$$f(v) \approx \sum_{m=0}^{M} f_m v^m, \quad |v| \leq L. \tag{53}$$

The approximation can be made arbitrarily good by taking M sufficiently large. Looking ahead to the result of filtering $U(t)$, we can see that only the odd powers of v can yield in-band components. Let us therefore simplify Eq.(53) to read

$$f(v) \doteq \sum_{k=0}^{K} f_{2k+1} v^{2k+1}, \tag{54}$$

where the symbol " $\doteq$ " means that the even powers have been omitted.

With $V(t)$ given by

$$V(t) = R \cos(\omega_s t + \varphi), \tag{55}$$

the output $U(t)$ is then

$$U(t) \doteq \sum_{k=0}^{K} f_{2k+1} R^{2k+1} [\cos(\omega_s t + \varphi)]^{2k+1}. \tag{56}$$

The powers of the cosine in this expression may be evaluated by the chain of equalities

$$(\cos x)^{2k+1} = (\tfrac{1}{2})^{2k+1} \left(e^{jx} + e^{-jx}\right)^{2k+1}$$

$$= (\tfrac{1}{2})^{2k+1} \sum_{m=0}^{2k+1} \binom{2k+1}{m} \left(e^{jx}\right)^{m} \left(e^{-jx}\right)^{2k+1-m}$$

$$= (\tfrac{1}{2})^{2k+1} \sum_{m=0}^{2k+1} \binom{2k+1}{m} e^{j(2m-1-2k)x}$$

$$= (\tfrac{1}{2})^{2k+1} \sum_{m=0}^{k} \binom{2k+1}{m} e^{j(2m-1-2k)x}$$

$$+ (\tfrac{1}{2})^{2k+1} \sum_{m=k+1}^{2k+1} \binom{2k+1}{m} e^{j(2m-1-2k)x},$$

36

or upon substituting $n = k + 1 - m$ in the first sum and $n = m - k$ in the second sum

$$(\cos x)^{2k+1} = (\tfrac{1}{2})^{2k+1} \sum_{n=1}^{k+1} \binom{2k+1}{k+1-n} e^{j(1-2n)x}$$

$$+ (\tfrac{1}{2})^{2k+1} \sum_{n=1}^{k+1} \binom{2k+1}{n+k} e^{j(2n-1)x}.$$

Since the binomial coefficients are identical in the two sums for the same index n, we can combine the sums as

$$(\cos x)^{2k+1} = (\tfrac{1}{2})^{2k+1} \sum_{n=1}^{k+1} \binom{2k+1}{n+k} 2\cos\left[(2n-1)x\right]$$

or, finally

$$(\cos x)^{2k+1} = 4^{-k} \sum_{n=1}^{k+1} \binom{2k+1}{n+k} \cos\left[(2n-1)x\right]. \tag{57}$$

If we substitute this in Eq. (56) we then have

$$U(t) = \sum_{k=0}^{K} f_{2k+1} R^{2k+1} 4^{-k}$$

$$\cdot \sum_{n=1}^{k+1} \binom{2k+1}{n+k} \cos\left[(2n-1)(\omega_S t + \varphi)\right]. \tag{58}$$

In this expression the terms involving

$$\cos\left[(2n-1)(\omega_S t + \varphi)\right]$$

are centered in frequency on an odd harmonic of ω_S. Even though the spectral width of these terms is proportional to the sum of the spectral widths of $R(t)$ and $\cos[\varphi(t)]$ multiplied by $(2k+1)$, we can usually assume that none of these spectra fall in the vicinity of ω_S. It is therefore an excellent approximation to use only the term for $n = 1$ in each of the inner sums of Eq. (58) to arrive at

$$U(t) = \left\{ \sum_{k=0}^{K} f_{2k+1} \binom{2k+1}{k+1} 4^{-k} [R(t)]^{2k+1} \right\}$$

$$\cdot \cos[\omega_s t + \varphi(t)]. \tag{59}$$

It will be noted that we have reinserted the time-dependence of R and φ which was left implicit in Eqs. (55)-(58).

In the CW-jamming case we are analyzing, it is useful to temporarily factor the first power of $R(t)$ out of the quantity in the braces, and to associate it with the phase modulated term so that we then have

$$U(t) = \left\{ \sum_{k=0}^{K} f_{2k+1} \binom{2k+1}{k+1} 4^{-k} [R^2(t)]^k \right\}$$

$$\cdot R(t) \cos[\omega_s t + \varphi(t)]. \tag{60}$$

The term multiplying the quantity in braces is then seen (from Eq. (32)) to be $V(t)$; we can also substitute the expression for $R^2(t)$ from Eq. (11) to obtain $U(t)$ in the form

$$U(t) = \left\{ \sum_{k=0}^{K} f_{2k+1} \binom{2k+1}{k+1} 4^{-k} [a^2 + b^2 + 2ab \cos(\omega t)]^k \right\}$$

$$\cdot [a \cos(\omega_s t) + b \cos(\omega_s t + \omega t)]. \tag{61}$$

In this form we see that $U(t)$ consists of carriers at ω_s and $\omega_s + \omega$ that are amplitude modulated by sinusoidal terms that are harmonics of ω; the largest of these harmonic modulation frequencies is at $K\omega$. We thus have the highest and lowest frequencies in $U(t)$ given by

$$\text{highest radian frequency in } U(t) = \omega_s + (K+1)\omega, \tag{62a}$$

$$\text{lowest radian frequency in } U(t) = \omega_s - K\omega. \tag{62b}$$

38

The most unfavorable situation therefore occurs when the jamming frequency is near the signal frequency so that

$$\omega \ll \text{transmission bandwidth,} \tag{63}$$

in which case all of the distortion frequencies pass through the filter and

$$W(t) \approx U(t). \tag{64}$$

We thus can substitute W(t) for U(t) on the left-hand side of Eq.(29); if we then compare this with Eq.(20) we see immediately that

$$H(r) = \sum_{k=0}^{K} f_{2k+1} \binom{2k+1}{k+1} 4^{-k} r^{2k+1}, \tag{65a}$$

and

$$h(r) \equiv 0. \tag{65b}$$

This yields the simpler expression

$$W(t) = H[R(t)] \cos[\omega_s t + \varphi(t)]. \tag{65c}$$

This is the model we will adopt in the ensuing analysis.

2.2.2.2.2 Shortcomings of Restricted Model

It must be recognized that in using the restricted model of Eq.(66) we are possibly ignoring the more serious suppression effects of the nonlinearity. The assumption that the phase shift is independent of drive level implies that the device exhibits no AM-to-PM conversion. This is certainly incorrect if the soft-limiting effects occur in a microwave power amplifier, and it is a difficult design problem to insure its truth even in low-power-level devices. Furthermore, the effect of AM/PM conversion can

39

be far more significant than the amplitude nonlinearity itself. From this previous study of the hard limiter, we expect maximum suppression due to amplitude effects to be of the order of 6 dB. However, it is possible to conceive of suppression effects much larger than this associated with the incidental phase modulation in a multiple-cavity power amplifier. The ensuing analysis of suppression associated with amplitude nonlinearities must therefore be viewed as only a first stage in the analysis of actual devices.

2.2.2.2.3 Suppression Ratios

The instantaneous RF power out of the nonlinear amplifier is given by

$$p(t) = \{H\lceil R(t)\rceil\}^2. \tag{67}$$

We denote by P the maximum available power from the device:

$$P = \text{peak power.} \tag{68}$$

Correspondingly, H must be constrained by

$$H(r) \leq P^{\frac{1}{2}}, \quad 0 \leq r \leq \infty. \tag{69}$$

It is helpful now to factor W(t) in a slightly different way. We define

$$G(r) = \frac{H(r)}{r}; \tag{70}$$

G(r) can be looked on as an amplitude-dependent voltage gain. We then have

$$W(t) = G\lceil R(t)\rceil \, R(t) \, \cos\lceil \omega_s t + \varphi(t)\rceil, \tag{71}$$

or, upon comparing with Eq.(3),

$$W(t) = G\lceil R(t)\rceil \, V(t). \tag{72}$$

If we refer back to Eq. (40) we see that $R^2(t)$ is an even periodic function with period

$$t_o = 2\pi/\omega. \tag{73}$$

Consequently, $R(t)$ also has this property as does $G[R(t)]$. We therefore can write

$$G[R(t)] = g_o + \sum_{n>0} g_n \cos(n\omega t) \tag{74}$$

where

$$g_o = \frac{1}{t_o} \int_{-t_o/2}^{t_o/2} G[R(t)] \, dt. \tag{75a}$$

and

$$g_n = \frac{2}{t_o} \int_{-t_o/2}^{t_o/2} G[R(t)] \cos(n\omega t) dt, \; n > 0. \tag{75b}$$

These coefficients may be put in a slightly nicer form by changing the variable of integration to be

$$x = \omega t,$$

so that

$$g_o = \frac{1}{2\pi} \int_{-\pi}^{\pi} G[\rho(x)] \, dx, \tag{76a}$$

$$g_n = \frac{1}{\pi} \int_{-\pi}^{\pi} G[\rho(x)] \cos(nx) dx, n > 0, \tag{76b}$$

where, in both expressions $\rho(x)$ is given by

$$\rho(x) = [a^2 + 2ab \cos(x) + b^2]^{\frac{1}{2}}. \tag{77}$$

If we now replace the factors G and V in Eq. (72) by their equivalent expressions given in Eqs. (74) and (35) respectively, we have

$$W(t) = \left[g_o + \sum_{n>0} g_n \cos (n\omega t) \right]$$

(78)

$$\cdot [a \cos(\omega_S t) + b \cos(\omega_S t + \omega t)],$$

or, using the standard trigonometric identity for the product of two cosines,

$$W(t) = a \, g_o \, \cos(\omega_S t) + b \, g_o \, \cos(\omega_S t + \omega t)$$

$$+ \sum_{n>0} \tfrac{1}{2} a \, g_n \cos(\omega_S t + n\omega t) + \sum_{n>0} \tfrac{1}{2} a \, g_n \cos(\omega_S t - n\omega t)$$

$$+ \sum_{n>0} \tfrac{1}{2} b \, g_n \cos[\omega_S t + (n+1)\omega t] + \sum_{n>0} \tfrac{1}{2} b \, g_n \cos[\omega_S t + (n-1)t].$$

(79)

Of all the terms involved in this expression, only the first term and the (n=1)-term in the last sum are at the signal frequency of ω_S. We can therefore write

$$W(t) = (a \, g_o + \tfrac{1}{2} b \, g_1) \cos (\omega_S t)$$

$$+ \text{ sinusoids at other frequencies.}$$

(80)

If we then denote the output signal power by P_S:

$$P_S = \text{power at frequency } \omega_S,$$

we have

$$P_S = (a \, g_o + \tfrac{1}{2} b \, g_1)^2.$$

(81)

All of the other terms in the expansion in Eq. (48) constitute potential interference or noise in subsequent detection.

42

operations and we can denote their power by

$$P_J = \text{power at frequencies} \neq \omega_S.$$

It would be tremendously cumbersome to arrive at the value of P_J by summing the squared coefficients, however. A much more direct way of arriving at this number is to equate it to the total power of $W(t)$ minus the power in ω_S. This total power is just the time average of the instantaneous power given by Eq. (67); denoting it by P_T, we have

$$P_T = \lim_{\tau \to \infty} \frac{1}{2\tau} \int_{-\tau}^{\tau} \{H[R(t)]\}^2 dt. \tag{82}$$

We can again use the periodic property of $R(t)$ to write this as the average over a single period of the difference frequency:

$$P_T = \frac{1}{2\pi} \int_{-\pi}^{\pi} \{H[\rho(x)]\}^2 \, dx.$$

This can be written in terms of the voltage gain G as

$$P_T = \frac{1}{2\pi} \int_{-\pi}^{\pi} \{\rho(x) \, G[\rho(x)]\}^2 dx. \tag{83}$$

We then express P_J as

$$P_J = P_T - P_S. \tag{84}$$

We turn now to the definition of suppression ratios. We observe first that if the amplifier were linear and operated under an _average_ power limitation, the output power P would be divided between signal and jamming in the same proportions as existed at the input. We would thus have

43

$$P'_S = \frac{S}{S+J} \ P = \frac{a^2}{a^2 + b^2} \ P$$

$$P'_J = \frac{J}{S+J} \ P = \frac{b^2}{a^2 + b^2} \ P$$

$\left. \right\}$ linear amplifier, average power limitation. (85)

For down-link-limited satellite repeaters where the main source of interference is the thermal noise power N at the down-link receiver and not the reradiated interference, the quantity of interest is the downlink SNR:

$$K_{S/N} = \gamma P_S/N, \tag{86a}$$

where

$$\gamma = \text{effective path power gain } (\gamma \ll 1). \tag{86b}$$

For the average-limited amplifier this SNR is

$$K'_{S/N} = \frac{\gamma a^2 P}{N(a^2 + b^2)} , \tag{87}$$

so that the SNR suppression may be defined by

$$\psi_{S/N} = \frac{K_{S/N}}{K'_{S/N}} = \frac{a^2 + b^2}{a^2} \ \frac{P_S}{S} . \tag{88}$$

For certain receiver cir itry calculations (to be discussed subsequently) we will be more ncerned with the ratios of sig-nal and interference to peak available output. For those analyses we will use the factors

$$\psi_{S/P} = P_S/P \tag{89}$$

and

$$\psi_{J/P} = P_J/P. \tag{90}$$

These are not measured relative to the values that would exist in a linear average-power limited device.

2.2.2.2.4 Summary of Relevant Formulas

It may be helpful to collect all of the relevant formulas in one place here. We have defined a drive-dependent voltage gain G that must satisfy

$$\rho G(\rho) \le P^{\frac{1}{2}}. \tag{91}$$

The input envelope ρ is given in terms of the relative phase of jamming and signal as

$$\rho(x) = [a^2 + 2ab \cos(x) + b^2]^{\frac{1}{2}}. \tag{92}$$

The output signal power is given by

$$P_S = (a\, g_0 + \tfrac{1}{2}\, b\, g_1)^2 \tag{93}$$

where

$$g_0 = \frac{1}{2\pi} \int_{-\pi}^{\pi} G[\rho(x)]\, dx, \tag{94a}$$

$$g_1 = \frac{1}{\pi} \int_{-\pi}^{\pi} G[\rho(x)]\, \cos(x)\, dx. \tag{94b}$$

The total output power is

$$P_T = \frac{1}{2\pi} \int_{-\pi}^{\pi} \{\rho(x)\, G[\rho(x)]\}^2 dx, \tag{95}$$

and the interference (or jamming) component of this is given by

$$P_J = P_T - P_S. \tag{96}$$

45

The three suppression factors are

$$\psi_{S/N} = \frac{a^2 + b^2}{a^2} \frac{P_S}{P} , \qquad (97)$$

$$\psi_{S/P} = P_S/P, \qquad (98a)$$

and

$$\psi_{J/P} = P_J/P. \qquad (98b)$$

In all of the expressions the numbers a and b are the signal and jamming amplitudes,

$$a^2 = S, \quad b^2 = J. \qquad (99)$$

2.2.2.3 The Saturating Amplifier

A reasonably good model for a "soft" limiter is provided by the saturating amplifier:

$$\left. \begin{array}{l} G(r) = C, \ 0 \le r \le r_o \\[6pt] rG(r) = Cr_o, \ r \ge r_o \end{array} \right\} \qquad (100)$$

That is, $G(\ ,$ provides constant gain below the threshold r_o, and constant output amplitude above it. In order to satisfy the peak power constraint, C and r_o must be related by

$$Cr_o = P^{\frac{1}{2}}. \qquad (101)$$

It is useful to take the input saturation level r_o as the independent variable in this equation and consequently to redefine G as

$$G(r) = \left\{ \begin{array}{ll} P^{\frac{1}{2}}/r_o , & 0 \le r \le r_o \\[6pt] P^{\frac{1}{2}}/r , & r \ge r_o \end{array} \right\} \qquad (102)$$

2.2.2.3.1 Analysis

Since

$$|a - b| \leq \rho(x) \leq a + b,$$

the analysis falls naturally into three separate cases:

Case I :	$r_o \geq a + b$	(103a)
Case II :	$\|a-b\| \leq r_o \leq a+b$	(103b)
Case III :	$r_o \leq \|a-b\|$.	(103c)

2.2.2.3.1.1 Case I

Although this case can be analyzed using trivial arithmetic, it is useful to use the formulas of Eqs. (92)-(99) to set the stage for the more difficult cases. Since

$$r_o \geq a + b \geq \rho(x), \tag{104}$$

G is given by the single expression

$$G(r) = P^{\frac{1}{2}}/r_o. \tag{105}$$

Substitution of this in Eqs. (94a) and (94b) yields

$$g_o = P^{\frac{1}{2}}/r_o, \tag{106a}$$

$$g_1 = 0, \tag{106b}$$

so that, from Eq. (94a),

$$P_S = a^2 P/r_o^2. \tag{107}$$

The total power, from Eq. (95), is

$$P_T = \frac{1}{2\pi} \int_{-\pi}^{\pi} \frac{P}{r_o^2} \lceil a^2 + 2ab \cos(x) + b^2 \rceil dx$$

47

or

$$P_T = \frac{a^2 + b^2}{r_o^2} \ P.$$ (108)

The interference component, from Eq.(96), is

$$P_J = P_T - P_S = b^2 P / r_o^2.$$ (109)

The suppression factors are then

$$\psi_{S/N} = \frac{a^2 + b^2}{a^2} \ \frac{P_S}{P} = \frac{a^2 + b^2}{r_o^2}$$ (110)

$$\psi_{S/P} = a^2 / r_o^2,$$ (111a)

and

$$\psi_{J/P} = b^2 / r_o^2 \ .$$ (111b)

Since

$$r_o^2 \geq (a + b)^2,$$ (112)

Eq.(110) shows that

$$\psi_{S/N} \leq \frac{a^2 + b^2}{a^2 + 2ab + b^2} \ < 1 \text{ unless } a = 0 \text{ or } b = 0.$$ (113)

Thus the signal power is suppressed from the level achievable in an ideal average-power-limited amplifier.

2.2.2.3.1.2 <u>Case II</u>

We now have

$$\underset{x}{\text{Min}} \ \rho(x) = |a-b| \leq r_o \leq a+b = \underset{x}{\text{Max}} \ \rho(x).$$ (114)

Let us first use the identity

$$\cos(x) = 1 - 2 \ \sin^2(x/2)$$

48

to rewrite Eq. (92) as

$$\rho^2(x) = (a+b)^2 - 4ab \sin^2(x/2). \tag{115}$$

We now define the _elliptic parameter_ m by

$$m = \frac{4ab}{(a+b)^2}, \tag{116}$$

in terms of which ρ can be written as

$$\rho(x) = (a+b)[1 - m \sin^2(x/2)]^{\frac{1}{2}}. \tag{117}$$

When $|x|$ is small ρ exceeds the clipping level r_0, and, conversely, when $|x|$ is near π, ρ is in the linear region. We define the breakpoint between these regions by x_0, which is given implicitly by

$$r_0 = \rho(x_0) = (a+b)[1 - m \sin^2(x/2)]^{\frac{1}{2}}, \tag{118a}$$

or explicitly by

$$x_0 = 2 \arcsin \sqrt{\frac{1}{m}\left[1 - \left(\frac{r_0}{a+b}\right)^2\right]}. \tag{118b}$$

We then have

$$G[\rho(x)] = \frac{\rho^{\frac{1}{2}}}{a+b}[1 - m \sin^2(x/2)]^{-\frac{1}{2}}, \quad 0 \le |x| \le x_0, \tag{119a}$$

$$G[\rho(x)] = \frac{\rho^{\frac{1}{2}}}{r_0} \qquad\qquad\qquad , \quad x_0 \le |x| \le \pi. \tag{119b}$$

The three constants to be determined are then

$$g_0 = \frac{1}{2\pi} \int_{|x| \le x_0} \frac{\rho^{\frac{1}{2}}}{a+b}[1 - m \sin^2(x/2)]^{-\frac{1}{2}} dx$$

$$+ \frac{1}{2\pi} \int_{x_0 \le |x| \le \pi} \frac{\rho^{\frac{1}{2}}}{r_0} dx; \tag{120}$$

49

$$g_1 = \frac{1}{\pi} \int\limits_{|x| \leq x_o} \frac{P^{\frac{1}{2}} \cos(x)}{a+b} [1-m \sin^2(x/2)]^{\frac{1}{2}} dx$$

$$+ \frac{1}{\pi} \int\limits_{x_o \leq |x| \leq \pi} \frac{P^{\frac{1}{2}}}{r_o} \cos(x) \, dx; \tag{121}$$

$$P_T = \frac{1}{2\pi} \int\limits_{|x| \leq x_o} P \, dx$$

$$+ \frac{1}{2\pi} \int\limits_{x_o \leq |x| \leq \pi} \frac{P(a+b)^2}{r_o^2} [1-m \sin^2(x/2)] dx. \tag{122}$$

The third expression is a simple trigonometric integral which can be evaluated as

$$\frac{P_T}{2} = \frac{x_o}{\pi} + \frac{(a+b)^2}{\pi r_o^2} [(1-m/2)(\pi-x_o) - (m/2) \sin(x_o)]. \tag{123}$$

The first two expressions can be partially evaluated to yield

$$g_o/P^{\frac{1}{2}} = \frac{\pi-x_o}{\pi r_o} + \frac{1}{\pi(a+b)} \int\limits_0^{x_o} \frac{dx}{[1-m \sin^2(x/2)]^{\frac{1}{2}}} \tag{124}$$

and

$$g_1/2P^{\frac{1}{2}} = \frac{\sin(x_o)}{\pi r_o} + \frac{1}{\pi(a+b)} \int\limits_0^{x_o} \frac{\cos x \, dx}{[1-m \sin^2(x/2)]} . \tag{125}$$

The integrals in Eqs. (124) and (125) can be evaluated in terms of incomplete elliptic integrals. However, for purposes of numerical calculations on a computer it is more efficient to

evaluate these integrals directly on the computer by any standard integration algorithm.

2.2.2.3.1.3 Case III

In this case

$$r_o \leq |a-b| = \underset{x}{\text{Min }} \rho(x), \tag{126}$$

so that G is given by Eq. (89a) with

$$x_o = \pi. \tag{127}$$

If we substitute this value of x_o in Eqs. (123)-(125) we arrive at

$$P_T = P, \tag{128}$$

$$g_o/P^{\frac{1}{2}} = \frac{1}{\pi(a+b)} \int_o^\pi \frac{dx}{\lceil 1-m \sin^2(x/2) \rceil^{\frac{1}{2}}} \tag{129}$$

and

$$g_1/2P^{\frac{1}{2}} = \frac{1}{\pi(a+b)} \int_o^\pi \frac{\cos x \, dx}{[1-m \sin^2(x/2)]} . \tag{130}$$

The integrals can now be expressed as complete elliptic integrals and it is worthwhile to do this because of the availability of excellent polynomial approximations for use on a computer. In both of the last two expressions we make the immediate substitution

$$x = 2\theta$$

to obtain

$$g_o/P^{\frac{1}{2}} = \frac{2}{\pi(a+b)} \int_o^{\pi/2} \frac{d\theta}{(1-m \sin^2\theta)^{\frac{1}{2}}},$$

and

51

$$g_1/2P^{\frac{1}{2}} = \frac{2}{\pi(a+b)} \int_0^{\pi/2} \frac{\cos(2\rho)d\rho}{(1-m \sin^2\rho)^{\frac{1}{2}}}$$

The first of these can be expressed immediately as a complete elliptic integral:

$$g_0/P^{\frac{1}{2}} = \frac{2}{\pi(a+b)} \; K(m). \tag{131}$$

In the second we make substitution

$$\cos(2\rho) = 1 - 2 \sin^2\rho$$

$$= (1-2/m) + (2/m - 2 \sin^2\rho)$$

$$= (1-2/m) + (2/m)(1-m \sin^2\theta)$$

to obtain

$$g_1/2P^{\frac{1}{2}} = \frac{2(1-2/m)}{\pi(a+b)} \int_0^{\pi/2} (1-m \sin^2\rho)^{-\frac{1}{2}} \; d\rho$$

$$+ \frac{4}{m\pi(a+b)} \int_0^{\pi/2} (1-m \sin^2\theta)^{\frac{1}{2}} \; d\rho.$$

This can be expressed as a combination of the two kinds of complete elliptic integrals:

$$g_1/2P^{\frac{1}{2}} = \frac{2}{\pi(a+b)} \; [(1-2/m) \; K(m) + (2/m) \; E(m)]. \tag{132}$$

2.2.2.4 Threshold Setting in Specific Applications, AGC

Before calculating any suppression curves it is necessary to establish some probable applications of soft-limiter characteristics.

52

2.2.2.4.1   Soft-Limiting Repeaters

An obvious use of a saturating amplifier characteristic is
in satellite or RPV repeater circuitry. The use of a partially-
linear amplifier can lessen the 6 dB signal suppression that
accompanies hard-limiting in the presence of strong jamming. In
order to gain any benefit from linear amplification, however,
the clipping level r_o must be set in accordance with the input
power level; equivalently there must be an automatic gain con-
trol (AGC) prior to the soft limiter.

Theoretically, the AGC voltage may be derived either from
peak power or from the average power or average envelope of the
received waveform. Use of a peak-following gain control makes
the threshold inordinately sensitive to pulsed jamming of low
average power, and should probably never be used. We can there-
fore assume some form of averaging. The optimum averaging
characteristic can generally be assumed to yield a threshold
setting of the general type:

$$r_o = f_2 \left[\frac{1}{T} \int_0^T f_1 [T(\tau)] d\tau \right], \tag{133}$$

where f_1 and f_2 are arbitrary nonlinear functions. A reasonable
requirement that scaling R by the factor A should scale r_o by
the same factor leads to the requirement on f_2 and f_1 that

$$f_2 \left[\frac{1}{T} \int_0^T f_1 [AR(\tau] d\tau \right] = A \ f_2 \left[\frac{1}{T} \int_0^T f_1 [R(\tau)] \ d\tau \right] \tag{134}$$

for any waveform $R(\tau)$. In particular this must hold for any
constant $R(\tau)$:

$$R(\tau) = x,$$

so that

$$f_2 \lceil f_1(Ax) \rceil = A \, f_2 \lceil f_1(x) \rceil \quad \text{for all } A, x. \tag{135}$$

If we let

$$h(x) = f_2[f_1(x)], \tag{136}$$

Eq. (135) can be rewritten as

$$h(Ax) = Ah(x) \tag{137}$$

which requires that

$$h(x) = \theta x \tag{138}$$

or

$$f_2 \lceil f_1(x) \rceil = \beta x = \beta \, f_1^{-1} \lceil f_1(x) \rceil$$

which, in turn means that

$$f_2(u) = \beta \, f_1^{-1}(u). \tag{139}$$

We can thus write Eq. (134) as

$$f^{-1} \lceil \frac{1}{T} \int_0^T f \lceil AR(\tau) \rceil \, d\tau \rceil = A \, f^{-1} \lceil \frac{1}{T} \int_0^T f \lceil R(\tau) \rceil d\tau \rceil. \tag{140a}$$

where

$$f \equiv f_1. \tag{140b}$$

Let us now substitute a two-valued R:

$$R(\tau) = \begin{cases} x, & 0 \leq \tau \leq \alpha T \\ y, & \alpha T < \tau \leq T \end{cases} \tag{141}$$

to obtain

$$f^{-1}[\alpha f(Ax) + (1-\alpha) f(Ay)] = A f^{-1}[\alpha f(x) + (1-\alpha) f(y)]. \tag{142}$$

54

Taking f of both sides of this equation we have

$$\alpha f(Ax) + (1-\alpha)\ f(Ay) = f\{Af^{-1}[\alpha f(x) + (1-\alpha, f(y)]\}$$

or, if we let

$$f[Af^{-1}(u)] = h(u),\qquad\qquad\qquad\qquad (143)$$

$$h[\alpha f(x) + (1-\alpha)f(y)] = \alpha f(Ax) + (1-\alpha)\ f(Ay).\qquad (144)$$

Differentiating both sides with respect to α gives

$$h'[\alpha f(x) + (1-\alpha)f(y)] = \frac{f(Ax) - f(Ay)}{f(x) - f(y)}$$

which is independent of α over $0 \le \alpha \le 1$ so that

$$h'(u) = \text{constant},\ f(x) \le u \le f(y).$$

Since x and y were arbitrary we have

$$h'(u) = \text{constant},\ \underset{x}{\text{Min}}\ f(x) \le u \le \underset{x}{\text{Max}}\ f(x).\qquad (145)$$

We now evaluate h'(u) in terms of f to arrive at

$$\frac{Af'\ [Af^{-1}(u)]}{f'[f^{-1}(u)]} = \text{constant}.$$

Taking logarithms of both sides of this equation we have

$$\log A + \log\left\{f'\left[Af^{-1}(u)\right]\right\} = \log(\text{constant}) + \log\left\{f'\left[f^{-1}(u)\right]\right\}$$

which, when differentiated again with respect to u yields

$$\frac{f''[Af^{-1}(u)]}{f'[Af^{-1}(u)]\ f'[f^{-1}(u)]} = \frac{f''[f^{-1}(u)]f^{-1}(u)}{f'[f^{-1}(u)]\ f'[f^{-1}(u)]}\ .\qquad (146)$$

55

If we write

$$\varphi(z) = \frac{zf''(z)}{f'(z)} \tag{147}$$

then Eq. (146) can be rewritten as

$$\varphi\lceil Af^{-1}(u)\rceil = \varphi[f^{-1}(u)], \underset{x}{\text{Min}}(f(x) \leq u \leq \underset{x}{\text{Max}} f(x), \text{ any } A.$$

We see immediately that as long as there is one nonzero value of $f^{-1}(u)$, then

$$\omega(z) = \text{constant}, \tag{148}$$

or

$$\frac{zf''(z)}{f'(z)} = C. \tag{149}$$

This last differential equation can be solved routinely. We let

$$v(z) = f'(z) \tag{150}$$

to obtain

$$\frac{v'(z)}{v(z)} = \frac{C}{z}$$

which can be integrated as

$$\log\lceil v(z)\rceil = c \log(z) + c_1$$

or

$$v(z) = c_2 z^c.$$

This in turn, upon substitution in Eq. (150) yields

$$p'(z) = c_2 z^c$$

or

$$f(z) = \frac{c_2}{1+c} z^{1+c} + c_3 \tag{151}$$

We thus have arrived at the most general form of Eq.(133), in which we now can write

$$f_1(r) = \alpha \, r^\nu + \gamma, \tag{152a}$$

$$f_2(u) = \beta f_1^{-1}(u) = \left(\frac{u-\gamma}{\alpha}\right)^{1/\nu}. \tag{152b}$$

If we substitute these in Eq.(133), we have

$$r_o = \beta \left\{ \frac{1}{\alpha} \left[-\gamma + \frac{1}{T} \int_0^T [\gamma + \alpha R^\nu(\tau)] dt \right] \right\}^{1/\nu} \tag{153}$$

or

$$r_o = \beta \left[\frac{1}{T} \int_0^T [R(\tau)]^\nu d\tau \right]^{1/\nu}.$$

The choice of an optimum value of ν must be based on a game-theoretic optimization to find the minimax solution for intermittent jamming of variable duty cycle and fixed peak power. It is necessary to defer this optimization for the present time and arbitrarily select the value $\nu = 2$ so that the threshold is set in terms of the rms input envelope.

2.2.2.4.2 Receiver Circuitry

A second application of soft limiting is in the processing circuitry in an AJ receiver for certain types of transmission. A possible modulation/detection configuration for FM transmissions is shown in Fig. 5. The function of the limiter in the receiver is to prevent the decoder correlations in the receiver from being swamped by an occasional hit by a jammer with large power.

In this configuration it is usually desirable to limit the inputs to the filter bank at a value slightly above the expected
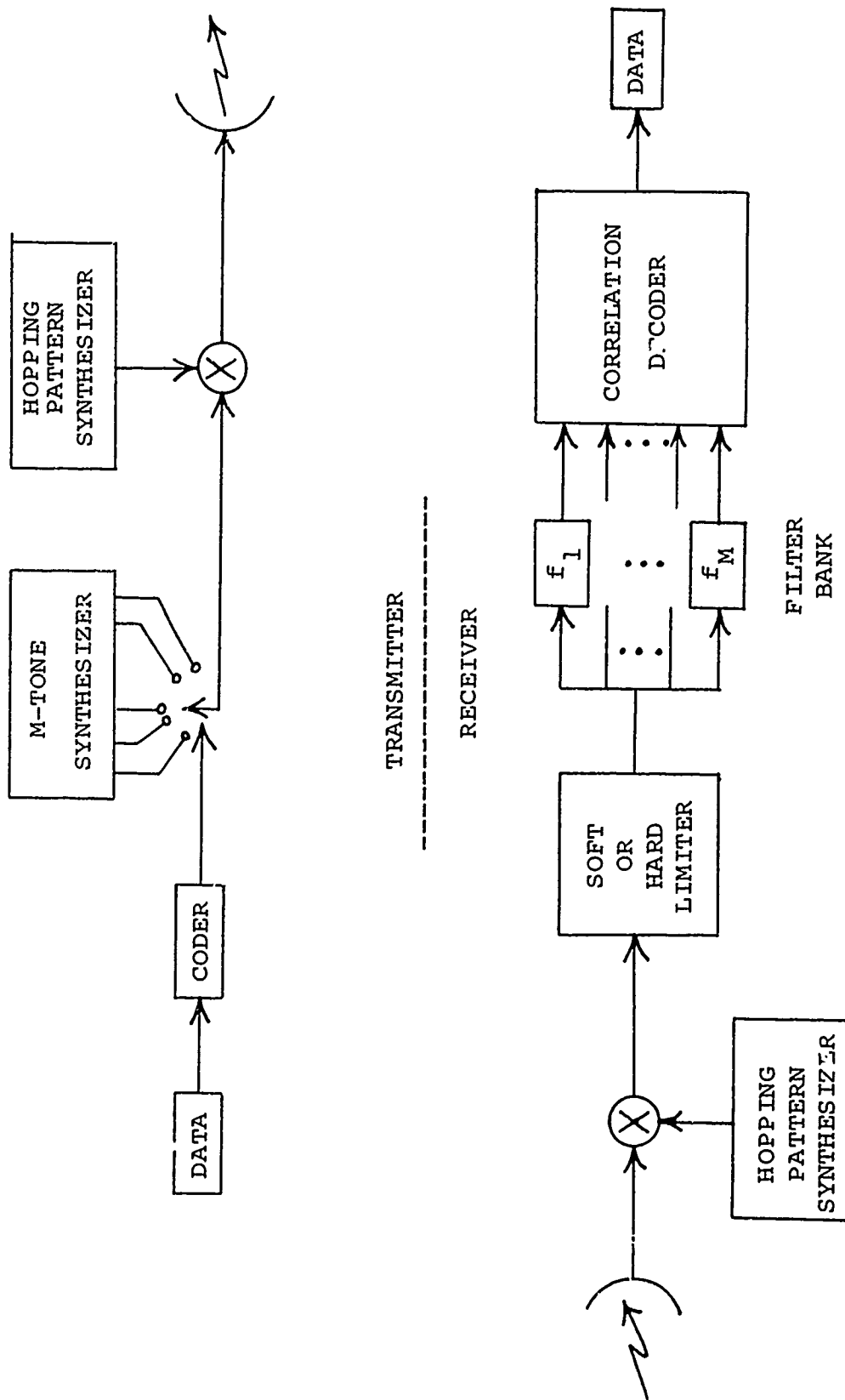
Figure 5. FH Transmission Block Diagram.

TRANSMITTER

RECEIVER

58

signal amplitude in order to achieve the maximum clipping of strong jammers with the minimum suppression of signal in the absence of jamming. On a line-of-sight transmission path it is usually possible to derive accurate estimate of the received power at the input to a soft limiter by adaptive measurements based on the outputs of the correlation decoder. Thus the clipping level r_o can be assumed to be set with reference to the signal amplitude a.

It should be noted that in this application we need to know both the signal and interference power at the limiter output relative to peak value. This is particularly true since an optimized jammer will attempt to spread his energy among a number of spectral regions that will yield on the order of magnitude of 0 dB J/S ratio at the limiter input when a hit occurs. Consequently we need to know not only the suppression of desired signal but also that of the total non-signal output. These are given in the already-defined notation as

$$\psi_{S/P} = P_S/P, \tag{154a}$$

$$\psi_{J/P} = (P_T - P_S)/P. \tag{154b}$$

2.2.2.5 Outline of Numerical Calculations

2.2.2.5.1 Cases and Parameters

The two cases we will analyze numerically are

    a)   the soft-limiting repeater

    b)   the receiver pre-clipper

In the soft-limiting repeater, it will be assumed that the clipping level is set with reference to the average input power

according to the relation

$$r_o^2 = B(a^2 + b^2).$$ (155)

The quantity of interest in this case is the additional suppression of signal below the value which would occur in an average-power-limited amplifier; this was given in Eq. (91) as

$$\psi_{S/N} = \frac{a^2 + b^2}{a^2} \frac{P_S}{P}.$$ (156)

In the case of the receiver pre-clipper we assume the clipping level to be set with reference to the average input _signal_ power according to the relation

$$r_o^2 = Ca^2.$$ (157)

The quantities of interest are the normalized jamming and signal suppressions

$$\psi_{S/P} = P_S/P,$$ (158a)

and

$$\psi_{J/P} = (P_T - P_S)/P.$$ (158b)

In Table 12 we summarize the system parameters to be used in the calculations.

2,2.2.5.2 Range of Parameters

The interesting effects that arise with soft limiters all result from the fluctuations of the envelope of signal and jamming. When either of these is 30 dB greater than the other the amplitude ripple of the resultant is only ± 3.2% corresponding to roughly a ± 1/3 dB variation of the instantaneous received power. Since it is unlikely that any important effects occur with ripple

60

TABLE 12. SYSTEM PARAMETERS

		SOFT-LIMITING REPEATER	RECEIVER PRE-CLIPPER
INPUT VARIABLES		jamming-to-signal ratio $$J/S = b^2/a^2$$	jamming-to-signal ratio $$J/S = b^2/a^2$$
		relative clipping level $$B = r_o^2/(a^2 + b^2)$$	relative clipping level $$C = r_o^2/a^2$$
OUTPUT VARIABLES		Absolute signal loss $$\psi_{S/P} = P_S/P$$	Signal suppression $$\psi_{S/P} = P_S/P$$
		relative signal suppression $$\psi_{S/N} = \frac{a^2 + b^2}{a^2} \; \frac{P_S}{P}$$	jamming suppression $$\psi_{J/P} = (P_T - P_S)/P$$

61

smaller than this it will suffice if we restrict calculations involving the jamming-to-signal ratio to the range

$$0.032 < b/a < 32. \tag{159}$$

We next observe that since the clipping level is normalized to either a or $\sqrt{a^2 + b^2}$, we can, in fact, set a equal to unity in all of the expressions:

$$a = 1, \tag{160}$$

so that b^2 becomes the input J/S ratio

$$J/S = b^2. \tag{161}$$

Similarly, since the output is normalized to P, we may take

$$P = 1 \tag{162}$$

in all of the expressions.

We next need to establish a useful range of clipping levels for the calculations. In the case of the soft-limiting repeater, a value of r_o equal to twice the rms envelope will lead to a 6 dB signal suppression in the absence of jamming; clearly, values of r_o larger than this need not be considered. There is no comparable natural choice for a lower end of the range of r_o values. We will therefore arbitrarily select -10 dB as the lower limit for the ratio of r_o to the rms envelope.

In the case of the FH receiver preclipper, the primary function of the preclipper is to prevent an occasional hit by a randomly hopped jammer from contributing more to the correlation outputs than the desired signal. Consequently r_o will never be set higher than the rms signal envelope and we can therefore restrict the upper end of the range of clipping levels to 0 dB. Again, there is no obvious choice for the lower end of the range

62

and we once more arbitrarily select -10 dB for the value to be used in calculations.

To summarize, the range of the clipping parameters B or C will be restricted to

$$-10 \text{ dB} \leq B \leq 6 \text{ dB}, \qquad (163a)$$

soft limiting repeater,

$$-10 \text{ dB} \leq C \leq 0 \text{ dB} \qquad (163b)$$

receiver preclipper.

2.2.2.5.3 Summary of Formulas

It is helpful to write the jamming-to-signal ratio as

$$\beta^2 = J/S, \qquad (164)$$

or, since we are taking

$$a = 1$$

in all of the expressions, we must have

$$b = \beta.$$

The range of values of β is $-30 \text{ dB} \leq \beta \leq 30 \text{ dB}$. The remaining parameter of the problem is then

$$r_o = \frac{\text{clipping level}}{\text{rms signal envelope}} \qquad (165)$$

which is determined by either the parameter C or the parameter B through the relations

$$B = \left(\frac{\text{clipping level}}{\text{rms input envelope}}\right)^2 = \frac{r_o^2}{1+\beta^2} \qquad (166a)$$

$$C = \left(\frac{\text{clipping level}}{\text{rms signal envelope}}\right)^2 = r_o^2. \qquad (166b)$$

63

These have ranges

$$-10 \text{ dB} \leq B \leq 6 \text{ dB},$$

$$-10 \text{ dB} \leq C \leq 0 \text{ dB}.$$

We define

$$R_{max} = 1 + \beta, \tag{167a}$$

$$R_{min} = 1 - \beta, \tag{167b}$$

and define three cases by

$$r_o \geq R_{max}, \text{ Case 1}, \tag{168a}$$

$$R_{min} < r < R_{max}, \text{ Case 2}, \tag{168b}$$

$$r_o \leq R_{min}, \text{ Case 3}. \tag{168c}$$

The suppression factors are

$$\psi_{S/N} = (1 + \beta^2) \, P_S \tag{169a}$$

$$\psi_{J/P} = P_T - P_S \tag{169b}$$

$$\psi_{S/P} = P_S. \tag{169c}$$

These in turn are given by

Case 1

$$P_S = 1/r_o^2, \tag{170a}$$

$$P_T = (1 + \beta^2) \, P_S; \tag{170b}$$

Case 2

$$P_T = \frac{\tau}{\pi} + \frac{(1 + \beta^2)(\pi - \tau) - 2\beta \sin\tau}{\pi r_o^2} \quad , \tag{171a}$$

$$P_S = \left[\frac{\pi - \tau - \beta \, \sin\tau}{\pi r_o} + \frac{1}{\pi} \int_o^{\tau} \frac{1 + \beta \, \cos\theta}{\sqrt{1 + \beta^2 + 2\beta\cos\theta}} \, d\theta \right]^2 \qquad (171b)$$

where, in both expressions

$$\tau = \text{arc cos} \left(\frac{r_o^2 - \beta^2 - 1}{2\beta} \right); \qquad (171c)$$

Case 3

$$P_T = 1, \qquad (172a)$$

$$P_S = \left(F_o + \beta F_1 \right)^2 \qquad (172b)$$

with

$$F_o = \frac{2}{(1+\beta)\pi} \, K(m), \qquad (172c)$$

$$F_1 = \frac{2}{(1+\beta)\pi} \left[(1-2/m) \, K(m) + (2/m) \, E(m) \right] \qquad (172d)$$

with K and E the complete elliptic integrals and

$$m = \frac{4\beta}{(1+\beta)^2} . \qquad (172e)$$

The formulas used for numerical calculation of the elliptic integrals are those given in Eqs. (17.2.18), (17.3.33), and (17.3.35) of Abramowitz and Stegun [1].

2.2.2.6 Special Cases and Asymptotic Values

It is useful to supplement the range of the calculated data by asymptotic expressions valid for large and small J/S ratio, and also to include closed-form calculations for J = S.

65

2.2.2.6.1 Equal Jamming and Signal Power

For the case of equal jamming and signal powers, we have

$$a = b = 1 \tag{173}$$

so that Eq.(92) becomes

$$\rho(x)[2 + 2\cos x]^{\frac{1}{2}} = 2|\cos x/2|. \tag{174}$$

If we define

$$g = a\, g_0 + \tfrac{1}{2} b\, g_1 = g_0 + \tfrac{1}{2} g_1 \tag{175a}$$

then

$$P_S = g^2, \tag{175b}$$

and g is given by

$$g = \frac{1}{2\pi} \int_{-\pi}^{\pi} (1 + \cos x)\, G[\rho(x)], \tag{176}$$

while P_T is, as before

$$P_T = \frac{1}{2\pi} \int_{-\pi}^{\pi} \{\rho(x)\, G[\rho(x)]\}^2\, dx. \tag{177}$$

Note that we can drop the magnitude signs in Eq.(174) for the range of values of x in the integral. We now substitute

$$G(r) = \begin{cases} 1/r_0, & 0 \le r \le r_0 \\ 1/r, & r \ge r_0 \end{cases} \tag{178}$$

to obtain

$$G[\rho(x)] = \frac{1}{2\cos(x/2)}, \quad 0 \le |x| \le 2\, \text{arc}\cos(r_0/2) \tag{179a}$$

$$G[\rho(x)] = 1/r_0, \quad 2\, \text{arc}\cos(r_0/2) \le |x| \le \pi, \tag{179b}$$

66

where we interpret the arc cosine as

$$\text{arc } \cos(r_o/2) = 0, \text{ if } r_o \geq 2$$

for arguments outside the usual range of definition.

We can now substitute this value for G in Eqs. (176) and (177). Both integrals are symmetric about $x = 0$ so that we need only include half of the range; furthermore, the expressions simplify by changing the variable of integration to

$$y = x/2.$$

We then obtain

$$P_T = \frac{2}{\pi} \int_0^{\pi/2} \{\rho(2y) \; G[\rho(2y)]\}^2 \, dy, \tag{180a}$$

$$g = \frac{4}{\pi} \int_0^{\pi/2} \cos^2 y \; G[\rho(2y)] \, dy, \tag{180b}$$

or, with

$$Y_o = \text{arc } \cos(r_o/2) \tag{181}$$

$$P_T = \frac{2}{\pi} \int_0^{Y_o} dy + \frac{2}{\pi} \int_{Y_o}^{\pi/2} \frac{\cos^2(y)}{\cos^2(y_o)} \, dy, \; r_o \leq 2 \tag{182a}$$

and

$$g = \frac{2}{\pi} \int_0^{Y_o} \cos(y) \, dy + \frac{2}{\pi} \int_{Y_o}^{\pi/2} \frac{\cos^2(y)}{\cos(y_o)} \, dy, \; r_o \leq 2. \tag{182b}$$

These can be evaluated immediately as

$$P_T = \frac{2}{\pi} \left[y_o + \frac{\frac{1}{2}(\pi/2 - y_o) - \frac{1}{4}\sin(2y_o)}{\cos^2(y_o)} \right] , \quad r_o \leq 2 \qquad (183a)$$

$$g = \frac{2}{\pi} \left[\sin(y_o) + \frac{\frac{1}{2}(\pi/2 - y_o) - \frac{1}{4}\sin(2y_o)}{\cos(y_o)} \right] , r_o \leq 2. \tag*{(183b)}$$

For $r_o > 2$, the input waveform is always in the linear region so that

$$\psi_{S/N} = 2/r_o^{\,2} = 1/B, \quad B \geq 2 \tag{184}$$

and

$$\psi_{S/P} = \psi_{J/P} = 1/r_o^{\,2} = 1/C, \quad C \geq 4 \tag{185}$$

Tables 13 and 14 give the suppression factors for this special case of S = J.

TABLE 13.   SUPPRESSION FACTOR FOR S/J = 0 DB
            SOFT-LIMITING REPEATER

Clip Level dB	$\psi_{S/N}$ dB
-10	-0.99
- 9	-1.00
- 8	-1.03
- 7	-1.06
- 6	-1.10
- 5	-1.15
- 4	-1.21
- 3	-1.30
- 2	-1.41
- 1	-1.55
0	-1.74
1	-2.00
2	-2.38
3	-3.00
4	-4.00
5	-5.00
6	-6.00

TABLE 14.   SUPPRESSION FACTOR FOR S/J = 0 DB
RECEIVER PRECLIPPER

Clip Level dB	$\Downarrow$ S/P dB	$\Downarrow$ J/P dB
-10	-3.96	-2.75
- 9	-3.97	-2.81
- 8	-3.98	-2.88
- 7	-4.00	-2.96
- 6	-4.01	-3.04
- 5	-4.04	-3.14
- 4	-4.07	-3.25
- 3	-4.11	-3.38
- 2	-4.16	-3.52
- 1	-4.22	-3.68
0	-4.31	-3.86

2.2.2.6.2   Asymptotic Values for Small J/S

For small values of J/S we can rewrite Eq.(62), for a = 1, as

$$\rho(x) \approx 1 + b \cos x + \tfrac{1}{2} b^2 - \tfrac{1}{2} b^2 \cos^2 x + O(b^3). \qquad (186)$$

If the clipping ratio B or C is larger than unity we then have the linear amplification case, and if B or C is smaller than unity we have the hard limiting case. In the former situation, the signal output is

$$\text{As } b \to 0 \begin{cases} P_S \to 1/r_o{}^2 = 1/B \text{ or } 1/C \\ P_J \to b^2/r_o{}^2 = J/BS \text{ or } J/CS \end{cases} \text{if } B > 1 \text{ or } C > 1. $$

$$(187)$$

If the reverse inequality holds, we have

$$G[\rho(x)] \sim 1/\rho(x), \quad r_o < 1, \qquad (188)$$

so that

$$P_T = 1, \tag{189}$$

and

$$g_o + \tfrac{1}{2} bg_1 \approx \frac{1}{2\pi} \int_{-\pi}^{\pi} \frac{1 + kcos\ (x)}{1 + bcos(x) + \tfrac{1}{2} b^2 sin^2 x + O(b^3)}\ dx. \tag{190}$$

The small-b approximation permits this integral to be written as

$$g_o + \tfrac{1}{2} bg_1 \approx \frac{1}{\pi} \int_{o}^{\pi} (1 + bcosx)[1 - bcosx + b^2cos^2x - \tfrac{1}{2} b^2sin^2x + O(b^3)]dx$$

which can be evaluated immediately as

$$g_o + \tfrac{1}{2} bg_1 \approx 1 - \tfrac{1}{4} b^2, \tag{191}$$

so that

$$P_S \approx 1 - \tfrac{1}{2} b^2 = 1 - \tfrac{1}{2} J/S, \qquad B \leq 1\ or\ C < 1 \tag{192a}$$

$$P_J \approx \tfrac{1}{2} J/S . \tag{192b}$$

(It should be pointed out that only half of the power represented by P_J appears at the original jamming frequency.)

The remaining possibility to be considered is that B or C is unity. In these two cases we have

$$r_o = \begin{cases} (1 + b^2)^{\frac{1}{2}} & if\ B = 1 \\ 1 & if\ C = 1 \end{cases} . \tag{193}$$

The first of these expressions can be approximated as

$$r_o \approx 1 + \tfrac{1}{2} b^2 + O(b^4)\ if\ B = 1. \tag{194}$$

From Eq. (186) we see that for either of the cases, clipping occurs for almost exactly half of each jamming cycle. It introduces no significant error to take this to be true with equality and

therefore obtain

$$P_T \approx \frac{1}{\pi} \int_0^{\pi/2} dx + \frac{1}{\pi} \int_{\pi/2}^{\pi} dx \frac{(1 + 3b \cos x + b^2)}{1 + b^2} \qquad (195)$$

$$g_0 + \tfrac{1}{2} bg_1 \approx \frac{1}{\pi} \int_0^{\pi/2} \frac{1 + b \cos x}{1 + b\cos x + \tfrac{1}{2} b^2 \sin^2 x + O(b^3)} dx$$

$$+ \frac{1}{\pi} \int_{\pi/2}^{\pi} \frac{(1 + b \cos x)}{1 + \tfrac{1}{2} b^2} dx. \qquad (196)$$

These integrals can be evaluated (using the usual small b approximations where necessary to obtain

$$P_T \approx 1 - (2/\pi) b + O(b^3) \qquad (197)$$

$$g_0 + \tfrac{1}{2} bg_1 \approx 1 - (1/\pi) b - (3/8)b^2, \qquad (198)$$

$$P_S \approx 1 - (2/\pi) b + (1/\pi^2 - 3/4) b^2, \qquad (199)$$

$$P_J \approx (3/4 - 1/\pi^2)b^2. \qquad (200)$$

We thus arrive at the final formulas for suppression ratios in the small J/S case:

$$\rho_{S/P} \rightarrow \rho_{S/N} \rightarrow \left\{ \begin{array}{ll} 1 & , \ B \leq 1 \text{ or } C \leq 1 \\ 1/B \text{ or } 1/C; & B > 1 \text{ or } C > 1 \end{array} \right\} \text{as } J/S \rightarrow 0;$$

$$(201)$$

$$\rho_{J/P} \sim \left\{ \begin{array}{ll} \tfrac{1}{2} J/S & , \ B < 1 \text{ or } C < 1 \\ (3/4 - 1/\pi^2)J/S & , \ B = 1 \text{ or } C = 1 \\ J/BS \text{ or } J/CS & , \ B > 1, \ C > 1 \end{array} \right\} \text{as } J/S \rightarrow 0.$$

$$(202)$$

71

2.2.2.6.3 Asymptotic Values for Large J/S

For large J/S, Eq. (92) becomes, for a = 1,

$$\rho(x) = b\left[1 + b^{-1}\cos x + \tfrac{1}{2} b^2 \sin^2 x + O(b^{-3})\right]. \qquad (203)$$

For any fixed value of C, the receiver preclipper is always ultimately in the hard-limiting situation as $b \to \infty$. We therefore have

$$P_T = 1, \text{ sufficiently large b, any C,} \qquad (204)$$

and

$$g_o + \tfrac{1}{2} g_1 \approx \frac{1}{\pi} \int_o^\pi \frac{1 + b \cos x}{b[1 + b^{-1}\cos x + \tfrac{1}{2} b^{-2}\sin^2 x]} \, dx. \qquad (205)$$

This latter integral simplifies to

$$g_o + \tfrac{1}{2} g_1 \approx \frac{1}{\pi} \int_o^\pi \left[\cos x + b^1\right]\left[1 - b^{-1}\cos x - \tfrac{1}{2}b^{-2}\sin^2 x + b^{-2}\cos^2 x\right] dx$$

which can be evaluated as

$$g_o + \tfrac{1}{2} g_1 \approx \tfrac{1}{2} b^{-1} + O(b^{-3}), \qquad (206)$$

which yields

$$P_S \sim \tfrac{1}{4} b^{-2} = \tfrac{1}{4} S/J, \quad \text{as } J/S \to \infty, \text{ any C} \qquad (207)$$

and

$$P_J \to 1. \qquad \text{as } J/S \to \infty, \text{ any C.} \qquad (208)$$

In this case of the soft-limiting repeater, the exact same result holds for all $B < 1$. We thus have

$$P_T \to 1$$

$$P_S \sim \tfrac{1}{4} \, S/J \Bigg\} \quad \text{as } J/S \to \infty, \text{ if } B < 1. \qquad (209)$$

$$P_S \to 1$$

If

$$B > 1$$

then for sufficiently large values of B the soft-limiting repeater looks like a linear amplifier with power gain

$$\frac{1}{B(J+S)}$$

so that

$$P_T = 1/B$$

$$P_S = \frac{S}{B(S+J)} \Bigg\} \quad \text{for sufficiently large } J/S, \ B > 1.$$

$$\psi_{S/N} = 1/B \qquad\qquad\qquad\qquad\qquad (210)$$

Again, we encounter a special case when

$$B = 1.$$

This leads to the threshold

$$r_o = (1 + b^2)^{\tfrac{1}{2}} \approx b + \tfrac{1}{2} b^{-1} + O(b^{-3}), \ B = 1. \qquad (211)$$

Since, from Eq. (173),

$$\rho(x) = b + \cos x + \tfrac{1}{2} b^{-1} \sin^2 x + O(b^{-2}), \qquad (212)$$

it is again an excellent approximation to assume that limiting occurs for exactly half of each jamming cycle. We then have

$$P_T = \frac{1}{\pi} \int_0^{\pi/2} dx + \frac{1}{\pi} \int_{\pi/2}^{\pi} \frac{[1 + 2b^{-1} \cos x + b^{-2}]}{1 + b^{-2}} \, dx,$$

$$g_0 + \tfrac{1}{2} g_1 = \frac{1}{\pi} \int_0^{\pi/2} \frac{1 + b \cos x}{b + \cos x + \tfrac{1}{2} b^{-1}} + \frac{1}{\pi} \int_0^{\pi/2} \frac{1 + b \cos x}{b + \tfrac{1}{2} b^{-1}} \, dx.$$

Using approximations for large b where necessary, these can be evaluated as

$$P_T = 1 - 2/(\pi b) + O(b^{-3}), \tag{213}$$

$$g_0 + \tfrac{1}{2} g_1 = \frac{3}{4b} - \frac{11}{6\pi b^2} + O(b^{-3}), \tag{214}$$

from which we find

$$\left. \begin{aligned} P_S &= (9/16) b^{-2} + O(b^{-3}) \\[1em] \psi_{S/N} &\to (9/16) \end{aligned} \right\} \quad J/S \to \infty, \; B = 1. \tag{215}$$

It is helpful to summarize here the asymptotic formulas for large J/S:

$$\left. \begin{aligned} \psi_{S/P} &\sim \tfrac{1}{4} \, S/J \\[1em] \psi_{J/P} &\to 1 \end{aligned} \right\} \quad \text{as } J/S \to \infty, \text{ for any C.} \tag{216}$$

$$\psi_{S/N} \to \begin{cases} 1/4, & B < 1 \\ 9/16, & B = 1 \\ 1/B, & B > 1 \end{cases} \quad \text{as } J/S \to \infty. \tag{217}$$

2.3 Doppler and Differential Doppler Simulation

2.3.1 Introduction

In this section we discuss the processing of Doppler and differential Doppler by the K-band modem, and its effects on the CSEL simulation. The reference which is used to describe the Doppler processing is TRW's Second Interim Technical Report [2].

The basic problem is as follows. The K_a band uplink from the ABNCP to the satellite utilizes wideband frequency hopping, at a center frequency of 38.0924 GHz for LES-9, and 36.7876 GHz for LES-8. Assuming a nominal 38 GHz frequency for numerical purposes, the Doppler shift on the nominal uplink signal is

$$f_d = \frac{v}{c} 38 \times 10^9, \tag{218}$$

where v is the radial velocity between the ABNCP and the satellite. If we denote the frequency-hop bandwidth by B Hz, then the maximum and minimum Doppler shifts on the transmitted signal are

$$f_{d_{max}} = \frac{v}{c} (38 \times 10^9 + \frac{B}{2}) \tag{219}$$

$$f_{d_{min}} = \frac{v}{c} (38 \times 10^9 - \frac{B}{2}), \tag{220}$$

and the differential Doppler shift between the top and bottom
of the transmitted spectrum is

$$f_{diff} = \frac{v}{c} B,$$ (221)

independent of the carrier frequency. Assuming v to be equal to
1000 fps, $v/c \cong 10^{-6}$, and

$$f_d = 38 \text{ kHz}.$$ (222)

As the maximum frequency error allowed in the signal received by
the satellite is 20 Hz, the transmitted symbols have to be frequency
corrected to remove the effects of differential Doppler. " In the
modem, frequency control is effected by adding or subtracting cor-
rections to the frequency command words supplied to the frequency
synthesizer. The frequency corrections include frequency hopping
differential Doppler compensation .... are performed in software
by the 1602 Rugged Nova" [Ref. 2, p. 2-7].

We thus have the situation wherein the transmitted signal is
pre-corrected for Doppler, so that there is effectively no Doppler
on the signal received by the satellite. However, in the simula-
tion, since there is no path length change there is no Doppler
shift, and pre-correction will actually cause a significant fre-
quency error in the imulated signal received by the satellite.
We must therefore determine a meaningful frequency shift to be
put on the modem which will simulate the combined effects of the
pre-correction for Doppler and the Doppler shift in a real trans-
mission.

2.3.2 Doppler Processing in the Modem

The Doppler measurement is performed on a down-link signal which has been mixed to a 20 MHz intermediate frequency. A description of the processing, as taken from [Ref. 2, p. 3-107] is as follows.

"A detailed block diagram of the Doppler frequency counter is illustrated in Fig. 1. [Note: Our Fig. 6]. The bit synchronizer (2-bit flip-flop counter) synchronizes the 200 ms gate (up clock) with the 20 MHz reference signal from the K-band terminal.

When the bit synchronizer is activated, the 22-bit binary counter is reset and enabled to count. A count of 3,970,000 is decoded, disables the 22-bit binary, and enables the modulo 30,000 up/down counter. The following activation of the bit synchronizer causes the count in the up/down counter to be parallel transferred to the holding register for output to the CPU on each 5 ms tick of the up-link clock. The output count of the up/down counter represents the Doppler frequency shift. The LSB of this counter represents 5 Hz and the MSB represents 40,960 Hz (5×2^{14} bits). The 16th bit of the count is a sign bit. The Doppler frequency count is accurate to ± 5 Hz."

The mathematical representation of this processing is straightforward. Let the 20 MHz reference actually be at $20 \times 10^6 + f_d$ Hz, where f_d is the Doppler shift. It will take T seconds to reach a count of 3,970,000, given by

$$(20 \times 10^6 + f_d)T = 3.97 \times 10^6. \tag{223}$$
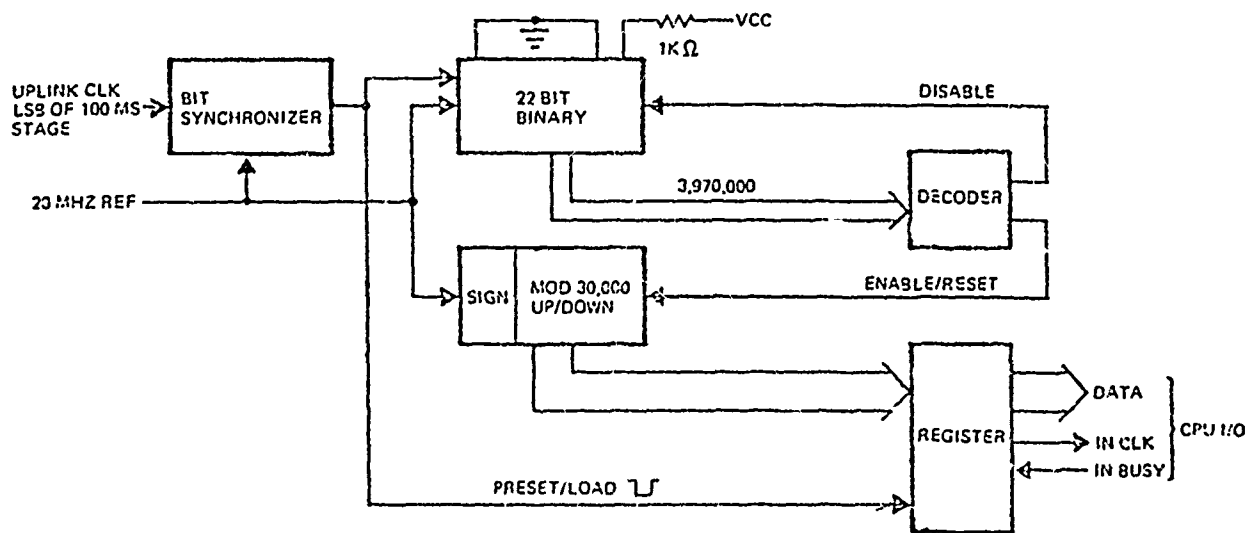
Figure 6. Doppler Frequency Measurement.
[From Ref. 2]

Therefore, in the remaining $0.2 - T$ seconds, a count of

$$(0.2 - T)(20 \times 10^6 + f_d) = 30 + 10^3 + 0.2 f_d \qquad (224)$$

will accumulate, which, when taken Mod 30,000, is equal to $0.2 f_d$.
Thus the resolution of this technique is 5 Hz.

Once the Doppler shift is measured, the software computes
an estimate to v/c, denoted by $\hat{\beta}$, using the basic relation:

$$\hat{\beta} = \hat{f}_d / f_{received} \qquad (225)$$

where $f_{received}$ is the receiver tuning frequency from which the
20 MHz IF signal was converted, and $\hat{f}_d$ is the estimated value of
f_d resulting from the instrumentation of Fig. 1. Then, if f_u is
the minimum uplink frequency, and f_h is the hopping frequency,
relative to the minimum uplink frequency, the software computes

$$\hat{\beta}(f_u + f_h) \qquad (226)$$

the total Doppler frequency shift of the transmitted signal.

The frequency synthesizer used by the modem to provide the
hopped carrier is a GR 1061. The output of the synthesizer is
multiplied by 16 in the modulator, so that the nominal carrier
frequency becomes 700 MHz; the synthesizer output ranges from
40 MHz to 50 MHz in order to accommodate the hopping. The soft-
ware commands the synthesizer to the frequency

$$40.55 \times 10^6 + R\{[f_h - \hat{\beta}(f_u + f_h)]/16\}, \qquad 227)$$

where $R\{\ \}$ indicates the rounding off of the frequency command
to the nearest 0.1 Hz, based on the value of the 0.01 Hz digit.
The synthesizer is actually commanded from the computer by a

32 bit BCD word in 0.1 Hz increments, resulting in a 1.6 Hz resolution in the transmitted frequency.

After multiplying by 16 and translating to K_a band, the frequency of the transmitted signal is

$$f_u + 16 \cdot R \{[f_h - \hat{\beta}(f_u + f_h)]/16\}, \tag{228}$$

and the frequency received by the satellite is

$$(1 + \beta)\left[f_u + 16 \cdot R\{[f_h - \hat{\beta}(f_u + f_h)]/16\}\right]. \tag{229}$$

If roundoff could be neglected, Eq. (12) would be

$$(1 + \beta)[f_u + f_h - \hat{\beta}(f_u + f_h)] = (f_u + f_h)(1 + \beta - \hat{\beta} - \beta\hat{\beta})$$

$$\cong (f_u + f_h)(1 + \beta - \hat{\beta}). \tag{230}$$

Equation (230) shows that in the absence of roundoff, and if $\hat{\beta} - \hat{\beta}$, the differential Doppler compensation is as desired. We next consider the simulation of Doppler compensation.

2.3.3 Doppler Compensation Simulation

Equation (228) shows that Doppler compensation is dependent on two factors, namely the ratio of estimated range rate to the speed of light, $\hat{\beta}$, and the effects of roundoff. A valid simulation of Doppler compensation would put, on each transmitted symbol, a Doppler compensation error given by

$$\text{Dopper Compensation Error} = f_u + f_h - \text{Eq. (229)}. \tag{231}$$

Thi⌐ is implemented by the following 3-step process.

Step 1. $\underline{\text{Estimation of } \hat{\beta}}$

    1. Select $f_{received}$, the RF frequency used for Doppler estimation.

    2. Select β, the normalized range rate.

    3. Form 20 MHz $+ \beta f_{received}$. This can be implemented by controlling a frequency synthesizer either manually or through CSEL.

    4. Implement, either in hardware or accurate software, the Doppler measurement loop of Fig. 6. Estimate $\hat{f}_d$.

    5. Compute $\hat{\beta} = \hat{f}_d / f_{received}$.

Step 2. $\underline{\text{Estimation of Doppler Compensation Error}}$

    1. Using $\hat{\beta}$ from Step 1, program CSEL to evaluate Eq. (229) for each transmitted symbol. The roundoff should be included.

    2. Compute the Doppler compensation error for each transmitted symbol given by Eq.(231).

Step 3. $\underline{\text{Inclusion of Doppler Compensation Error}}$

    1. Add to the frequency of each transmitted symbol the frequency error of Step 2.

2.4 Repeater Jamming

Jammer strategies for the TRW Spread Spectrum Modem-Processor
(SSMP) have been describe and evaluated in other studies. Here
we consider a jammer technique known as repeater jamming. We
describe what is meant by repeater jamming and how the jamming
signal may be generated. We determine the appropriate signal
decision statistic taking into account the effects of matched
filtering, limiting, random frequency and random phase. We
evaluate the probability of decision error for the particular
jamming signal. An analysis is also included which describes
the effect of partial chip jamming when the jamming time is com-
pletely known and when it is unknown. Several strategies are
discussed for the case of unknown jamming time. The analyses
demonstrate that repeater jamming is in general more efficient
than random noise.

2.4.1 Introduction

This section considers the effects of repeater jamming.
It is well known that the most successful jamming occurs when
the jamming signal is of the same format as the desired data
signal. We therefore consider the case where the repeater
jammer consists of a set of equal strength tones with spacing,
f_o, equal to the data frequency spacing and with some total
width large enough to cover all possible Doppler shifts.

It is recognized that such a jamming signal has a non-constant
amplitude which may be undesirable from the point of view of jam-
mer final power amplifier; but more important, from the point of

82

view of performance analysis, limiter signal suppression will not
be optimum. It will be shown that the desired signal can be pro-
duced by using a periodic linear FM signal which has a constant
amplitude.

The repeater jammer operates in the following fashion. The
desired signal comes on the air on some frequency-hopped center
frequency. The signal appears in one of M frequency cells within
this frequency-hopped band. The band is actually $q + M$ fre-
quency cells wide where q is a non-negative integer. The re-
peater jammer estimates the frequency-hopped band and begins
transmission of jamming tones. If signal transmission began at
time $t = 0$ then the jammer power appears in the receiver at
time $t = t_j$. This time delay is due to the frequency estimation
procedure as well as to the path delay between the desired signal
transmitter and jammer and between the jammer and receiver.

The jammer bandwidth must cover the full range of Doppler
shift in order to guarantee jammer/signal coincidence with
probability one. If the maximum Doppler shift is $B/2$ Hz then
the jammer bandwidth is B Hz. The desired signal has duration
T seconds and the tone spacing is then taken as $f_o = 1/T$ Hz. The
jammer tone spacing is also f_o Hz.

If the jammer has bandwidth less than B Hz then the probability
of landing in the limiter bandwidth is less than one. For
example, if the jammer bandwidth is $W_J = B/4$ and if the jammer
continually steps his signal over the total bandwidth B, then on
the average the jammer appears in the limiter with a 0.25 proba-
bility. The jammer is less effective, but may choose to

1) Concentrate more power in the smaller bandwidth
2) Transmit less power overall.

83

An optimum jammer bandwidth and power versus decision error pro-
bability exists. In this section, we address the full bandwidth
jammer problem.

Two random occurrences must be considered in the analysis.
First, due to the unknown Doppler shift the jammer will appear on
a random frequency within each frequency cell. Second, there will be
a random phase associated with the jammer with respect to the de-
sired signal. In the absence of additive noise, an error will
never occur when the jammer tone amplitude is less than half of
the signal amplitude.

A decision as to which one of the M tones was transmitted
must be made. The composite signal is limited, and the limiter
output is matched filtered. The matched filter outputs from
N consecutive chips are added together to form the decision statis-
tic. The analysis below must therefore also consider any suppres-
sion effects due to limiting. The frequency cell having the largest
summed output is chosen as the transmitted frequency.

2.4.2 Effects of Random Frequency

Figure 7 displays a typical frequency cell of width f_o and
center frequency f_c Hz.

$$
\begin{array}{ccc}
\bullet & & \bullet \\
\bullet & & \bullet \\
\bullet & & \bullet \\
\bullet & & \bullet \\
\bullet & \bullet & \bullet
\end{array}
$$

$$f_c - f_o/2 \qquad f_c \qquad f_c + f_o/2$$
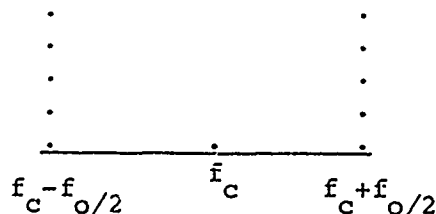
Figure 7. Typical Frequency Cell

A jammer may arrive within the cell at any random frequency $f_c + \delta$ where $|\delta| \le f_o/2$. We determine the degradation due to the Doppler shift ambiguity δ.

We assume that the jammer signal has the form

$$v_J = J\, e^{j2\pi(f_c+\delta)t} \qquad\qquad t_J \le t \le T. \tag{232}$$

Then the matched filter output, m_J is equal to

$$m_J = \frac{1}{T} \int_{t_J}^{T} v_J e^{-j2\pi f_c t}\, dt$$

$$= J\, \frac{(T-t_J)}{T}\, e^{j\pi\delta(T+t_J)}\, \text{sinc } \pi\delta(T-t_J), \tag{233}$$

where sinc x is defined as

$$\text{sinc } x = \frac{\sin x}{x} \tag{234}$$

and

$$T = 1/f_o. \tag{235}$$

Let us assume that $t_J = 0$. The most degradation occurs when $\delta = \pm f_o/2$. Then $|m_J| = 2J/\pi$ and there is a 4 dB loss over the case when $\delta = 0$ (i.e., no frequency ambiguity).

We therefore can do the jammer analysis by at first ignoring the random frequency occurrence and then modifying the jammer power by the appropriate degradation factor.

2.4.3 Generation of Jammer Signal

We assume at the outset that the jammer knows his delay time t_J exactly. In Section 2.4.5 we assume that t_J is completely unknown. We are interested in generating a jammer signal which has a uniform power spectrum made up of equispaced lines with the total bandwidth B and a constant envelope. Since B is large in our case, we can accomplish this by using periodic linear FM.

We have several choices of signal generation. In all but Case 3 the jammer will be on the air $(T-t_J)$ seconds. The linear FM signal may repeat every

1) T/R seconds, where T is the chip duration and R is the number of repeats per chip interval. This guarantees a sweep over B Hz for all repeats, except in general the last repeat, when the instantaneous frequency is B Hz.

2) T seconds and have an instantaneous frequency of $B(t-t_J)/(T-t_J)$ Hz. Then B Hz will be swept once every T Hz.

3) T seconds and have an instantaneous frequency of B Hz. During the hopped frequency estimation interval $0 \leq t < t_J$ the FM signal would begin to sweep according to the previously estimated frequency; then at time t_J it would switch to the new frequency.

Figure 8 displays the frequency sweep for Cases 1 through 3.

a) Case 1   R = 4

b) Case 2

c) Case 3
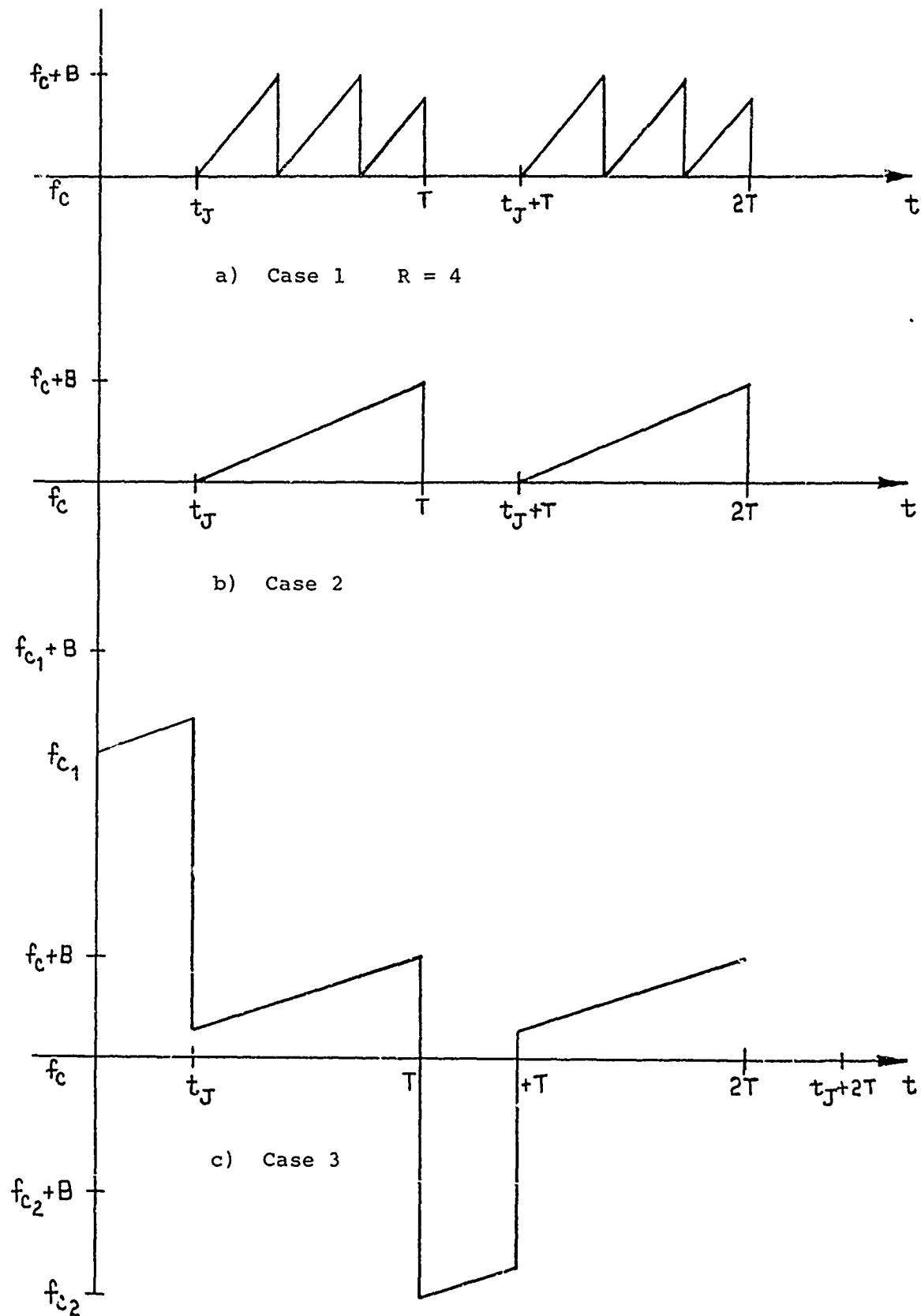
Figure 8   Several Methods of Jammer Generation
(f_c = dehopped frequency)

87

Since the jammer signal is periodic, the signal spectrum will be a line spectrum which is most desirable for jamming an FSK signal. In case 1 lines will be spaced every $R/T = Rf_o$ Hz. Therefore, only 1 out of every R possible frequency bins can be jammed. This is not an effective jamming procedure. Both cases 2 and 3 have spectra with lines spaced every f_o Hz, which is what we desire. In case 3, there is no clear advantage of keeping the jammer on during the t_J second interval since it is most likely that the new hopped frequency is far removed from the previous frequency. There is a B/F chance of jamming where B is the jammer bandwidth and F is the total hopped bandwidth.

The jamming signal will therefore be

$$v_{J'} = J' \exp\left[j2\pi\left\{ \left(f_c + \delta\right)\left(t - t_J\right) + B\left(t - t_J\right)^2 / 2\left(T - t_J\right)\right\}\right]; \quad t_J \le t \le T.$$

(236)

The jammer matched filter output is found to be equal to

$$m_{J'} = \frac{J'}{T} \sqrt{\frac{\pi}{2K}} \, e^{-j\frac{4\pi^2 \delta^2}{K}} \left[F\left\{\sqrt{\frac{2K}{\pi}}\, T + \sqrt{\frac{2\pi}{K}}\, \delta \right\} - F\left\{\sqrt{\frac{2\pi}{K}}\, \delta \right\}\right]$$

(237)

where

$$K = \pi B/(T - t_J)$$

(238)

and $F\{\cdot\}$ is the complex Fresnel integral,

$$F(x) = \int_o^x e^{j\frac{\pi}{2} t^2} \, dt.$$

(239)

For the cases of interest to us we can use the approximate relationship

$$F(x + y) - F(y) \approx F(x)$$

(240)

since $y = \delta\sqrt{2\pi/K}$ is extremely small.

88

Therefore,

$$|m_{J'}| \cong \frac{J'}{T} \sqrt{\frac{\pi}{2K}} \left| F\left\{\sqrt{\frac{2K}{\pi}} \; T\right\} \right| \tag{241}$$

which is independent of the frequency ambiguity, δ.

We wish to choose the jammer amplitude, J', such that the energy density of the linear FM is equal to that of the pure tone jammer. We find that this is the case when

$$\frac{(J')^2}{2B} = J^2 T \tag{242}$$

or

$$J' = \sqrt{2BT} \; J. \tag{243}$$

Then the matched filter output is equal to

$$|m_{J'}| = J \sqrt{\frac{(T-t_J)}{T}} \left| F\left\{\sqrt{\frac{2B}{(T-t_J)}} \; T\right\} \right| \tag{244}$$

Comparing this to the pure tone case with $t_J = 0$ we find

$$|m_{J'}| = \frac{J}{\sqrt{2}} \; . \tag{245}$$

Thus, whereas the pure tone case could have a 4 dB degradation due to frequency ambiguity, the linear FM has no frequency ambiguity degradation but does have a 3 dB degradation built in (for the same jammer energy density). We shall therefore do our analysis for the pure tone case and no frequency ambiguity and then degrade the results by 3 dB. This will give the true linear FM or pure tone jamming performance.

2.4.4 Jamming Probability

We have assumed a frequency hopped MFSK modulation with N chips of length $T = 1/f_0$ seconds to comprise a data transmission.

89

After dehopping, the desired signal will appear in one frequency cell. Jammer noise will appear in all frequency cells within the limiter bandwidth. The receiver processes the data by limiting the composite signal, matched filtering the M frequency cells, and then summing the energy in each cell over N chips. The largest total energy corresponds to the frequency decision.

There will be (M-1) cells with only jammer power. The limiter matched filter output will be designated by m_J. One cell will have both desired and jammer power and its output will be designated by m_i where the subscript i refers to the i'th chip. Then the probability of deciding the wrong frequency is given by

$$P_e = Pr\left\{ \sum_{i=1}^{N} |m_i|^2 \leq N|m_J|^2 \right\} \tag{246}$$

We now include the random phase, φ, with respect to the desired signal. The jammer signal is given by

$$v_J(t) = J' \exp\left[j2\pi\left\{ f_c(t-t_J) + \frac{\varphi}{2\pi} + B \frac{(t-t_J)^2}{2(T-t_J)} \right\} \right]; \quad t_J \leq t \leq T \tag{247}$$

and the desired signal is given by

$$v_s(t) = S \exp[j2\pi f_c t] \; ; \quad 0 \leq t \leq T. \tag{248}$$

The limiter input contains $v(t) = v_J(t) + v_s(t)$. The output of the limiter will contain the strongest signal plus a suppressed version of the weaker signal. We therefore write the limiter output as

$$w_\ell(t) = v_J(t) + \beta \, v_s(t) \tag{249}$$

where β is the suppression (or enhancement factor when $|v_s| > |v_J|$) and the normalizing constant $1/\sqrt{|v_J|^2 + |v_s|^2}$ has been omitted for simplicity. The value of β can be found in Fig. 9, which, for convenience of the reader, is Fig. 1, repeated.
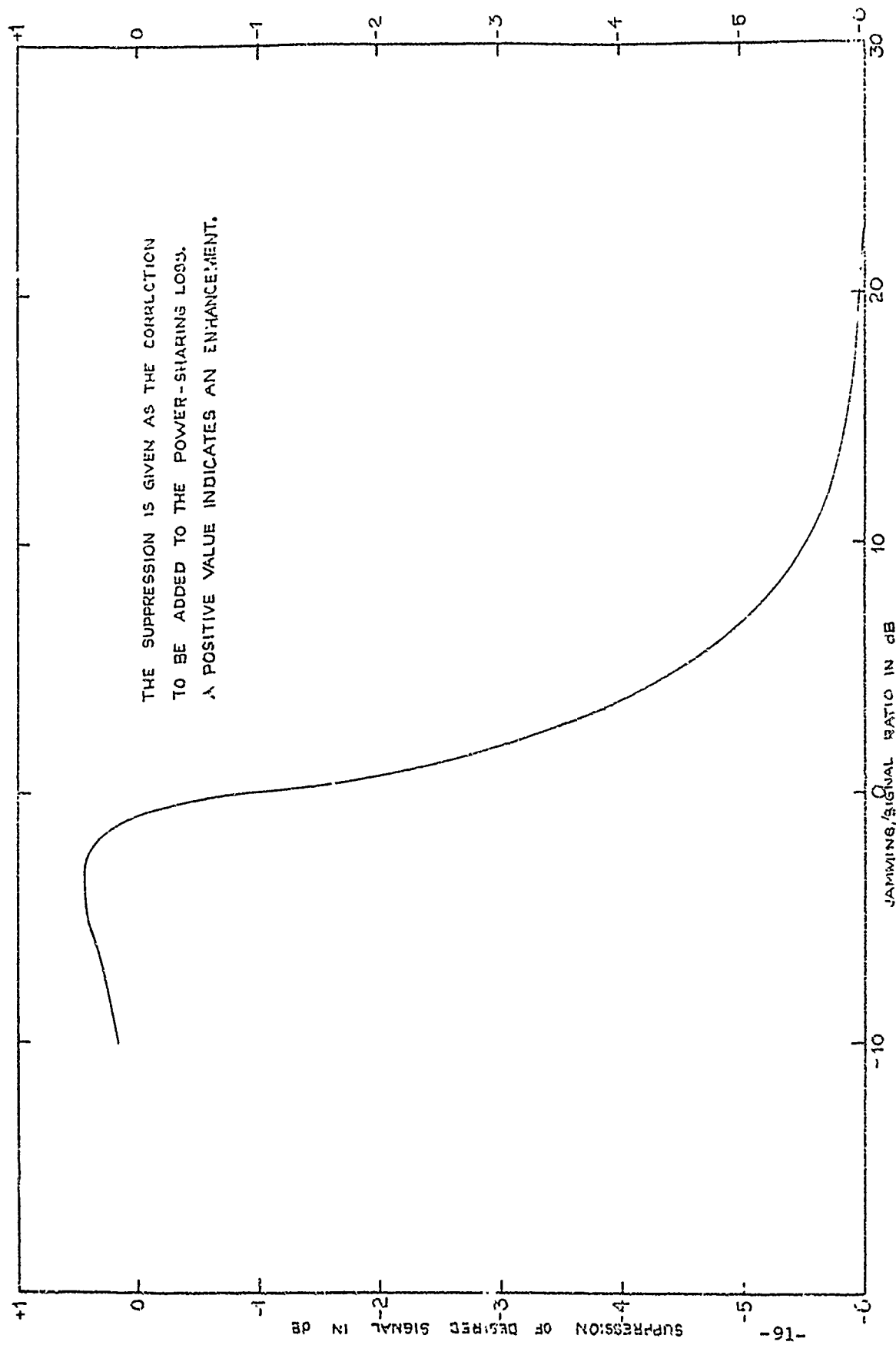
90

THE SUPPRESSION IS GIVEN AS THE CORRECTION
TO BE ADDED TO THE POWER-SHARING LOSS.
A POSITIVE VALUE INDICATES AN ENHANCEMENT.

JAMMING/SIGNAL RATIO IN dB

SUPPRESSION OF DESIRED SIGNAL IN dB

Figure 9. Hard Limiter Suppression Factor

Seven matched filter outputs contain only the effects of $v_J(t)$ and give

$$|m_{J'}| = \frac{J'}{T} \sqrt{\frac{\pi}{2K}} \left| F\left\{ \sqrt{\frac{2K}{\pi}} \; T \right\} \right| \qquad \text{(FM)} \qquad (250)$$

$$|m_J| = J \frac{(T-t_J)}{T} \left| \text{sinc} \; \pi \delta (T-t_J) \right| \quad \text{(pure tone)} \qquad (251)$$

The eighth matched filter output can be written as

$$m_i = m_J + \beta \; S \; e^{j\varphi_i}. \qquad (252)$$

Squaring we have

$$|m_i|^2 = |m_J|^2 + 2\beta S \text{Re}\left\{ m_J \; e^{-j\varphi_i} \right\} + \beta^2 S^2 \qquad (253)$$

For the pure tone case where m_J is real

$$|m_i|^2 = |m_J|^2 + 2\beta S \; |m_J| \cos \varphi_i + \beta^2 S^2. \qquad (254)$$

For the linear FM case we have

$$m_{J'} = J \sqrt{\frac{T-t_J}{T}} \left\{ C(x) + j \; S(x) \right\} e^{-j \frac{4\pi^2 \delta^2}{K}} \qquad (255)$$

where

$$x = T \sqrt{\frac{2B}{T-t_J}} \qquad (256)$$

and $C(x)$ and $S(x)$ are the real and imaginary parts of the Fresnel integral $F(x)$. Most of the time x is very large so that

92

$$m_{J'} \approx J \sqrt{\frac{T-t_J}{T}} e^{-j\left(\frac{4\pi^2 \delta^2}{K} - \pi/4\right)} \tag{257}$$

and

$$|m_i|^2 = |m_{J'}|^2 + 2\beta S |m_{J'}| \cos \varphi_i' + \beta^2 S^2 \tag{258}$$

where

$$\varphi_i' = \varphi_i + \frac{4\pi^2 \delta^2}{K} - \pi/4. \tag{259}$$

The condition for an error to occur is therefore

$$\sum_{i=1}^{N} \cos \varphi_i' < - \frac{N}{2} \frac{\beta S}{|m_J|} = \gamma. \qquad -\pi \le \varphi_i' \le \pi \tag{260}$$

If the signal to jammer amplitude ratio is $\rho = S/J$ then

$$\gamma = - C\rho \tag{261}$$

where

$$\frac{N\beta}{2C} = \begin{cases} \dfrac{(T-t_J)}{T} \left| \text{sinc } \pi\delta(T-t_J) \right| & \text{(pure tone)} \\[2em] \sqrt{\dfrac{(T-t_J)}{T}} \left| F \left\{ \sqrt{\dfrac{2\beta}{(T-t_J)}} \, T \right\} \right| & \text{(FM)} \end{cases} \tag{262}$$

2.4.4.1 Probability Density Function

The probability density function of $Z = \sum \cos \varphi_i$ must be determined to evaluate the jammer performance. This is difficult when N is larger than 2. We demonstrate how the pdf is found when $N = 2$. We then state numerical results which we obtained for $N = 3,4$.

Let $x = \cos \varphi$ with $p(\varphi) = 1/2\pi, -\pi < \varphi < \pi$. Then since

$$p(x) = 2p(\varphi) \left| \frac{d\varphi}{dx} \right| \tag{263}$$

93

it is easily found that

$$p(x) = \frac{1}{\pi \sqrt{1-x^2}} \, , \quad -1 < x < 1. \tag{264}$$

If we now desire the pdf of y where

$$y = x_1 + x_2 \tag{265}$$

we have

$$p(y) = \frac{1}{\pi^2} \int_{x=-1}^{1} \frac{1}{\sqrt{1-x^2}} \, \frac{1}{\sqrt{1-(y-x)^2}} \, dx. \tag{266}$$

This is most easily evaluated using transform techniques. If $P(\omega)$ is the Fourier transform of $p(x)$, then

$$p(y) = \frac{1}{2\pi} \int_{\omega=-\infty}^{\infty} P^2(\omega) \, e^{j\omega y} \, d\omega. \tag{267}$$

It is easy to show that

$$P(\omega) = J_0(\omega) \tag{268}$$

where $J_0(\omega)$ is the zero'th order Bessel function of the first kind. Then [Ref. 3, Eq. 8.13.8]

$$p(y) = \frac{2}{\pi} K\left(\frac{1}{2}\sqrt{4-y^2}\right)^* \qquad |y| < 2 \tag{269}$$

where $K(x)$ is the elliptic integral, equal to

$$K(x) = \frac{\pi}{2} \left[1 + \left(\frac{1}{2}\right) x + \left(\frac{1\cdot 3}{2\cdot 4}\right)^2 x^2 + \left(\frac{1\cdot 3\cdot 5}{2\cdot 4\cdot 6}\right)^2 x^3 + \ldots \right], \, |x| < 1. \tag{270}$$

The desired pdf for

$$z = \sum_{1}^{N} x_i = \sum_{i=1}^{N/2} y_i \qquad (271)$$

is

$$p(z) = \frac{1}{2\pi} \int_{\omega=-\infty}^{\infty} J_0^N(\omega) e^{j\omega z} d\omega. \qquad (272)$$

This is easy to evaluate numerically using FFT techniques and impossible to evaluate analytically for $N > 2$. The numerical results for $N = 3,4$ are shown in Figs. 10 and 11 where the pdf and cdf are displayed. Table 15 lists the data for these figures.

TABLE 15. MULTIPLE CHIP PHASE PROBABILITIES

System	3 Chip		4 Chip	
$-\gamma$	PDF	CDF	PDF	CDF
0	.2853	0.5000	.2873	0.5000
1/8	.2854	0.4632	.2779	0.4646
1/4	.2856	0.4275	.2686	0.4295
3/8	.2859	0.3918	.2593	0.3965
1/2	.2863	0.3560	.2501	0.3646
5/8	.2869	0.3202	.2408	0.3340
3/4	.2876	0.2843	.2316	0.3045
7/8	.2884	0.2483	.2222	0.2761
1	.2864	0.2122	.2127	0.2490
1 1/8	.2153	0.1824	.2030	0.2230
1 1/4	.1863	0.1575	.1930	0.1983
1 3/8	.1649	0.1356	.1826	0.1748
1 1/2	.1476	0.1162	.1718	0.1527
1 5/8	.1327	0.0987	.1602	0.1319

TABLE 15 (cont'd)

System	3 Chip		4 Chip	
-Y	PDF	CDF	PDF	CDF
1 3/4	.1195	0.0830	.1476	0.1127
1 7/8	.1077	0.0688	.1333	0.0952
2	.9677(-1)	0.0561	.1137	0.0796
2 1/8	.8655(-1)	0.0446	.9478(-1)	0.0668
2 1/4	.7681(-1)	0.0344	.8173(-1)	0.0558
2 3/8	.6738(-1)	0.0254	.7099(-1)	0.0463
2 1/2	.5802(-1)	0.0176	.6175(-1)	0.0380
2 5/8	.4846(-1)	0.0110	.5362(-1)	0.0308
2 3/4	.3823(-1)	0.0056	.4637(-1)	0.0246
2 7/8	.2615(-1)	0.0015	.3982(-1)	0.0192
3	0	0.0	.3387(-1)	0.0147
3 1/8			.2842(-1)	0.0108
3 1/4			.2340(-1)	0.0076
3 3/8			.1877(-1)	0.0049
3 1/2			.1448(-1)	0.0029
3 5/8			.1048(-1)	0.0013
3 3/4			.6755(-2)	0.0007
3 7/8			.3268(-2)	0.0003
4			0	0.0
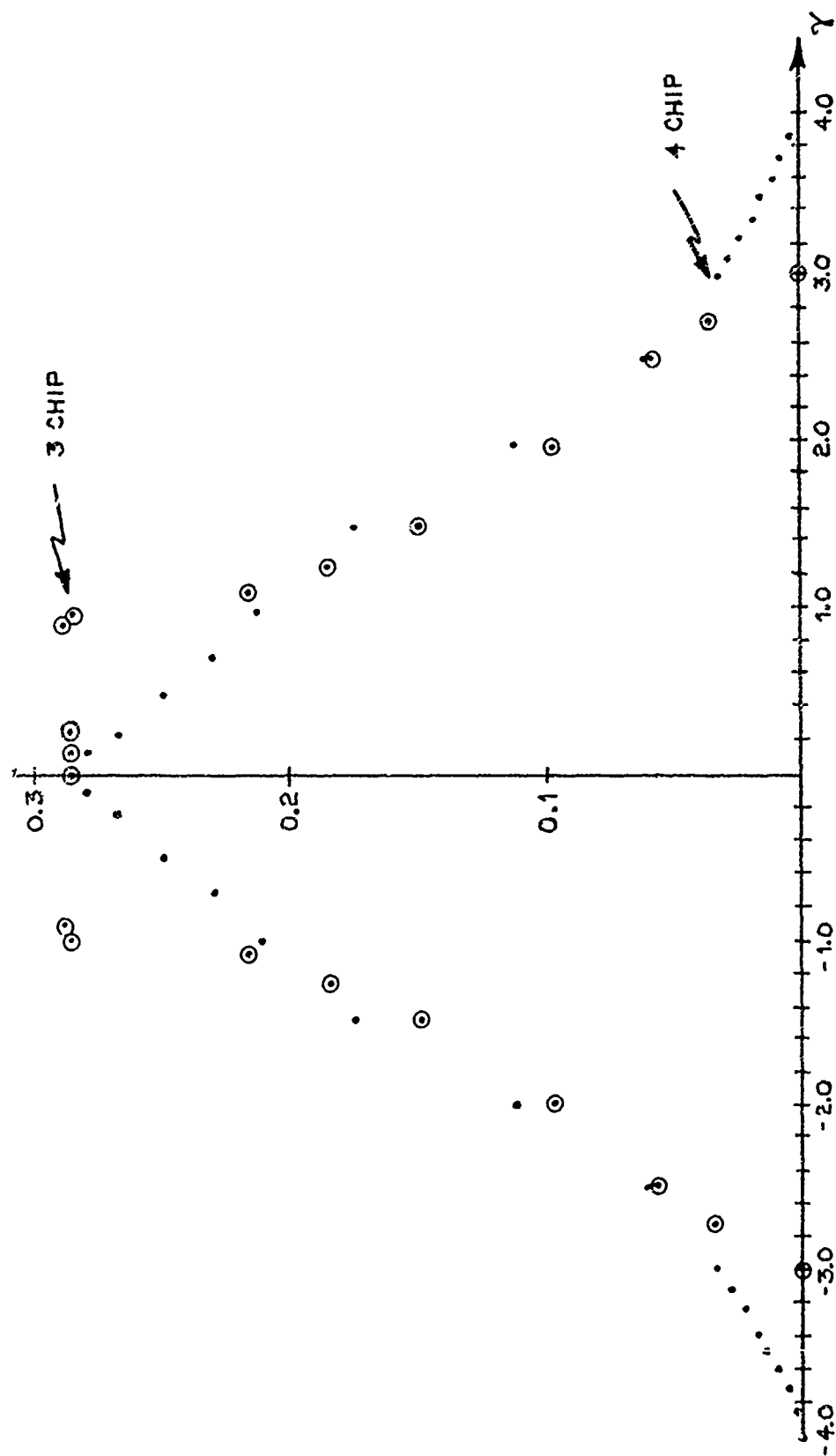
Figure 10   PDF of System

97
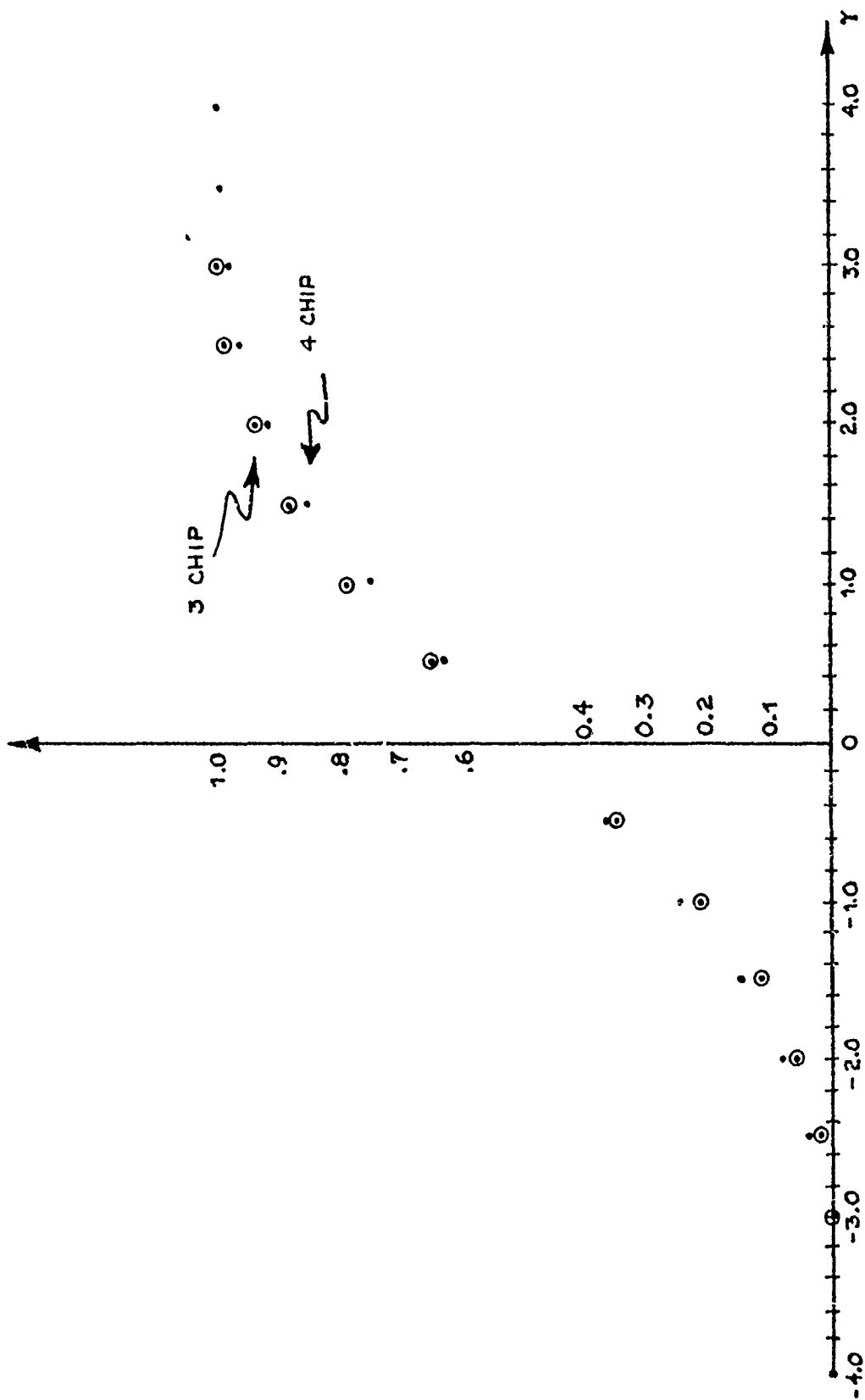
Figure 11 CDF of System

98

2.5 LES 8/9 Simulation Experiments

This section describes a preliminary sequence of experiments to be performed using the CSEL facility to simulate and test the LES 8/9 processor and system. Three forward link simulation experiments are discussed, the first being a validation of the PSP model of the satellite processor, the second being a testing of the downlink simulation, and the third being a simulation of jamming on the forward uplink. The initial evaluation will be performed using digital computer simulation, as shown in Figure F-4 of an internal AFAL report describing the CSEL facility ("the CSEL document"). We will first outline the performance of tests based on this figure, which is reproduced as Fig. 12 of this section.

2.5.1 Test Series 1. Forward Link Simulation

The first test series is the forward link simulation, with the K-band uplink and the UHF downlink. It is assumed that the ˙. and UHF modems exist, but that the satellite is being simulated by the PSP. The test configuration is shown in Fig. 12. We start by putting 75 bps data into the modem processor. This is encoded and 8 FSK transmitted at K-band through the K-band terminal. The AJ protection is put onto the transmitted signal by frequency-hopping at a rate of 200 hops per second;   75 bps @ $R = \frac{1}{2} = >$ 150 bps. 8 FSK reduces this to 50 symbols/sec. Each symbol is hopped over four frequencies, resulting in 200 frequency hops per second, or a duration of 5 ms per frequency.

The K-band transmitted power is 2 W, and the antenna gain is 51 dB. The frequency is 38 GHz. The satellite antenna gain is 42.7 dB for the disc, 25 dB for the horn. The received power is

$$P_R = \frac{P_T \, G_T \, A_R}{4\pi \, R^2} \qquad\qquad (273)$$

99
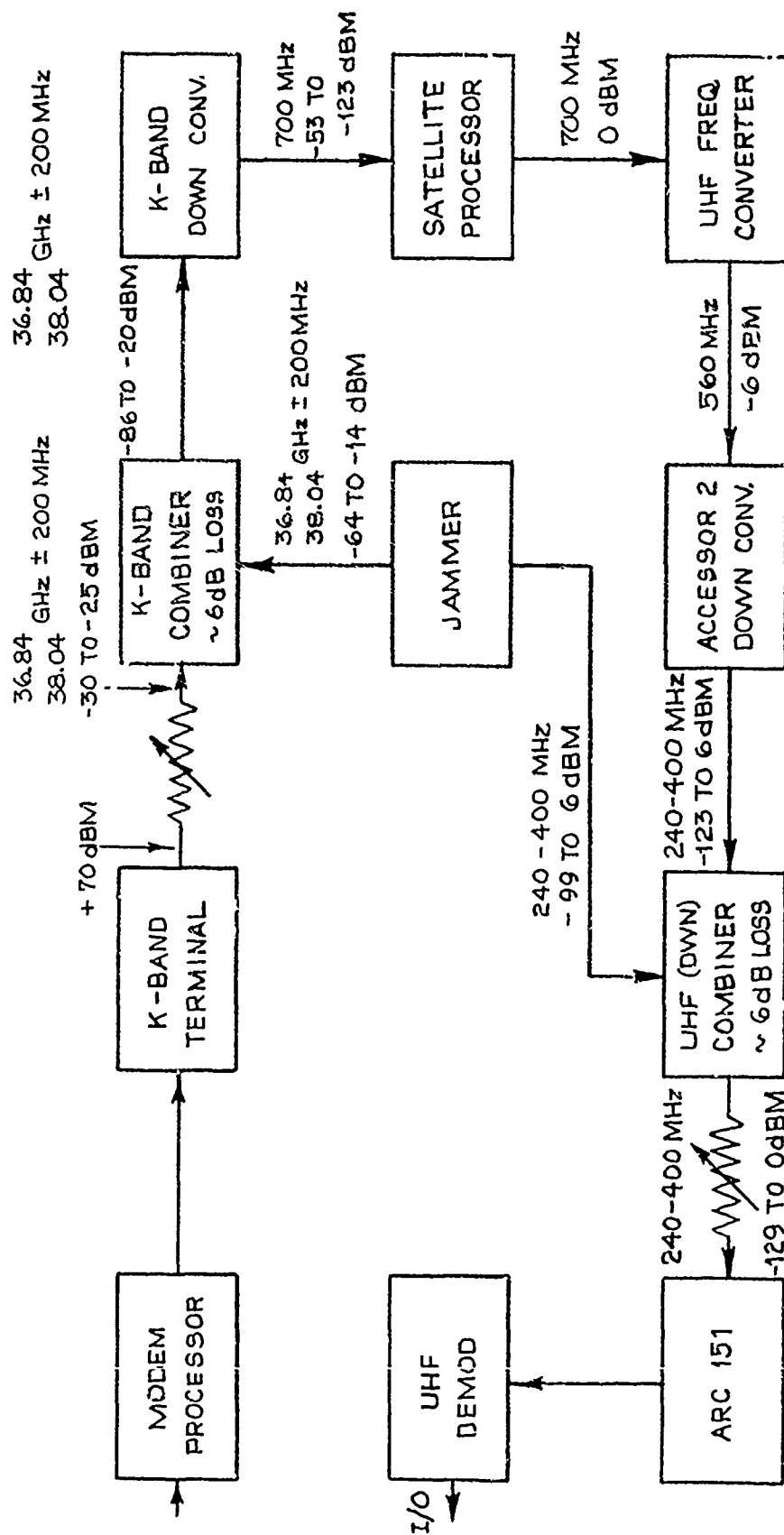
Figure 12. Forward Link
K-Band – UHF Simulation

100

Since:

$$P_T = 3 \text{ dBW}$$

$$G_T = 51 \text{ dB}$$

$$A_R = -28 \text{ dBm}^2 \qquad \text{(Horn)}$$

$$-10 \log_{10}(4\pi) = -11$$

$$20 \log_{10} R = -151 \text{ dBm}^2 \qquad \begin{cases} R \cong 20 \times 10^3 \text{ nm} \\ = 37 \times 10^6 \text{ meters} \end{cases}$$

or
$$P_R = -136 \text{ dBW}$$
$$-106 \text{ dBm.} \qquad (274)$$

To this received power, one must add atmospheric losses. Assuming no rain, this would range from nearly 0 dB for vertical transmission to about 30 dB for horizontal transmission. If, for a nominal worst case, we add a 20 dB propagation loss, the received power will be -126 dBm. The power shown on Fig. 12 at the satellite processor input ranges from - 53 to -123 dBm. The lower level, -123 dBm, is in good agreement with our estimate of -126 dBm. However, the -53 dBm level seems unnecessarily strong for LES 8/9 simulation, as, in clear weather, the received power would be -106 dBm maximum.

The K band horn system has an 8 dB noise figure, or an N_o of -166 dBm/Hz. Therefore the E_b/N_o for a 75 bit per second rate is then

$$\frac{E_b}{N_o} = \frac{P_R T_b}{N_o} = -126 - 19 + 166 = +21 \text{ dB.} \qquad (275)$$

This, it should be recalled, is with a 20 dB atmospheric loss; with no loss, it is 41 dB.

If an E_b/N_o of 0 dB were desired, and the maximum signal strength were -106 dBm, then

$$0 \quad = \quad -106 - 19 - N_o \qquad (276)$$

$$N_o \quad = \quad -125 \text{ dBm/Hz}, \qquad (277)$$

which is, as expected, 41 dB above the receiver noise level. If this noise were spread over a bandwidth of B MHz,

$$P_N = -65 + 10 \log_{10} B \text{ dBm.} \qquad (278)$$

The K band down converter has, according to Fig. 12, a loss of about 35 dB (the figure is ambiguous, showing a loss of 33 dB at -20 dBm in, and 37 dB at -86 dBm in). Assuming a 6 dB combiner loss, the jammer would require a maximum output power of

$$P_{J_{max}} \cong -65 + 35 + 6 + 10 \log_{10} B$$
$$= -24 + 10 \log_{10} B \text{ dBm.} \qquad (279)$$

in order to achieve a 0 dB SNR. The jammer on Fig. 12 has an output power ranging from -14 to -64 dBm. If this is not sufficient power to achieve 0 dB, at the standard signal power level, then 0 dB SNR jamming would be accomplished by decreasing the signal power at the processor input while running at maximum jamming power.

With these preliminary power considerations settled, let us now consider specific tests to be run on the forward link. We can broadly divide them into two classes, namely noise and jamming tests, and acquisition tests. We consider them in that order.

2.5.1.1 Noise and Jamming Tests

The first set of tests, noise and jamming, have two purposes. First, the performance of the forward link is to be checked out against white Gaussian noise, to validate the simulation system and model. Secondly, having shown the system and model to be valid, the effects of various types of jammers will be tested and compared to theoretical results.

Table 16, taken from Lindsey and Simon [4], shows the word and bit error probabilities (P_E and P_B, respectively) of a non-coherent 8-FSK system using optimum detection.* This is a lower bound on the error which can be attained by the processing used in the satellite.

TABLE 16. OPTIMUM 8-FSK ERROR PROBABILITY:
INCOHERENT DETECTION

E_b/N_o (dB)	Word Error Probability P_E	Bit Error Probability P_B
0.00	0.34075232	0.19471561
3.01	0.10403854	0.59450594 (-1)
4.78	0.28086227 (-1)	0.16049273 (-1)
6.02	0.70613553 (-2)	0.40350601 (-2)
7.00	0.16994870 (-2)	0.97113545 (-3)
7.78	0.39791019 (-3)	0.22737724 (-3)
8.45	0.91543186 (-4)	0.52310392 (-4)
9.02	0.20826269 (-4)	0.11900725 (-4)
9.54	0.47052477 (-5)	0.26887130 (-5)

---

*The error probabilities of Table 16 are written in the form 0.XXX(-N), which is equivalent to 0.XXX 10^{-N}.

For 8'ary FSK, word and bit error probability are related by

$$P_B = \frac{4}{7} P_E,$$ (280)

that is, the bit error probability is 4/7 the word error proba-
bility. It should be noted that the signal-to-noise ratio in
Table 16 is $10 \log_{10}(E_b/N_o)$. E_b, in turn, is $P_s T_s/3$, where P_s
is the transmitted symbol power, T_s is the transmitted symbol
duration, and the factor of 3 occurs because there are three
bits encoded into each transmitted symbol. For the 8-FSK trans-
mission, $T_s = 20$ ms, corresponding to 50 symbols/second, while the
bit rate into the 8FSK encoder is 150 bits per second.

To further complicate the situation, the unencoded bit rate
at the transmitter modem input is 75 bps, corresponding to an
input bit duration T_b of 13.33 ··· ms. This has a bit energy
of +3 dB relative to an equal-power 20 ms, 3 bit symbol. We
will make clear, in this report, the exact time duration being
used 'n a table or figure.

The processing in LES 8/9 is not optimum, and one would ex-
pect the error rate to differ from that of Table 16. Deviations
from optimality include

a)   The matched-filters in the 8-FSK receiver are
     implemented using 2-bit quantization of both the
     input signal and the reference frequencies;

b)   Hard limiting of the IF signal;

c)   Frequency hopping within the symbol, which cause
     phase discontinuities in the dehopped signal.

There is an experimental curve, attributed to Lincoln Laboratory,

104
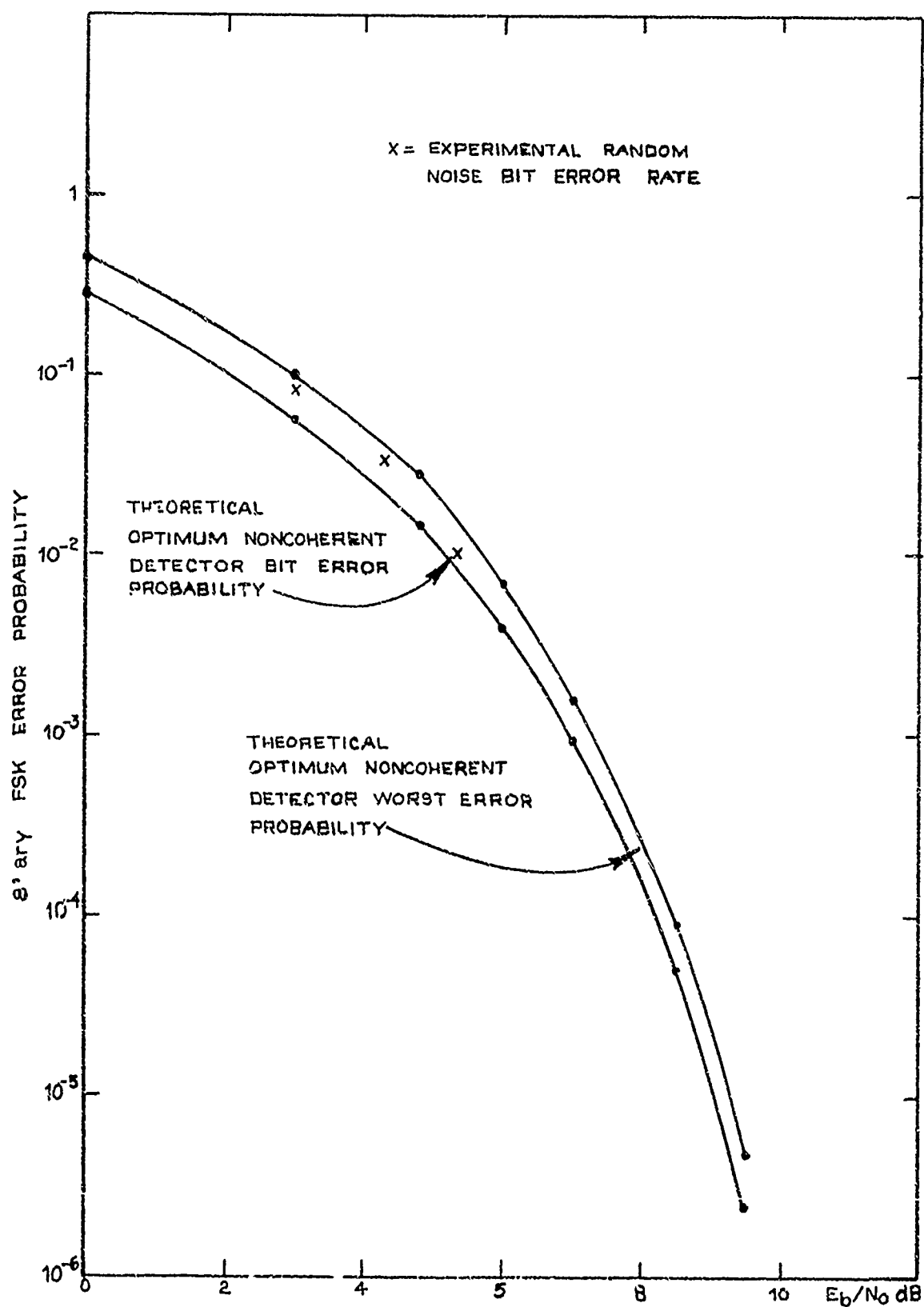
Figure 13. 8-FSK Error Rate, Gaussian White Noise Channel

of the bit error rate as a function of signal-to-Gaussian noise ratio. Three points from this curve, shown as x's, are reproduced in Fig. 13, along with the bit and word probabilities of Table 16.

2.5.1.1.1 Experiment 1. PSP Model Validation

The first experiment is to validate the curves of Fig. 14, thereby showing the satellite processor is being simulated properly. This is best done on a step-by-step basis, in the following sequence.

1.5.1.1.1.1 Experiment 1A. Optimum 8-FSK Modem Simulation

Simulate the optimum non-coherent detector 8-FSK modem. This will differ from the LES 8/9 satellite receiver by

1) not frequency hopping;

2) not using the limiter;

3) quantization of the signal and the reference to at least 6 bits.

The word error probability of the PSP should be measured as a function of additive Gaussian noise. This is done by comparing the FSK frequency commanded at the modem to the FSK frequency decided by the PSP. The signal-to-noise ratio should be varied over the range 0 to +10 dB, keeping the noise constant and varying the signal level. The sampling rate used in the simulation should be the same as in the satellite processor, namely 64 samples of the I and of the Q process in a 20 ms symbol. The 75 bps data into the modem should come from a suitable digital test source, such as a pseudo-random number generator.

106

The PSP has a 16 dB noise figure at the 700 MHz input. Therefore the noise power density is -158 dBm/Hz, and the (bit) signal-to-noise ratio for a 20 ms symbol is

$$\frac{E_b}{N_o} = \frac{P_s \, T_s}{3 \, \cdot \, _o} = P_s - 17 + 158 - 4.8$$

$$= P_s + 136 \text{ dB}. \qquad (281)$$

Therefore, in order to have a 0 dB signal-to-noise ratio due solely to the PSP's noise figure,

$$P_s = -136 \text{ dBm}. \qquad (282)$$

However, the PSP is specified to have an input signal range of -123 to -53 dBm with the result that a -136 dBm signal is too weak for it to process. It is therefore necessary to add external noise, and use a stronger signal. If we add external noise which is equivalent to increasing the front end noise by 21 dB, 0 dB SNR would be achieved with a $P_s = -115$ dBm, within the range of the PSP. Therefore the added noise should have a density of

$$N_o = -137 \text{ dBm/Hz}. \qquad (283)$$

The receiver's noise figure can be neglected with this additive noise, as it is 21 dB above KTF. The total noise power is

$$P_N = -77 + 10 \log_{10} B \text{ dBm} \qquad (284)$$

in a bandwidth of B MHz.

Experiment 1A could be run with a signal power into the PSP ranging from -115 dBm, for a 0 dB E_b/N_o, to -105 dBm, for a +10 dB E_b/N_o, with the additive noise kept constant at a density of -137 dBm/Hz at the PSP input.

107

The results of Experiment 1A should match the curve marked "Optimum Non-coherent Detector Word Error Probability", of Fig.13. However, the absence of an AGC or limiter, might result in a signal level out of the range of the A/D converter. If the experimental curve deviates significantly from the theoretical, consideration should be given to either increasing both P_S and N_O to get into the A/D converter's range, or increasing the number of bits in the A/D converter, to increase its dynamic range.

Following Experiment 1A, the modeling should start to include the omitted effects of the LES 8/9 satellite processor. As each effect is added, the experimental curves should be rerun. Once an effect is added, it should be kept in the simulation model for the remainder of the satellite tests. An appropriate test sequence would be

2.5.1.1.1.2 Experiment 1B Limiter

Repeat Experiment 1A, with the limiter added to the simulated receiver. With the limiter present, the error probability should be only a function of SNR, and not of the absolute values of P_R or N_O. This relation should hold until the limiter does not bring the signal into the range of the A/D converter.

2.5.1.1.1.3 Experiment 1C Quantization

The purpose of this is to show the change in error rate due to the use of 2-bit quantization of the A/D converter and the matched filter reference waveform. The number of bits used should be decreased from those used in Experiments 1A and 1B, to 2 bits. With the limiter and 2-bit processing, the error curve should move from the optimum toward the experimental points shown on Fig. 13. Note that the Fig. 13 curve is a bit error curve; the word error for an 8-FSK system is 7/4 the bit error.

2.5.1.1.1.4 Experiment 1D Frequency-Hopping

The purpose of this is to show the change in error rate due to frequency hopping. This should be accomplished in two steps. First, the signal should be hopped at the transmitter and de-hopped with zero frequency error at the PSP. The measured error rate in this case, as compared with that of Experiment 1C, will show the effects due to the phase discontinuities in the four subchips which make up a single FSK symbol. Second, frequency errors should be introduced in the de-hopping to show the effect of incorrect frequency estimation. The most simple error to put in is a constant error independent of the transmitter frequency. This error can be varied up to the FSK frequency separation. A more complicated error to put in is one which is a function of the instantaneous transmitted frequency. This can be, initially, under program control as follows. Asssume an error in measuring center-frequency Doppler. Let the center frequency be f_c, and the error in center frequency Doppler be be e_{fc}. Then, if the transmitted frequency is f, the error in the received signal will be

$$e_{fc}\left[1 + \frac{f-f_c}{f_c}\right] = \frac{f}{f_c}\,e_{fc}. \tag{285}$$

This error can be programmed into the PSP.

The error rate measured in Experiment 1D, which includes frequency hopping, limiting, and quantization, should agree with the Lincoln Laboratory data.

109

2.5.1.1.2 Experiment 2   Downlink Simulation

The result of Experiment 1 will be to confirm that the up-link modeling is correct through the 8'ary FSK detector. A second experiment is needed to verify that the UHF downlink modulation is being properly simulated. To do this, the full forward link of Fig. 12 is used, and the bit error rate from the modem processor input to the UHF demodulator output is measured.

Figure 14, which is Fig. 3.14-6 of the TRW report [2], shows the performance curve for the demodulator decoder. It plots the decoder output bit error probability as a function of the input channel error probability; the input channel error probability is the 8-FSK bit error probability. Experiment 1 will provide the channel error rate as a function of the E_b/N_o for the transmitted 8'ary FSK signal. This can thus be converted into a predicted bit error rate at the output of the downlink through Fig. 14. The experiment consists of the measurement of the channel error rate, conversion of this to a predicted decoded bit error rate, and comparison of the predicted bit error rate to the measured bit error rate.

Figure 15 shows two theoretical curves of bit error rate out of the decoder as a function of the 8-FSK uplink E_b/N_o. The curves were generated by using the theoretical bit error rate curve of Fig. 13, with the decoder curve of Fig. 14. Since the Lincoln Laboratory experimental points of Fig. 13 are close to the theoretical, the measured decoded bit error rate should be close to the curve of Fig. 15. It is seen that the two curves are identical in shape, but separated by 3 dB. The curve marked "T_b = 6.66 ms" is based on the energy in the 150 bps encoded

110
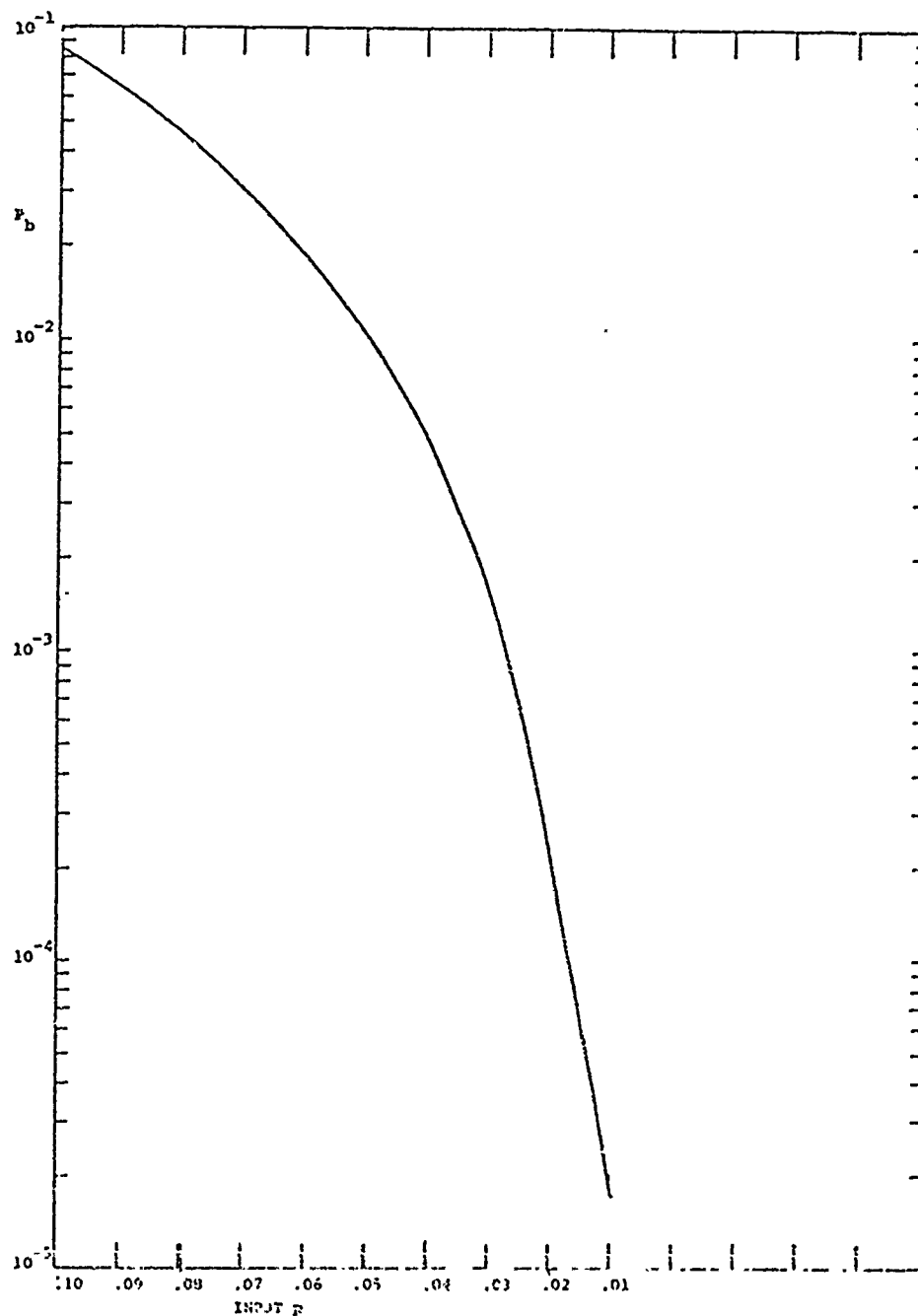
Figure 14. Forward Link Bit Error Probability as Function of Input Error Probability. (From Ref. [2])

111
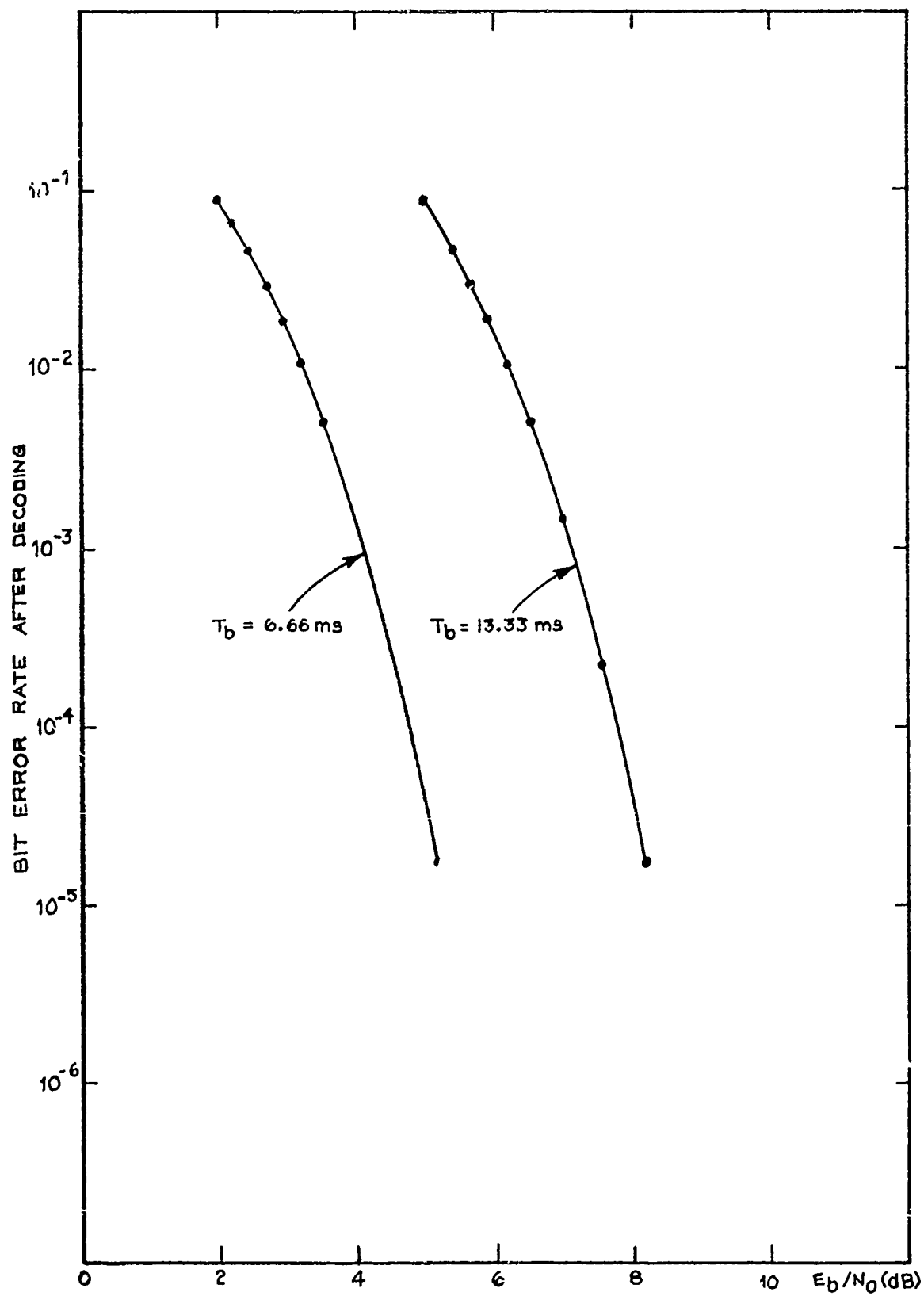
Figure 15. Predicted Forward Link Bit Error
Probability After Decoding

112

bits which are transmitted as the 8-FSK data, and correspond exactly to the theoretical curve of Figure 1. The curve marked "$T_b = 13.33$ ms" is based on the energy in the 75 bps data going into the transmitter modem.

In this experiment, the downlink should be at a high enough signal-to-noise ratio that the ARC 151 receiver noise does not cause errors.

2.5.1.1.3   Experiment 3   Forward Link Jamming Test

With the completion of Experiments 1 and 2, there should be confidence that the forward link signal processing functions of the satellite are being properly simulated. The emphasis can can then switch to forward link jamming and acquisition tests. We will consider repeater jamming in this section.

Repeater jamming can be used to reduce the power required by the jammer. In repeater jamming, the signal radiated by the transmitter is intercepted, and its frequency estimated. Then a jamming signal of bandwidth B is transmitted, centered on the intercept frequency. Since B is significantly less than the total RF bandwidth, W_T, there is a large possible saving for repeater jamming relative to full-band jamming.

The implementation of the repeater jamming uses a Hallicrafter Sweeplock receiver. The FSK signal is 20 ms long, and is transmitted as a sequency of four frequency hopped chips, each of 5 ms duration. In Section 2.4 we presented an analysis of the repeater jammer, and showed that a delay of 3/5 of a chip would decrease the jammer effectiveness by $1/(1-0.6)$, or 8 dB relative to full-chip jamming; this would still be in the order of 11 dB more effective than full-band jamming. The first repeater jamming experiment will be to test

113

the efficiency of repeater jamming. With the signal level of
the desired signal set at a nominal value, such as -113 dBm,
the jammer level can be varied over the E_o/J_{OM} range of 20 to
40 dBm. There will be a range of about 6 or 8 dB over which
the error rate is significant, with the exact value depending
on the amount of the chip which is jammed. The parameter α
is 0 if the entire chip is jammed, 1 if none of the chip is
jammed, and varies linearly between these two extremes.
Using whatever jamming waveform is selected, the repeater
jamming should be tested over the range $\alpha = 0$ to 1, at
discrete steps; typical values of α might be 0, 0.2, 0.4, 0.9.
The bit error probability can then be measured as a function of
E_o/J_{OM} and α, and compared with the full-band multitone and noise
jamming error probabilities. While the error probability can be
measured either in the PSP receiver or after error detection in
the strike force receivers, the error rate should be measured at
the same place for all jamming tests.

Following this experiment, the effect of receiver noise should
be included in the tests. At high signal-to-noise ratios, such as
20 dB, the error rate should be the same as in the absence of noise.
Noise effects should start being seen with E_b/N_o in the order of
6 dB, as shown in Fig. 13.

The repeater jamming tests, with and without receiver noise,
will show the performance of the repeater jamming system as
operating with the present LES 8/9 satellite processor. Repeater
jamming operates on only part of the received signal. The satellite
processor, as presently designed, processes the entire chip. If,
however, the processor where to adaptively measure the received
signal and integrate only over the unjammed portion, one would

expect that the jamming efficiency would be decreased. For values of α near 1, where most of the chip is unjammed, the performance should approach that of the unjammed signal. For values of α near 0, where most of the chip is jammed, the amount of energy in the unjammed portion of the chip is small, and the receiver thermal noise would be a limiting factor. The PSP can be used to simulate an LES 8/9 processor which integrates over only the unjammed part of each chip, and the error probability measured as a function of α, E_o/J_{OM} and E_b/N_o. This simulated processor will have an ECCM capability against repeater jamming which is not found in the present processor.

It is axiomatic that for a given ECCM one can develop a new ECM technique. In this case, the ECM response would be to develop a receiver which can estimate the received frequency in a time interval which is sufficiently short as to cause the processor to be thermal noise limited. One would expect that, given either sufficient sweep capability or parallel processing, the transmitted frequency can be estimated in a time equal to the reciprocal of the frequency uncertainty. Therefore, to jam with a frequency uncertainty of, say 10 kHz, would require only a 0.1 ms intercept time. The simulation of a repeater jammer should include exploring trade-offs between intercept time and chip processing time.

SECTION 3

NAVSTAR GPS STUDIES

3.1 Introduction

The NAVSTAR Global Positioning System (GPS) is a satellite navigation system which will allow the user to determine his three-dimensional position and velocity. The GPS Phase 1 Program is a space-based radio navigation concept validation program that precedes the full scale development of the GPS. As part of Phase 1, AFAL is developing a generalized development model (GDM) of the GPS user equipment. The GDM system will include the hardware and software to receive and process GPS navigational signals, along with inertial and auxiliary navigation sensor data in some modes, and determine optimum estimates of three dimensional postion, velocity, and system time for display to the user.

The GDM will be part of the CSEL facility, and experiments will be part of the CSEL facility, and experiments will be run as required to determine system parameters. The purpose of this section is to determine means of simulating the GPS signal and channel characteristics, to a degree that will permit accurate and reliable testing of the GDM. We take a general point of view, allowing for a variety of different receiver types and GPS signaling schemes. Future studies will consider the specific requirements needed for the Phase 1 system.

This section is divided into two main parts. Section 3.2 summarizes some possible configurations for the GPS, as well as possible uses of the simulation facility. The errors incurred in the system are reviewed, and some methods of correction by the receiver are discussed, since they have a significant

116

impact on the necessary simulation accuracy. Some important
aspects of the receiver structure are pointed out, and finally,
the general structure of the simulator is defined. In the
discussion of Section 3.2, only the global features of a simu-
lation facility are discussed. Section 3.3 extends the analysis
to include detailed problems in the instrumentation of the simu-
lation system hardware and software.

3.2 General Problems of GPS/GDM Simulation

3.2.1 A Survey of Possible GPS Structures

GPS is designed primarily for military use, but civil
applications are also envisioned, which has some impact on
the types of receivers that can be used.

The full system is to have 24 satellites in 12 hour orbits,
such that any point of the earth is covered by at least 4 satel-
lites. The user position is determined from the measured path
delay differences (hyperbolic multilateration). The downlink sig-
nals at 1.2 or 1.6 GHz are modulated by pseudo-random binary
sequences for the delay determination. Orthogonal sequences are
used for each satellite. The bandwidth is 10 MHz. In addition
the satellites also transmit information on satellite ephemerides,
clock drifts, as well as measured and predicted data on the ionos-
phere and the troposphere. The ionospheric data may consist of
Global data on the total electron content, and readily available
data on ionspheric parameters such as to F2, MUF, etc. The tropo-
spheric data are mainly of importance for low elevation satellites,
and could consist of parameters for a surface refractivity model.

The data are collected at the ground control stations which
send them to the satellite, from where they are relayed to the

117

users. Two different modes are possible; the satellites may be transmitting simultaneously or sequentially. By simultaneous transmission a more precise timing results due to the higher stability of the satellite clocks, and uncertainties in the satellite receiver trajectories between successive transmissions in a sequential mode. On the other hand some interference between the different satellite signals are unavoidable by simultaneous transmission.

3.2.2 Advantages of a Simulation Facility

The primary application of the simulation Facility is to test the receivers (GDM's) before the actual channels are available. By using a software controlled simulation it is possible to test receivers under both average and adverse atmospheric conditions. By simple program changes it is also possible to evaluate several GPS downlink data schemes.

When the satellites are in orbit the simulator is still of great value for providing easy in-house tests, particularly for new receivers requiring down-link data that has not yet been included in the GPS system. In fact, large parts of the entire GPS can easily be tested.

It is considered imperative that the simulator is flexible, so that it can respond to advances in ionospheric and tropospheric prognostication, as well as to changes in the overall system. A hybrid approach with RF building blocks for constructing the channel is suggested with a software control of the channel parameters and part of the channel configuration.

To determine the components needed, and the software complexity, it is necessary to study the errors that can be incurred in the system.

118

3.2.3 Sources of Position Errors in the GPS

3.2.3.1 Satellite Ephemerides

If we start at the satellite, the first error source is the errors in the satellites own estimate of position, velocity, etc. These errors can be caused by erroneous distance measurements by the ground reference stations, which can be influenced by the atmosphere, clock errors multipath, and inaccurate trajectory estimates between position updates. A receiver using direct Faraday rotation information also needs an accurate estimate of the polarization of the transmitted waveform.

3.2.3.2 Clock Errors

Satellite clock errors affect the position estimates if the four satellite transmissions needed to determine the position are not completely synchronized. For the sequential transmission mode the less accurate receiver clocks can also be a major source of error.

3.2.3.3 Multipath Errors

Multipath propagation can also seriously impair the performance of the GPS. It can arise by either atmospheric reflection and refraction effects, or by ground (or sea) reflection. The effect of ground reflections can be evaluated relatively easily. If the receiver is h feet above a smooth reflecting surface, and the satellite elevation is is θ, then the differential delay of the reflected path is

$$\delta = 2h/c \sin \theta, \qquad\qquad (286)$$

119

where c is the velocity of light. Due to the 10 MHz PRN signal-
ling, only reflection delayed less than 100 nsec will affect the
estimate (this assumes a linear matched filter receiver, for re-
ceivers with nonlinearities, e.g. hard limiters, larger delays
will also have a significant effect). Thus only atmospheric
multipath and low ground multipath is important.

One way of estimating the delay is to use a threshold 6 dB
down from the peak output of a matched filter. The errors re-
sulting from a 50 nsec delayed perfect reflection is illustrated
in Fig. 16, assuming an ideal triangular signal auto-correlation
function. With a reflection coefficient of .8, corresponding to
a 14 dB multipath fading, calculations have shown that errors
range between -33 feet and +11 feet.

If a hard limiter is used in front of the matched filter, and
if only one satellite signal is received at a time, the error is
smaller at small delays, but persists for delay almost as long
as the entire duration of the PRN sequence. However, this way
errors less than 7 feet can be obtained with a threshold 12 dB
below the peak of the matched filter output. For this type of
receiver, large delay multipath should be simulated when applic-
able. For most other receivers, delays less than 100 nsec are
sufficient to test the performance against multipath.

3.2.3.4 Ionospheric Propagation Effects

The refractive index along the signal path causes excess
delays. The main error is incurred in the ionosphere, where the
refractive index can be related directly to the electron density.
For frequencies well above the gyro- and plasma frequencies of the
ionosphere (as is the case here, these frequencies are of the order
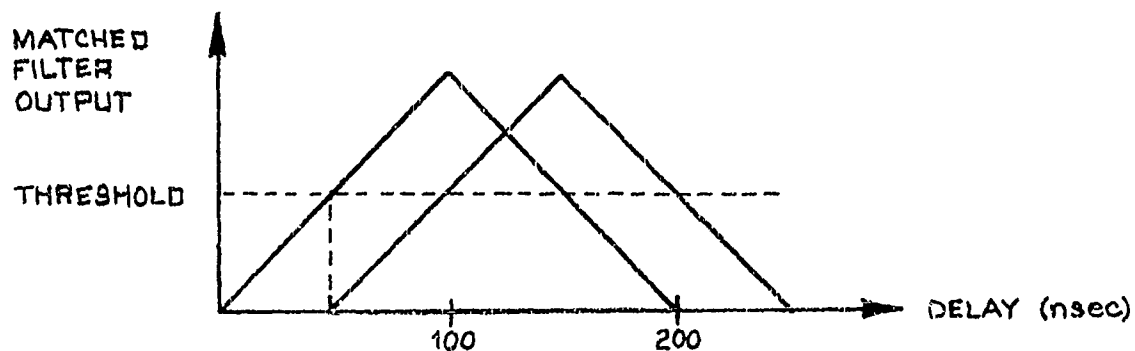
(a) Direct and Reflected Signals.
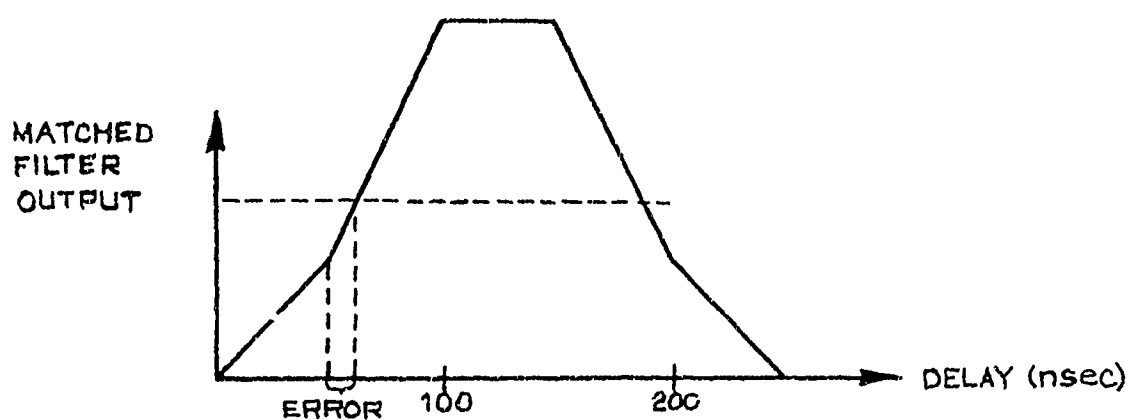
(b) Signals Adding In-Phase,
     Resulting in a 10 ft. Error
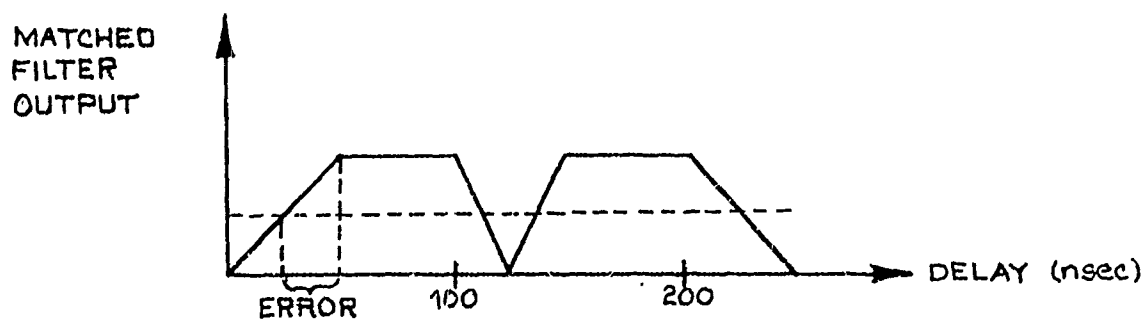
(c) Signal Adding Out of Phase,
     Resulting in a -25ft. Error

Figure 16 Matched Filter Multipath Effects

121

of 1 - 10 MHz) we can ignore the influence of the geomagnetic
field and electron collisions. The refractive index n is given
by

$$n^2 = 1 - \frac{f_o^2}{f^2} \qquad (287)$$

where f_o is the plasma frequency, and f the transmitting frequency.
We have (in rationalized MKSA units)

$$f_o^2 = \frac{4\pi e^2}{m} N(h) = 80.7\ N(h), \qquad (288)$$

where e and m is the electron charge and mass, respectively, and
N(h) is the electron density as a function of height. The maximum
value of N(h) determines the critical frequency of the F2 layer,

$$N_M = 1.24 \times 10^{-2} \times (f_o F2)^2. \qquad (289)$$

The integral of N(n) along the signal path is called the total
electron content (TEC), and can be related directly to the propa-
gation delay due to the ionosphere,

$$\tau = \frac{1.34 \times 10^{-7}}{f^2}\ TEC. \qquad (290)$$

Typical values for the total vertical electron content are in
the range of 10^{16} - 10^{18} electrons/m^2 for f = 1.6 GHz. This
corresponds to delays in the range of .5 - 50 nsec. The delays
at the lowest elevation (5°) can be 2 to 4 times as big.

The ionosphere also introduces a differential Doppler shift,
mainly due to the deviation of the signal path from the geometric
path. This Doppler shift can also be related to the electron density,
but only approximately to the total electron content.   The Doppler

shift is relatively small and can potentially improve the position accuracy of a receiver utilizing this information.

Faraday rotation information can also be useful to a receiver, since it provides information about the TEC. As a first order approximation, the following expression is often used,

$$\Omega = \frac{2.97 \times 10^{-2}}{f^2} \times \overline{M} \times TEC, \qquad (291)$$

where $\overline{M}$ is an average quantity depending on the angles the path makes with the magnetic field, and vertical.

Aside from the delay, Doppler, and Faraday rotation effects, the irregularities of the ionosphere causes a flat fading of the received signal (scintillation). The statistics of scintillation are fairly well studied, and prove quite easy to simulate. We shall not dwell much more on this aspect of the problem here.

3.2.3.5 Tropospheric Propagation Effects

Normal tropospheric effect can be calculated by using a model for the standard atmosphere (Altschuler and Kalaghan, [5]). Typically, the range error are 7 feet with a 90° elevation, and 80 feet with a 5° elevation. Under adverse weather conditions, this can be considerably worse, especially at low elevations where the signal may have to travel through a rain or snow storm over a fairly large distance. The troposphere also introduces a small Doppler shift.

3.2.3.6 Other Error Sources

Of the many remaining error sources we mention the additive
noise (cosmic noise, receiver noise, etc.) which can have drastic
effects on the range accuracy, especially during deep signal fades,
or when a satellite is near the sun as see from the receiver. Also
interference from other GPS satellites, and man-made interference
has to be taken into account.

3.2.4 Corrective Procedures to Reduce the Error

The errors discussed in the previous section consist of a
predictable error bias and a random component. By eliminating or
reducing the bias term in the receiver, substantially better range
accuracies can be achieved. It is therefore important that the
simulator produces both the predictable and unpredictable components,
such that a realistic performance results, whether the receiver
removes the predictable component or not. Since it is not clear just
how much a particular receiver will be able to predict, it is im-
portant that the simulator is easily modified. Thus a software
approach is called for.

3.2.4.1 Satellite Ephemerides and Clock Drift

Errors in these parameters will be controlled by relaying
the appropriate information directly to the user on the down link
data stream. The satellite Ephemerides are accurately tracked by
the satellite and the ground control station, as is the satellite
clock. The receiver clock is less critical in most cases. It is
estimated that the clock errors and the errors due to satellite
ephemerides can be held to 5 feet each.

3.2.4.2 Multipath Corrections

Although serious multipath is expected to occur only a
fraction of the time in the overall system, certain environments
will be associated with persistent multipath propagation. As
pointed out in Section 4.3, such multipath conditions can result
in relatively large errors. The smart receiver will then use an
adaptive equalizer, adaptive antenna, or simply a tilted antenna
nulling out the specular point of reflection (this can be done
if satellite and receiver position are known with respect to the
reflecting surface).

3.2.4.3 Ionospheric Models for Single Frequency Users

The low cost medium accuracy users are expected to receive
just the 1.6 GHz signal, and correct for the ionospheric delay
using a locally generated model. We discuss some proposed models
and the time scales that can be expected in the residual errors.
The Bent model (Bent et al., [6]) uses a large amount of measured
data to construct an empirical ionosphere model. This model con-
sists of three exponential top side layers, a parabola near the
F2 maximum, and a bi-parabola for the lower ionosphere. The
profile is determined by predicted values of the following param-
eters: The critical frequency f_oF2, the height of maximum density
h_m, the half thickness of the bottom side layer y_m, the half thick-
ness of the topside layer y_t, and the decay constants k_i for the
lower, middle and upper topside exponential layers. Corrections
using this model are reported to result in root mean square residual
group delay ranging from 1 to 20 nsec, and mean residual delay between
-4 and 17 nsec. The cumulative probability distribution of the

delays is calculated in the above reference, as well as some station-station correlation. Generally 70 to 90% of the day time ionosphere is eliminated.

A simple model was developed at AFCRL (Klobuchar and Allen, [7]), which computes the TEC estimates from measured predicted values of f_oF2. The use of this algorithm is limited, but gives good results when applied near the data gathering station.

The Applied Physic Laboratory of John Hopkins University (Pisacane et al. [8]) considered three algorithms, one based on long term predictions, and two capable of real time corrections. The basic algorithm is based on an 11-parameter model using parabolas for the E, F1, and F2 layers. The second algorithm is an analytic model describing the deviations from the first model, while the third algorithm is an empirical model, also based on the first al-gorithm. For the data considered, the typical time delays are on the order of 10 to 50 nsec, 86 nsec being the largest vertical time delay encountered. The RMS residuals range from approximately 0 to 20 nsec, with algorithm II being consistently better than algorithm III, which again is better than algorithm I. Several cumulative distributions of the rms residual delays are presented, as well as station-station correlations.

A Stanford University model (Waldman and da Rosa, [9]) use an empirical expansion of the electron content as a function of time, season, and an index of solar activity. The data from the reference stations are interpolated to give the local TEC estimate. The inclusion of real time measurements are suggested in a second model. Typical vertical time delays encountered range from 5 to

50 nsec. while residual rms errors found are 1 to 20 nsec. The cumulative distribution of the residuals are calculated.

The University of Illinois (Rao et al., [10]) considers several methods for correcting the ionospheric delay. Mainly near real time measurements, and varying amounts of past data from other stations are used. In all, eight models are considered, of which two are chosen as representative. With the simple model, residuals up to 10 nsec are found, while 7 nsec is typical for the more sophisticated model. Distributions of residuals are calculations under various evaluation conditions.

3.2.4.4 Other Ionospheric Corrections

The best way of correcting for the excess ionospheric delay is to utilize the fact that the delay is inversely proportional to the frequency. By transmitting two frequencies it is possible to eliminate the trans-ionospheric delay completely, at least in theory. Errors result mainly from the facts that the two frequencies do not follow the same path, and deviations from the inverse square law. The frequencies used for the GPS are 1.2 and 1.6 GHz, and it is estimated that ionospheric effects can be ignored completely by this method. The disadvantage is the cost of the receiver, since twice as many correlations are needed. This method is therefore only to be used for high precision users where cost is not a primary factor.

There is also the possibility of measuring the Faraday rotation of the received waveforms. This is also costly to implement for simultaneous satellite transmissions, and does not take into account the part of the electron layer outside the bulk of the geomagnetic field. This approach only has merit by a sequential

127

transmission mode, and requires detai.ed attitude data on the
down link.

3.2.4.5 Tropospheric Corrections

In the troposphere model developed at AFCRL (Altschuler and
Kalaghan, [5]), the range corrections are calculated as a
rational function of height, elevation and surface refractivity.
In the case of unknown surface refractivity, average values are
determined from an empirical formula depending on height, latitude,
and calendar month.

Standard deviations of the residual delays are found as
6.75 nsec (83.8 nsec total delay) at a 5° elevation, and .6 nsec
(7.9 nsec total delay) at a 90° elevation.

3.2.5 Short Term Variations in the Atmosphere

It is important for a realistic simulator to take the time
variations of the channel into account, since it will affect both
the correlation procedure and position estimates for a receiver
using smoothing of past delays (as implemented by a Kalman filter,
for instance). Few data are available at this moment, so we study
here mainly the available results on the sources of such time vari-
ations. Many of these results can be found in standard ionospheric
texts, such as Al'pert [11] and Davies [12].

The slow diurnal and seasonal variations are usually pre-
dictable, but the change that occurs at sunrise and sunset often
is associated with rather steep gradients, giving rise to large
residual errors (slowly varying). Other slow hard-to-predict
variations are associated with solar flare, sudden magnetic com-
mencement, sudden soxmic noise absorption, etc. The time scale is
relatively large, and therefore not important to the present con-
siderations.

128

Other regular slowly varying effects are steady winds, atmospheric rotation, and tidal waves. Somewhat smaller time scales are associated with irregular winds, where typical parameter are

wind velocity   70 m/sec
correlation time   100 min or less
vertical scale   6 km
horizontal scale   100 km

Small periods are also encountered in connection with internal waves in ionosphere, which propagate at frequencies below the Väsäilä frequency

$$\omega_g = \frac{g}{C} \sqrt{\gamma - 1}, \quad \gamma = \frac{C^2}{gH}, \tag{292}$$

where g is the gravitational accelleration, C the velocity of sound, and H the scale height ($= kT/mg$). Periods are approximately 5 min. in the E region, and 10 to 15 minutes in the F region. These waves are often associated with the experimentally found traveling ionospheric disturbances (TID).

Even smaller time scales are found for diffusion and ion-production, -recombination, and -attachment processes. Time constants down to a few tenth of a second can be found.

Some experimental data on the variations of the excess ionospheric delay have been reported by Misyura et al. [13]. Measuring fluctuation in Faraday rotation and differential Doppler shift, they find that the auto-correlation function is well approximated by an expression of the form

$$K(\tau) = e^{-\alpha \tau^2} \cos \gamma \tau \tag{293}$$

129

the typical correlation time is 8 to 20 sec, and the corresponding
vertical scale is approximately given by

$$X = \tau V_{sat} \frac{h}{h_{sat}} , \qquad (294)$$

where V_{sat} is the satellite horizontal velocity, h the ionosphere
height (average) and h_{sat} the height of the satellite. This is
based on a simple model of ionospheric irregularities.

3.2.6 The Effect of the Receiver Type on Simulator Complexity

It is clear that a complex receiver also requires a complex
simulator. A two-frequency receiver requires twice as many channels
as a single frequency receiver, and a receiver measuring Doppler
shift requires the inclusion of random frequency offsets. We
classify here the receiver types, and discuss the corresponding
requirements on the simulator. The discussion is not intended to
exhaust all possible configuration, but only as a guide to determine
the necessary simulation setup. The main point is that a highly
flexible simulator is a must.

1) A receiver measuring distance only, without much concern
    for velocity or high accuracy, will use little smoothing
    of the measured delays. Hence a simple single frequency
    model is sufficient, and time-variations can be ignored.
    Often the tropospheric effects are negligible, and need
    not be simulated.

2) If the receiver measures distance only, and uses a
    Kalman or constant-gain filter to update position and
    velocity, it can be important that short term variations
    are included in the simulator model.

130

3) A high precision receiver using delay and Doppler measurements, complete with filtering to estimate position and velocity, will require simulation of Doppler shift also, and short term time variations may have to be included.

4) A high precision receiver using two frequency reception is complicated mainly by the added channels needed. If the frequencies are transmitted sequentially, time-sharing is possible, however.

5) A medium precision receiver using single frequency delay measurements with ionospheric and tropospheric corrections can improve its accuracy considerably by using the information from its inertial navigation system. All measurements can be converted to position and velocity estimates using a Kalman filter. This requires a rather sophisticated simulation since errors in the inertial guidance system has to be simulated.

3.2.7 A Summary of the Simulator Structure and Requirements

For the purposes of the simulator, we shall assume that the satellite RF ranging signals are available without down link data. Also a synchronization signal is available for modulation of the down link data. The general structure of the simulating facility, as operation in conjunction with the GDM, is shown in Fig. 17. Depending on the desired channel information, the computer may deliver down link information to the satellite signal modulators, and general information to the GDM, such as local time and any atmospheric information that would be locally available to the receiver. It can also provide simulated receiver trajectories and inertial guidance outputs. The down link signals are passed through the individual channel simulators. The most complex configuration is when two frequencies are received simultaneously from all four satellites. Eight channels are needed then. The

131
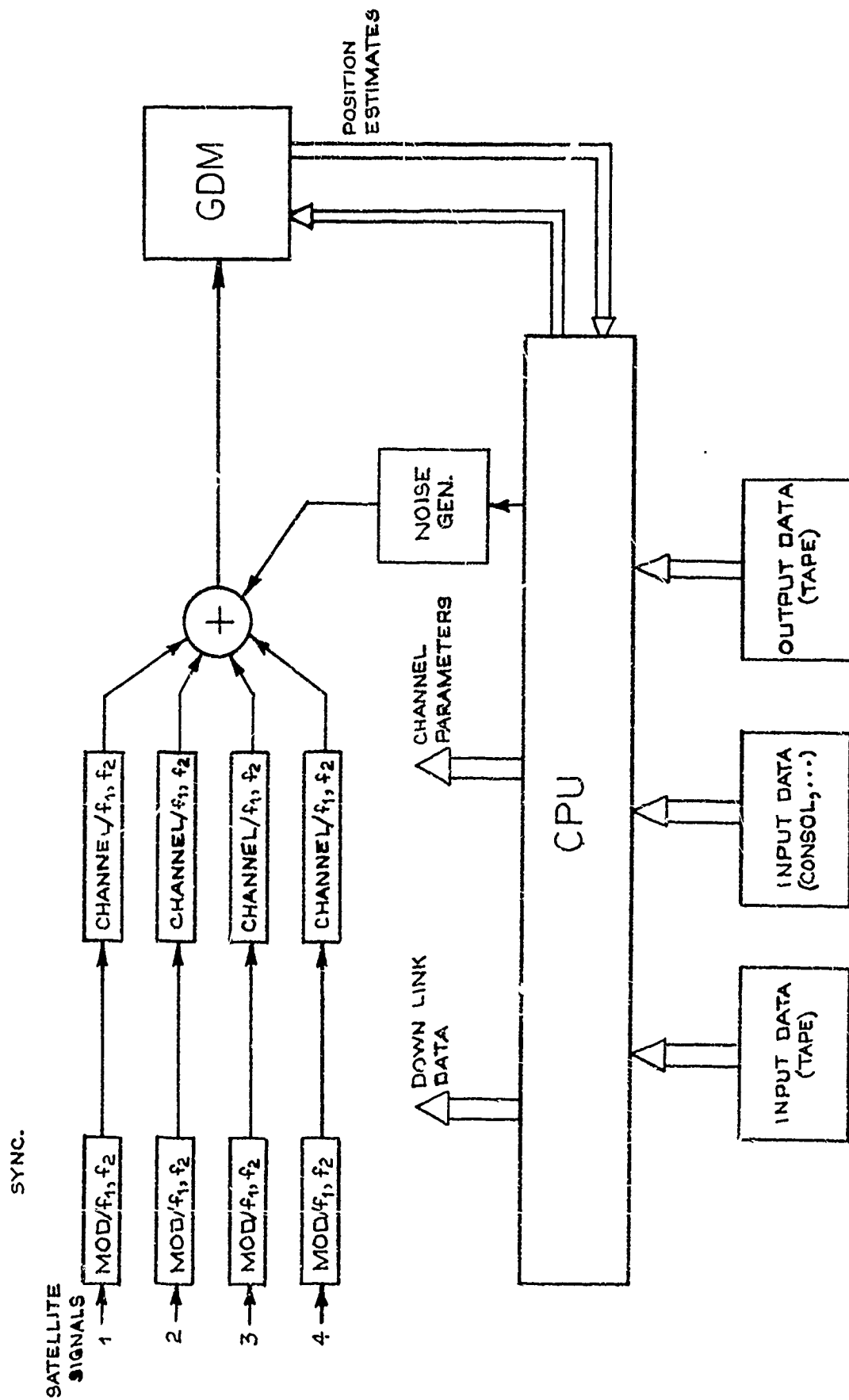
Figure 17. General GPS Simulation Scenario

132

simplest configuration is the case of single frequency reception and
sequential transmission. In this case only one channel and one
signal modulator is necessary. Thermal-noise is added, assuming
(unrealistically) that the additive noise is independent of the
direction of the signal.

The position and velocity estimates may be analyzed directly
by the same computer, in real time, or may be recorded together
with the pertinent channel and satellite data for off-line analysis.
The data supplied to the channel may be from a locally generated model
atmosphere, or may consist of actual recorded data of the total
electron content. The information needed can include

- Satellite trajectories and velocities.
- Satellite Powers.
- Uncertainties in satellite trajectories.
- Hour, day, month.
- Ionosphere model parameters.
- RMS of ionospheric delay residuals reduced to vertical.
- Time scale of residuals.
- Troposphere model parameters.
- RMS of tropospheric delay residuals.
- Time scale of residuals.
- Additive noise power, may be different for each
  satellite.
- Receiver longitude, latitude, and height.
- Receiver velocity, or trajectory.

The structure of each channel is illustrated in Fig. 18. The
parameters needed are
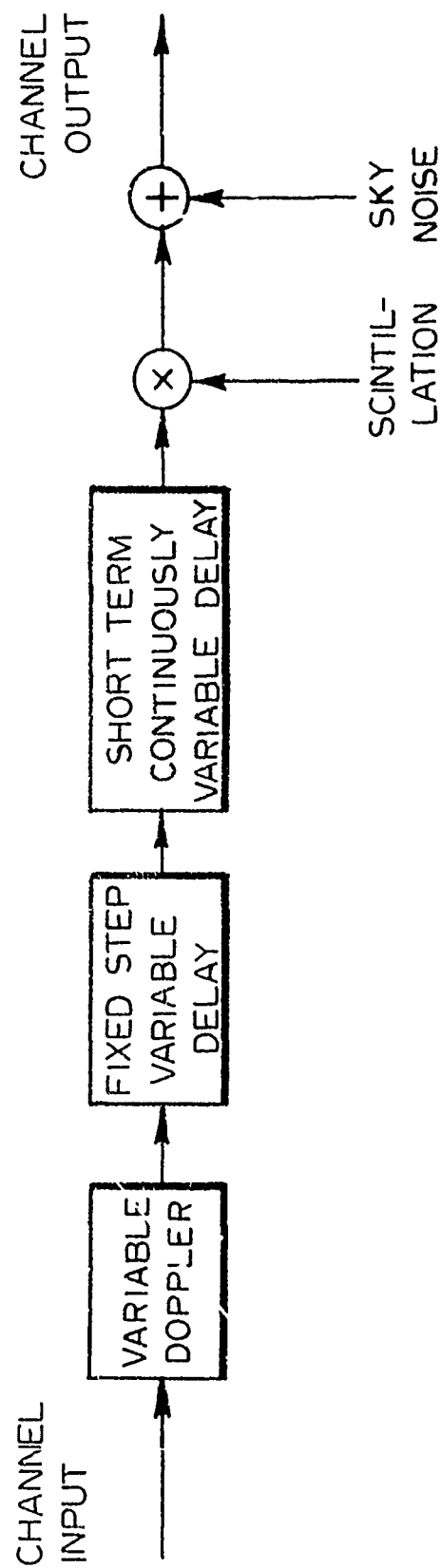
Figure 18. General Channel Structure

- Doppler shift

- Gross delay

- Short term delay

- Scintillation index

- Scintillation spectrum (probably fixed)

- Sky noise power (may be lumped into
   receiver noise).

The simulator shown does not include the multipath effect that can arise. A relatively simple simulation of atmospheric and ground multipath can be included by inserting a 2 to 3 tap delay line after the summation in Fig. 17. This ignores the fact that the different satellite signals do not suffer from the same multipath effect, and a uniform bias will be introduced in all the range estimates. An equally simple, and more meaningful, method is to introduce multipath in just one channel. Of course, a completely realistic simulation requires independent multipath effects on each channel, and dependent on the satellite elevation.

3.3 Specific Problems of GPS/GDM Simulation

In Section 3.2 we presented a general discussion of the GPS system, with the purpose of defining the necessary simulator features. This was accomplished for several possible system configurations and receiver strategies. Due to the general nature of the problem only the global features of a simulation facility were considered. This section extends the analysis to consider

- expected GDM receiver structure

- simulator integration into AFAL/CSEL

- use of CSDL/4-SV Satellite simulator

135

- application of new techniques developed at SIGNATRON for constructing delay lines with computer controlled variable delay

- GDM antenna assembly simulation

- stabilization of clock-controlled Satellite-receiver delays using a digital feedback link

- simulator hardware and software requirements.

While the section contains a detailed analysis of these aspects, at this point we will summarize its contents, and bring out the most important aspects of the problem.

In Sections 3.3.1 through 3.3.3 we discuss various aspects of the simulation requirements, concluding in Section 3.3.4 in a summary of several methods of implementation, alternative configurations, and possible compromises. The best system configurations are selected after the software and hardware requirements are treated in Sections 3.3.6 and 3.3.7. The alternative configurations are based on new techniques developed in Section 3.3.5 for controlling and creating the required delays. The following discussion centers around the system configurations shown in Figs. 19 and 20.

Figure 19 shows a block diagram of the simulation facility configured so that all signals, at both L1 and L2 frequencies, are generated with independent satellite signal generators. Eight such generators are needed. Each signal generator consists of a digitally controlled frequency synthesizer, exciter, and up-converter. The frequency synthesizer forms the unmodulated base-band signal (~ 10 MHz) with appropriate Doppler, and the carrier frequency Doppler at a 70 MHz intermediate frequency. The exciter modulates the IF carrier with externally supplied code signals superposed with down link data. A 70/560 MHz up converter assures the applicability of the CSEL exciters. We have based

136
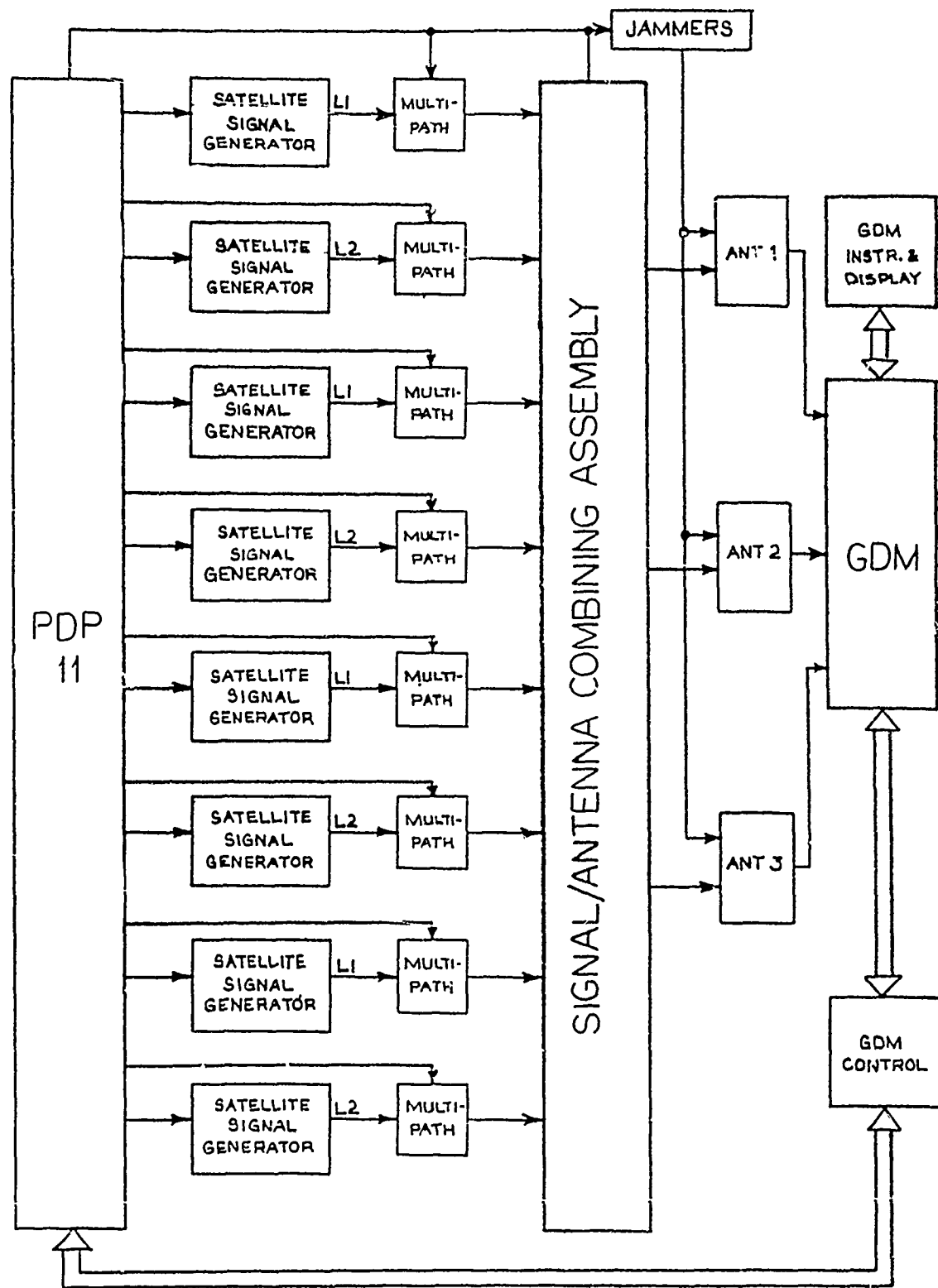
Figure 19. GPS/GDM Simulation Facility, Alternative 1.

137
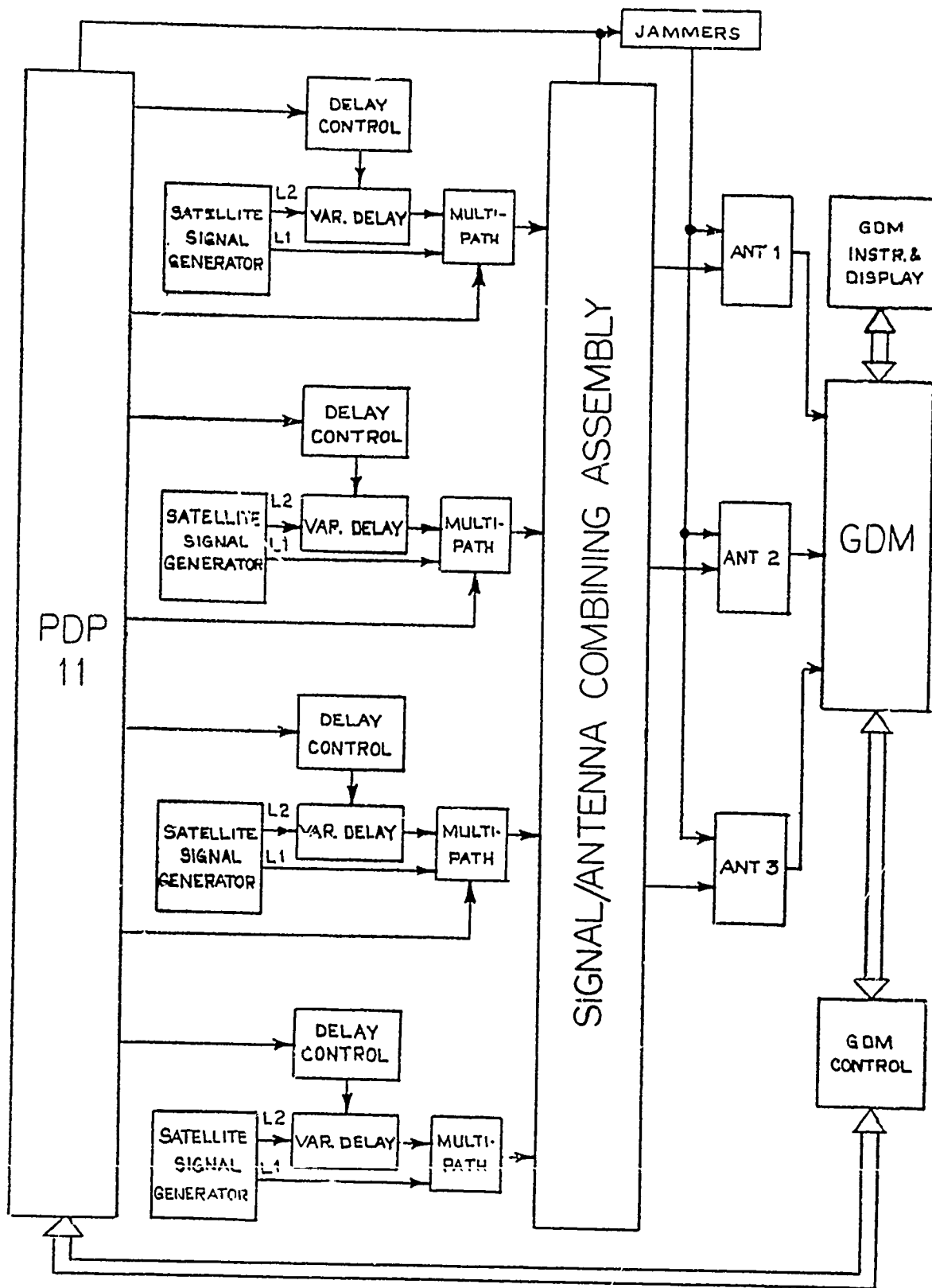
Figure 20. GPS/GDM Simulation Facility, Alternative 2

our analysis on the frequency synthesizer structure developed
at the Charles Stark Draper Laboratories, and shown in Fig. 21.
The specifications of the synthesizer accuracy are shown in
Table 17.

Since the synthesizer supplies the appropriate Doppler
shifts to both the carrier and the modulation, it is possible
to achieve the required differential satellite-receiver delays
by adjusting the Doppler. This Doppler has to be pre-computed
very accurately since a deviation of the desired delay from the
actually achieved delay will not be corrected, thus limiting
the duration of the simulation due to accumulating delay errors.
This phenomena is analyzed in Section 3.3.5.1, and the theoretical
errors seem acceptable. However, under practical circumstances
several factors not accounted for can result in inaccurate delays.
Hence, a technique is suggested which will close the loop and
immediately correct delay errors. This technique, described
in detail in Section 3.3.5.2, consists of directly measuring the
delay on the baseband signal before carrier modulation, com-
paring it with the desired delay, and using the error to cor-
rect the Doppler. The technique is relatively inexpensive to
implement since it is almost all digital. Use of it simpli-
fies the initial set-up of the system, and allows for arbitrary
long simulation runs.

The multipath in Fig. 19 requires a variable delay unit.
Several simple ways of implementing such a unit, under direct
computer control, are presented in Section 3.3.5. We shall not
discuss this unit in detail here. However, the method illus-
trated in Figs. 32 thru 34 appears very promising. The number
of multipath units to be used depends on how precise a simulation
is desired of the more critical propagation conditions, and also
on the practical limitations in providing the antenna with the

139

Figure 21. Dynamic NAVSTAR Frequency Synthesizer,
as Developed by CSDL.

140

TABLE 17. DYNAMIC NAVSTAR-FREQUENCY-SYNTHESIZER
OUTPUT-WAVEFORM PERFORMANCE GOALS
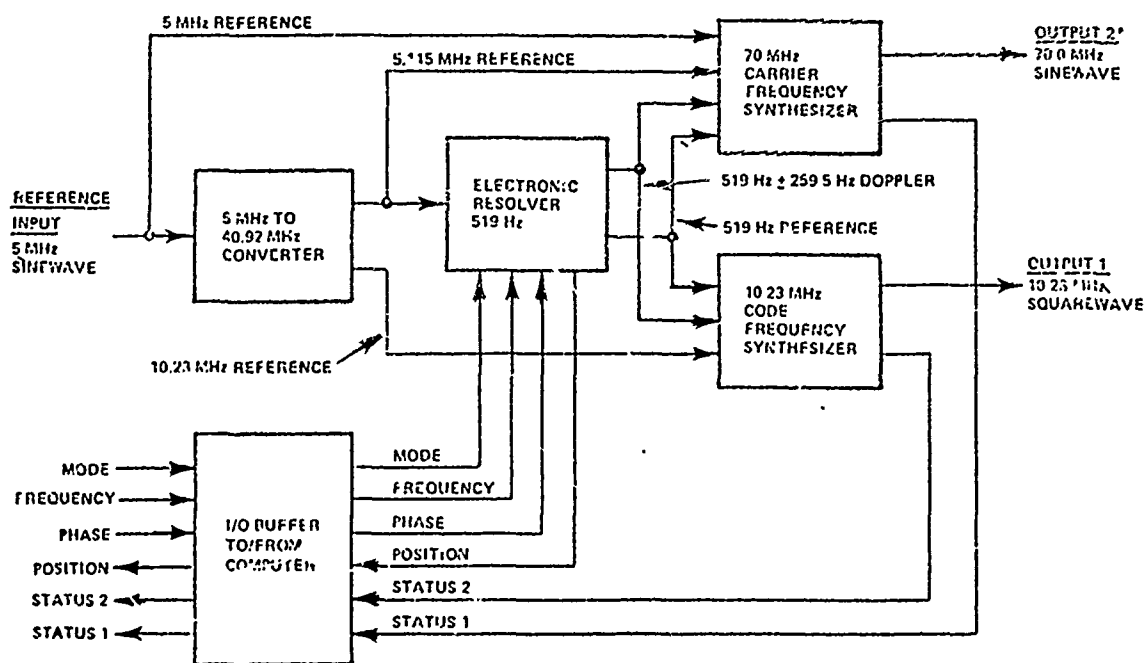
	10.23 MHz CODE SQUAREWAVE	70.0 MHz CARRIER SINEWAVE (TO BE HETERODYNED TO 1.57542 GHz)
AMPLITUDE	TTL squarewave	+7 dBm into 50 Ω
DOPPLER SHIFT	0 ±259.5 Hz in 2^{22} steps of 0.124 mHz	0 ±39,961 Hz in 2^{22} steps of 19 mHz (corresponds to a minimum resolution of 0.01 ft/s at 1.57542 GHz).
PHASE RESOLUTION	One part in 308 of a full cycle (0.3 ns)	One part in 256 of a full cycle.
PHASE STABILITY	$\leq$1 - ns rms in a 100 Hz Bandwidth over the simulation interval ($\leq$1 ns corresponds to a position uncertainty of $\leq$1 ft)	One part in 64 rms when measured in a 1 Hz bandwidth over a measurement interval of 1 s (one part in 64 is equivalent to 0.01 ft at 1.57542 GHz. When measured over a 1-s interval, this permits resolution of 0.01 ft/s).
MAXIMUM FREQUENCY RATE (ACCELERATION)	3.25 Hz/s	500 Hz/s (this is approximately a 10-g acceleration).
MAXIMUM NUMBER OF CHANGES IN FREQUENCY IN 1 s	100	100

141

correct signals. This last task is indicated in Fig. 19 by the

block named 'Signal Antenna Combining Assembly'. Realizations

of this assembly are discussed in Section 3.3.5.4, and the preferred

implementation is shown in Fig. 22 for a 3-element antenna.

It uses four-way combiners plus attenuators and phase shifters

to simulate the antenna pattern. The complexity of this assembly

suggests the option of using an omnidirectional antenna as a com-

promise in the simulation. Other alternatives, such as providing

part of the signal at IF or digitally, are discussed in the

main body of the memo. L-band jammers are available in CSEL.

The simulation is controlled by a computer (PDP-11) and

assisted by an independent GDM control unit. The tasks of the

computer and the GDM control are discussed in Section 3.3.6.

The alternative configuration in Fig. 20 is similar to that

of Fig. 19,   the only difference being in the use of four,

instead of eight, satellite signal generators. These generate

both the L1 and L2 frequencies, with the proper Doppler shifts

on the carriers. The Doppler on the modulation sequence is

referred to   the L1 carrier, such that Doppler control can

accomplish the desired delay of the L1 signal in the same way

as before. The L2 signal will be delayed by the same amount,

and it is therefore necessary to have a delay line for simulating

the additional delay that the L2 signal receives from the ionos-

phere. The only difference between the signal generator used

here, and the one used before, is the need for an additional

70-MHz carrier frequency synthesizer (see Fig. 21), and the

up-converters and exciters also needed for the L2-frequency

signal generator in the first approach (Fig. 19). Delay feed-

back can be used as before to stabilize the delay of the L1

signal.

142
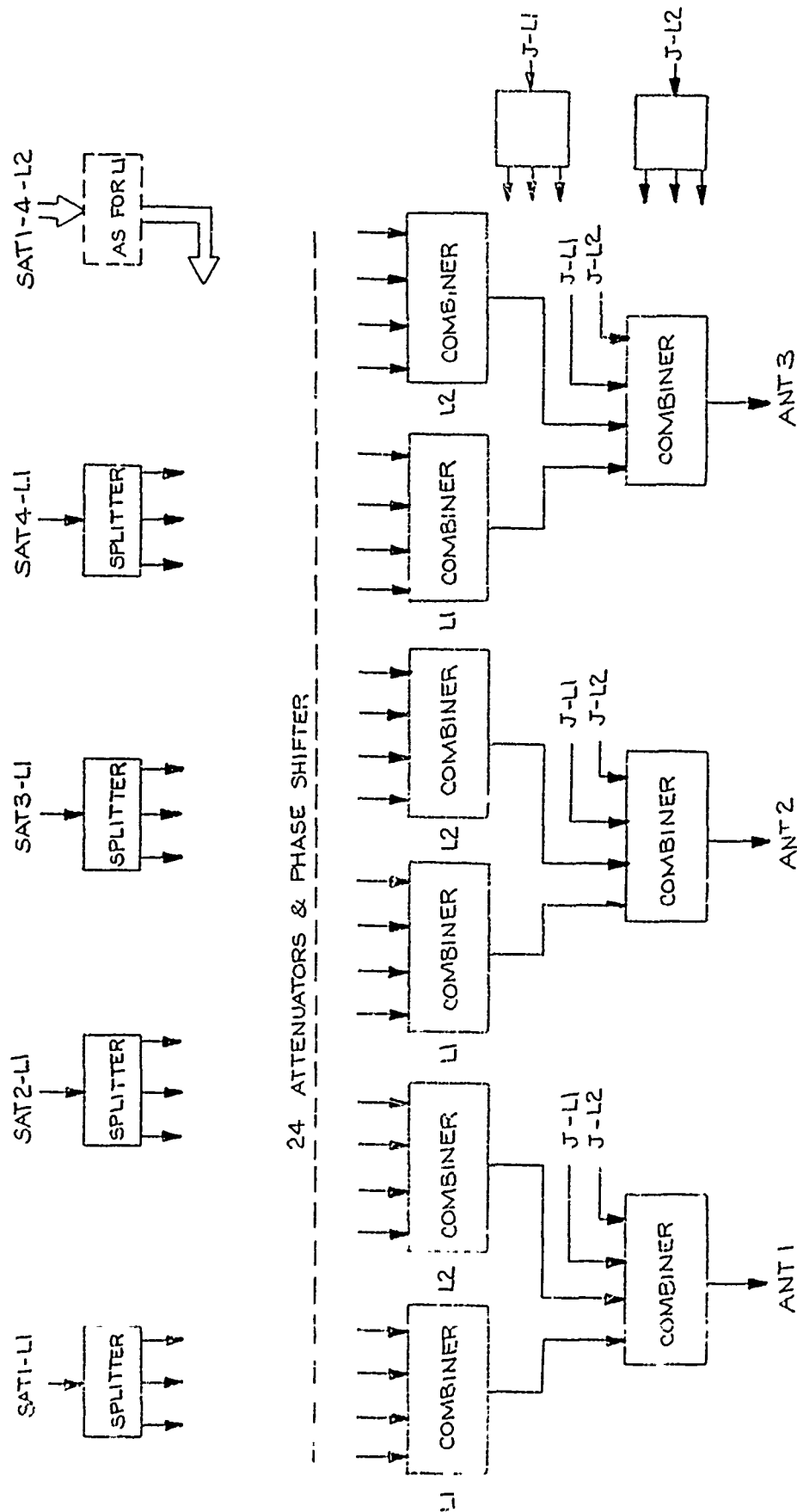
Figure 22. The Full RF Signal Combining Network

The additional delay required for the L2-signal is accomplished with a variable delay line controlled directly by the computer, as indicated in Fig. 20. The variable delay is the same unit as needed for multipath simulation, and is discussed in detail in Section 3.3.5.3. The trade-off between the two approaches lies in the difference between the cost of a frequency synthesizer (less the carrier synthesizer) and the cost of the variable delay line.

3.3.1 Background

In this study we take a direct view at the solution of the problem of simulating the NAVSTAR/GPS environment, with the purpose of testing the Generalized Development Model (GDM) receivers. This solution is based on available information on the projected GPS format, the proposed functions of the GDM receivers, and the maximum use of existing equipment in the AFAL/CSEL simulation facility. It is also assumed that a frequency synthesizer is available which is similar to the Dynamic 4SV Simulator designed by the Charles Stark Draper Laboratories.

In the remaining part of this section we present a brief background description of the GPS and the relevant AFAL/CSEL facilities.

3.3.1.1 A Summary of the GPS

The Global Positioning System is designed to provide worldwide high accuracy navigation data to military and civilian users. Position is determined by a hyperbolic multilateration involving four or more satellites. The user determines range and range rate for each satellite by using a 10 Mbps code modulated on the carrier.

144

The satellite will transmit both a protected and a clear code. In addition, various data are transmitted down to aid the user in determining time and improving the postion estimate. Each satellite transmits two frequencies, L1 ~ 1.6 GHz and L2 ~ 1.2 GHz. High precision users employ both frequencies for the elimination of the ionospheric delay errors, while less demanding users will only use L1, possibly combined with an algorithm eliminating part of the ionospheric delay. For this reason only the L1 carrier is provided with a clear code. Ionospheric data may be transmitted from the satellite to help the determination of the delay error.

The main data on the satellite system are listed in Table 18. Further data can be found in the review paper by Cretcher [14].

The receivers are grouped into categories of varying degrees of accuracy and complexity. The GDM receivers will be of relatively high complexity, and this means that a high precision simulation is required. Other receivers may, of course, also be tested by the same simulation facility. A description of the likely GDM features is given in Section 3.3.1.2.

3.3.1.2 The AFAL/CSEL Facilities

The Communication Systems Evaluation Laboratory was first applied to the testing of receivers designed for the LES 8/9 communication satellite links. An ordinary transmitter-channel simulator-receiver configuration was not possible since the satellite modified the signal. A simulation of the satellite was called for. CSEL was developed to test these and similar systems, primarily for jamming protection.

LES 8/9 uses UHF and Ka-band frequencies, and the majority of the available equipment work at these frequencies. For other

145

TABLE 18. GPS DATA

Orbits	Period:	12 hr circular
	Inclination:	63°
	Satellites per orbit:	8, equally spaced
	Number of orbits:	3, at 120° angles

Spacecrafts	Power:	est. 450 W
	Weight:	est. 900 lbs.
	Clock Stability	10^{-13}

Signals	L1 carrier:	$\sim$ 1.6 GHz
	L2 carrier:	$\sim$ 1.2 GHz
	Protected code:	L1, L2
	Clear code:	L1
	Code rate:	10 Mbps
	Data rate:	$\sim$ 50 bps

requirements X- and L-band equipment are also included. Since
the GPS works at L-band frequencies, we shall mainly describe
some of this equipment.

The major components of the CSEL simulation facility are

- spectrum and interference generator (SIG)
- roof top antenna facility
- satellite simulator
- computers and peripheral systems.

The SIG consists of two accessors and a jammer at L-band,
a switching network, up/down converters to UHF, X-, or Ka-band,
signal combiners, and a digital controller complex. The signals
(accessors) are generated with a random amplitude (selectable
spectrum), modulated at a rate up to 50 Mbps with BPSK or QPSK at
560 MHz (exciters), and filtered and heterodyned to an L-band
frequency, selectable in steps of 16 Hz. The signal combiners
include a switch between up-link and down-link combiners for
satellite communication applications. Each combiner has inde-
pendent amplitude control for each accessor and jammer, the accessors
are combined directly, and accessors and jammers fed to two inputs
of a four-way combiner (either uplink or down-link) with two spare
inputs. The uplink and down-link combiners have different dynamic
ranges. 700 MHz to 560 MHz conversion is available so that the
exciters can be used on 700 MHz IF signals also. The digital con-
troller complex performs the real-time digital control of swit-
ching, amplitude, frequency selection, filtering, etc.

The Ka-band roof top facility is designed for tests using
the actual satellite (with locally controlled jamming and receiver
parameters) and for pre-launch tests of the airborne system. It
consists of

147

- radome and pressurization system

- antenna pedestal with computer controlled servo systems

- a series of Ka-band antennas

- computer interface.

The satellite simulator terminal consists of a programmable signal processor (PSP) and two FFH/PN modems (Flexible Frequency Hopping/Pseudo-Noise). The FFH/PN contains a frequency synthesizer producing one of 2^{24} frequency shifts with a minimal resolution of 3.25 Hz. The frequency is modulated at a maximum rate of 1.28 MHz. This is not sufficient for applications to GPS.

The hardware is provided with extensive computer support via the digital controller complex. Direct control is furnished by a PDP 11/20 computer (16 bit words) designed to supervise most of the real time experiments. A PDP 11/45 is used as back-up and for some real-time applications requiring more speed.

3.3.2 Objectives of Simulation

The main objective of the simulation facility will be to test the contemplated General Development Model (GDM) receivers. A variety of different factors influence the scope of this problem, and these factors will be singled out in this section in order to describe the tests that can be performed.

3.3.2.1 Receiver Tests

The test of the receivers may be performed on two levels. First it is necessary to be able to track down errors and deficiencies in the many different classes of receivers that can be encountered. Second, it is desirable to have a facility which in a unified and systematic manner evaluates the performance of receivers, checks against specifications and performs an overall comparative analysis of competing systems.

With a well equipped simulation facility such as CSEL, these tests can be done both prior to, and after the launch of the satellites with considerable savings in effort. Prelaunch tests are the only way of securing workable receivers for the first evaluation of the GPS. After launch of the phase I satellites, the receivers can be tested in the simulation facility for performance with future satellite configurations, as well as future signaling formats. Even more significant is the greater ease of tracking down receiver errors due to the local control of the satellite signals. The reproducibility of experiments is equally important in this context. Thus the effect of changes made in the receiver can easily be checked under conditions that may only occur relatively seldom in the final implementation. The reproducibility is also necessary for the comparative analysis of several receivers. Jamming can be introduced quite simply without having to perform expensive experiments in the field.

In order to see the amount of features that can be tested, we now briefly discuss some aspects of the expected receiver design.

3.3.2.2 Brief Description of GDM Features

The objective of the GDM receiver series is to provide high anti-jam equipment for validation testing of the NAVSTAR GPS and identification of complexity and cost associated with meeting the high anti-jam requirement. The major functions involved in this are shown in Fig. 23.

The high performance receiver assembly is constructed as a Kalman filter using both satellite signals and auxiliary inputs to determine its position. The use of inertial components makes it possible for the receiver to keep accurate track of its position during long periods of signal loss. The Inertial Measurement Unit (IMU) may also assist in refining the navigation solution during periods of normal signal reception. A barometric altimeter can stabilize the vertical component of the inertial system. The effect of the filtering is to average over several measurements, so that a particular position estimate will depend on both past and present signal delays and accelerometer outputs. For this to work ideally, the time constants of the receiver filter should be smaller than those of the channel (including unpredictable receiver motions). It is not a priori known how this receiver will be implemented, but anything between almost completely software and almost completely hardware approaches is possible.
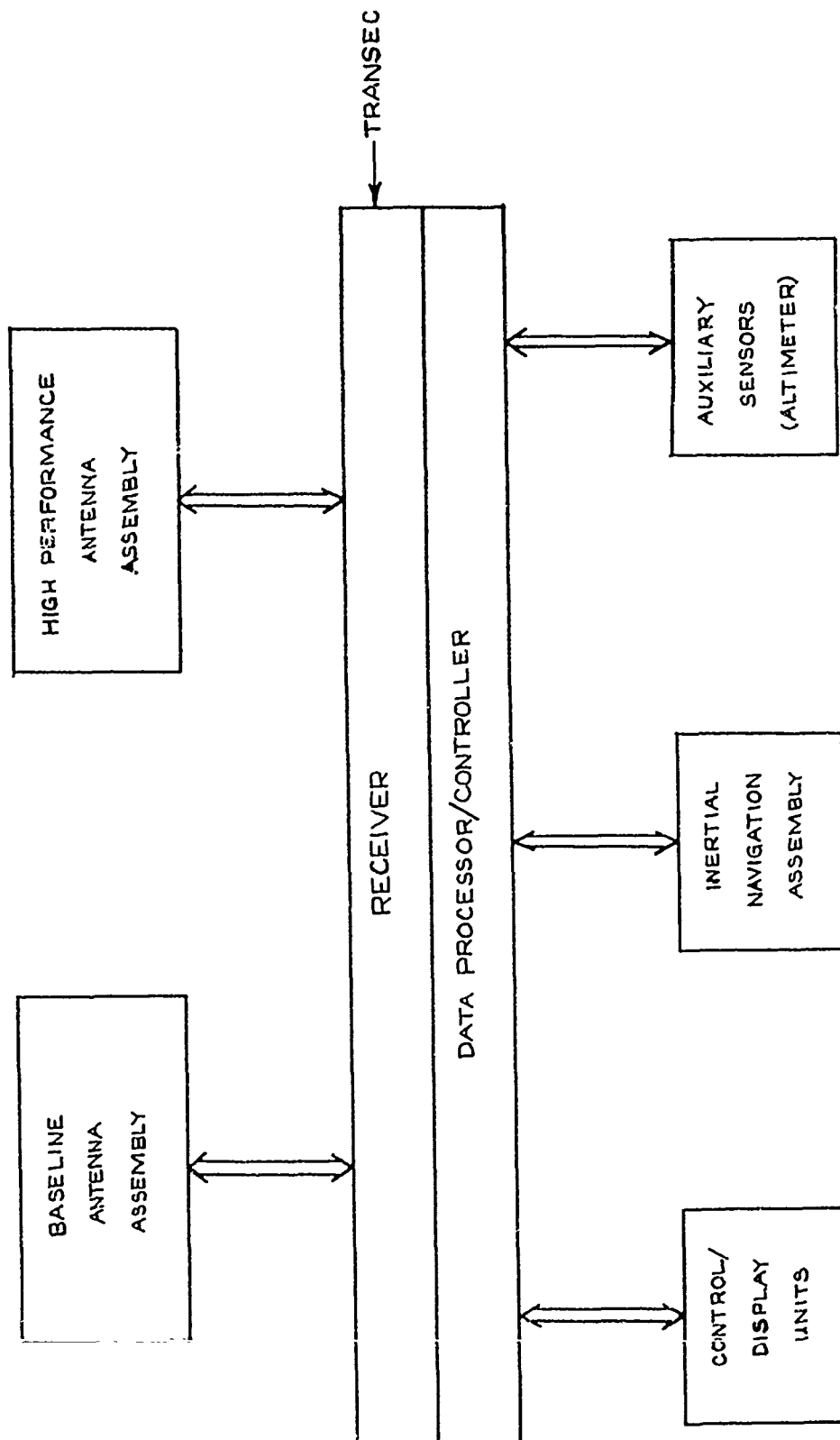
Figure 23. Functional Diagram of GDM Receiver.

The antenna system is an important part of the GDM receiver, as it is the first step in jamming suppression. The receiver is scheduled to operate with both a baseline antenna and a high-performance antenna. Both antenna systems will operate with satellites at an elevation of 5° or more. A high performance antenna may use new advanced technology, with multi-element arrays to improve the suppression of jamming and multipath. Several configurations are possible, and the antenna operation may be integrated with the receiver operation in a way to make realistic simulation difficult. However, the operation with the baseline antenna is relatively easy to simulate. The baseline antenna assembly consists of two conformal crossed slot antennas to provide hemispheric coverage and a conformal annular slot antenna providing low angle coverage. The assembly may provide only one, two, or three RF inputs to the receiver. Therefore the antenna can be included in the simulation, and RF input provided directly at the input to the preamps.

The receiver will be able to operate in several modes all of which may be tested by simulation. The primary GDM receiver models are determined by combinations of several factors.

- 4 to 5 satellite signals received simultaneously
- 2 satellite signals received at a time
- L2 signals only received sequentially, L1 signals simultaneously
- L1 & L2 signals received
- L1 only
- inertial signals utilized
- altimeter measurements used
- ionosphere model used (L1 only)
- troposphere model used.

In addition, the system may operate in several secondary modes,

- Receiver self-test.
- Inertial system ground alignment.
- Inertial system in-air alignment
- Inertial navigation only.
- Initial acquisition.

The receiver shall satisfy requirements for initial signal acquisition, reacquisition, and synchronization recovery under specified conditions of jamming and vehicle motion. The degree to which these requirements are satisfied can be tested by the simulation.

3.3.2.3 Satellite Effects

The signals transmitted from the satellites contain both ranging waveforms with a low sidelobe auto-correlation function, and binary data with information on the satellite's position, velocity, clock, attitude, as well as ionospheric and tropospheric data. This information may be transmitted on either of the two carriers L1 $\sim$ 1.6 GHz, and L2 $\sim$ 1.2 GHz.

The motion of the satellite affects the received signals, creating Doppler, Doppler changes, etc. For the purpose of testing the receiver, it is adequate to assume a circular orbit around the inertial center of the earth. It will be practical to simplify this trajectory further and approximate it by small piecewise linear segments.

153

3.3.2.4 Propagation Effects

Another objective of the simulation is to test the response
of the GDM receiver to several important propagation phenomena.
The receiver may include software designed to correct some of the
errors induced by propagation effects, and realistic tests of
this software are needed for meaningful evaluation of the recei-
ver. We now summarize some of the effects that may be found.

The troposphere will cause errors in the delay estimate
due to a velocity of propagation slightly smaller than the free
space velocity of light. This effect is particularly pronounced
for low elevation satellites, and the tropospheric delay is there-
for to be calculated for several points of the satellite trajec-
tory, and under representative atmospheric conditions. Prefer-
ably a stochastic model should be used in order to avoid the
perfect behavior that could arise if the receiver happens to be
using the same model.

The ionosphere can introduce even larger delay errors. The
receiver can compensate for these errors in two ways. The best
is to use the two frequency reception technique, taking advantage
of the fact that the delay is inversely proportional to the square
of the frequency. Thus both frequencies need to be incorporated
in the simulation, and differential delay properly simulated
including deviat ᵒns from the theoretical formula.

The relevant theory of ionospheric delay was discussed in
Section 3.2, along with a summary of several empirical ionos-
phere models.

The atmosphere may introduce a Doppler error which is due
to the deviation of the path from the straight line between

154

transmitter and receiver. It is shown in Appendix A that this
frequency error is

$$\Delta f = \frac{f}{c} \dot{\alpha}_s (n_0 \sin \theta_1 - \sin \theta_0) R_0$$

where

$$\dot{\alpha}_s = \text{angular velocity of the satellite}$$

$$n_0 = \text{surface refractivity}$$

$$R_0 = \text{Radius of Earth}$$

$$\theta_1 = \text{incidence angle of arriving path}$$

$$\theta_0 = \text{incidence angle to the satellite.}$$

A rough calculation in Appendix A indicates that the ionospheric
Doppler can be ignored. At low elevations strong gradients in
the troposphere may cause a noticable shift in frequency, but
it will not be necessary to simulate this effect unless the
receiver is equipped to compensate for this error.

Ionospheric inhomogenities can cause fluctuations in both
delay and amplitude (scintillation) of the received signal, due
to the combined motions of the satellite, the receiver, and the
ionosphere. The time scale of ionospheric fluctuations was estimated
in an earlier memo to be on the order of seconds or longer. This
should be large enough to avoid significant effects on the recei-
ver dynamic filters. In addition the rms fluctuation of the electron
density is believed to be so small (10^{11} electrons/m^3 estimated by
Booker, [15], out of approximately 10^{15} electrons/m^3) that the cor-
responding delay fluctuations can be ignored.

Scintillation at the frequencies involved is relatively small
as it generally follows an inverse power law with frequency.
It is convenient to describe the scintillation in terms of the

155

m parameter of the Nakagami m-distribution. This parameter can be related to the various scintillation indices. The variation with frequency is

$$\log \frac{m_1}{m_2} \Big/ \log \frac{f_1}{f_2} = \eta_m. \tag{295}$$

The spectral index η_m ranges from 2 to 4, with the most likely value around 3. The m-parameter at 1.2 to 1.6 GHz can be over 1000 resulting in only a few percent scintillation. Thus it may not be necessary to include this effect either.

Multipath can result in much deeper fades and significant delay errors. The order of magnitude of delay errors that can be expected were analyzed in a previous memo for a receiver of the passive matched filter type. Similar errors can be expected for an active filter receiver. Since the multipath will also induce erroneous Doppler shifts, it is clear that some multipath capability should be included in the simulation facility.

3.3.2.5 Jamming Tests

The simulation facility should provide for various kinds of jamming tests, such as CW, pulse, and repeat jamming. The effect of multiple jammers can be simulated in connection with the baseline antenna. More complicated tests of the antijam capability of the high performance antenna system might be possible using the CSEL roof-top facility and available airborne or ground band jamming transmitters.

The jamming may cause deteriorated navigation accuracy, prolonged or complete absence of initial acquisition, as well as lack of reacquisition or synchronization capability. This may occur for one or all satellites. It is for these situations that a

simulation involving the inertial system is important.

3.3.2.6 Summary of Features to be Exercised

We now collect the results of the discussions in the previous sections, and summarize the total amount of features that should, or might, be tested by the simulation. The relative importance of some of the various effects to be simulated is briefly touched upon.

1)   Selection of four satellites for best GDOP when more than four satellites can be received. This is of secondary importance for checking GDM operation, and can be omitted when the cost per satellite simulated is high. Alternatively a simple low accuracy fifth satellite can be used.

2) $r, \dot{r}$ measurements

3)   Data demodulator

4)   Kalman filter dynamics

5)   Inertial Measurement Unit errors. Important during jamming experiments.

6)   GDM computer programs, local performance estimates, etc.

7)   Sequential or simultaneous signal processing. See Section 2.2 for details.

8)   Atmospheric corrections, both ionospheric and tropospheric. Important for medium accuracy receivers using only the L1 frequency.

9)   Jamming immunity.

10) Multipath protection.

11) Operational modes.

12) Performance with partial satellite loss.

157

13) Base-line antenna assembly.

14) High performance antenna assembly. A complete test with this antenna may be too costly.

15) Initial acquisition performance,

16) Reacquisition.

17) Synchronization recovery.

18) Data recovery.

3.3.3 Requirements for a Successful Simulation

In this section we discuss in more detail some of the requirements that must be met by the individual parts of the simulator. This includes both configuration and accuracy requirements.

3.3.3.1 Satellite Related Requirements

Each satellite emits two frequencies, L1 ~ 1.6 GHz and L2 ~ 1.2 GHz. The data and protected sequence are modulated at a rate of 10 M bits/sec. It is assumed that the transmitting band-width is 20 MHz, such that the sidelobes in the signal spectrum can be ignored.

The Doppler shift introduced by the satellite can be calculated using the notation defined in Fig. 24.   The radial velocity is seen to be

$$v_r = v_{sat} \cos (\theta + \alpha)$$

$$= \frac{R}{R_s} \, v_{sat} \cos \theta. \tag{296}$$

For a 12 hour period satellite in a circular orbit, we have

$$R_s = 20218 \text{ km}$$

$$v_{sat} = 3870 \text{ m/s}.$$

158
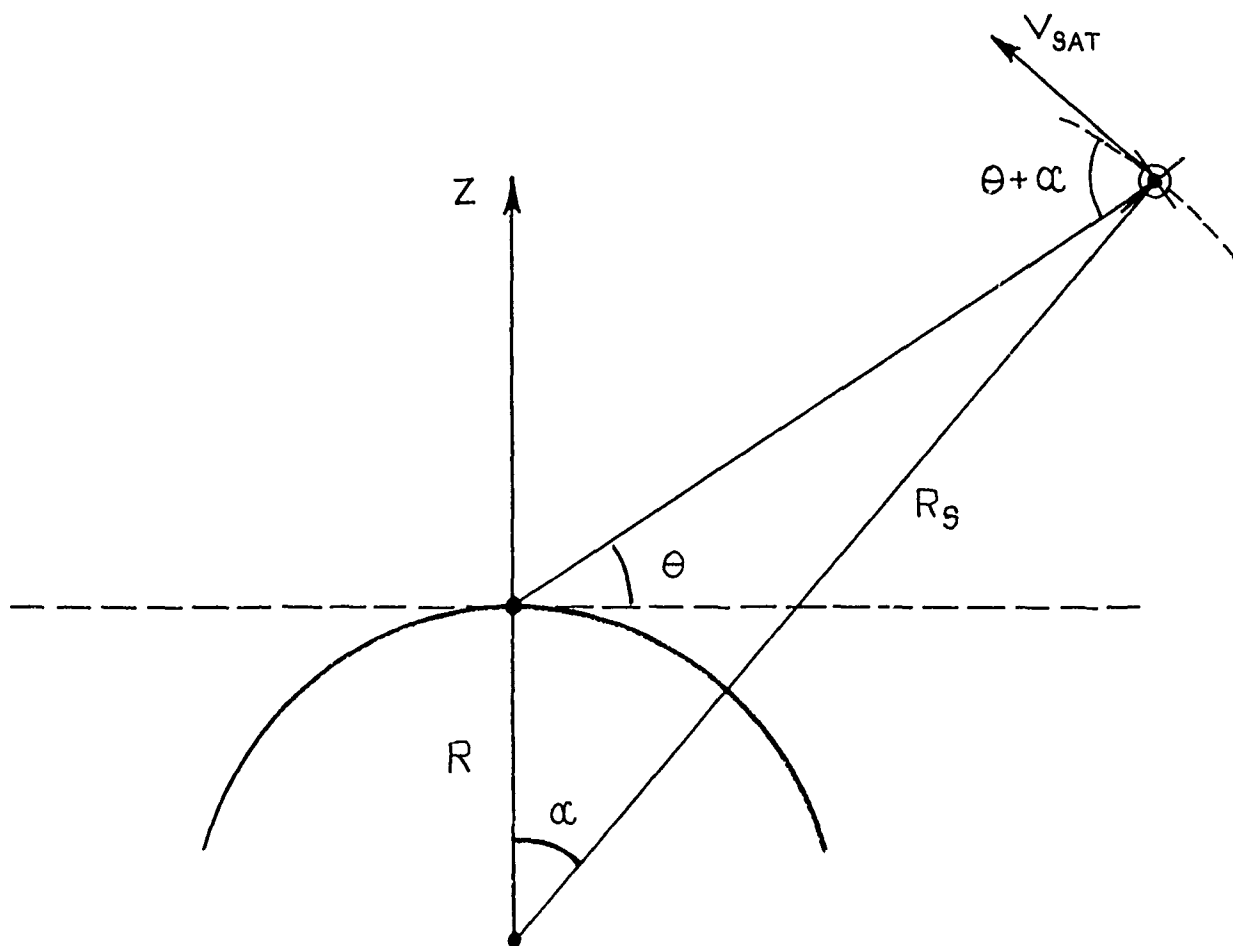
Figure 24.   Geometry for Satellite
             Doppler Calculation.

159

R is the earth radius

$$R = 6374 \text{ km.}$$

At the lowest elevation of $\theta = 5^O$, we have

$$v_r = 1215 \text{ m/s,}$$

giving a Doppler shift at 1.6 GHz of 6.5 kHz. This calculation ignores the effect of the rotation of the earth, which depends on the latitude and longitude of the receiver as well as the orientation of the satellite orbit. If the satellites follow the rotation of the earth, the above value is a worst case, if not, 10 kHz can be taken as the worst case value.

To generate the Doppler shifts a frequency synthesizer is required which shifts both the L1 and L2 carriers, as well as the modulation rate. Without going into the precise construction of the synthesizer, we can still discuss the main feature of its operation. The functional diagram is shown in Fig. 25. The synthesizer is conceived as a completely digitally controlled device, with the main input being the Doppler. Direct read-out of the phase is possible, and the current phase can be reset when desired. When only the frequency is input, the current phase is computed digitally by simply adding the binary number representing the frequency of the phase accumulator at a fixed rate. The digital phase is converted to a low frequency analog phase, which again is converted to the modulation frequency and IF or RF. The synthesizer discussion is based on a design resolution criterion of < 1 nsec delay errors, and < .01 ft/sec velocity errors.

The rate at which the frequency synthesizer is controlled determines the accuracy of the simulated trajectory. For practical

160
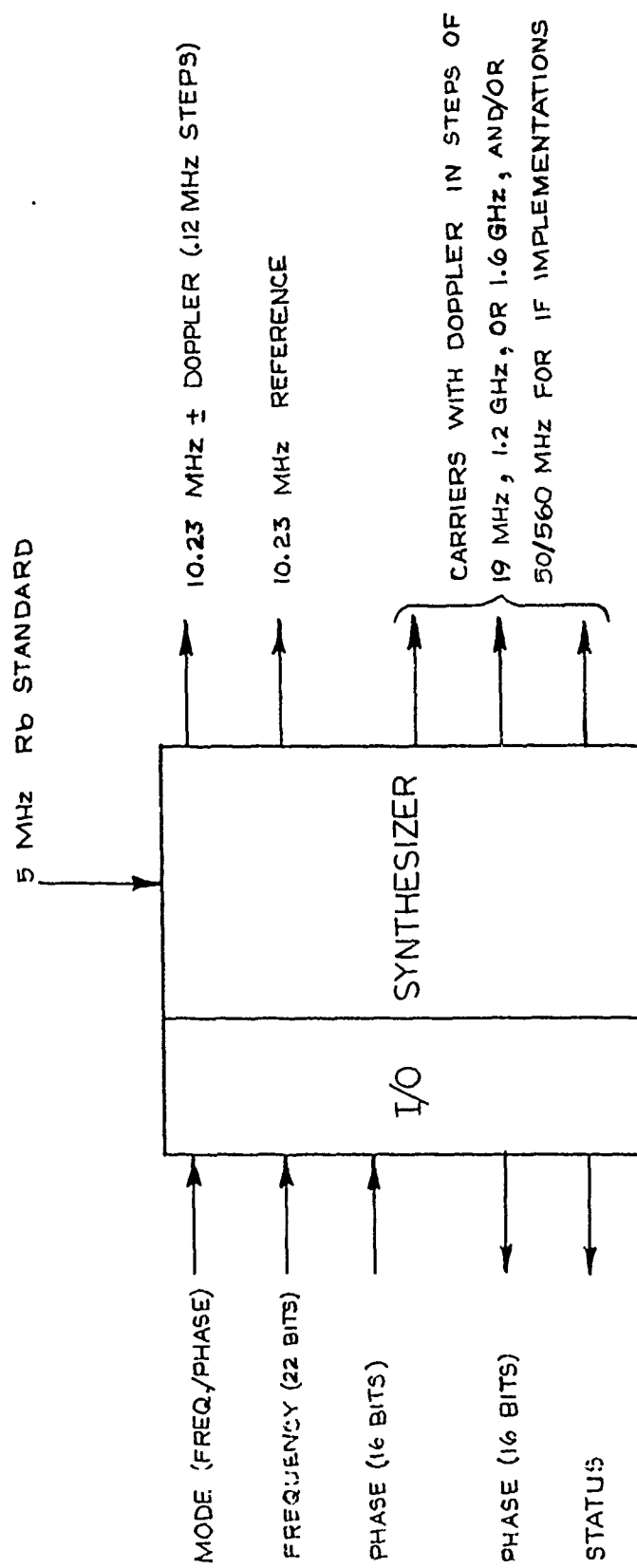
Figure 25. Frequency Synthesizer.

reasons a maximum of 100 Doppler updates per second is considered.
We can then evaluate the worst case postion errors due to
this Doppler sampling. Assuming a maximum acceleration of
10 G, the velocity may change by as much as 1 m/sec in a 10 msec
interval. This is considerably larger than the synthesizer reso-
lution, but will result in adequate trajectory representation
over several samples, as the receiver performs some averaging.
However, the successiv Doppler shifts must be carefully cal-
culated so as to average out the errors over several updates.
We shall see later that this is particularly important when
controlling the delays with the frequency synthesizer.

The update time interval chosen is of the same order of
magnitude as the maximum differential delay between two satel-
lites. Table 19 shows the delay between signals from a
satellite at zenith, and a satellite at an elevation of θ°.

TABLE 19. MAXIMAL DIFFERENTIAL DELAYS

θ	Delay, msec
0°	17.8
5°	16
10°	14
15°	12.8
20°	11
25°	9.5
30°	8.1

Thus one satellite may be updated up to two times after reception before the corresponding signal from another satellite is received. This is important for some considerations concerning delay control in Section 3.3.5.

3.3.3.2 Propagation Effects

The delay introduced by the ionosphere is discussed in Section 3.2. It was found that ionospheric delays can be as large as 50 nsec, and up to 200 nsec at a 5° elevation of the satellite. At 1.2 GHz at most 350 nsec can be expected. It was seen in Section 2 that Doppler effects in the ionosphere can be ignored.

Tropospheric delays were calculated by Altschuler and Kalaghan [5] who found delays of 7 nsec at vertical incidence and 80 nsec at a 5° elevation. In total, at most 300 to 400 nsec atmospheric delay can be expected, and this has to be calculated for each satellite with the accuracy required (1 nsec).

The path scintillation, and the sky noise (if necessary) do not require great accuracy, since reproducibility is the only important factor here.

As discussed in Section 3.2, multipath delays greater than 100 to 200 nsec need not be simulated directly, since the reflected signal appears as noise at larger delays. Great accuracy is not required in the differential delay, since the performance will not be much different at relatively close delays. The requirements are based on short delay and deep fades, and longer delays with an arbitrary phase relationship between the direct and reflected signals. Delays smaller than 10 nsec should not be necessary. Accuracy requirements on the attenuation

163

are not very stringent either; only the case of near perfect

reflection and a 180° phase shift requires some care, as it can

result in complete signal fades.

3.3.3.3 Simulation of Auxiliary Sensors

The simulator shall provide X, Y, Z acceleration inputs
to the GDM receiver, as well as barometric altitude. These inputs
may be provided directly to the GDM data processor, or via the de-
signated interfaces.

The accuracy required of the acceleration inputs may be de-
termined by the accuracy of the inertial system itself. The
maximum accuracy can be found without reference to the particular
device, however. If the accelerations are updated 100 times per
second, and a velocity uncertainty less than .01 feet/sec is
desired, then the necessary acceleration accuracy is approximately
.3 m/s^2. The inertial trajectory (i.e., as computed from inertial
input) is then approximated by sections of constant acceleration.
The accelerations needed for the simulation can be calculated as
output of a digital filter, or directly by the formula

$$q_n = \frac{r_{n+1} - 2r_n + r_{n-1}}{\Delta^2} \tag{297}$$

where Δ = .01 sec.

The altitude measurement uncertainty is given by the proper-
ties of the altimeter. It need not be given with any greater
accuracy than the system accuracy of 1 nsec., and may be orders of
magnitude larger with conventional barometric altimeters.

3.3.3.4 Antenna Effects

Some antenna effects need to be included in the simulation,
as they may have rather important consequences for the performance.
Simulation of the . gh performance antenna is not considered feasible

164

at this stage, however, so we concentrate on the baseline antenna system. The simulator supplies RF signals to the preamplifier for each antenna. It is generally reasonable to assume that the antennas are so closely spaced that any differential delay can be disregarded. If this is not the case, a short delay can be introduced using tapped coaxial cable delay lines. This complicates the combining of the satellite signals somewhat, and should be avoided if possible. It is necessary for receivers using widely spaced antennas combined with software corrections based on attitude estimates. In this case it may also be necessary to provide attitude sensors to the receiver.

3.3.3.5 Best Achievable Accuracy

The accuracy obtainable with an optimal receiver is found in terms of the Cramér-Rao bound in Appendix B. Based on a transmitter power of 450 W, a receiver noise temperature of 300° K and a distance of 12,000 km, the lower bound of the ranging error is determined as a function of the additonal gain due to the integration and the antenna pattern. The results are repeated in Table 20. With an antenna gain of 20 dB, and a processing gain of 30 dB, a ranging error of less than one foot is theoretically possible. This substantiates the soundness of the high-resolution requirements of the simulator.

TABLE 20.   THEORETICAL ACCURACY BOUNDS

Total Gain [dB]	Ranging Error [feet]
20	26
25	14.6
30	8.2
35	4.6
40	2.6
45	1.5
50	.82

3.3.3.6 Summary of Effects to be Simulated

We now list the total number of parameters included in the simulation, as emerging from the discussion above.

1) Attenuation, not critical

2) Delay, 1 ns accuracy

3) Doppler, 19 mHz accuracy

4) Scintillation, as in 1)

5) Multipath delay 0 - 200 ns, resolution not critical

7) Inertial system parameters, see Section 3.3.3.3.

8) Altitude (Barometric)

9) Data

10) Number of satellites, maximum 5

11) Jamming waveforms

12) Individual antenna input, degree of complexity depending on conditions

13) Attitude measurements (optional)

3.3.4 How to Meet the Requirements

In this section we discuss how to accomplish the tasks set out in Section 3.3.3. The main thrust is on the division of the system into IF/RF hardware, digital hardware, and software.

3.3.4.1 Tasks to be Implemented

A large amount of the tasks are inherently software oriented. This includes the computation of satellite and receiver trajectories, coordinate transformation, range and range rate calculations, as well as generating the necessary auxiliary data and parameters (inertial system, altimeter, command of GDM display systems, etc.). All of these calculations are fairly standard and computational procedures exist in most cases.

166

The atmospheric delay calculations will clearly also require software control. The ionospheric model uses pseudo ionospheric parameters, some of which may also be supplied to the receiver, either directly or via the downlink data modulation. As an example, the NASA-DBA model (Bent et. al., [6]) is specified by seven parameters

(1) The critical frequency f_oF2

(2) The height of the F2 layer (h_m)

(3) The half thickness of the bottom side layer (y_m)

(4) The half thickness of the top side layer (y_t)

(5) k_1, decay constant for lower third of top side layer

(6) k_2, decay constant for middle third of top side layer

(7) k_3, decay constant for upper third of top side layer.

These parameters are computed from generally available observations, such as f_oF2, maximum usable frequency factor, daily solar flux, running average of monthly solar flux, magnetic dip, geographic and magnetic latitude, time of day, season, etc. In addition to performing these calculations, it can be necessary to add a random term to the computed delay to avoid the GDM receiver, using the same model, calculating the ionospheric delay exactly. The tropospheric model requires similar calculations. The parameters involved were described in the previous memo on the GPS simulation facility.

The remaining tasks can be implemented in hardware. This includes

- Generation of satellite signals with Doppler shifts

- Modulation of p-sequences and down-link data

- Multipath

- Noise

- Jamming (interference)

- Construction of inputs to antenna elements

- Scintillation.

These tasks can be achieved in various IF/RF/Digital configurations which will be discussed later.

3.3.4.2 Methods of Implementation

In the most desirable system the entire simulation is performed in one on-line operation. This would permit real-time operator control of the vehicle trajectory with immediate display of the navigation performance. As a result, easier determination of worst case receiver conditions could be performed. Unfortunately, the amount of numerical computations necessary to accomplish such a task is tremendous and a practical computer capacity prohibits such operation. The software tasks are therefore divided into off-line and on-line computations. The description of these tasks is presented in Section 3.3.6 with an approximate evaluation of the complexity involved.

The items designed for a hardware implementation are treated in Sections 3.3.5 and 3.3.7. We do not discuss the implementation of the frequency synthesizer, but only the use of a synthesizer in constructing a realistic model of the channel. The main problems with the creation of a variable delay and the handling of the GDM antenna are treated in Section 3.3.5, while Section 3.3.7 contains the hardware requirements for various configurations. Some of the main alternatives involved in the choice of system configurations are

1)   IF or RF channel simulation

2)   open or closed loop delay control

3)   where to introduce jamming.

A number of alternatives causing compromises in simulation performance are treated in the next paragraph.

3.3.4.3   Compromises of the Complete Implementation

As has been mentioned earlier, the simulation of the complete GDM, including the high performance antenna assembly, may be impractical when too many antenna elements are involved. We shall therefore restrict ourselves to consider use of the baseline antenna assembly only. This leaves us with the baseline simulator configuration in Fig. 26.   Of course, this does not necessarily mean that the high performance antenna cannot be included if it only has a few elements.

It will be seen in Section 3.3.5 that even the baseline antenna can require a large amount of RF circuitry due to the several antennas and their directional patterns. At the cost of a less informative simulation this can be reduced by

a)   Consider omnidirectional antennas and ignore individual fading.

b)   Use of only one antenna element in the transfer of the signals to the GDM, and supply the GDM with the information necessary for neglecting the remaining elements.

A major contribution to the cost of the simulation facility is the need for eight frequency synthesizers to represent the two-frequency transmissions from the satellites. With an alternative method discussed in Section 3.3.5, four frequency synthesizers
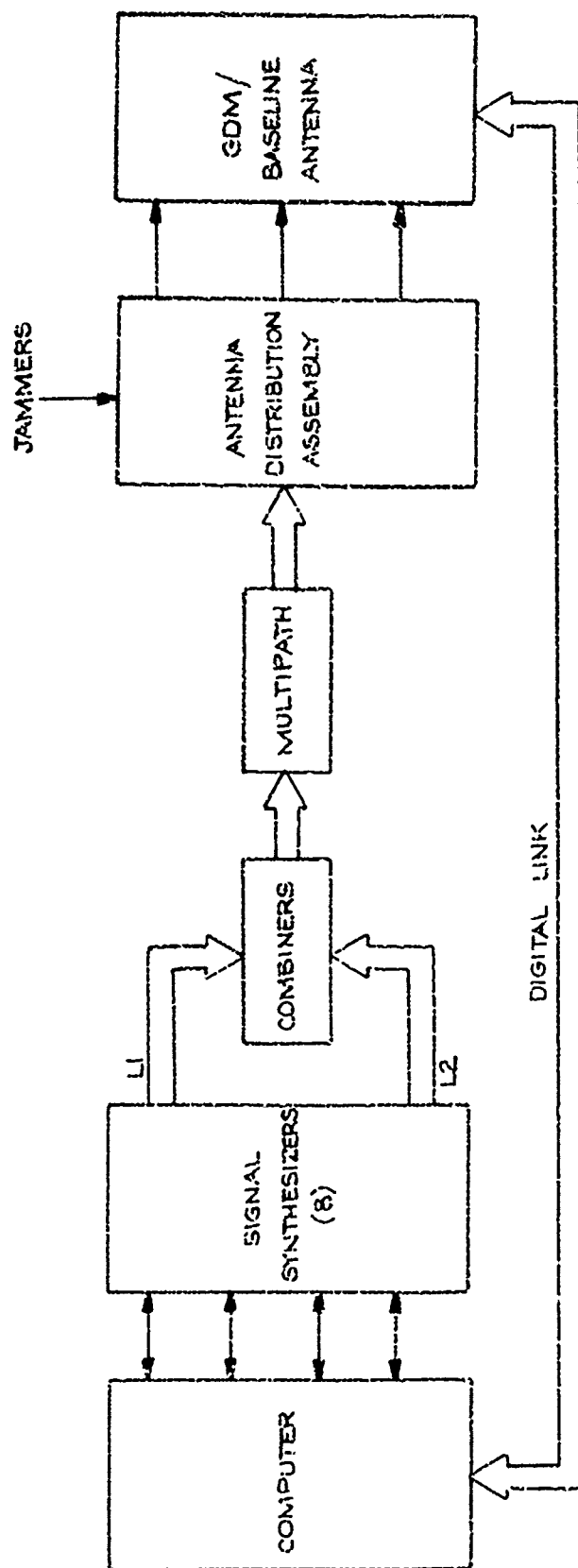
Figure 26. Baseline Configuration of Simulation Facility.

and four variable-delay lines are needed. A substantial reduction
of hardware requirements can be achieved by only testing the range
and range rate performance on a single satellite-receiver path.
The configuration is sketched in Fig. 27. In this approach only
one channel is simulated in hardware, and the rest are represented
by digital links supplying the information directly to the GDM
computer. The implementations of this method requires signifcant
modifications of the GDM software and, as a consequence, can not
serve to evaluate a large part of the software performance. It
will still be possible, however, to check the K-filter operation,
the utility of inertial and auxiliary parameters, the position and
velocity computation program, GDOP performance, in fact anything
but antenna performance, pseudo-range and range rate correlations,
and GDM software efficiency.

Other simplifications include the elimination of all or part
of the multipath, scintillation, and noise capabilities, all of which
are deemed to be of secondary importance.

3.3.5 Methods of Implementing some of the Requirements

We discuss here some of the requirements that may need a
hardware implementation. Excluded is the construction of the
frequency synthesizer, as it has been treated elsewhere. The main
problem is the simulation of delays, and we will present four
methods of implementing these delays. These methods consist of
open loop and closed loop clock control, and two tapped delay line
configurations. We will also briefly discuss the construction of
the antenna inputs.
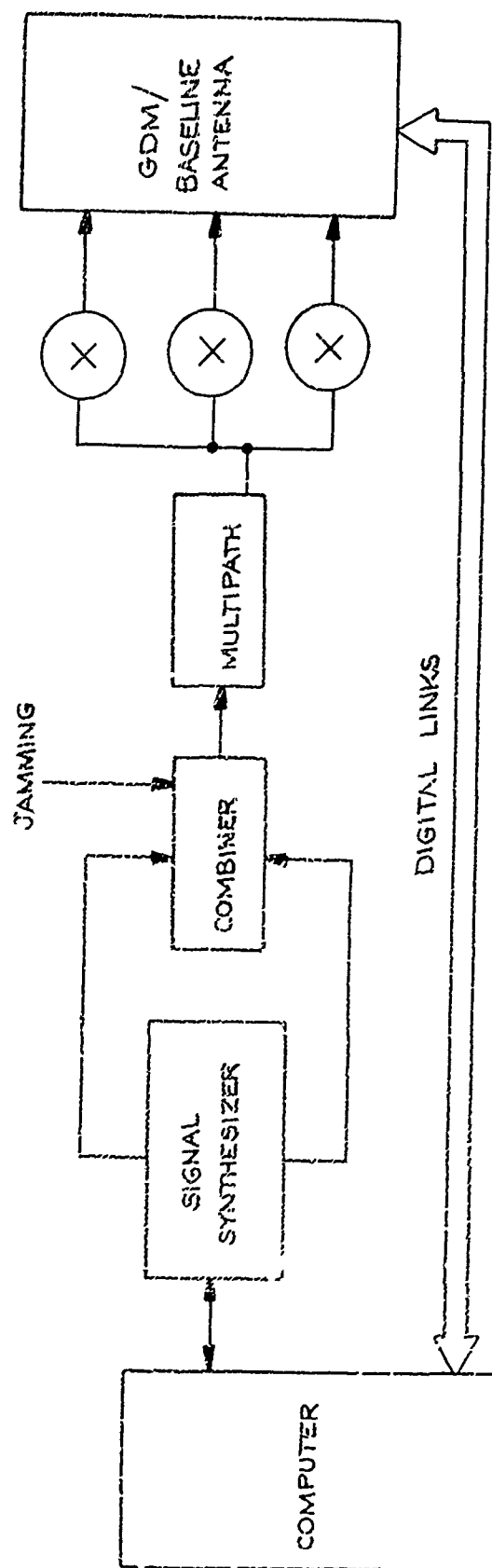
Figure 27. A Reduced Hardware Configuration.

3.3.5.1 Open Loop Clock Control of Delay and Doppler

If all satellites are controlled by independent clocks, running one clock faster than another will affect both carrier and modulation and effect a linearly increasing delay, since the receiver will receive in a fixed time more pulses from one satellite than from the other. In practice we can not expect independent clocks per se, but rather a series of frequency synthesizers as in Fig. 26.

Delays are controlled easily using these synthesizers by simply controlling the Doppler frequency input. Some errors may be introduced in this approach due to Doppler quantization and other uncertainties. We analyze first the delay errors accumulated over a given time assuming that the Doppler is stepped at intervals of $\Delta = .01$ sec and with independent quantization errors of 10 mHz.

Suppose that at time $t=T$ the carrier phase is $\omega_o(t-T) + \varphi_o$, and that at this time the frequency changes to ω_1. The phase at time t is then

$$\varphi(t) = \omega_1(t-T) + \varphi_o$$

or

$$\varphi(t) = \omega_o \left(t - T + \frac{(\omega_1 - \omega_o)}{\omega_o} (t-T) \right) + \varphi_o. \qquad (298)$$

Thus a time delay at $T+\Delta$ of

$$\tau_1 = \frac{\omega_o - \omega_1}{\omega_o} \Delta \qquad (299)$$

has been effected. The total delay after n changes in frequency is

173

$$\tau_n \ = \ \frac{\Delta}{\omega_o} \ \sum_{i=1}^{n} \ (\omega_o - \omega_i). \tag{300}$$

If the frequency changes continually, this can be written

$$\tau(t) \ = \ \int_{T}^{T+t} \frac{\omega_o - \omega(\sigma)}{\omega_o} \ d\sigma. \tag{301}$$

Let us call the Doppler offset

$$\delta\omega \ = \ \omega_o - \omega. \tag{302}$$

We consider two types of errors, namely the case of a constant Doppler offset error, and the case of independent uniformly distributed frequency errors due to random quantization errors.

Assuming the frequency resolution at 1.6 GHz is 19 mHz we have a maximum offset of 9.5 mHz ($\sim$ 10 mHz). If a constant error of 10 mHz exists in the Doppler, the error after T sec is

$$\delta\tau_{max} \ = \ T \ \times \ \frac{10 \ mHz}{f_o}. \tag{303}$$

When the center frequency is 1.6 GHz and a maximum delay error of 1 nsec is allowed, then we get

$$T \ \leq \ 1 \ nsec \ \times \frac{1.6 \ GHz}{10 \ mHz} \ = \ 160 \ sec.$$

Thus a constant frequency error of this magnitude implies that the simulation can only run 2 to 3 minutes without excessive delay errors.

The second case, which appears more likely, can be analyzed by calculating the variance $\overline{\delta\tau^2}$ of the delay error, since now it is assumed that $\overline{\delta\tau} = 0$. We have from Eq. (300)

174

$$E\left\{\delta\tau^2\right\} = \frac{\Delta^2}{\omega_o^2} \sum_{i=1}^{T/\Delta} \overline{(\delta\omega_i)^2}$$

$$= \frac{\Delta\ T}{f_o^2}\ \overline{\delta f^2}\ . \tag{304}$$

If δf has a rectangular distribution on $|\delta f| \leq f_1$, $f_1 = 10$ mHz, we get

$$\overline{\delta f^2} = \frac{1}{3}\ f_1^2\ .$$

If we allow $\sigma_{\delta\tau} = 1$ nsec, and $\Delta = .01$ sec, then the allowable time is

$$T \leq \frac{(1\ \text{nsec})^2\ (1.6\ \text{GHz})^2}{.01 \times \frac{1}{3}\ (10\ \text{mHz})^2} = 7.68 \cdot 10^6 \text{ sec.}$$

This time is so large, that errors during normal simulation can usually be ignored.

Thus only biased errors can have a significant effect, and we easily see how to eliminate any bias that may arise in the quantization process itself. It simply consists of tracking the phase, and controlling the Doppler to keep a bounded phase error. This is easily done digitally, and eliminates the bias completely.

However, there may still be errors introduced in the later analog stages of the synthesizer, and such errors will accumulate. In addition, there can be problems in setting up the initial time delay for a simulation experiment. Since the loop is not closed, errors in the initial delay will not disappear. In the next section we develop a very simple digital technique for closing the loop, thus eliminating the uncertainties left in the above scheme.

175

3.3.5.2 <u>Doppler Control with Delay Feedback Compensation</u>

The principle of the feedback loop is shown in Fig. 28. The delay with respect to a known reference is measured directly on the 10 Mbps baseband sequence before modulating it on the carrier and before filtering to remove the sidelobes. Thus in effect infinite bandwidth is available to measure the delay, and high accuracy is possible. The measured delay is compared with the desired delay funished by the computer, and if it is too large, a positive Doppler correction is added to the computed Doppler, thus allowing the delay to diminish. Since the feedback loop is all digital the implementation is extremely simple. It also turns out that independent clocks can be used for the Doppler updates and for the delay measurements so that the configuration is very flexible. This last feature holds when the desired Dopplers and Delays are computed according to the simple formula

$$\tau_{n+1} = \tau_n + \omega_n \Delta, \tag{305}$$

where Δ again is the period between Doppler updates. This amounts to approximating the trajectory by linear segments before applying the inputs to the synthesizer. As discussed in Section 3.3.3.1, velocity errors of 1 m/sec can then occur over short periods of time, while the average error will be much smaller.

Fig. 29 shows how the coder/delay sampler can be implemented. Both the reference 10 MHz sequence, and the satellite 10 MHz +Doppler sequence are used to drive M-sequence generators or other similar code generators. At regular intervals a segment of the reference sequence is frozen in a shift register. This shift register has to be at least as long as the shift register in the generator so that a particular segment only occurs once in the entire sequence. At the time the reference sequence is frozen, a counter

176
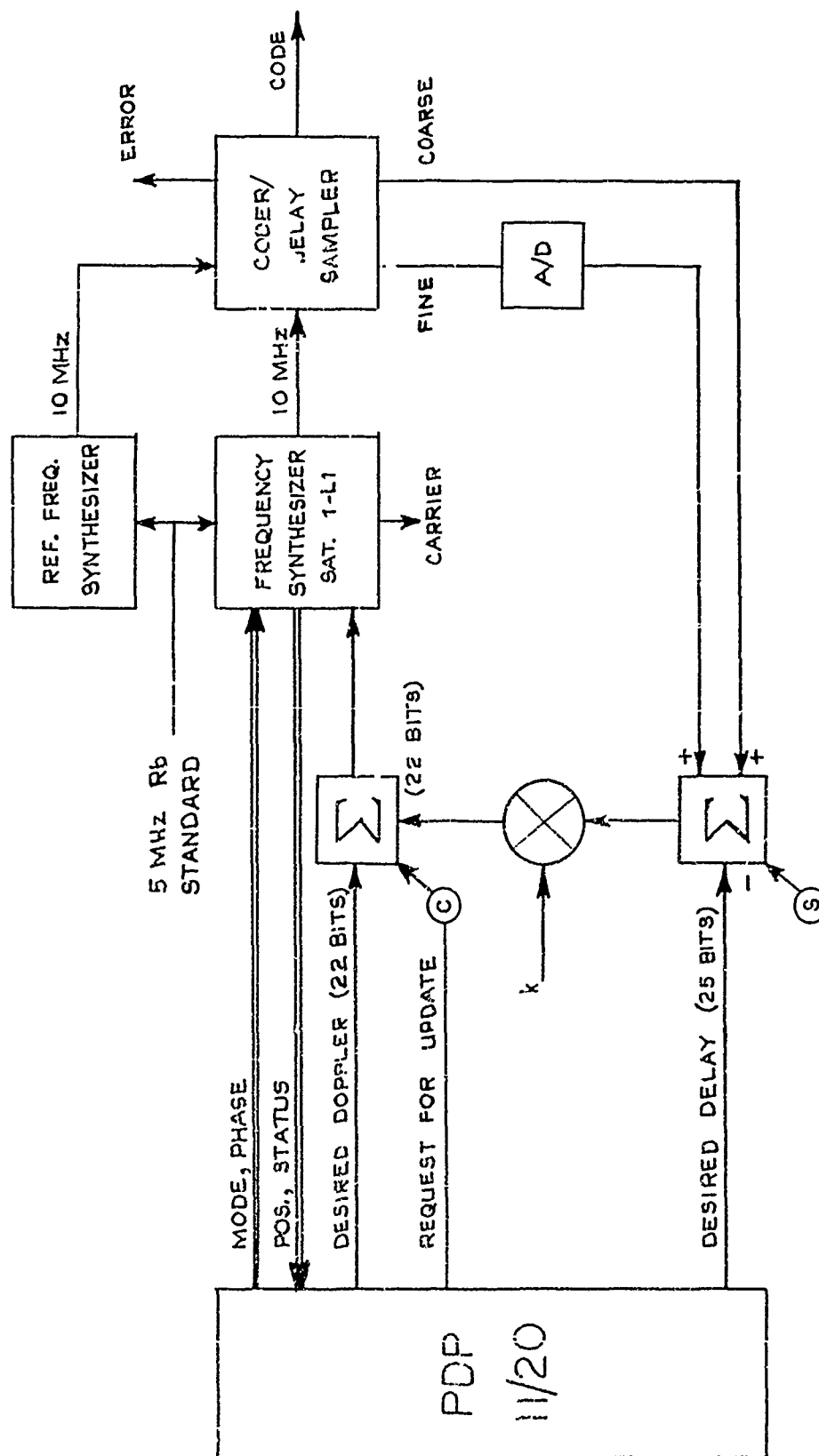
Figure 28. Automatic Delay Correction of Satellite Signals
(L1 Carrier for Satellite No. 1 Only).
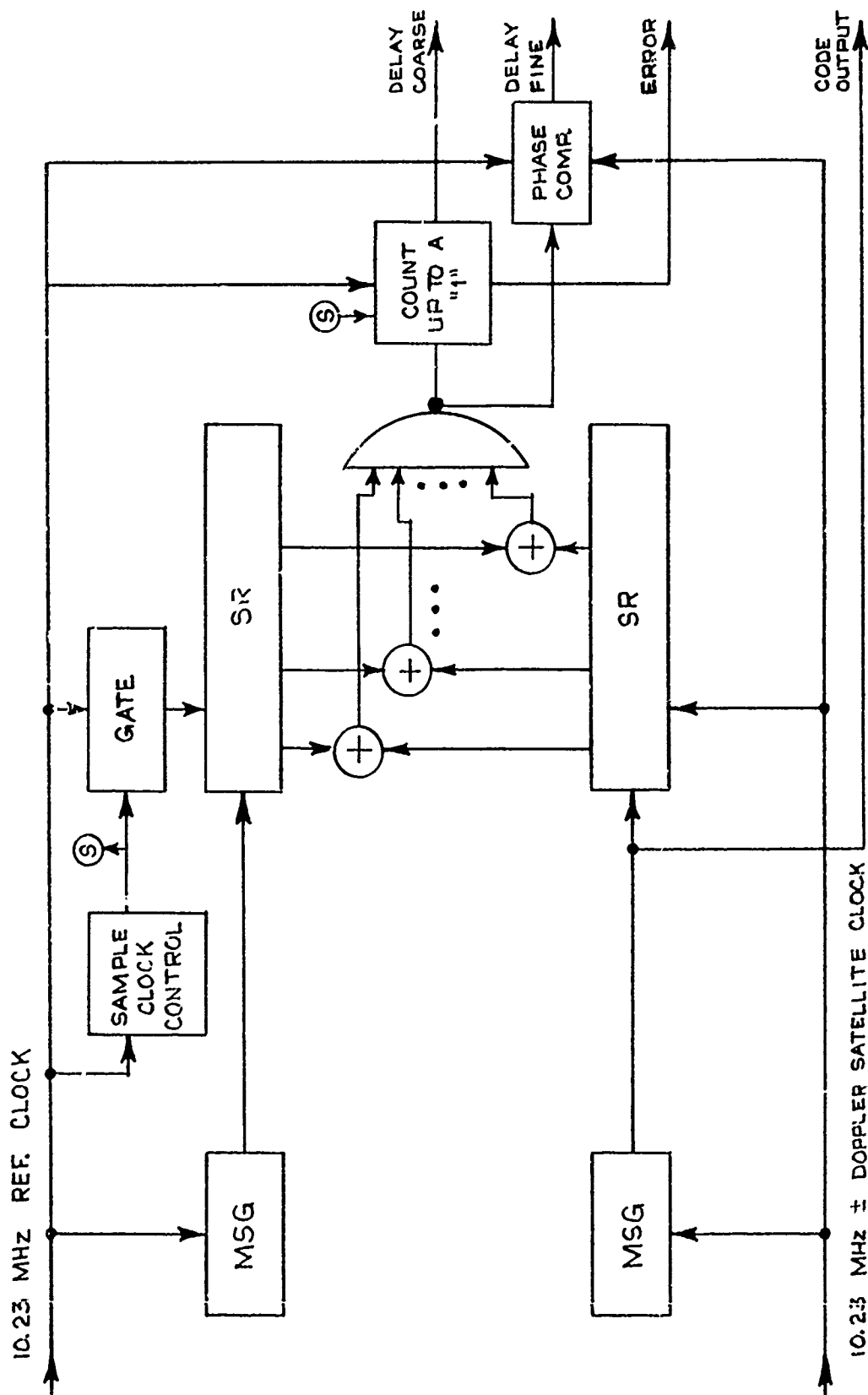
Figure 29.   Satellite Coder/Delay Sampler.

178

starts which only stops when the same segment is detected in the satellite signal. The detection is accomplished by a bitwise Exclusive-OR'ing of the two sequences, followed by a NOR'ing of their outputs. When the NOR gate output is a 1, the two shift-register sequences are identical. This will determine delay with respect to the reference to within 100 ns (coarse delay estimate). The fine delay estimate is found by measuring the phase between the two clock sequences. This is the only part of the delay sampler that may not be completely digital. It can be implemented by a simple integrator and wideband sample and hold devices followed by an A/D converter. It can also be accomplished by counting at a much higher rate, or by correlating the two clock sequences. With the last approach it is necessary to use the output of the shift register comparison to resolve the phase ambiguity. It is clear, however, that a simple inexpensive implementation can be achieved.

Since only relatively small segments are used, the relative time contraction of the two sequences will not influence the resulting estimate of the delay. The circuit in Fig. 29 can be used for each satellite and each transmitted frequency, a total of 8 times. Only the reference clock, and the related clock filling the reference shift register, is shared by all satellites.

Each satellite and frequency will be transmitting mutually orthogonal sequences. A simple way of accomplishing this is to use shifted M-sequences. A sequence generated by, say, a 33-stage shift register will not repeat itself for a period of

$$(2^{33} - 1) \times 100 \text{ nsec} = 859 \text{ sec.}$$

179
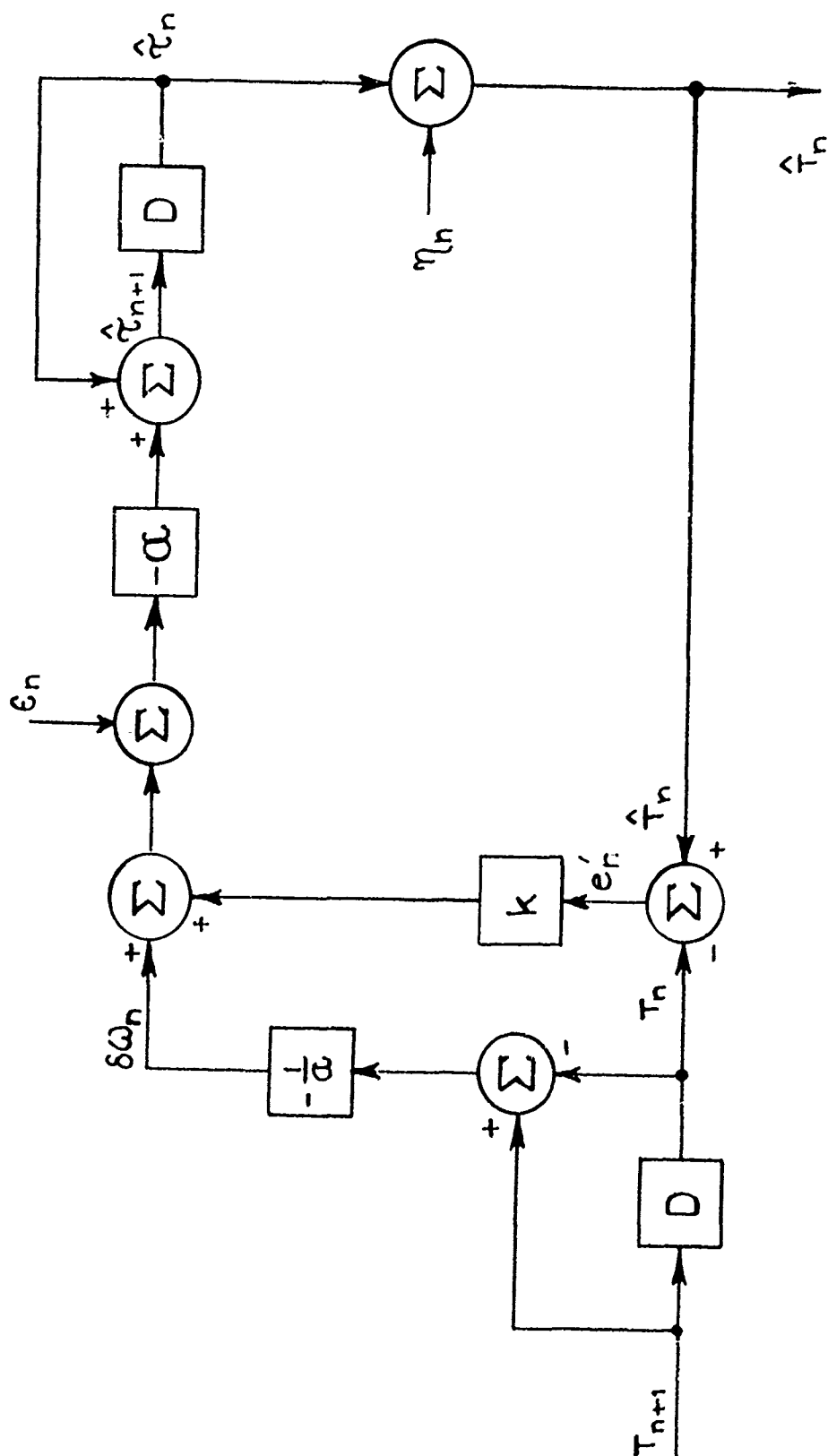
Figure 30. Model of Closed-Loop Frequency/Delay Synthesizer.

If eight shifted versions of the sequence are used they will be orthogonal over a period of approximately 107 sec, much more than needed for controlling the differential delays shown in Table 19. Although it is convenient to use an M-sequence, the circuits will work with any finite stage sequence generator, so that nonlinear secure codes can also be used. The only requirement is that the shift-registers are long enough to assure that the segments only occur once in the entire sequence.

We now analyze the performance of the closed loop system in Fig. 28. It is assumed that the desired Doppler and delay are related by Eq. (305), and it is therefore possible to model the closed loop by the circuit in Fig. 30 . The notation used in the figure is as follows. The desired Dopp' δw_n is computed directly from the desired delay's T_n. The additive error ϵ_n is due to quantization errors in both the desired Doppler and in the Doppler correction. The factor α is given by

$$\alpha = \frac{\Delta}{w_o} ,$$

(306)

where Δ is the Doppler update period. η_n is observation noise. $\hat{\tau}_n$ is the actually implemented delay while $\hat{T}_n$ is the delay observed by the delay sampler in Fig. 29. The feedback gain k is to be chosen subject to stability and accuracy requirements.

We write the equation of evolution for the closed loop system in terms of the error in the implemented delay,

$$e_n = \hat{\tau}_n - T_n,$$

(307)

181

and get

$$e_{n+1} = (1 - \alpha k) e_n - \alpha k \eta_n - \alpha \epsilon_n. \tag{308}$$

This is independent of the actual desired Doppler $\delta \omega_n$, and holds even if the delays are measured at a slower rate than the Doppler updates. The error depends only on the initial error and the uncertainties ϵ_n an η_n. The loop is stable as long as

$$|1 - \alpha k| < 1. \tag{309}$$

Assuming constant gain k and zero-mean independent errors, we have

$$\overline{e_{n+1}^2} = (1 - \alpha k)^2 \overline{e_n^2} + \alpha^2 \sigma_\epsilon^2 + \alpha^2 k^2 \sigma_\eta^2. \tag{310}$$

The steady state error for a stable system is

$$\overline{e_\infty^2} = \frac{\alpha}{k} \frac{\sigma_\epsilon^2 + k^2 \sigma_\eta^2}{2 - \alpha k}. \tag{311}$$

The value of k minimizing this error is

$$k_0 = \frac{1}{\alpha \sigma_\eta^2} \left[\sqrt{\left[\frac{\alpha^2 \sigma_\epsilon^2}{2}\right]^2 + \alpha^2 \sigma_\epsilon^2 \sigma_\eta^2} - \frac{\alpha^2 \sigma_\epsilon^2}{2} \right] \tag{312}$$

and the minimum steady state error is

$$\overline{e_{\infty,0}^2} = \frac{\alpha^2 \sigma_\eta^2}{2} + \sqrt{\left[\frac{\alpha^2 \sigma_\eta^2}{2}\right]^2 + \alpha^2 \sigma_\epsilon^2 \sigma_\eta^2}. \tag{313}$$

182

As we shall see later, however, this optimal value is not practical because it results in too long an integration time.

If the errors ϵ_n, η_n, contain a bias, the mean steady state error is

$$\overline{\iota}_{\infty} = -\frac{1}{k}\,\overline{\epsilon} - \overline{\eta}. \tag{314}$$

This shows why it is not desirable to choose k too small.

Before considering numerical examples, let us see what happens if the gain is allowed to vary. Then Eq. (308) becomes

$$e_{n+1} = (1 - \alpha\,k_n)\,e_n - \alpha\,\epsilon_n - \alpha\,k_n\,\eta_n. \tag{315}$$

For zero-mean errors it is easily found that the optimal value of k_n is

$$k_n = \frac{1}{\alpha}\,\frac{\overline{e_n^2}}{\overline{e_n^2} + \sigma_2^2} \tag{316}$$

The error variance then satisfies the equation

$$\overline{e_{n+1}^2} = \alpha^2\,\sigma_\epsilon^2 + \frac{\overline{e_n^2}\,\sigma_\eta^{\cdot 2}}{\overline{e_n^2} + \sigma_\eta^2}. \tag{317}$$

The steady state solution to this nonlinear equation is just Eq. (313). It is interesting to note that Eq. (315) suggests a nonlinear feed-back scheme which will eliminate the initial error instantly.

If we take

$$k_n = \frac{1}{\alpha}\,\frac{e_n'^2}{e_n'^2 + \sigma_\eta^2} \tag{318}$$

183

where $e_n' = e_n + \eta_n$ is the measured error, then we have

$$e_{n+1} = e_n \frac{\sigma_\eta^2}{e_n'^2 + \sigma_\eta^2} - \alpha \, \varepsilon_n - \eta_n \frac{e_n'^2}{e_n'^2 + \sigma_\eta^2}. \qquad (319)$$

If e_n' is large, then

$$e_{n+1} \sim - \alpha \varepsilon_n - \eta_n .$$

If e_n' is small,

$$e_{n+1} \sim e_n - \alpha \, \varepsilon_n \sim -\alpha \, \varepsilon_n - \eta_n .$$

The nonlinear feedback therefore reduces the error to that of observation. By using a running average of $e_n'^2$ instead of the instantaneous value, smaller errors result. For zero-mean errors the uncertainty is

$$\sigma_\tau^2 = \sqrt{\sigma_\eta^2 + \alpha' \, \sigma_\eta^2}. \qquad (320)$$

This is in contrast to the case where a constant gain is chosen which requires several measurements before the initial error is reduced. However, the steady state performance of the constant gain filter is much better.

The constant gain loop performance is mainly determined by the corresponding time constant. We shall arbitrarily define this time as the time in which the initial error is reduced by 90%, i.e.,

$$t_{10\%} = n \, \Delta,$$

where
$$|1 - \alpha h|^n = .1.$$

We now consider a numerical example. We take

$$\Delta = 0.01 \text{ sec}$$
$$f_o = 1.6 \text{ GHz}$$
$$\alpha = 9.95 \cdot 10^{-13} \text{ sec}^2$$
$$\sigma_\epsilon = 10^{-2} \text{ sec}^{-1}$$
$$\sigma_\eta = 5 \text{ nsec} .$$

The minimum steady state error is found from Eq. (313),

$$\overline{e_\infty^2} \simeq \alpha \, \sigma_\epsilon \, \sigma_\eta \simeq 5 \times 10^{-24} ,$$

or
$$\sigma_\tau \simeq 2.2 \text{ psec.}$$

Thus extreme accuracy is theoretically possible with unbiased errors, but it requires a very small value of k, and hence a long convergence time. Using Eq. (312) it is found that

$$\tau_{10\%} \sim 40 \text{ min.}$$

It is therefore necessary to consider more realistic values of k. If k is chosen such that

$$n = \tau_{10\%}/\Delta = 100,$$

$$\alpha k \simeq 2.3 \cdot 10^{-2}.$$

Then we find from Eq. (311).

$$\sigma_\tau = \overline{e_\infty^2} = 0.54 \text{ nsec}.$$

With this value of k the steady state bias in Eq. (314) can also be ignored if $\overline{\eta} = 0$, and $\overline{\epsilon} < \sigma_\epsilon$.

If the nonlinear feedback in Eq. (318) is used, immediate convergence results, but the error is limited by the observation error

$$\sigma_\tau \sim \sigma_\eta = 5 \text{ nsec}.$$

In conclusion, excellent performance can be obtained using the constant gain closed loop. The choice of the gain is mainly determined by reasonable bounds on the convergence time, which again is determined by the amount of biased error in the Doppler offset, as well as the stability of the frequency synthesizer.

3.3.5.3 Tapped Delay Line Implementations

A disadvantage of the technique in Section 3.3.5.2 is that independent frequency synthesizers are needed for all eight channels (2 frequencies per satellite). As an alternative, four synthesizers can be used, each generating both the L1 and L2 frequencies. In this way the Doppler will still be correct on both frequencies, but it will not be possible to simulate the difference between the ionospheric delays at the two frequencies. This differential delay

186

will in all likelihood be less than 150 nsec, and it may therefore be more economical to use a tapped delay line to simulate this part of the system.

The conceptually simplest way of implementing the tapped delay line is to have a long line with taps spaced at 1 to 2 nsec, and then simply switch from one tap to another as the delay changes. This is illustrated in Fig. 31. It is immaterial whether the carrier is upconverted before or after the line with this configuration. The variable delay is designed for the 1.2 GHz signal, but it will usually be performed at IF, say, a 70 MHz or 560 MHz signal directly from the synthesizer. To preserve phase continuity when the delay is switched, it is desirable to space the taps an integral number of wave lengths. The implementation in Fig.31 may require several hundred electronic switches, which may be too complicated. A method requiring fewer taps is shown in Fig. 32, where a delay is changed in steps by powers of 2. Again, phase continuity is obtained by constraining the lengths of the lines to integral multiples of the wavelength. The control of the line in Fig. 32 is also simpler since it is derived directly from the binary representation of the delay. It is necessary to switch between two delay lines at intervals no smaller than the delay, since otherwise information could get lost in the switching process. This will also avoid large delay switching transients, but will require more delay lines. It may be possible, however, to time-share the second delay line between the four satellites, since the maximum delay of approximately 200 nsec is much smaller than the rate of updating (once every 10 msec at most). An alternate method requiring slightly more complex switching circuitry and a knowledge of the next delay before the change, is illustrated in
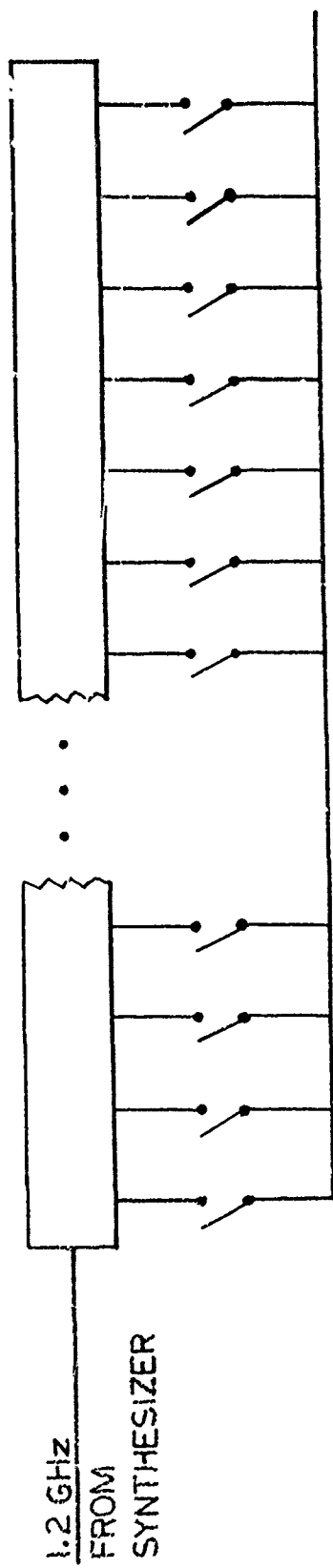
Figure 31.   Switched Tapped Delay Line.

1.2 GHz
FROM
SYNTHESIZER
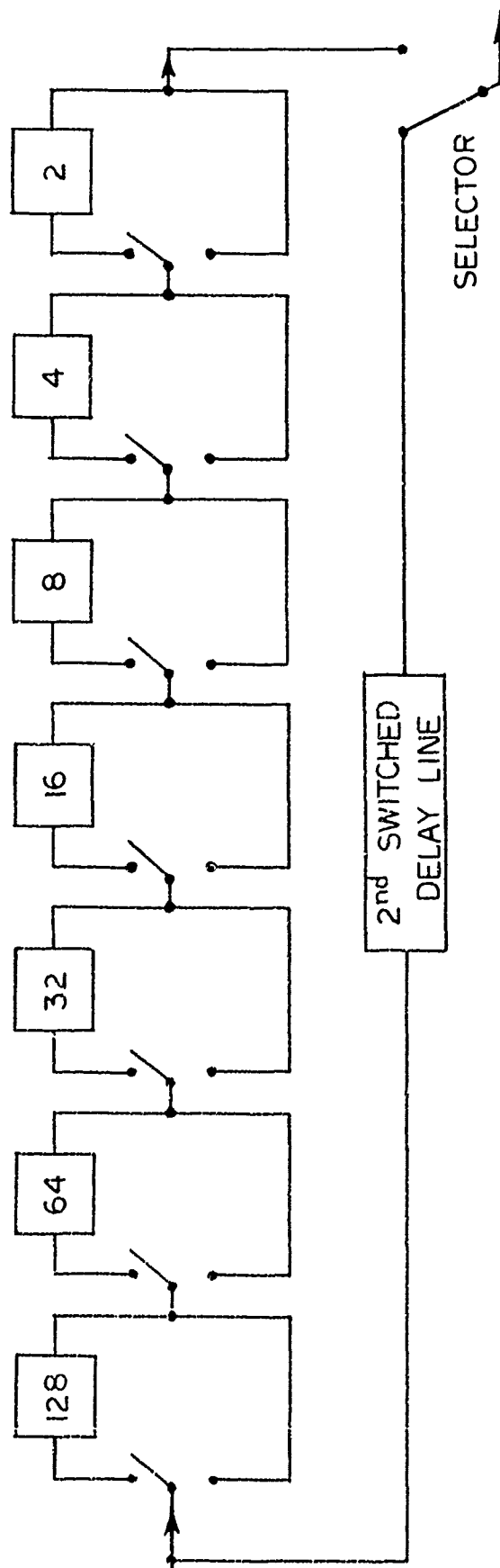
Figure 32. Switched Tapped Delay Line With Logarithmically Increasing Number of Taps.

189

Fig. 33 for a delay line of maximum length 7. The principle is simply to set up the next delay using the currently unused delay segments and an alternate output to be switched; only the output switch is activated at the time of change of delay. Fig. 33 only shows the connections required; the set-up of the switches is very simple, and is shown in Fig. 34. The technique assumes that the delay only changes by increments of one unit of delay. This is a very reasonable assumption in most applications, including the one of concern here.

One final method deserves mention. It utilizes the simple delay line simulation in Fig. 31, but with variable tap gains rather than switches. It also takes advantage of the bandlimiting in the transmitter to use more widely spaced taps. It can be shown that the optimal spacing is slightly denser than the Nyquist spacing. It is then necessary to weight several taps near the delay. Figure 35 shows some typical tap gains as a function of the delay. The exact number of taps required using this approach can only be calculated after a detailed system analysis, but a rough estimate can be obtained if we assume

(1) Delay maximum 150 ns

(2) Bandwidth 20 MHz

(3) Tap Spacing $\dfrac{3}{4W}$.

It is then seen that only 5 to 11 taps are needed. Thus this approach can offer substantial savings in the number of taps, but the control of the gains requires somewhat more complicated circuitry.

DELAY LINE CONNECTIONS   DELAYS SWITCHED
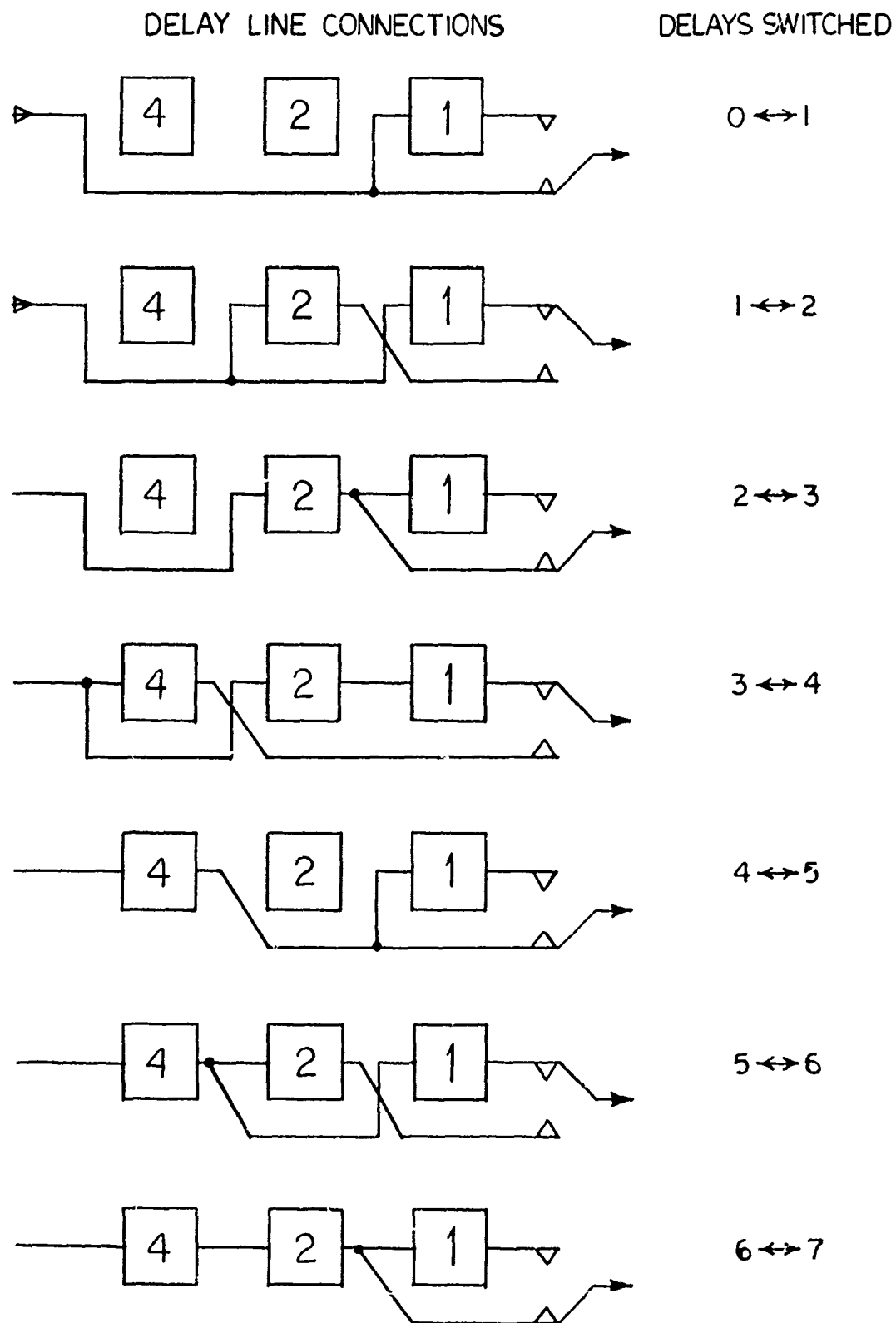
Figure 33.   Alternative Switched Tapped Delay
              Line Signal Flows.

191
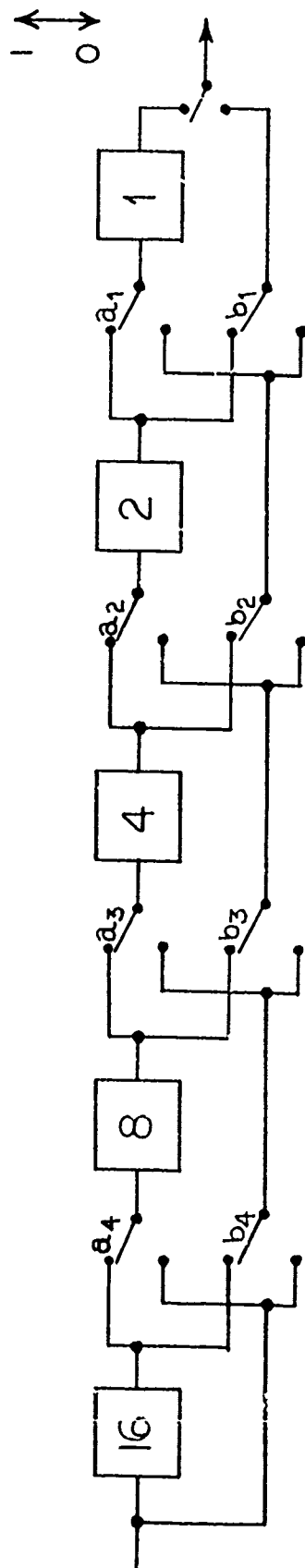
Figure 34. Diagram of Switch Set-Up for Alternative Switched Tapped Delay Line.
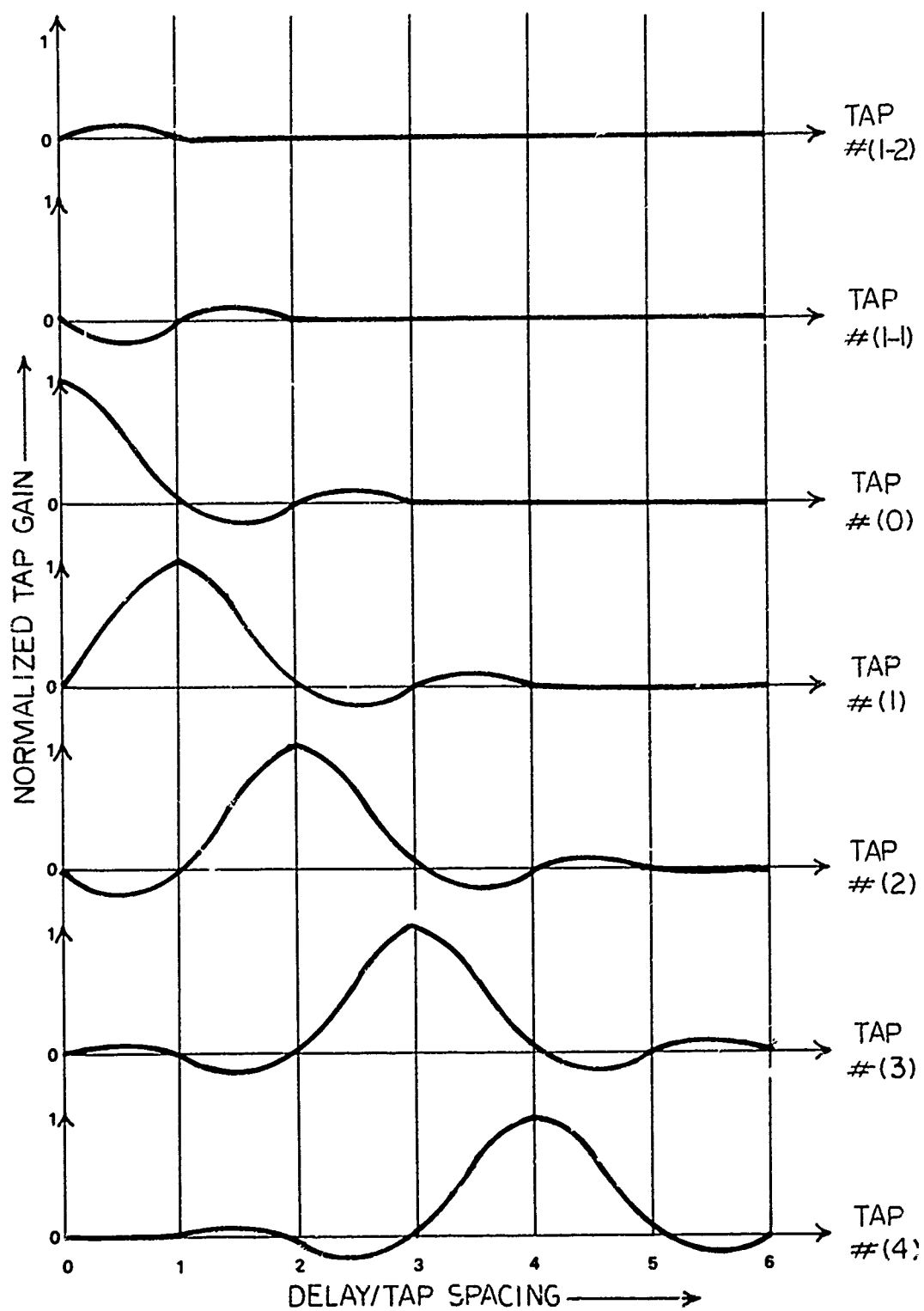
Figure 35. Typical Tap Gains
Tap Spacing .72/W

193

3.3.5.4 Antenna Signal Distribution

As discussed in Section 3.3.2.2, it is necessary to provide separate inputs to each antenna in the assembly. This i..cludes the phasing and attenuation of all eight satellite signals for each antenna. We assume at most three antennas, as in the baseline assembly. The L1 and L2 carriers for each satellite as well as at least one L1 jammer and one L2 jammer go into each antenna.

Two different approaches are possible. One is to keep all carriers and jammers at an intermediate frequency (e.g., 70 MHz) all the way from the frequency synthesizer through multipath and antenna combination networks and only heterodyne up to the L1 or L2 frequency at the antenna input. This will at least save some mixers, since there are fewer antennas than satellites and jammers. The other approach is to work at RF throughout, which will result in some savings since some of the L-band equipment already exists at CSEL. An implementation requiring 10 mixers and 3-way splitters, nine four-way combiners, and up to 24 attenuator and phase shifters is shown in Fig. 36. If the receiver uses only one antenna output when extracting a particular signal, then phase shifters are not necessary. The attenuators may also be omitted without seriously affecting the quality of the simulation since no relative attenuation corresponds to a worst case of omnidirectional antennas. However, some attenuation may be important when one antenna is designed for low elevation satellites, while the other antennas are aimed at high elevation satellites. Fig. 37 shows part of a corresponding all-IF combination networks. The requirements in this case are three L-band hybrids, six mixers, and six IF 5-way combiners. The number of attenuators and phase shifters is as before.
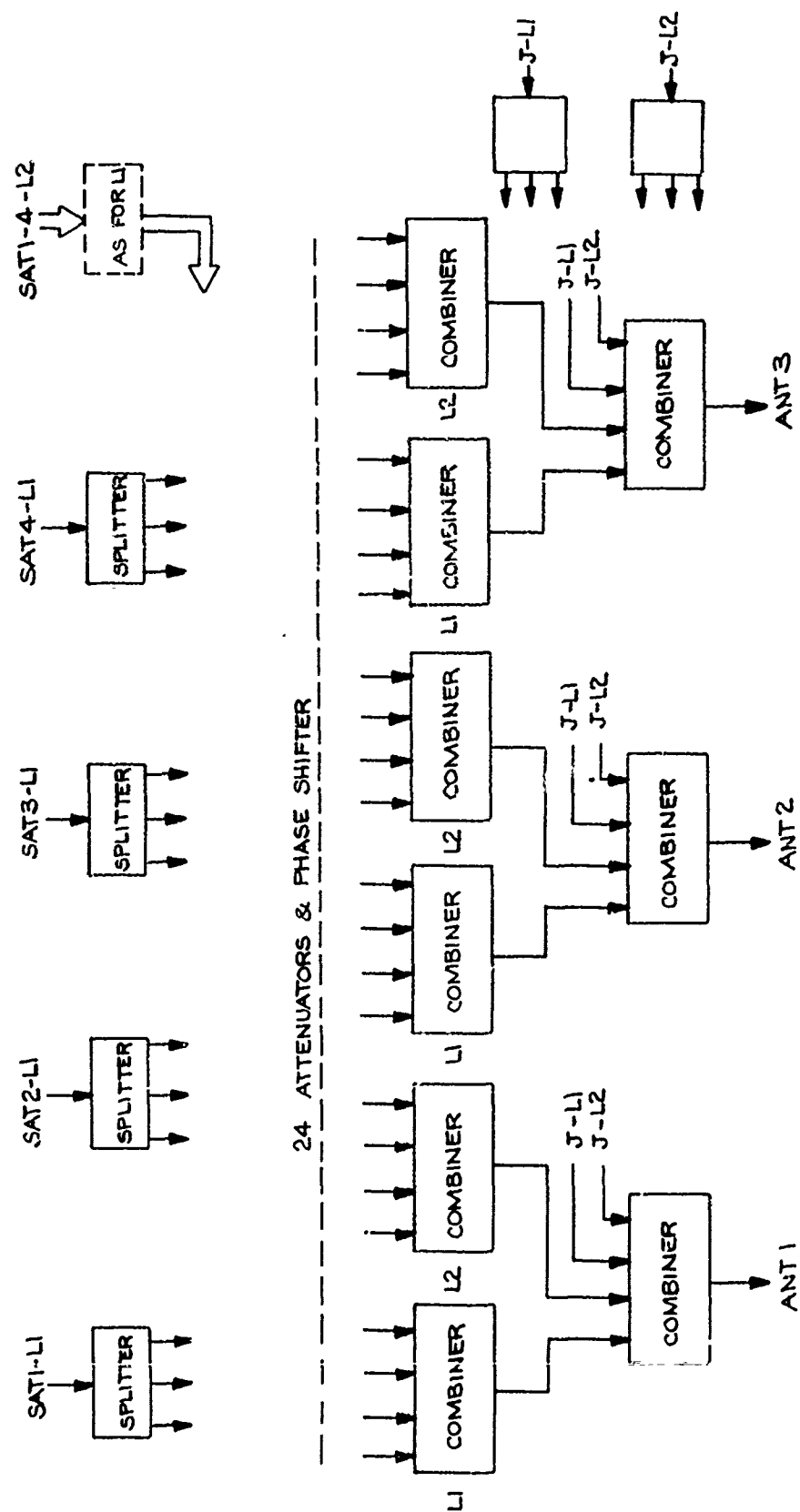
Figure 36. The Full RF Signal Combining Network.

195
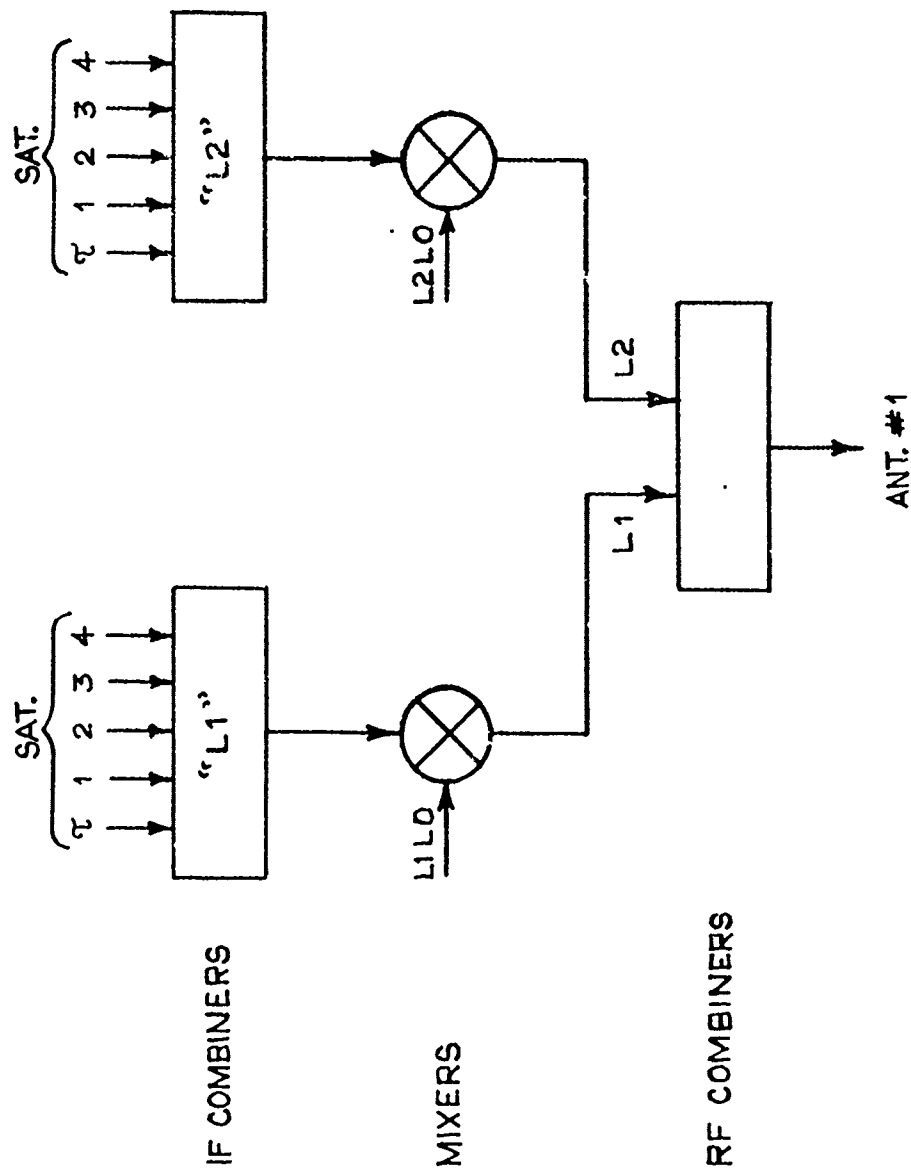
Figure 37. Part of the IF Signal Combining Network.

3.3.5.5   Summary and Recommendations

We have in this section discussed the implementation of variable delays and the simulation of the antenna reception.

The two main methods of implementing delay are

(1)   Eight independent frequency synthesizers, with delay controlled by Doppler. The feedback method of Section 3.3.5.2 is recommended to stabilize the delay.

(2)   Four independent frequency synthesizers, with delay controlled by Doppler. They would create both L1 and L2 signals but with the correct delay only for the L1 (1.6 GHz). The additional delay of the L2 carriers is implemented using four tapped delay lines, such as the ones in Figures 31 through 33.

The choice between the two methods should be based on the relative costs of delay line vs. synthesizer implementation.

3.3.6   Software and Computational Requirements

The simulation facility requires a fair amount of software due to necessary flexibility of the system. Various degrees of flexibility can be obtained depending on how much real-time analysis is desired. We will here make a rough sketch of the requirements of the simplest scheme, where all computations are done beforehand, and only the minimum amount of data recorded for the real-time simulation.

197

3.3.6.1 Calculations that can be done before the Simulation

Many of the calculations can be done most economically beforehand. This includes the satellite trajectory and atmospheric effects. The receiver parameters are also included, but if desirable, certain real-time control of the receiver is possible at the cost of a much more complex computer programming effort. Table 21 lists the necessary program functions in the three stages: Pre-simulation, simulation, and post-simulation. Table 22 groups some of the data storage requirements for the off-line pre-simulation and post-simulation stages.

3.3.6.2 Real-Time Data Requirements

We now discuss the data rates and computational requirements of the simulation. It is assumed that the delay feedback of Section 3.3.5 is used, and that the Doppler is to be computed from Eq. (305), so that only the delay need to be recorded on the input tape. The parameters needed on this tape are listed in Table 23. Some of these parameters should be updated at the maximal rate of 100 per second, while others can be updated at a much slower rate. The high rate data will often be sufficiently slowly varying so that a differential encoding, or more advanced prediction error correcting methods, can reduce the data rate considerably. We now discuss the required data rates with these considerations in mind.

The down-link data are low rate, less than 100 bits per second, so only one bit is required at each update time if we assume 100 updates/sec.

The number of bits needed in the delay is determined by the accuracy of the frequency synthesizer and the largest delay possible.

TABLE 21.   INDIVIDUAL PROGRAMMING STEPS REQUIRED

Pre-Simulation

READ IN   Satellite trajectory parameters

                                 receiver trajectory parameters

                                 multipath data

                                 scintillations, attenuation

                                 ionospheric model

                                 tropospheric model

                                 antenna parameters

                                 mode of simulation, status, etc.

COMPUTE   Satellite trajectories

                                 receiver trajectory

                                 Satellite to receiver paths

                                 ionospheric delay

                                 tropospheric delay

                                 downlink data

                                 antenna pattern effects

                                 delay and Doppler

                                 jamming

                                 inertial parameters

                                 auxiliary parameters

PRINT   Status

                                 data read in

                                 trajectory information

RECORD   delay (and possibly Doppler)
                                 downlink data

TABLE 21   (cont'd)

RECORD (cont'd)   Inertial and auxiliary parameters

                                   multipath conditions

                                   actual receiver position (velocity
                                     altitude) for quick real-time
                                     analysis

                                   run-time status

                                   antenna gains per satellite
                                     receiver antenna

                                   jamming (type, on/off)

SIMULATION

    READ   tape generated

    COMPUTE   Doppler from delay

    PRINT/DISPLAY   error estimate

    RECORD   estimated position, velocity,
                                     time-of-day estimated ionospheric
                                     and tropospheric correction,
                                     range and range rate

POST SIMULATION
   ANALYSIS

    READ   Pre-simulation recordings

                                   simulation result

    ANALYZE   errors, performance

TABLE 22. OUTLINE OF DATA TO BE STORED

1) Status Record
2) 4 Satellite trajectories, ephemerides
3) Receiver Trajectory
4) Inertial Parameters
5) Auxiliary sensor parameters
6) Jamming parameters (type, position, power,···)
7) Ionosphere Model Parameters
8) Tropospheric Model Parameters
9) Ionospheric Delays
10) Tropospheric Delays
11) Satellite-Receiver Path Data
12) Antenna Parameters
13) Antenna Attenuation, phase, relative to jamming
14) Delay and Doppler
15) Multipath Parameters
16) Path attenuation and scintillation
17) Downlink Data
18) Computed Data, total (tape)
19) Measured Data, total (tape)
20) Results of analysis.

TABLE 23. INPUT PARAMETER FOR SIMULATION

1)	Downlink data
2)	Delay
3)	Inertial parameters
4)	Altitude data
5)	Multipath, delay(s) and reflection coefficient(s)
6)	Antenna combining factors, scintillation
7)	Actual receiver position, velocity, and altitude
8)	Jamming; power, type.
9)	Miscellaneous status parameters defining simulation mode.

When the delay is directly encoded, the required resolution is 1.25×10^{-13} seconds in order to get 20 mHz Doppler resolution at 1.6 GHz. With a maximum differential delay of 20 msec, it is found that 38 bits are required. A more efficient method is to initially record the desired delay, and then implement only the Doppler during the simulation. This will require 22 bits for the Doppler with a maximum Doppler shift of about 40 kHz, a saving of 16 bits. With a slight increase in the real-time computations, we can encode changes in the Doppler shift instead. With a maximum acceleration of 10 g, we find that only 10 bits are needed with a resolution of the acceleration of

$$\delta g = \frac{\delta v}{.01 \text{ sec.}} = \frac{.003048 \text{ m/sec}}{.01 \text{ sec}} \sim .3 \text{ m/s}^2.$$

The same resolution is required for the acceleration parameters of the inertial system, giving 10 bits per coordinate, or 30 bits total. Differential encoding of the accelerations can reduce this to 12 bits total with a maximum jerk of 100 m/s^3. Additional input from the gyro may be needed. It should be sufficient to reserve 16 bits for these and other auxiliary sensors except the altimeter.

Direct encoding of the altitude could require as much as

$$\log_2 \frac{100,000 \text{ ft.}}{1 \text{ ft.}} \approx 20 \text{ bits.}$$

Differential encoding, however, should only require 4 to 5 bits in order to specify the altitude with sufficient accuracy.

Multipath parameters include delay and reflection coefficient. The reflection coeficients need only be determined initially. Since only delays in the range of 0 to 200 nsec are required for the

203

simulation, at most 8 bits are needed to specify the delay. Differential encoding can reduce this to 4 to 5 bits, and this can be reduced even further by updating the delay at a much smaller rate, as the exact delay need not be very precise. At most four delays will be used, one for each satellite, and most of the time one will be enough to test the multipath protection of the receiver.

The receiver antenna signals require up to 24 attenuators and phase-shifters, or complex multipliers. A rudimentary antenna test may be performed with somewhat fewer elements, but we consider the worst case here. The 48 numbers will be very slowly varying. A 10-bit quantization and direct encoding would require 480 b'ts, while with differential encoding, 96 bits should be sufficient. The quantization noise can be eliminated by filtering.

The actual receiver position, velocity and attitude parameters can be encoded directly with 3 x 16 bits for position, 3 x 22 bits for velocity, and 48 bits for other parameters such as roll, pitch and yaw. This amounts to 162 bits. Differential encoding may reduce this to about 3 x 10 bits (pos. or velocity only) plus 3 x 4 bits, at total of only 42 bits.

The jamming parameters should not require updates during regular simulation, so it is not necessary to assign any bits to these parameters.

To account for other parameters such as simulation modes, data formats, etc., an absolute worst case should be 48 bits.

The results of the discussion above are given in Table 24. Both the maximum and minimum ratio given (96 kbps, 28 kbps) can be implemented with standard recording techniques. The smaller rates allow for longer simulations and fewer tape reading errors. The numbers given are worst-case, and additional savings should be possible when designing the final system.

TABLE 24. REAL-TIME DATA REQUIREMENTS

Parameters (See Table 6-3)	Bits/10 msec, direct encoding	Bits/ 10 msec differential encoding
1	1	1
2	152 (88)	40
3	30-60	12-28
4	20	4-5
5	32	20
6	480	96
7	162	42
8	0	0
9	48	48
TOTAL	861-955	263-280

3.3.7 Hardware Requirements

The exact hardware requirements will depend on the choice of the configuration, of which many alternatives have been discussed in the previous section. Two such alternatives are shown in Figs. 38 and 39.

The system in Fig. 38 is based on independent clock or Doppler control of both the L1 and L2 frequencies. It consists of eight signal generators, containing frequency synthesizers (Section 3.3.3.1), exciters, possibly a delay feed-back loop as described in Section 3.3.5.2, and possibly up-converters to bring the simulated satellite signals to the desired L-band frequency. If the signals are converted to RF the complete multipath test can be carried out with only four delay lines, while otherwise eight delay lines would be needed. However, in all likelihood it will be sufficient with only one or two multipath delay lines to test the implications of severe multipath conditions on the GDM. The signals are combined in an assembly providing signals from all satellites to up to three antennas. A GDM controller/interface assembly supplies control signals to the GDM along with the inertial and remaining auxiliary parameters. It also sends the GDM estimates back to the CSEL computer for on-line analysis and recording. Alternatively, it may contain a separate tape drive for direct recording of the GDM data.

The configuration in Fig. 39 is identical except for the use of only four signal generators and four variable delay lines. The signal generator must supply both the L1 and L2 signals with the proper Doppler shifts and a common delay as required for the L1 channel. The signal generator will be a slightly more complex than the one used in Fig. 38 since it requires one extra carrier frequency synthesizer. The variable delay line represents the

206
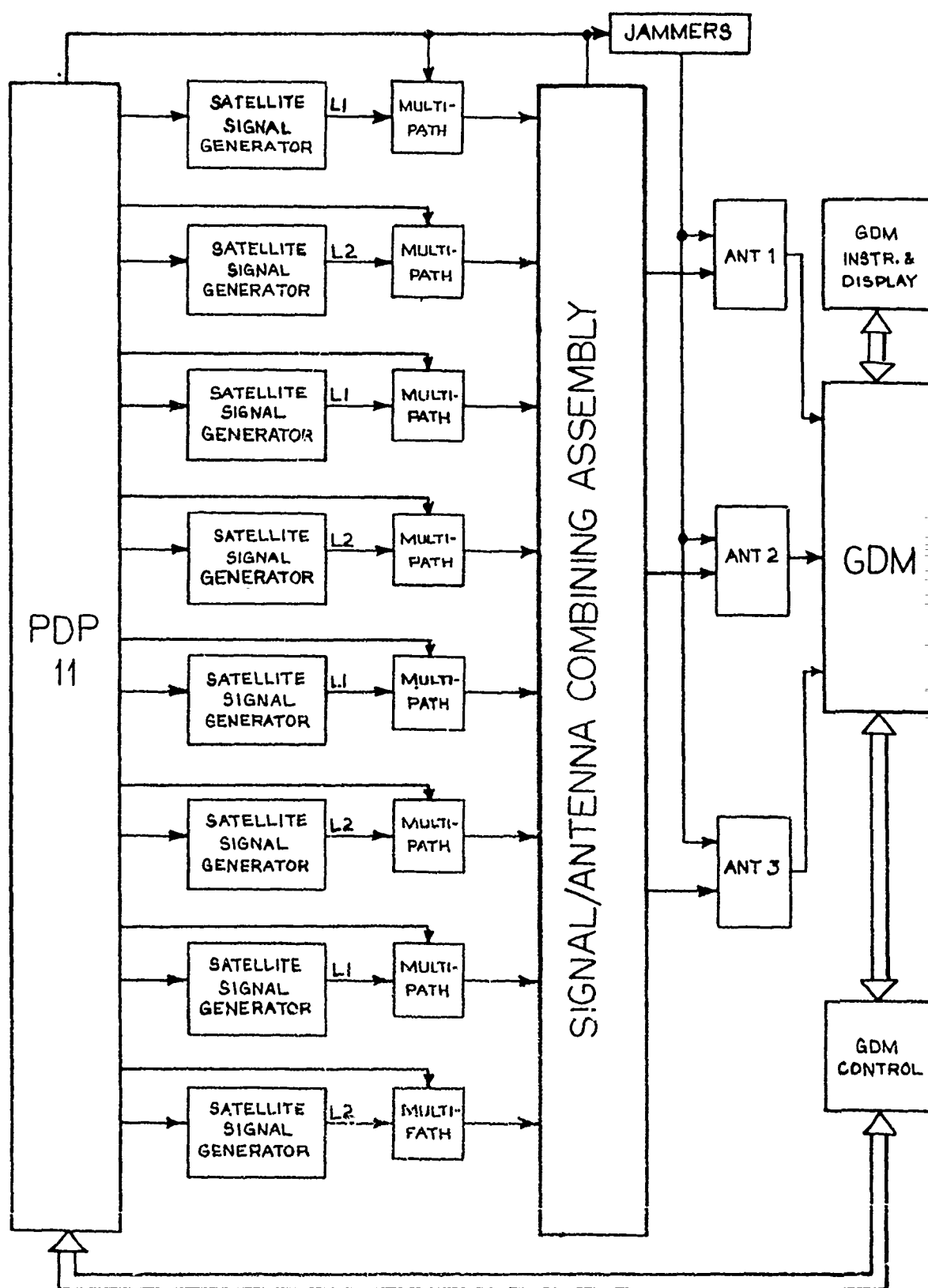
Figure 38. GPS/GDM Simulation Facility, Alternative 1.
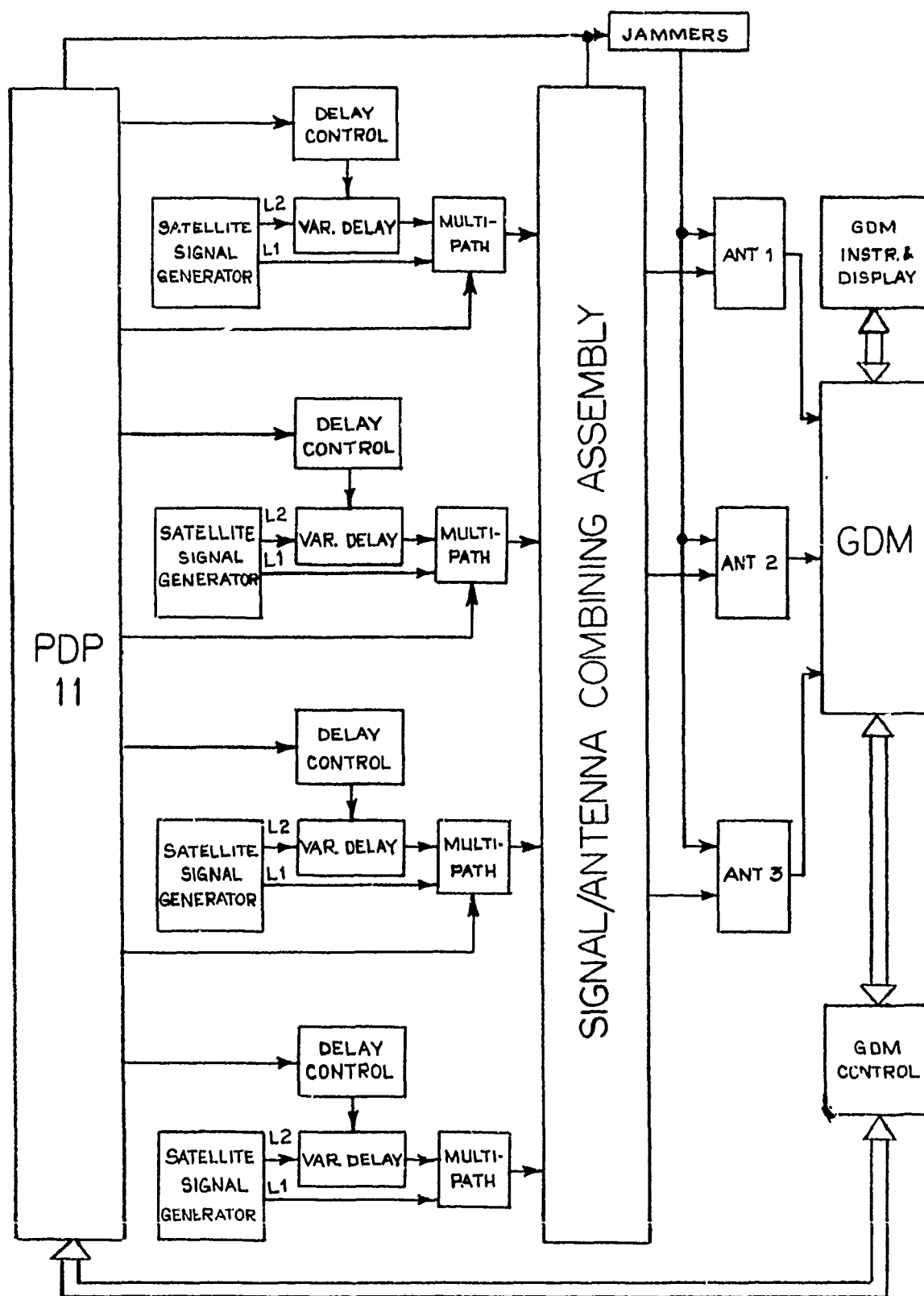
Figure 39. GPS/GDM Simulation Facility, Alternative 2

208

differential ionospheric delay, and may be implemented by any
of the methods discussed in Section 3.3.5.3. We now try to assess
the amount of hardware needed.

3.3.7.1 IF/RF Hardware

The requirements for various configurations are listed in
Table 25 (a-d). Table 26 shows the total number of parts re-
quired for a full RF implementation, as well as the currently
available parts.

3.3.7.2 Digital Hardware and Interface Requirements

The digital interfaces of the simulation facility fall into
two categories. One consisting of interfaces with the governing
computer (PDP-11/20/45), and one consisting of interfaces with
the GDM.

The GDM interface can include some processing capability as
indicated by the term "GDM CONTROL" in Figs. 38, 39. It may
interface the GDM either through the GDM control/display assembly
or directly to the data processor via an extension of the vehicle
instrumentation system. In either case, special test programs are
required for the GDM to override the actual auxiliary sensors
and initial measuring unit output and to accept the inputs supplied
by the GDM control assembly. Provisions should also be made for
the transmission of pseudo range, range rate, estimated position
and velocity, estimated ionospheric delay and satellite clock,
etc. The GDM controller can be controlled by a microprocessor,
supervising the flow of data to and from GDM and PDP-11/20, and
to a tape drive recording the results of the simulation. Alter-
natively a simpler interface can be used with all control retained
by the PDP-11/20 or the PDP-11/45.

TABLE 25(a). HARDWARE REQUIREMENTS

UNIT	PARTS	NUMBER OF PARTS
Satellite Signal Generator, Alternative 1	Frequency synthesizer Supplying IF carrier and 10 MHz square wave, both with and without Doppler.	8
	Code generators a: without delay feedback b: with delay feedback	 8 16
	Exciters (not including jamming)	 12
	IF/RF converters a: RF propagation Simulation b: IF propagation Simulation	 8 0

TABLE 25(b). HARDWARE REQUIREMENTS

UNIT	PARTS	NUMBER OF PARTS
Satellite Signal Generator, Alternative 2	Frequency synthesizer supplying 10 MHz square wave and 2 IF carriers, with proper Doppler shifts	4
	Code generators a: without delay feedback b: with delay feedback	 8 12
	Exciters (not including jamming)	12
	IF/RF converters a: RF propagation Simulation b: IF propagation Simulation	 8 0
Variable Delay	Tapped Delay Lines with Digital control (Section 5.3)	4

TABLE 25(c).   HARDWARE REQUIREMENTS

UNIT	PARTS	NUMBER OF PARTS
Multipath	L-Band combiners	
	a) RF implementation	4
	b) IF implementation	0
	Delay Lines	
	a) Full RF implementation	4
	b) Full IF implementation	8
	c) Minimal RF implementation	1
	d) Minimal IF implementation	2

TABLE 25(d). HARDWARE REQUIREMENTS

UNIT	PARTS	NUMBER OF PARTS
Jamming and Antenna Assembly RF Implementation	3-way splitters	6
	Attenuator & Phase-shifter or I & Q Multiplier	≤ 24
	Jammers, incl.Code Gen. and exciters	2
	4-way L-band Combiners	5-9
Jamming and Antenna Assembly IF Implementation	L-Band Combiner	2
	IF/RF Converters	6
	IF 5-way Combiners	6
	IF 3-wav Splitters	10
	Attenuator & Phase-shifter or I & Q Multiplier	≤ 24
	Jammers	2

TABLE 26. TOTAL REQUIREMENTS FOR ALL RF IMPLEMENTATION WITHOUT DELAY FEEDBACK. ALTERNATIVE 2 IN PARENTHESIS

PARTS	NUMBER OF PARTS	CSEL AVAILABILITY
Frequency Synthe- sizer	8(4)	1
Code Generator, excl. jamming	8	0
RF Exciters, excl. Jamming	12	4
IF/RF Converters	8	3
Variable Delay Line	0(4)	0
Multipath Units	4	0
L-band Combiners	13	1
L-band Splitters	10	?
Variable Atten. & Phaseshift	24	0
Jammers	2	1

Interfaces with the simulation facility are needed in the following places:

1)   Frequency synthesizers
2)   Variable delay, if applicable
3)   Multipath units
4)   jamming units, optional
5)   antenna assembly.

The interface may contain all of the delay feedback (if applicable) logic (Fig. 28), or the measured delay may be fed back into the computer for a recomputation of the desired Doppler shift.

3.3.8 Summary and Conclusions

We have outlined the requirements for a reliable simulation of GPS/GDM receivers and suggested both the general structure of the simulator as well as some particular implementations of the more critical elements. The division of hardware and software functions has been made, together with a list of the necessary parts and the complexity of alternative implementations.

Use of CSEL existing equipment has been taken into consideration, in particular the following CSEL parts can be used:

- jamming generator
- signal combiners with amplitude control
- exciters (SIG), including fading
- clock, 5 MHz Rb
- switching assembly
- digital control complex
- computer and interface facilities.

215

A number of new parts are required, including:

- high precision frequency synthesizers
- variable-delay lines (trade-off against synthesizers)
- multipath
- antenna assembly, as required
- extensive off/on-line software support
- GDM software modifications, as required.

The main alternatives in the implementation are:

1) Implementation of variable delays. This can be achieved with independent Doppler control of the synthesizers, either open loop or closed loop using the baseband delay measurement technique of Fig. 28 . All eight frequencies can be controlled by using eight such frequency synthesizers, or by using only four (one for each satellite) combined with a short variable delay line for simulating the differential ionospheric delay of the L1-L2 signals. Several ways of implementing the delay are presented in Sections 3.3.5.2 through 3.3.5.3.

It appears that the most economical implementation is with four satellite simulators and four variable delay lines using the baseband/digital technique described in connection with Fig. 33 . The question of whether the delay feedback is necessary to stabilize the delay accuracy cannot be determined without testing directly the high precision frequency synthesizer. It is recommended that a delay measurement technique similar to the one in ⌐. 29 be used unless a complete receiver with single ranging capability is immediately available.

2) Implementation of the channel portion at IF or RF. From the point of view of antenna signal distribution, there is no major differences in the complexity of the implementation in

216

either case. However, the RF approach lends itself more readily to realistic modifications, and exploits the capabilities of the CSEL facility to a much higher degree. This approach is therefore preferable.

3) <u>Implementation of the antenna distributors</u>. As a first approach a single-antenna GDM can be used. This may be sufficient to test the most important features of the majority of the GDM receivers with a baseline antenna assembly. Testing of proper antenna utilization and problems which occur when switching between antennas may require that independent signals be applied to each antenna. A possible configuration is shown in Fig. 36. It is suggested that this problem be decided upon at a later stage of the simulator analysis. Simulation of GDM's with high performance antenna assemblies will require considerably more study and will depend strongly on the type of antenna used.

The feasibility of testing the high performance antennas and the use of the roof top facility are questions open for future study.

SECTION 4

SATELLITE SIGNAL PROPAGATION

4.1 Introduction

Sections 2 and 3 were concerned with system aspects of the
LES 8/9 and NAVSTAR GPS simulation. In this section we address
certain satellite signal propagation properties. It is intended
as a guide in the setting of desired and jamming signal parameters.
The section is divided into two main parts. Section 4.2 is prima-
rily the result of a literature survey on satellite signal scin-
tillation and the effect of the earth's atmosphere on satellite sig-
nal propagation. Section 4.3 addresses the problem of generating,
on a digital computer, probability density functions for use in
realistic simulation of scintillation.

4.2 Properties of Satellite Signals

In the absence of multipath, one would expect that the path
between a ground station and a satellite would present a nearly
ideal non-fading channel. However, measurements made on satellite
signals have shown that scintillation fading does occur. The fading
is dependent on time of day, season of the year, latitude, and radio
frequency. It is primarily due to small scale irregularities in the
electron density in the F layer of the ionosphere, at altitudes rang-
ing from 225 to 400 km. Thus, the same scintillation behavior would
be found at aircraft altitudes, e.g., 9 to 12 km, as at earth stations.

In this section we present a survey of current results in satel-
lite propagation, as an aid in determining the proper means of simu-
lating satellite signal scintillation. The section is divided in-
to subsections. In Section 4.2.1 the time and space dependence of
scintillations are reviewed. In Section 4.2.2, measures of scintil-
lation data are presented. Measured and modeled scintillation data

218

are compared in Section 4.2.3. In Section 4.2.4, the frequency
dependence of scintillation is discussed. Atmospheric effects
are discussed in Section 4.2.5.

4.2.1 Time and Space Dependence of Satellite Scintillation

Ionospheric scintillation can cause both signal enhancement
and fading. In this subsection we discuss the temporal and
geographic extent of this scintillation. The material in this
section, including the figures, comes primarily from the review
paper by Aarons, Whitney, and Allen, "Global Morphology of Ionos-
pheric Scintillations", Proc. IEEE, Vol. 59, No. 2, Feb., 1971,
pp. 159-172. [16]

Two areas of the earth are particularly troubled by fading,
namely the high latitudes and the equatorial region. This is
shown graphically in Fig. 40.   The density of darkening on Fig. 40
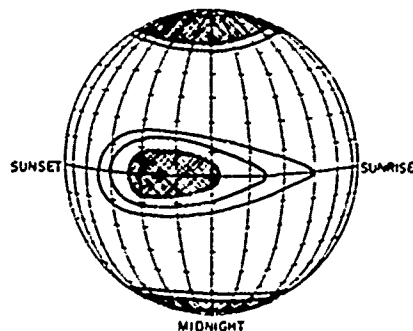
Figure 40.   The irregularity structure at night. The density of the
hatched are represents the occurence of deep fading.

is proportional to the occurrence of deep fades. From this figure
it is seen that the geographical extent of fading is great, with
the high latitude region extending from approximately 57° to the
pole, and the equatorial region being approximately 15° on either
side of the equator.

In the polar cap region, scintillation is both permanent and at a high rate. At lower latitudes, but still within the high latitude range, diurnial effects begin to be seen; high scintillations occur around midnight, and low scintillations during the day time hour. Figure 41 shows data on the fade duration and fade rate measured at Thule, Greenland, at a frequency of 136 MHz; the peak-to-peak fading is seen to range from 15 dB at night to 4 dB in the day, with corresponding fade periods of from 2 to 60 seconds. Observations made near the boundary of the high latitude region have shown 10%, 50%, and 90% fade rates of 2, 6, and 10 fades per minute, with occasional fades lasting several minutes.
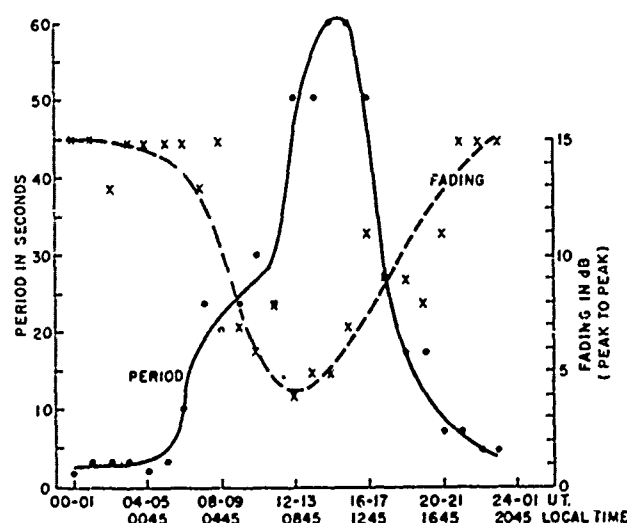
Figure 41. Fading period and amplitude for Thule during quiet period of October 21, 22, 23, 1968, with A_p's of 2, 1, and 3.

As contrasted to the more continual scintillation of the animal region, equatorial scintillations start abruptly, reach a maximum in several minutes, and last for several hours. The fade rate in equatorial regions is a factor of 2 to 10 slower than that in auroral regions. The fade intensity shows both a

220

pronounced diurnal and a seasonal variation. Figures 42 and 43
present data taken at Ghana. Figure 42 shows a maximum in both
scintillation rate and intensity occurring around midnight, and
a minimum occurring during the day; the scintillation index, S,
will be discussed in Section 4.2.2. Note that in contrast to
Fig. 41 which has a scale of fades duration in seconds, Fig. 42
plots the inverse scintillation rate in scintillations per minute.
Figure 43 shows a maximum scintillation to occur in September and
March, and a minimum to occur in June and December. The data of
both Figs. 42 and 43 were taken at VHF using the Intelsat II
satellite.

Since the scintillation is due to irregularities in the F-
layer electron density, the scintillation rate is due to move-
ment of the irregularities. The F-layer drifts eastward
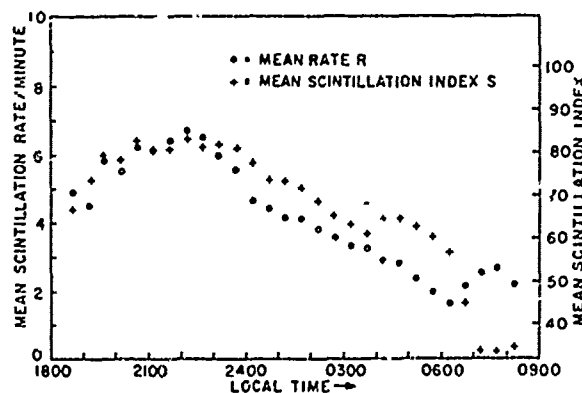
Figure 42. The diurnal variation of mean rate and mean
scintillation index in Ghana.

% OF TIME SCINTILLATION EXCEEDS S

36
30
24
18
12
6
0

S = 30

S = 70

CANARY BIRD SCINTILLATION – SEASONAL EFFECT

M J J A S O N D J F M A M
1967   1968
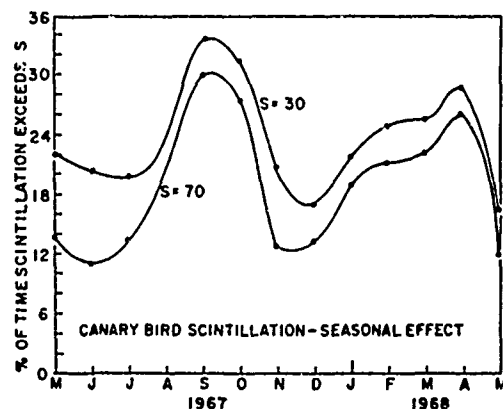
Figure 43.   The seasonal dependence of scintillation
for Accra, Ghana.

at nights at 70 to 140 meters/sec., and westward during the day
at 140 to 280 meters/sec. The east-west size of the ground pat-
tern of the irregularities ranges from 100 to 400 meters, and
the axial ratios, or ratio of north-south to east-west extent are
greater than 60:1. This has significant implications for aircraft-
to-satellite transmission, as the scintillation rate for an air-
plane traveling east-west will be determined by the rate at which
the projections of irregularities are traversed, while an airplane
traveling north-south will have essentially the same scintillation
rate as ground-based system.   In addition these effects would
cause the fade rate of a jamming signal to generally differ from
that of a communication signal being jammed.

4.2.2 Measures of Scintillation

In the previous section we have discussed scintillation, without qualitatively describing it. The purpose of this subsection is to provide analytic measure of scintillation. Experimental data will be shown in Section 4.2.3.

The conventional measure of scintillation is based on the distribution of either the amplitude or the power of the received signal. In Briggs and Parkin, [17], four measures of scintillation are given, namely S_1, S_2, S_3, and S_4. If the instantaneous amplitude of the received signal is $R(t)$, the instantaneous power is defined as $R^2(t)$. Then:

$$S_1 \equiv \frac{\overline{|R - \overline{R}|}}{\overline{R}} \tag{321}$$

$$S_2 = \frac{\left[\overline{\left(R - \overline{R}\right)^2}\right]^{\frac{1}{2}}}{\overline{R}} \tag{322}$$

$$S_3 = \frac{\overline{|R^2 - \overline{R}^2|}}{\overline{R}^2} \tag{323}$$

$$S_4 = \frac{\left[\overline{\left(R^2 - \overline{R}^2\right)^2}\right]^{\frac{1}{2}}}{\overline{R}^2} \tag{324}$$

For a number of years, Air Force Cambridge Research Laboratories has used, as their measure, the scintillation index, or SI. SI is defined (e.g., Whitney, H.E., Aarons, J., Allen, R.S., Seeman, D.R., [18]; Whitney, H.E., [19]) as:

$$SI = \frac{P_{max} - P_{min}}{P_{max} + P_{min}} \tag{325}$$

where P_{max} is the third peak down from the maximum, and P_{min} is the third minimum up from the lowest excursion in the given sample period. Both P_{max} and P_{min} are measured in dB, and AFCRL generally utilizes 15 minute sample periods. In analyzing experimental data, AFCRL has found it useful to divide data into six groups, depending on the scintillation index. These are shown in Table 27, from Whitney et.al. [19] along with the corresponding value of $P_{max} - P_{min}$. The higher the group number, the deeper the scintillation.

TABLE 27. RELATION OF GROUP TO SCINTILLATION INDEX AND FADING

Groups	Scintillation index (%)	$P_{max} - P_{min}$ (dB)
0	<20	<1.7
1	20 to 39	1.7 to 3.6
2	40 to 59	3.7 to 5.9
3	60 to 79	6.0 to 9.4
4	80 to 89	9.5 to 12.7
5	$\geq$90	$\geq$ 12.8

Table 28, also taken from Whitney et.al., [19], shows the percent occurrence of 15 minute scintillation indices, measured at Hamilton, Mass., Narssarssuaq, Greenland, and Huancayo, Peru at a frequency of 136 MHz. The data are grouped according to local time (2200-0200, 1000-1400, and 0000-2400), and magnetic index (0-3, 4-9, and 0-9), and show the diurnal and latitudinal variation of scintillation. In addition, the magnetic index is seen to affect the auroral (Greenland) scintillation index to a much greater extent than the mid-latitude (Massachusetts) or equatorial (Peru) scintillation index.

224

TABLE 28. PERCENT OCCURRENCE OF 15-MIN SCINTILLATION INDICES FOR MAGNETIC INDEX AND LOCAL TIME VARIATION FOR ATS-3, 136 MHz

Hamilton, Massachusetts, 1968-1970

K	|	Group (2200-0200)						|	Group (1000-1400)						|	Group (0000-2400)					
		0	1	2	3	4	5		0	1	2	3	4	5		0	1	2	3	4	5
0-3		72.0	12.8	7.2	4.4	1.26	2.34		94.41	4.5	0.8	0.2	0.04	0.05		85.93	8.5	2.9	1.6	0.43	0.64
4-9		58.6	17.5	8.5	6.1	3.48	5.82		90.65	6.9	1.4	1.0	0.05	0.00		74.47	13.0	5.8	3.2	1.42	2.1
0-9		69.75	13.6	7.4	4.7	1.63	2.92		93.92	4.8	0.9	0.3	0.04	0.04		84.15	9.2	3.4	1.8	0.58	0.87

Narssarssuaq, Greenland, 1968-1971

K	|	Group (2200-0200)						|	Group (1000-1400)						|	Group (0000-2400)					
		0	1	2	3	4	5		0	1	2	3	4	5		0	1	2	3	4	5
0-3		13.0	15.1	15.8	17.9	12.3	26.0		55.06	26.0	10.5	4.8	1.78	1.86		36.1	21.7	14.6	10.8	6.0	10.8
4-9		1.7	5.3	11.4	18.5	15.8	47.3		19.0	17.9	19.7	14.6	11.0	17.8		8.8	11.3	15.5	17.1	13.2	34.1
0-9		11.2	13.5	15.0	17.9	12.9	29.5		50.49	24.9	11.7	6.0	2.98	3.93		32.0	20.2	14.7	11.8	7.0	14.3

Huancayo, Peru, 1968-1970

K	|	Group (2200-0200)						|	Group (1000-1400)						|	Group (0000-2400)					
		0	1	2	3	4	5		0	1	2	3	4	5		0	1	2	3	4	5
0-3		43.0	7.9	6.5	6.7	4.4	31.5		78.73	21.0	0.25	0.0	0.01	0.01		70.3	11.8	3.2	2.7	1.6	10.4
4-9		41.7	9.3	5.6	7.4	5.2	30.8		83.14	16.3	0.37	0.19	0.0	0.0		67.5	10.8	3.3	3.6	2.3	12.5
0-9		42.7	8.2	6.3	6.8	4.6	31.4		79.29	20.4	0.27	0.02	0.01	0.01		69.9	11.7	3.2	2.8	1.7	10.7

Local time

225

The Nakagami m-distribution has been proposed to describe scintillation, in an attempt to both unify the descriptions of scintillation and provide a single analytic description of the distribution of scintillation (Whitney, e.al., [19], Nakagami, M., [20]). The m-distribution is a single parameter distribution, which, by choice of m, will match many experimental and analytic distributions. The m distribution has the probability density function

$$p(R) \equiv M(R,m,\overline{R}^2) = \frac{2m^m R^{2m-1}}{\Gamma(m)(\overline{R}^2)^m} \exp\left(-m \frac{R^2}{\overline{R}^2}\right), \qquad (326)$$

$$m = \frac{\left(\overline{R}^2\right)}{\left(R^2 - \overline{R}^2\right)^2} \geq \frac{1}{2}. \qquad (327)$$

If m is equal to 0.5, the m distribution becomes equal to the one-sided Gaussian distribution, while if m is equal to 1, it becomes equal to the Rayleigh distribution. Higher values of m cause the distribution to be more concentrated, as shown in Fig. 44 (Nakagami, [20]). It is evident from the definition of m that
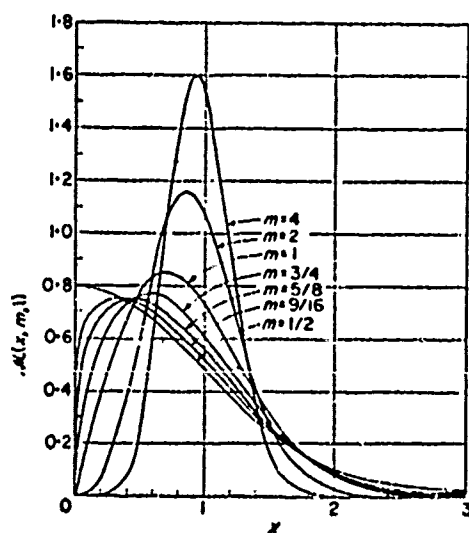
$$m = 1/S_4^2. \qquad (328)$$

Figure 44. Probability density function of the m-distribution.

226

Two transformations which are useful in working with the m-distribution are those for the squared envelope and for the received power in dB. In the squared-law case, if $y = R^2$, then

$$p(y) = \frac{m^m}{\Gamma(m)} \left(\frac{y}{\overline{R^2}}\right)^m \frac{1}{y} \exp\left(-m \frac{y}{\overline{R^2}}\right). \qquad (329)$$

This can be identified as a chi-squared distribution with 2m degrees of freedom, and a variance of $\overline{R^2}$ in the underlying Gaussian process. However, while m must be an integer for the chi-squared distribution, m need only be any real number greater than 0.5 for the m-distribution.

In the second case, if $x = 20 \log_{10} R$, then

$$p(x) = \frac{2m^m}{M\Gamma(m)} \exp\left\{m\left(\frac{2x}{M}\right) - e^{2x/M}\right)\right\}, \qquad (330)$$

where
$$M = 20 \log_{10} e. \qquad (331)$$

Computer processing has been performed at AFCRL to relate the scintillation index to the parameter m. [19] A graph of this relation is shown in Fig. 45.

While the m-distribution is useful because it only has one parameter, other researchers , e.g., Rino and Fremouw [21] claim that its fit to experimental data is not always accurate, and prefer to use a complex Gaussian representation in which the powers of the in-phase and quadrature components are not equal. In particular, if the received field is represented as the sum of a constant value plus a random component

$$\vec{E}(\vec{r}) = \overline{\vec{E}(\vec{r})} + \vec{E}_o(\vec{r}) \; \psi(\vec{r}), \qquad (332)$$

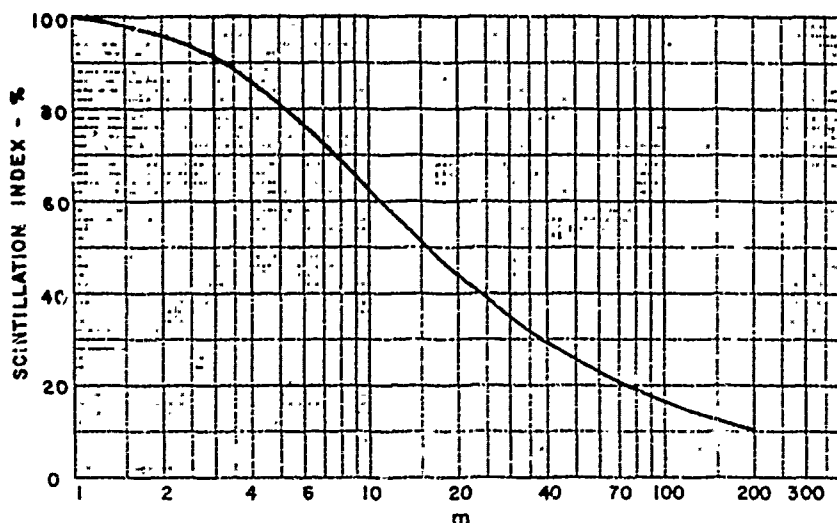where the overbar indicates the ensemble average, $\vec{r}$ is the direction vector, and

227

Figure 45. Scintillation index vs m.

$$\psi \quad = \quad x + jy, \tag{333}$$

where x and y are zero-mean, correlated Gaussian random variables. The phase reference of $\vec{E}(\vec{r})$ is defined in terms of a vector $\vec{\eta}$ such that

$$\overline{\vec{E}(\vec{r})} \quad = \quad \vec{E}_o(\vec{r}) \, (\eta_x + i \, \eta_y). \tag{334}$$

The variances of x and y, normalized to the total intensity I, are defined as σ_T^2. Summarizing,

$$\overline{I} \quad = \quad \overline{E_o}^2 \left(\sigma_T^2 + \eta_x^2 \right), \tag{335}$$

where

$$\sigma_T^2 \quad = \quad \sigma_x^2 + \sigma_y^2. \tag{336}$$

Also, by definition,

$$C_{xy} \quad = \quad \frac{\overline{xy}}{I}. \tag{337}$$

Using the auxiliary definitions

$$B \quad = \quad \sigma_x^2 - \sigma_y^2 + 2j \, C_{xy} \tag{338}$$

$$2\delta \quad = \quad \underline{/B} \quad = \quad \tan^{-1} \frac{2C_{xy}}{\sigma_x^2 - \sigma_y^2}, \tag{339}$$

228

then it can be shown that

$$S_4^2 = 2\sigma_T^2 \left(1 - \sigma_T^2\right)\left[1 + \frac{|B| \cos 2\delta}{\sigma_T^2}\right] + \sigma_T^4 \left(1 + \frac{|B|^2}{\sigma_T^4}\right). \qquad (340)$$

4.2.3 Comparison of Measured and Modeled Scintillation Data

The purpose of a model is to give a representation of physical data — scintillation in this case — which can be conveniently used to approximate a physical process. In this subsection we will present comparisons between measured and modeled scintillation distributions.

Figure 46, from Aarons et. al. [22], shows a comparison of the experimental distributions of VHF (136 MHz) scintillations from ATS3 recorded at Hamilton, Massachusetts, with cumulative
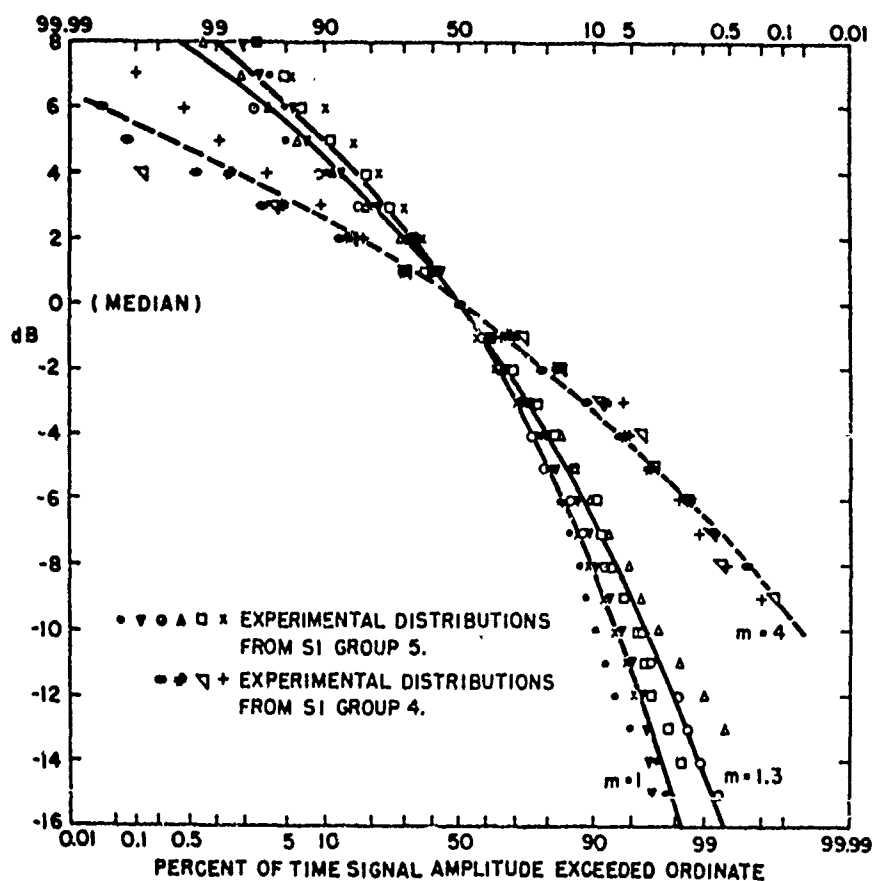

Figure 46. Comparison of Theoretical m-Distributions (Solid Line for m=1 and 1.3, Dashed for m=4) With Experimental Distributions From S.I. Groups 4 and 5 (136 MHz).

229

distributions using the m-distribution with m = 1, 1.3, and 4. The m-distribution is seen, for these data, to provide a good fit over the approximated 20 dB scintillation range.

Figure 47, taken from Rino et.al. [23], shows experimentally determined probability density functions for simultaneous VHF (137.5 MHz) and UHF (412 MHz) transmissions from ATS5, also recorded at Hamilton, Massachusetts. Two theoretical distributions are shown as dotted and solid curves, one the two-dimensional Gaussian, and the other the log normal. Based on a chi-square goodness of fit test, the fit of the Gaussian is better than that of the log normal. The parameters of the Gaussian distribution are given in Table 29. Also shown in Fig. 47 are circles which correspond to m-distributions with the same values of intensity on $m = 1/S_4^2$. It is seen that the fit of the m-distribution to the measured data are good.

Figure 48 shows UHF (250 MHz) scintillation data for transmission from TACSAT I by the Naval Electronics Laboratory Center (Paulson and Hopkins, [24]. Local time is 10 hours later than that shown on the figure, i.e., the figure is for 2420 to 0100 hours local time. Paulson and Hopkins note that the data "look Gaussian". However, the data of Fig. 48 have an excellent fit to the m-distribution with m = 1. This is shown in Fig. 49, in which the data of Fig. 48 are replotted along with a family of cumulative m-distributions. It is seen that, until the measured data go into the noise level, the m = 1 curve is followed quite clo: ·ly.

To summarize, while there is still debate as to the exact law followed by the first-order distribution, it appears from the cases examined that the m-distribution can be used as an approximation to the envelope for engineering purposes. If, however, phase is important, the Rino and Fremouw complex Gaussian model should be considered.
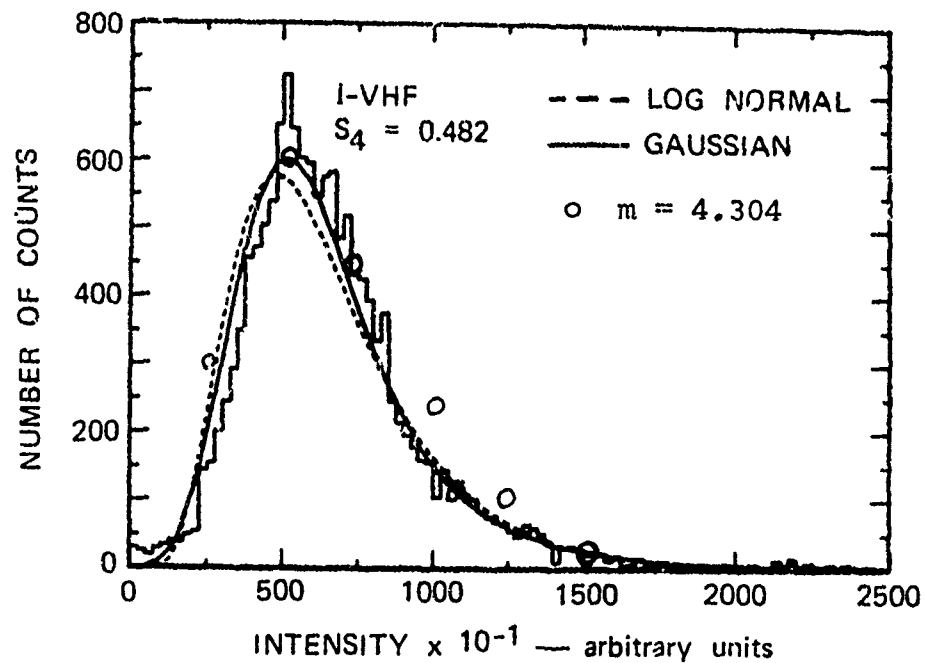
(a)   VHF ⟨I⟩ = 6700
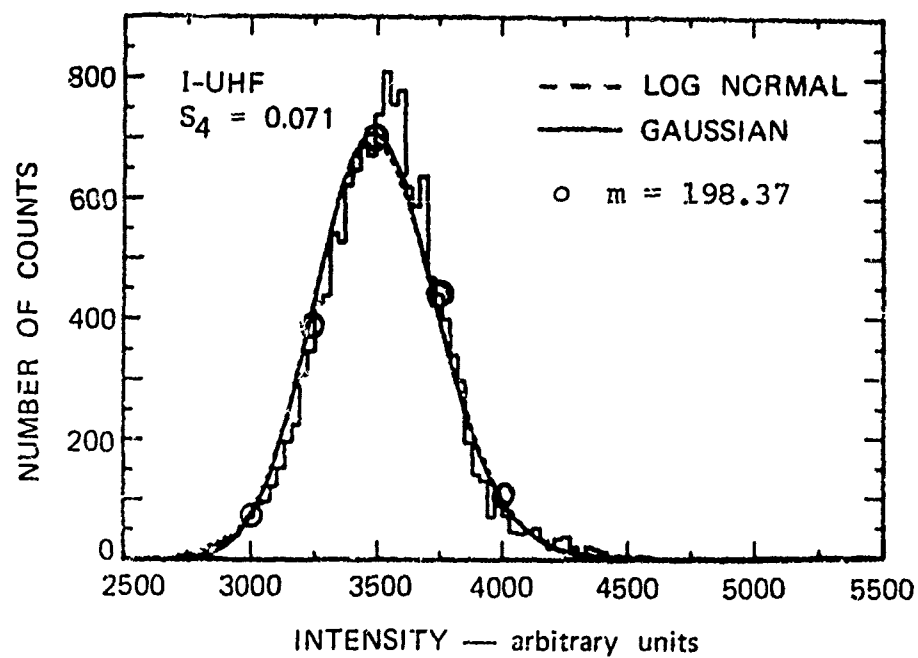
(b)   UHF ⟨I⟩ = 3523

Figure 47. Data Block I Histograms 14400 Samples.

231
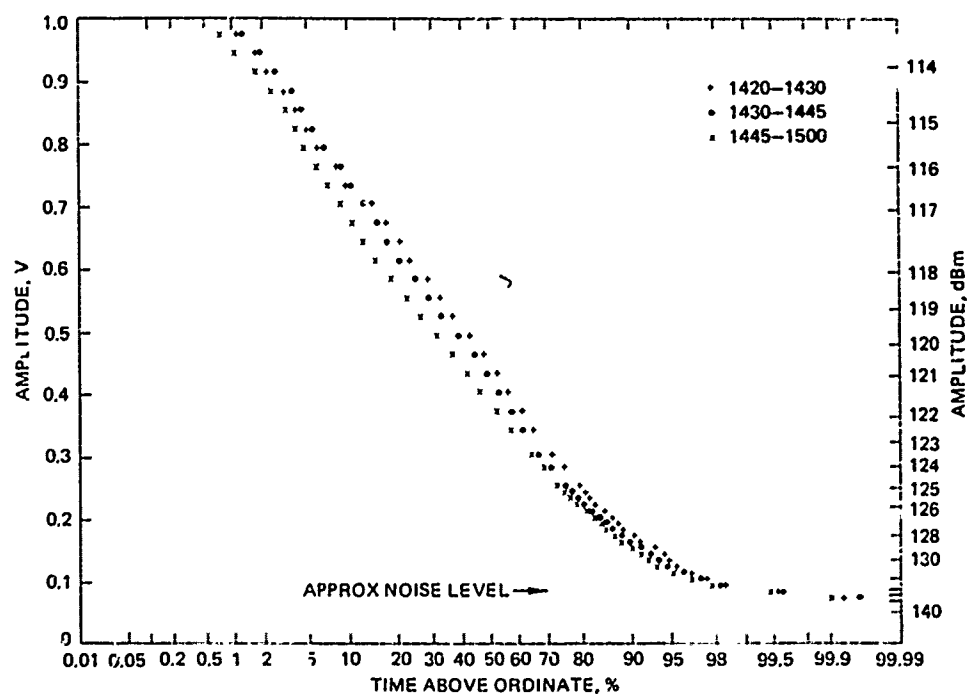
Figure 48. Example showing three cumulative amplitude distributions for records made on the night of 23 September 1972 GMT. (250 MHz)

TABLE 29. PARAMETERS OF GAUSSIAN DISTRIBUTIONS OF FIGURE 47

Frequency	S_4	σ_T^2	$|B|$	$\angle B$	σ_x^2
VHF (137.5 MHz)	0.482	0.310	0.2604	0°	0.0248
UHF (412 MHz)	0.0711	0.021	0.0189	5°	0.00105

232

Figure 49. Cumulative Form of the Nakagami Distribution:
Valid for m ≥ 0.5.

4.2.4 Effects of Frequency on Scintillation Distributions

As shown in Whitney et.al. [18]   observations which have
been made on radio stars indicate a frequency dependence of
scintillation which, when expressed in terms of the m parameter,
takes the form

$$\frac{\log(m_1/m_2)}{\log(f_1/f_2)} = \gamma_m, \tag{341}$$

where m_1 and m_2 are two values of m measured in simultaneous
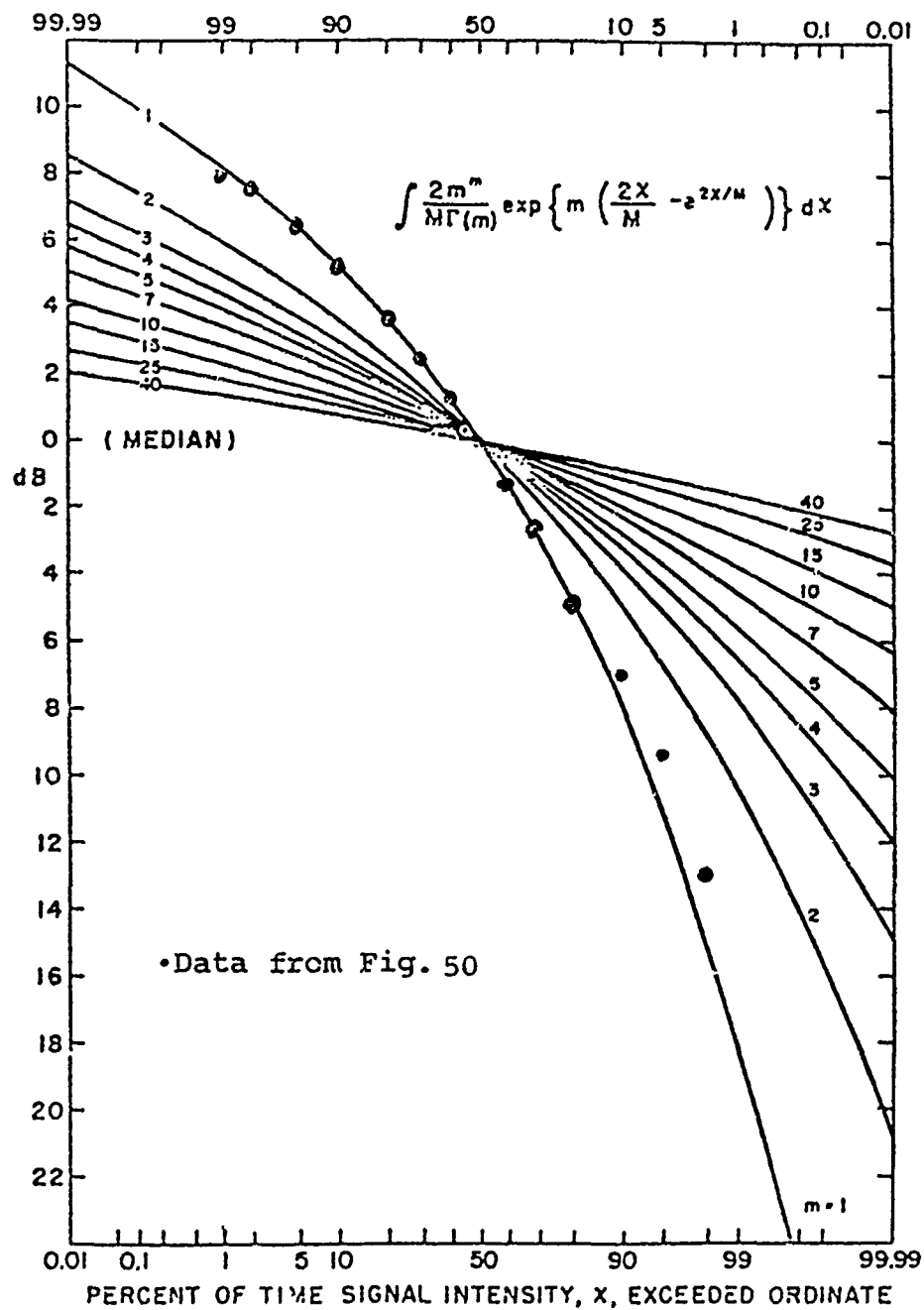observations at frequencies f_1 and f_2. The parameter γ_m, while
ideally a constant, is actually a random variable. Figure 50
shows a histogram of γ_m made from 119 records at 137 MHz and
412 MHz (Whitney, [19] using ATS-3 and ATS-5 data. This data
give an average γ_m of 2.62, and a median of 2.65. As a comparison,
the data of Fig. 42,   using ATS-5 measurements, have $\gamma = 3.49$.

The extrapolation of VHF/UHF data into SHF and higher fre-
quencies indicates that the scintillation will decrease rapidly.
For example, at 2.3 GHz relative to 250 MHz,

$$m(f=2.3 \text{ GHz}) = \left(\frac{2.3 \text{ GHz}}{250 \text{ MHz}}\right)^{2.62} m(f=250 \text{ MHz})$$

$$= 335 \text{ m } (f=250 \text{ MHz}). \tag{342}$$

Since the minimum value of m is 0.5,

$$m(f = 2.3 \text{ GHz}) \geq 117.5. \tag{343}$$

As can be seen from Fig. 49   and m of 117.5 will have very
little scintillation. Figure 51,   from Paulson and Hopkins [24]
shows simultaneous 2.3 GHz and 250 MHz TACSAT I amplitude distri-
bution data. It is seen that, indeed, little scintillation was
measured at 2.3 GHz; Paulson and Hopkins estimate the peak-to-
peak 2.3 GHz scintillation measured during their tests to be in
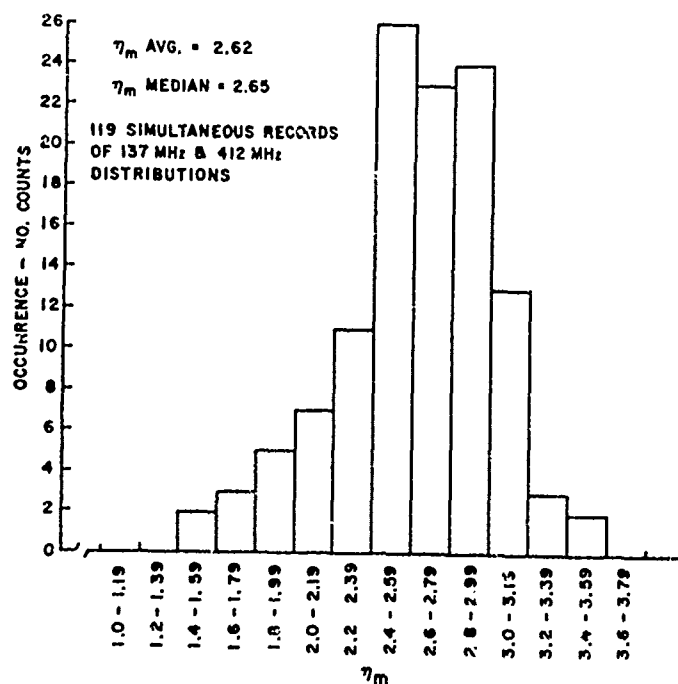the range of 2 to 5 dB.

234

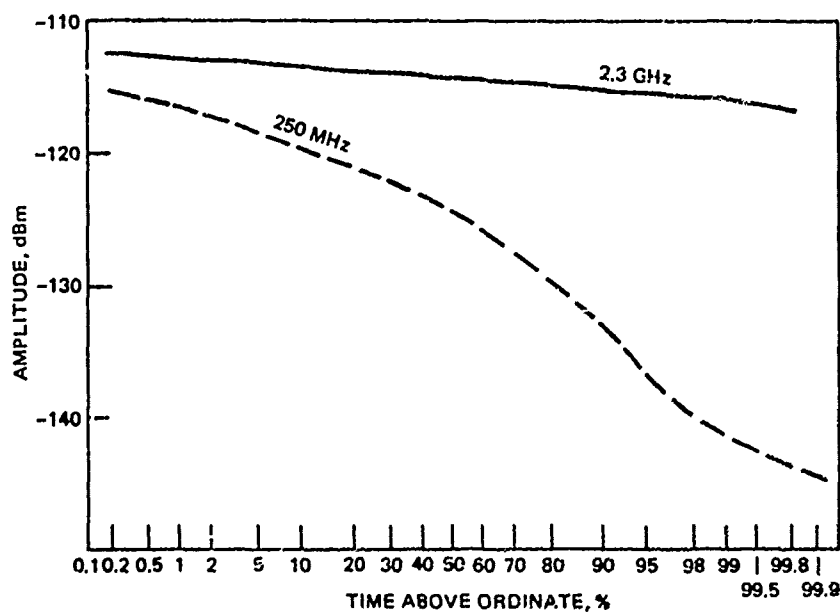Figure 50. Histogram of Spectral Index η_m.

Figure 51. Comparison of cumulative amplitude distributions
for TACSAT I UHF and S-band signals; Guam,
11 October 1972, 0945 to 9050 GMT.

4 and 6 GHz scintillation data have also been measured in the equatorial region over a 15 month period by COMSAT [25]. It was found that peak-to-peak scintillations were in the order of 4 to 6 dB; therefore fades below the median level can be estimated to be about half of this, or 2 to 3 dB.

4.2.5 Atmospheric Effects on Signal Propagation

The principal effect of the atmosphere on satellite propagation is to cause attenuation at millimeter wavelengths due to oxygen and water vapor absorption. Figures 52, 53, 54, from a review article by Altshuler et.al., [26] present some theoretical and experimental data at 15 and 35 GHz. Figure 52 shows calculated attenuations to a satellite as a function of zenith angle, rainfall rate, cloud water vapor content, and humidity. It is seen that attenuations in excess of 10 dB are predicted in rainy weather, and up to nearly 10 dB even in clear weather. Figure 53 presents measurements made at 15 and 35 GHz, which confirm the predictions of Fig. 47   Figure 54 shows the tribution of attenuation, as a function of zenith angle.

The data for Figs. 53   and   54   were measured over the six month period   January to July 1966, at the AFCRF Prospect Hill radio observatory in Waltham, Massachusetts, and, as Altshuler et.al. point out, are applicable c 'y to locations having a climate comparable to that of the   ston area. Brookner [27] has generated a set of "universal' curves, in which attenuation is given as a function of angle for 9 combinations of rain rate and cloud water content, at frequencies of 16, 35, and 94 GHz. The combinations of parameters used are shown in Table 30, and his 16 and 35 GHz data, in Fig. 55.   Also shown on Fig. 55 are curves of rainfall rates for various cities in the United States.

236
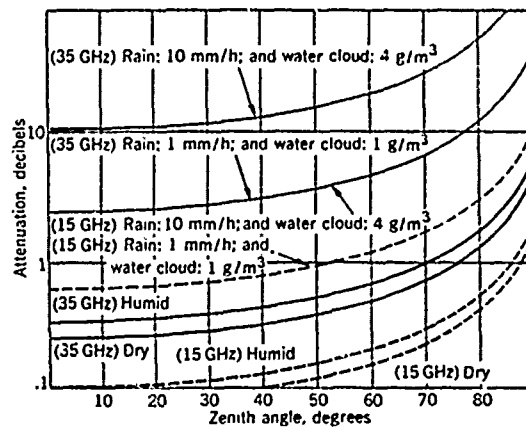
Figure 52.   Total atmospheric attenuation at
              15 GHz and 35 GHz (calculated).
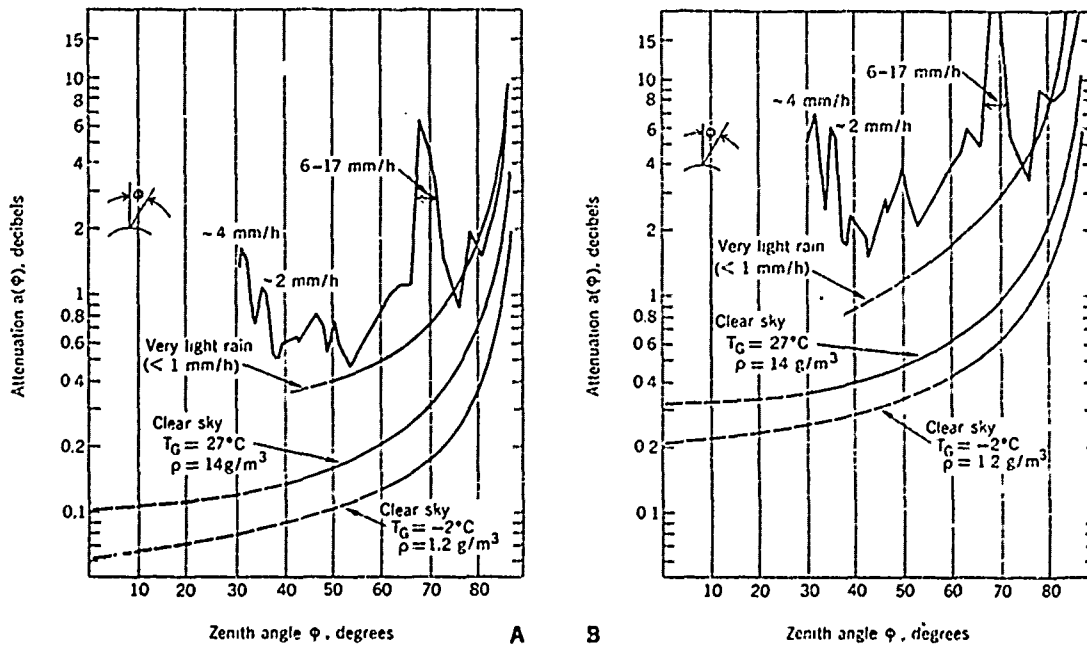
Figure 53. Total atmospheric attenuation at (A) 15 GHz and (B) 35 GHz.
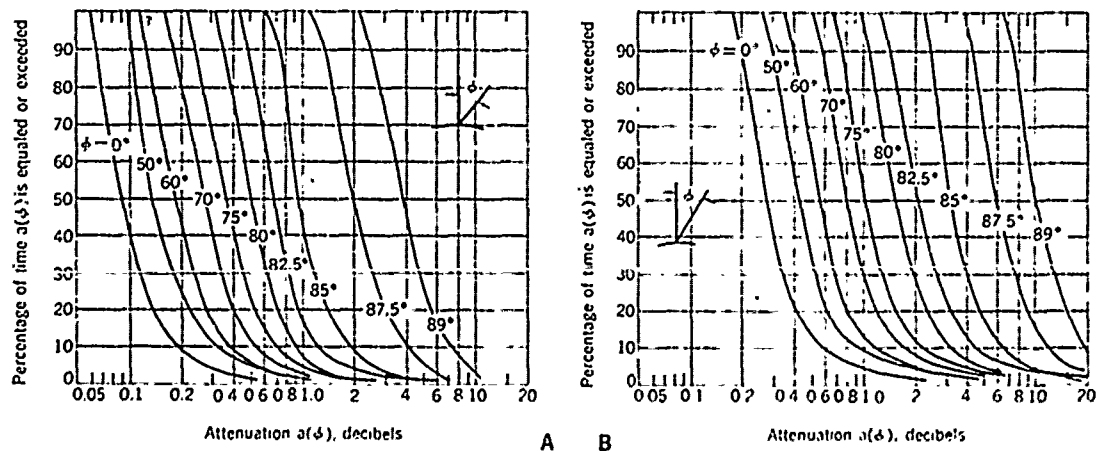
Figure 54.   Total atmospheric attenuation distribution at (A) 15 GHz
              and (b) 35 GHz.   237

TABLE 30. WEATHER MODELS USED IN THE CALCULATION OF ATTEN-
UATION AND SKY TEMPERATURE

Weather Type	Clear	Cloudy				Rainy			
Model No.	1	2	3	4	5	6	7	8	9
Pressure	x	x	x	x	x	x	x	x	x
Temperature	x	x	x	x	x	x	x	x	x
Clouds									
1		x				x			
2			x				x		
3				x				x	
4					x				x
Rain									
1						x			
2							x		
3								x	
4									x

238
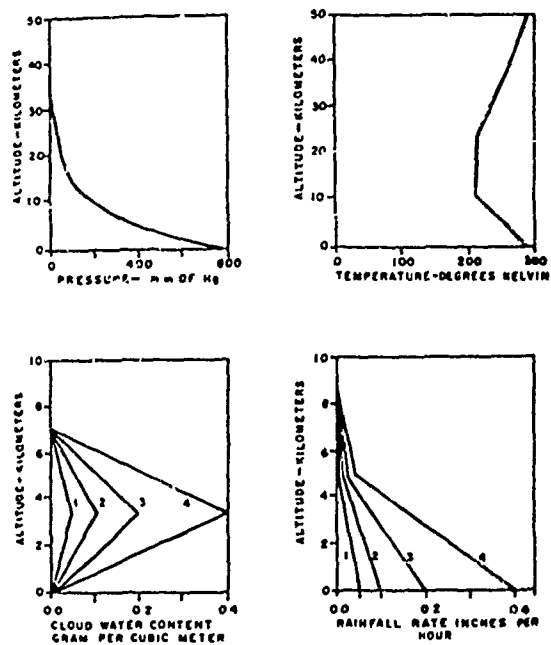
Altitude Profiles of Pressure,
Temperature, Cloud Water Content
and Precipitation
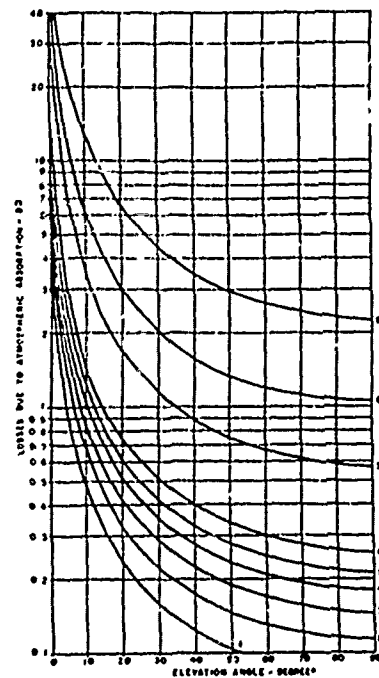
16 GHz Signal Losses Due to
Atmospheric Absorption
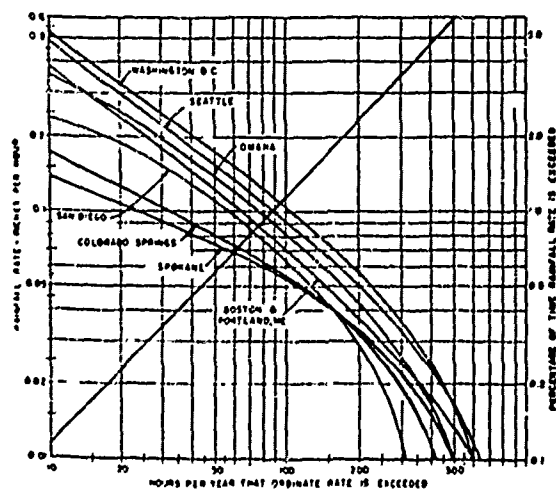
Frequency of Occurrence of Rain-
fall of a Given Intensity
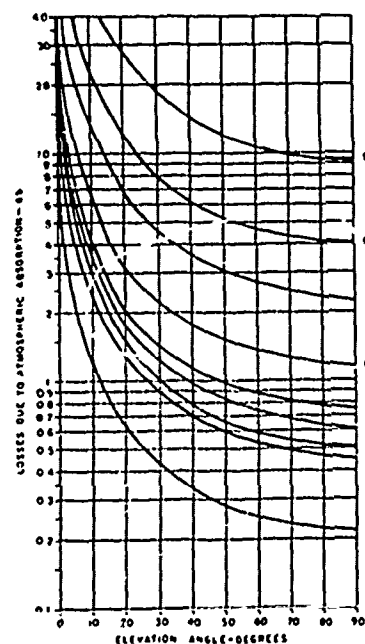
35 GHz Signal Losses Due to
Atmospheric Absorption

Figure 55.   16 and 35 GHz Attenuation Curves.

4.3 Simulation of Scintillation Statistics

4.3.1 Introduction

In the previous section we have reviewed the modeling of
radiowave scintillation. Two distinct groups of thought exist.
One favors the Nakagami m-distribution described completely by
its m parameter and mean parameter Ω; the other favors a complex
Gaussian distribution with quadrature components of unequal vari-
ance and mean*. It appears that the Gaussian distribution may
be a better approximation.   However , it is trivially easy
to find an approximating m-distribution and very difficult
to find the parameters for an approximating complex Gaussian dis-
tribution. On the other hand, for synthetic channel simulation it
is far easier to generate the Gaussian scintillation statistics.
In the following sections we present the methods of generating the
m and Gaussian distributions, and the methods of fitting experimental
data to the distributions.

4.3.2 Generation of Scintillation Statistics

The starting point of the scintillation statistics generation
is a uniform random variable of value $0 \leq u \leq 1$. It is assumed
that the communication laboratory computers are capable of generat-
ing a sufficient number of independent uniform random variables
for any communication experiment.

4.3.2.1 Nakagami m-Distribution

We let r and u respectively be Nakagami m- and uniform random
variables with probability density functions(pdf)

---

* The phase is usually chosen so that one component has zero mean.

240

$$f_R(r) = \frac{2m^m R^{2m-1} e^{-mr^2/\Omega}}{\Gamma(m)\Omega^m} \qquad r \geq 0 \qquad (344)$$

$$f_U(u) = 1 \qquad\qquad 0 \leq u \leq 1 \qquad (345)$$

$\Gamma(m)$ is the gamma function of m. m need not be an integer. A direct generation of the Nakagami variate from the uniform variate is obtainable by equating equal probabilities or equivalently by setting the cumulative density functions equal to each other.

The cumulative density function (cdf) of r and u are equal to

$$F_R(r) = \frac{2m^m}{\Gamma(m)\Omega^m} \int_{R=0}^{r} R^{2m-1} e^{-\frac{mR^2}{\Omega}} dR \qquad (346)$$

$$F_U(u) = \int_{U=0}^{u} du = u \ . \qquad (34^\sim)$$

Therefore, the Nakagami variate is generated by solving

$$u = F_R(r) \qquad (348)$$

for r.

Making the change of variables

$$t = \sqrt{\frac{m}{\Omega}} R^2 , \qquad (349)$$

Eq. (346) becomes

$$F_R(r) = \frac{1}{\Gamma(m)} \int^{\frac{mr^2}{\Omega}} t^{m-1} e^{-t} dt \qquad (350)$$

which is the defining integral for the incomplete gamma function, $P(m, mR^2/\Omega)$, and the probability integral of the χ^2-distribution, $P(2mR^2/\Omega | 2m)$.

The solution of

$$u = P\left(m, \frac{mr^2}{\Omega}\right) \tag{351}$$

for R is still a hard problem due to the complex nature of the incomplete gamma or χ^2-distribution. Nonetheless with the function tabulated on a digital computer given m, Ω and the present generated value of u, r can be found.

Complete tabulation is unnecessary when m is limited to integer and 1/2 values. Then the recursion relationship

$$P(a + 1, x) = P(a, x) - \frac{x^a e^{-x}}{\Gamma(a+1)} \tag{352a}$$

can be used with

$$P(1, x) = 1 - e^{-x} \tag{352b}$$

or

$$P(1/2, x) = \text{erf } x$$

Erf x is defined as the error function of x

$$\text{erf } x = \frac{2}{\sqrt{\pi}} \int_0^x e^{-t^2} dt \tag{353}$$

and may be approximated to almost 10^{-5} accuracy by

$$\text{erf } x = 1 - (a_1 t + a_2 t^2 + a_3 t^3) e^{-x^2} \tag{354a}$$

$$t = 1/(1 + px) \tag{354b}$$

$$p = 0.47047 \tag{354c}$$

$$a_1 = 0.3480242 \tag{354d}$$

$$a_2 = -0.0958798 \tag{345e}$$

$$a_3 = 0.7478556 \tag{354f}$$

242

When m is equal to 1 the direct transformation is given by

$$r = \sqrt{-\Omega \ln(1-u)} \tag{355}$$

Finally, we can generate R for arbitrary m, without an incomplete gamma function tabulation by choosing the closest integer m', less than m and interpolating according to the relationship

$$\left[1 - P\left(\frac{mR^2}{\Omega}, m' - \frac{1}{2}\right)\right]\left[\frac{W^2}{2} - \frac{W}{2}\right] + \left[1 - P\left(\frac{mR^2}{\Omega}, m'\right)\right]\left[1 - W^2\right]$$

$$+ \left[1 - P\left(\frac{mR^2}{\Omega}, m' + \frac{1}{2}\right)\right]\left[\frac{W^2}{2} + \frac{W}{2}\right] = u \tag{356a}$$

where

$$W = m - m' > 0 \tag{356b}$$

4.3.2.2 Complex Gaussian Distribution

The Gaussian distribution may be generated easily by two different methods. One method utilizes the central limit theorem by summing a number of uniform random numbers together. This method uses many uniform random numbers and thus may limit the number of independent Monte-Carlo samples in any communications experiment. This is particularly true on mini-computer simulators. In addition, the distribution is only valid for variates up to plus and minus half the number of summed uniform random numbers. The second method is again a direct transformation method. It is accurate for all ranges of variate and may only be slightly longer in generation time than the former method. It utilizes very few uniform random numbers.

4.3.2.2.1 Central Limit Approach

The central limit theorem is quite good when as few as 12 independent uniform random numbers are added together. Therefore,

243

by adding n independent uniform random numbers together, with $n \geq 12$, the sum is approximately Gaussian with mean equal to n/2 and variance equal to n/12. If we have a Gaussian random variable, x, with mean μ_x and variance σ_x^2 then we must form

$$x = \frac{\sum_{k=1}^{n} u_k - \left(\frac{n}{2} - \mu_x\right)}{(n/12\sigma_x)^{1/2}} .$$

(357)

Repeating (14) with parameters μ_y and σ_y^2 gives a second Gaussian variate, y, which is independent of x.

A total of 2n, or at least 24, uniform random variables are required to generate the two complex Gaussian components x and y.

4.3.2.2.2 Direct Method

A Rayleigh random variable multiplied by the sine and cosine of a uniform random variable is well known to give two independent Gaussian random variables. It is very simple to determine the Rayleigh variable by direct transformation. The Rayleigh pdf is given by

$$f_R(r) = \frac{r}{\sigma^2} e^{- r^2/2\sigma^2} \quad r \geq 0$$

(358a)

and the cdf is given by

$$F_R(r) = 1 - e^{- r^2/2\sigma^2}$$

(358b)

so that

$$u_1 = 1 - e^{- r^2/2\sigma^2}$$

(359)

must be solved for r. We have

244

$$r = \sqrt{-2\sigma^2 \ln(1-u_1)}$$

or since u_1 and $(1-u_1)$ are both uniform random variables between zero and unity

$$r = \sqrt{-2\sigma^2 \ln u_1} \qquad (360)$$

is the generation relationship for a Rayleigh random variable. Then we can generate the two complex Gaussian components x and y according to

$$x = \mu_x + \sigma_x \sqrt{-2\ln u_1} \cos 2\pi u_2 \qquad (361a)$$

$$y = \mu_y + \sigma_y \sqrt{-2\ln u_1} \sin 2\pi u_2 \qquad (361b)$$

We note that only two uniform random variables are required so that we can have an order of magnitude greater number of samples in any communication experiment when the direct transformation method is used.

4.3.3 Correlated Scintillation Variables

Very often it will be necessary to generate correlated scintillation variables. This can be accomplished by adding two independent variables together with the appropriate weighting factor related to the desired correlation. In the case of Gaussian statistics the resultant sum is again Gaussian. However, for Nakagami m statistics the resultant sum is no longer Nakagami m distributed! We now demonstrate this latter fact.

Let R_1 and R_2 be jointly independent Nakagami m variables such that their joint pdf is given by

$$f_{R_1,R_2}(r_1,r_2) = \frac{4m^{2m}(r_1 r_2)^{2m-1} e^{-\frac{m}{\Omega}(r_1^2 + r_2^2)}}{\Gamma^2(m)\Omega^{2m}} \qquad \begin{array}{l} r_1 \geq 0 \\[4pt] r_2 \geq 0 \end{array}$$

$$(362)$$

We wish to determine the distribution of R

$$R = \sqrt{r_1^2 + \rho r_2^2} \tag{363}$$

where ρ is the desired correlation. Introducing an auxiliary variable S

$$S = r_2 \tag{364}$$

the desired pdf of R is given by

$$f(R) = \int_{S=0}^{\infty} f(R,S)\,dS \tag{365}$$

where

$$f(R,S) = \frac{f_{R_1,R_2}(\sqrt{R^2-\rho S^2},S)}{|J|} \tag{366a}$$

and the Jacobian J is given by

$$J = \begin{vmatrix} \dfrac{\partial R}{\partial R_1} & \dfrac{\partial R}{\partial R_2} \\[2ex] \dfrac{\partial S}{\partial R_1} & \dfrac{\partial S}{\partial R_2} \end{vmatrix} \tag{366b}$$

and is evaluated at

$$R_1 = \sqrt{R^2 - \rho S^2} \tag{367a}$$

$$R_2 = S \ . \tag{367b}$$

We find that

$$|J| = \left(R^2 - \rho S^2\right)^{1/2} \Big/ R \tag{368a}$$

$$r_1 r_2 = S\left(R^2 - \rho S^2\right)^{1/2} \tag{368b}$$

$$r_1^2 + r_2^2 = R^2 + (1-\rho) S^2 \tag{368c}$$

so that

$$f(R,S) = \frac{2m^m R e^{-mR^2/\Omega}}{\Gamma(m)\Omega^m} \cdot \frac{2m^m S^{2m-1}(R^2-\rho S^2)^{m-1} e^{-m(1-\rho)S^2/\Omega}}{\Gamma(m)\Omega^m}$$

(369)

For the case of small correlation, we make the approximation

$$S^{2m-1}\left(R^2-\rho S^2\right) \approx R^{2m-2}\, S^{2m-1} - (m-1)\rho\, S^{2m+1}\, R^{2m-4}$$

(370)

The integration in (365) can then be performed to obtain the pdf

$$f(R) \approx \frac{2m^m R^{2m-1} e^{-mR^2/\Omega}}{(1-\rho)^m \Gamma(m)\Omega^m} - \frac{\rho(m-1)2m^m R^{2m-3} e^{-mR^2/\Omega}}{(1-\rho)^{m+1}\Gamma(m)\Omega^{m-1}}$$

(371)

We see that even when ρ is small R is not Nakagami m-distributed. When the correlation between r_1 and r_2 is almost zero then

$$f_R(R) \approx \frac{2m^m R^{2m-1} e^{-mR^2/\Omega}}{(1-m\rho)\Gamma(m)\Omega^m} \qquad \rho \approx 0$$

(372)

and R is again Nakagami m-distributed.

Since the condition $\rho \approx 0$ is not always met it is recommended that the Gaussian scintillation statistics be used.

4.3.4 Determination of Scintillation Parameters

From the points of view of generation, generation of correlated variables and best data fit, it is recommended that the scintillation statistics be considered complex Gaussian. Unfortunately, this assumption leads to a complicated parameter determination when we are constrained to work with amplitude data alone. We discuss three methods of determining the distribution parameters. One method is a parameterization method which results in a family of pdf's. This

method uses average amplitude squared and fourthed data and requires the generation of a histogram of the data followed by a goodness-of-fit test with each pdf in the family. The second method makes a Taylor series expansion of the complex Gaussian pdf. Four moments of the amplitude data are required. Using an iterative approach the Gaussian parameters are determined.

Both of the above methods assume that only amplitude data is available. We present a third method which assumes that the complex signal is available. Then the pdf parameters are trivially available by simple mean, variance and correlation measurements on the quadrature signal components. It goes without saying that the third method is the one recommended.

4.3.4.1 Parameterization Method

The parameterization method is described in detail in Rino and Fremouw [21], and is summarized here. If a is the received signal amplitude then the statistical average $\langle a^2 \rangle$ and $\langle a^4 \rangle$ are determined from the data. $\langle \cdot \rangle$ represents the ensemble average. The scintillation index S_4 defined as the normalized standard deviation of a^2 is then determined

$$S_4^2 = \sqrt{\frac{\langle a^4 \rangle - \langle a^2 \rangle^2}{\langle a^2 \rangle^2}} \ . \tag{373}$$

The scattering cross-section, σ^2, equal to the fraction of the incident power that is randomized by the scattering medium, is then determined as a function of functions g_1 and g_2. We have

248

$$\sigma^2 = \frac{g_1}{g_2 - 2g_1} \left[\sqrt{1 + \frac{(g_2 - 2g_1)S_4^2}{g_1^2}} - 1 \right]$$

(374)

We next compute a complex quantity B

$$B = -\frac{\sigma^2 \, e^{j\frac{1}{2} \arctan \left[\frac{f_1 \tan u_1 + f_2 \tan u_2}{1 - \tan u_1 \tan u_2 \sec^2 \theta} \right]}}{\left[\left(1 - \tan u_1 \tan u_2 \sec^2 \theta\right)^2 + \left(f_1 \tan u_1 + f_2 \tan u_2\right)^2 \right]^{1/2}}$$

(375)

where

$$\tan u_1 = 2\lambda z \sec \rho / \pi (\xi \beta)^2$$

$$\tan u_2 = 2\lambda z \sec \theta / \pi \xi^2$$

$$f_{1,2} = 1 + \tan^2 \begin{Bmatrix} \cos^2 \varphi \\ \sin^2 \varphi \end{Bmatrix}$$

$$\beta = a^2 \cos^2 \psi + \sin^2 \psi$$

ξ = transverse-scale size

ψ = magnetic dip angle at the ionosphere penetration point

a = axial ratio

ρ = declination

φ = azimuth

λ = wavelength

z = height

(376)

Next we compute the inphase and quadrature component variances, σ_x^2 and σ_y^2, and their correlation, C_{xy}

$$\left.\begin{array}{l} \sigma_x^2 = \left[\sigma^2 + \text{Re}(B) \right]/2 \\[2mm] \sigma_y^2 = \left[\sigma^2 - \text{Re}(B) \right]/2 \\[2mm] C_{xy} = \text{Im}(B)/2 \end{array}\right\}. \tag{377}$$

We note that all the above parameters are still a function of g_1 and g_2.

The complex Gaussian pdf of x and y is given by

$$f_{x,y}(x,y) = \frac{\exp\left\{ -\left[(x-\mu_x)^2/\sigma_x^2 - 2\,C_{xy}(x-\mu_x)y/\sigma_x\sigma_y + y^2/\sigma_y^2 \right]/2\left(1 - c_{xy}^2\right) \right\}}{2\pi\,\sigma_x\sigma_y\sqrt{1 - c_{xy}^2}}. \tag{378}$$

With the amplitude a defined as

$$a = \sqrt{x^2 + y^2} \tag{379a}$$

and

$$x = a\cos\theta \tag{379b}$$

$$y = a\sin\theta \tag{379c}$$

the pdf of a and θ is

$$f(a,\theta) = a\,f_{x,y}(a\cos\theta, a\sin\theta) \tag{380}$$

and the pdf of a is

$$f_A(a) = \int_{\theta=0}^{2\pi} a\,f_{x,y}(a\cos\theta, a\sin\theta)\,d\theta \tag{381}$$

The pdf of a must be determined point by point for discrete a by numerical integration. A large number of discrete a will be necessary since the histogram of the data must be fit to (381). It is estimated that at least 200 integrations of (381) would be necessary to represent it smoothly. Even if only 5 combinations

250

of g_1 and g_2 are taken to have a family of 5 pdf, a total of 1000 integrations of (381) is required. This must be followed by 5 goodness of fit tests. In all an excessive amount of computation is required in order to determine the complex Gaussian parameters.

We next propose a method which is computationally easier but which may possess convergence problems under certain conditions.

4.3.4.2 Taylor Estimation

Using (378) the ν'th moment of the amplitude a, $\langle a^\nu \rangle$ is given by

$$\langle a^\nu \rangle = \int_{-\infty}^{\infty} \int_{-\infty}^{\infty} \frac{(x^2 + y^2)^{\nu/2}}{2\pi \sigma_x \sigma_y \sqrt{(1 - C_{xy}^2)}} \; e^{-\frac{1}{2(1-C_{xy}^2)}\left[\frac{(x-\mu_x)^2}{\sigma_x^2} - \frac{2C_{xy}(x-\mu_x)}{\sigma_x \sigma_y} + \frac{y^2}{\sigma_y^2}\right]} dx dy$$

(382)

The moment may then be expanded in a Taylor series about some arbitrary values $\mu_{xo}, \sigma_{xo}^2, \sigma_{yo}^2$ and C_{xyo}. We have

$$\langle a^\nu \rangle \approx \langle a^\nu \rangle_o + \frac{\partial \langle a^\nu \rangle}{\partial \mu_x}\bigg|_o \Delta \mu_x + \frac{\partial \langle a^\nu \rangle}{\partial \sigma_x^2}\bigg|_o \Delta \sigma_x^2 +$$

$$\frac{\partial \langle a^\nu \rangle}{\partial \sigma_y^2}\bigg|_o \Delta \sigma_y^2 + \frac{\partial \langle a^\nu \rangle}{\partial C_{xy}}\bigg|_o \Delta C_{xy} \qquad (383)$$

where subscript o indicates evaluation at $\mu_{xo}, \sigma_{xo}^2, \sigma_{yo}^2$ and C_{xyo} and the delta quantities equal

251

$$
\left.
\begin{aligned}
\Delta \mu_x &= \mu_x - \mu_{xo} \\
\Delta \sigma_{xo}^2 &= \sigma_x^2 - \sigma_{xo}^2 \\
\Delta \sigma_{yo}^2 &= \sigma_y^2 - \sigma_{yo}^2 \\
\Delta C_{xy} &= C_{xy} - C_{xyo}
\end{aligned}
\right\}
\tag{384}
$$

The philosophy behind the Taylor expansion method is to describe four moments of the amplitude and solve for the actual four Gaussian parameters $\mu_x, \sigma_x^2, \sigma_y^2$ and C_{xy}. Writing the four equations in matrix form we have

$$
\hat{\underline{A}} = \underline{A}_o + \underline{F}_o \underline{\Delta}
\tag{385}
$$

where the _measured_ four moments of the amplitude data, $\hat{\underline{A}}$, is

$$
\hat{\underline{A}} =
\begin{bmatrix}
\langle a^{\nu_1} \rangle \\
\langle a^{\nu_2} \rangle \\
\langle a^{\nu_3} \rangle \\
\langle a^{\nu_4} \rangle
\end{bmatrix}
\tag{386}
$$

the _theoretical_ moments evaluated at μ_{xo}, σ_{yo}^2 and C_{xyo}, $\underline{A}_o$, is

$$
\underline{A}_o =
\begin{bmatrix}
\langle a^{\nu_1} \rangle_o \\
\langle a^{\nu_2} \rangle_o \\
\langle a^{\nu_3} \rangle_o \\
\langle a^{\nu_4} \rangle_o
\end{bmatrix}
\tag{387}
$$

252

$$\cdot\left\{F_o\right\}_{ij} = \left.\frac{\partial \langle a^{\nu_i} \rangle}{\partial \alpha_j}\right|_o \qquad \alpha_1 = \mu_x, \ \alpha_2 = \sigma_x^2 \qquad (388)$$

$$\alpha_3 = \sigma_y^2, \ \alpha_4 = C_{xy}$$

and

$$\underline{\Delta} = \underline{\alpha} - \underline{\alpha}_o = \begin{bmatrix} \mu_x - \mu_{xo} \\[2mm] \sigma_x^2 - \sigma_{xo}^2 \\[2mm] \sigma_y^2 - \sigma_{yo}^2 \\[2mm] C_{xy} - C_{xyo} \end{bmatrix} \qquad (389)$$

Theoretically, the Gaussian parameter set, $\underline{\alpha}$, is found by solving

$$\underline{\alpha} = \underline{F}_o^{-1}(\hat{\underline{A}} - \underline{A}_o) + \underline{\alpha}_o \qquad (390)$$

We comment on this direct solution. First and foremost with respect to accuracy the solution $\underline{\alpha}$ will only be close to the true set if $\underline{\alpha}_o$ is close to the true set. A priori we do not know a good set $\underline{\alpha}_o$ to choose. Thus, $\underline{\alpha}$ will be a poor estimate in general. (Below we describe a method of choosing $\underline{\alpha}_o$.) To circumvent this problem an iterative method should be employed. First $\underline{\alpha}_o$ is chosen in some way. Then $\underline{\alpha}_1 = \underline{\alpha}$ is determined from (406). This set of parameters will be inaccurate but closer to the true set than $\underline{\alpha}_o$. Next, $\underline{\alpha}_1$ is used as the new expansion point and a better approximation $\underline{\alpha}_2$ is found. This continues until the difference between the new and previous parameter set is minimal. Mathematically, the iteration procedure is described by

$$\underline{\alpha}_{i+1} = \underline{F}_i^{-1}(\hat{\underline{A}} - \underline{A}_i) + \underline{\alpha}_i . \qquad (391)$$

Convergence of (391) to the true set will be rapid when the ratio of the largest to smallest eigenvalue of $\underline{F}_i$ is small.

The second comment on the Taylor expansion method pertains to the evaluation of the $\underline{F}$ matrix. Just as in the parameterization method, numerical integration is required. Here we have 16 double integrals to evaluate on each iteration. Thirty iterations would require the same computational requirements as the 5 family parameterization method (1000 integrations). We circumvent this drawback by explicitly evaluating the moments using the moment generating function.

Given a pdf $f(x)$ the moment generating function, $\Phi(\beta)$, is defined as the expected value of $e^{j\beta x}$. Then the moments of x, m_n, are given by

$$\left. \frac{d^n \Phi(\beta)}{d\beta^n} \right|_{\beta=0} = j^n m_n.$$ (392)

We now determine the moments $\langle a^{\nu_i} \rangle$ required for solving (391) directly.

4.3.4.2.1 Determination of $\langle a^{\nu_i} \rangle$

Let us define the vectors $\underline{Y}$, $\underline{A}$ and $\underline{K}$ where

$$\underline{Y} = \begin{bmatrix} x \\ y \end{bmatrix}$$ (393a)

$$\underline{A} = \begin{bmatrix} \mu_x \\ 0 \end{bmatrix}$$ (393b)

$$\underline{K} = \begin{bmatrix} \sigma_x^2 & c_{xy}\sigma_x\sigma_y \\ c_{xy}\sigma_x\sigma_y & \sigma_y^2 \end{bmatrix}$$ (393c)

254

Components x and y are jointly correlated Gaussian components with correlation C_{xy}, means μ_x and 0, respectively, and variances σ_x^2 and σ_y^2, respectively. $\underline{K}$ is the covariance matrix. The squared amplitude of these quadrature components is given by

$$Q = \underline{Y}^T \, \underline{Y} \, . \tag{394}$$

The moment generating function of Q is [28]

$$\Phi_Q(\beta) = e^{-\frac{1}{2}(f-g)}/h^{1/2} \tag{395}$$

where

$$\left.\begin{aligned}
f &= \underline{A}^T \, \underline{K}^{-1} \, \underline{A} \\
g &= \underline{A}^T \, \underline{K}^{-1} \, \underline{L}^{-1} \, \underline{A} \\
h &= |\underline{L}|
\end{aligned}\right\} \tag{396}$$

and

$$\left.\begin{aligned}
\underline{L} &= \underline{I} - j2\beta\underline{K}.
\end{aligned}\right.$$

It is readily found by substitution that

$$\underline{f} = \mu_x^2/\sigma_x^2(1-C_{xy}^2) \tag{397}$$

$$\underline{L} = \begin{bmatrix} 1 - j2\beta\sigma_x^2 & -j2\beta C_{xy}\sigma_x\sigma_y \\ - j2\beta C_{xy}\sigma_x\sigma_y & 1-j2\beta\sigma_y^2 \end{bmatrix} \tag{398a}$$

$$\underline{L}^{-1} = \frac{1}{1-4\beta^2\sigma_x^2\sigma_y^2(1+C_{xy}^2) - j2\beta(\sigma_x^2+\sigma_y^2)} \begin{bmatrix} 1-j2\beta\sigma_y^2 & j2\beta C_{xy}\sigma_x\sigma_y \\ j2\beta C_{xy}\sigma_x\sigma_y & 1-j2\beta\sigma_x^2 \end{bmatrix}$$

$$\tag{398b}$$

$$g = \mu_x^2 / h\sigma_x^2 (1-C_{xy}^2) \tag{399}$$

and

$$h = 1-4\beta^2 \sigma_x^2 \sigma_y^2 (1+C_{xy}^2) - j2\beta(\sigma_x^2 + \sigma_y^2) \tag{400}$$

An extremely lengthy but systematic application of (392) yields the following results:

$$m_1 = D_4 (D_2 + 1/2) e^{D_1+D_2} \tag{401}$$

$$m_2 = \left[D_4^2 (D_2^2 + 3D_2 + 3/4) + D_3(2D_2-1) \right] e^{D_1 + D_2} \tag{402}$$

$$m_3 = \left\{ D_4^3 \left(D_2^3 + \frac{15}{2}D_2^2 + \frac{45}{4}D_2 + \frac{15}{18} \right) + D_4 D_3 \left(6D_2^2 + 10D_2 - 3/2 \right) \right.$$

$$\left. + 8D_3^2 D_2/D_4 \right\} e^{D_1 + D_2} \tag{403}$$

$$m_4 = \left\{ D_4^4 \left(D_2^4 + 14D_2^3 + \frac{105}{2}D_2^2 + \frac{105}{2}D_2 + \frac{105}{16} \right) \right.$$

$$+ D_4^2 D_3 \left(12D_2^3 + 52 D_2^2 - 7D_2 - 21 \right)$$

$$+ D_3^2 \left(44D_2^2 + 28D_2 + 9 \right)$$

$$\left. + 40D_3^3 D_2/D_4^2 \right\} e^{D_1 + D_2} \tag{404}$$

where

$$\left. \begin{aligned}
D_1 &= - \mu_x^2/2\sigma_x^2 (1 - C_{xy}^2) \\
D_2 &= \mu_x^2/2\sigma_y^2 (1 - C_{cy}^2) \\
D_3 &= 4\sigma_x^2 \sigma_y^2 (1 + C_{xy}^2) \\
D_4 &= 2(\sigma_x^2 + \sigma_y^2)
\end{aligned} \right\} \tag{405}$$

Equations (401) to (405) specify the required $\underline{A}_i$ matrix in (391). The $\underline{F}_i$ matrix requires the derivatives of the m_j with respect to the parameters μ_x, σ_y^2, and C_{xy}. These in turn are functions of the derivatives of the D_ℓ. Defining

$$\{\underline{D}\}_{\ell j} = D_\ell^{j*} \equiv \frac{\partial D_\ell}{\partial \alpha_j} \qquad j, \ell = 1, 2, 3, 4 \tag{406}$$

we have

$$\underline{D} = \begin{bmatrix} 2D_1/\mu_x & -D_1/\sigma_x^2 & 0 & 2C_{xy}D_1/(1-C_{xy}^2) \\ 2D_2/\mu_x & 0 & -D_2/\sigma_y^2 & 2C_{xy}D_2/(1-C_{xy}^2) \\ 0 & D_3/\sigma_x^2 & D_3/\sigma_y^2 & 8C_{xy}\sigma_x^2\,\sigma_y^2 \\ 0 & 2 & 2 & 0 \end{bmatrix} \tag{407}$$

Finally, the derivatives of the moment are given by

$$\frac{\partial m_1}{\partial \alpha_j} = \left(D_1^j + D_2^j \right)m_1 + \left[D_4^j\left(D_2 + \frac{1}{2}\right) + D_4 D_2^j \right] e^{D_1 + D_2} \tag{408}$$

$$\frac{\partial m_2}{\partial \alpha_j} = \left(D_1^j + D_2^j \right)m_2 + \left[2D_4 D_4^j\left(D_2^2 + 3D_2 + 3/4\right) + \right.$$

$$\left. D_4^2\left(2D_2 + 3\right)D_2^j + D_3^j\left(2D_2 - 1\right) + 2D_3\,D_2^j \right] e^{D_1 + D_2} \tag{409}$$

---

* D_ℓ^j is not to be confused with D_ℓ raised to the j'th power. When D_ℓ is to be raised to be a power the power will be explicitly written as a number not a variable.

257

$$\frac{\partial m_3}{\partial \alpha_j} = \left(D_1^j + D_2^j\right)m_3 + \left[3D_4^2\ D_4^j\left(D_2^3 + \frac{15}{2}D_2^2 + \frac{45}{4}D_2 + \frac{15}{18}\right)\right.$$

$$+ D_4^3\left(3D_2^2 + 15D_2 + \frac{45}{4}\right)D_2^j + \left(D_3 D_4^j + D_4 D_3^j\right)$$

$$\left(6D_2^2 + 10D_2 - 3/2\right) + D_4 D_3\left(12D_2 + 10\right)D_2^j$$

$$+ 8D_2^j\ D_3^2/D_4 + 16D_3 D_3^j D_2/D_4 - \left.8D_3^2 D_2 D_4^j/D_4^2\right] e^{D_1 + D_2}$$

(410)

$$\frac{\partial m_4}{\partial \alpha_j} = \left(D_1^j + D_2^j\right)m_4 + \left[4D_4^3\ D_4^j\left(D_2^4 + 14D_2^3 + \frac{105}{2}D_2^2 + \frac{105}{2}D_2 + \frac{105}{16}\right)\right.$$

$$+ D_4^4\left(4D_2^3 + 42D_2^2 + 105D_2 + \frac{105}{2}\right)D_2^j$$

$$+ \left(2D_4 D_4^j D_3 + D_4^2 D_3^j\right)\left(12D_2^3 + 52D_2^2 - 7D_2 - 21\right)$$

$$+ D_4^2 D_3\left(36D_2^2 + 104D_2 - 7\right)D_2^j$$

$$+ 2D_3 D_3^j\left(44D_2^2 + 28D_2 + 9\right) + D_3^2\left(88D_2 + 28\right)D_2^j$$

$$+ 120D_3^2 D_3^j D_2/D_4^2 + 40D_3^3\ D_2^j/D_4^2 - \left.80D_3^3\ D_2 D_4^j/D_4^3\right] e^{D_1 + D_2}$$

(411)

Equations (407) to (411) specify the $\underline{F}_i$ matrix so that (391) can now be easily solved using any standard matrix inversion sub-routine.

4.3.4.2.2 Interpretation of m_j

The m_j are the moments of the squared amplitude so that the data must be used to measure

258

$$\underline{\hat{A}} = \begin{bmatrix} m_1 \\ m_2 \\ m_3 \\ m_4 \end{bmatrix} = \begin{bmatrix} \langle a^2 \rangle \\ \langle a^4 \rangle \\ \langle a^6 \rangle \\ \langle a^8 \rangle \end{bmatrix} \tag{412}$$

For ease of measurement we may assume that the distribution of a is close to a Nakagami m-distribution then by measuring $\langle a^2 \rangle$ and $\langle a^4 \rangle$ we have

$$m = \frac{\langle a^2 \rangle^2}{\langle a^4 \rangle - \langle a^2 \rangle^2} \tag{413}$$

$$\Omega = \langle a^2 \rangle . \tag{414}$$

Then since

$$\langle a^{2n} \rangle = (\Omega/m)^n (m+n-1)(m+n-2)\ldots m \qquad n = 1,2\ldots \tag{415}$$

for the m-distribution we have

$$\underline{\hat{A}} = \begin{bmatrix} \Omega \\ (\Omega/m)^2 (m+1)m \\ (\Omega/m)^3 (m+2)(m+1)m \\ (\Omega/m)^4 (m+3)(m+2)(m+1)m \end{bmatrix} \tag{416}$$

4.3.4.2.3 Starting Point $\underline{\alpha}_o$

We arbitrarily determine a starting point $\underline{\alpha}_o$. We assume that the scintillation statistics are close to a Rayleigh distribution of the form

$$f(a) = \frac{a}{\sigma^2} e^{\frac{a^2}{2\sigma^2}} \qquad a \geq 0 . \tag{417}$$

259

Then the mean of $\langle a^2 \rangle$ is simply equal to $2\sigma^2$ and we have as $\underline{\alpha}_0$

$$\underline{\alpha}_0 = \begin{bmatrix} 0 \\ \langle a^2 \rangle/2 \\ \langle a^2 \rangle/2 \\ 0 \end{bmatrix} \tag{418}$$

4.3.4.3 Complex Signal Method

This method assumes that the complex signal $x+jy$ is available. Then the phase of the signal is chosen so that $\langle y \rangle = 0$. The data is used to determine

$$\left. \begin{aligned} \mu_x &= \frac{1}{N} \sum_{j=1}^{N} x_j \\ \sigma_x^2 &= \frac{N}{N-1} \left[\frac{1}{N} \sum_{j=1}^{N} x_j^2 - \mu_x^2 \right] \\ \sigma_y^2 &= \frac{1}{N-1} \sum_{j=1}^{N} y_j^2 \\ C_{xy} &= \frac{1}{(N-1)\sigma_x\sigma_y} \sum_{j=1}^{N} x_j y_j \end{aligned} \right\} \tag{419}$$

The complex Gaussian distribution is thus trivially determined.

4.3.5 Summary

In summary, we have seen that the complex Gaussian distribution is easiest to generate; the direct transformation method being preferred. If the scintillation data is available in complex form then the parameters of the complex Gaussian distribution are easily found. If only amplitude data is available, the parameter estimation problem is much more difficult. It may be solved most easily by using the Taylor expansion method by using Equations (391), (401) to (405), (407) to (411) and (412).

260

SECTION 5

SUMMARY, CONCLUSIONS, AND RECOMMENDATIONS

Sections 2 through 4 of this report have investigated three specific uses of the CSEL facility. Section 2 described the use of CSEL in LES 8/9 simulation, with analyses of limiter performance, Doppler simulation, repeater jamming, and a systematic means of simulation validation. Section 3 described the use of CSEL in NAVSTAR GPS simulation, discussing the GPS system configuration, sources of errors, analytic models, and interfacing with CSEL. Section 4 describes the properties of satellite signals and means of generating signals with specified amplitude and phase statistics.

We have shown that, depending on the J/S ratio, either a soft or a hard limiter can minimize signal suppression. When J/S > 1, the soft limiter is optimum, but its threshold is a function of the J/S ratio. We have shown that for an FH system, repeater jamming is in general more efficient than either random noise or multitone jamming. For the LES 8/9 system, in particular, we have outlined a series of start-up simulation tests, for validating the PSP model, testing the downlink simulation, and simulating the uplink jamming.

Our GPS studies recommend means of simulating delays by adjusting the Doppler shift. A closed loop method is suggested for correcting Doppler errors. Means are proposed for implementing variable multipath delay, one by use of switched delay lines, and the other by means of a gain-controlled tapped delay line. The study shows that proper antenna simulation is a complex matter, and suggests considering the use of an omnidirectional antenna pattern in the CSEL simulation. Finally, an alternative simulation configuration

261

is discussed, which uses half as many satellite signal generators as does the full configuration, but requires a computer-controlled delay line.

Effects of scintillation and atmospheric attenuation on the satellite signal were examined. The present state of knowledge on scintillation indicates that if only the envelope of the scintillation is of interest, it can be approximated by a Nakagami m-distribution. However, if both envelope and phase are of importance, the complex Gaussian model of Rino and Fremouw appears to be the most appropriate model available at the present time. Detailed methods of simulating both of these distributions on a digital computer are given.

The DOD laboratories encompass many facilities. To the best of our knowledge, CSEL is unique among them, being the only laboratory which allows real-time hybrid simulation of complete avionics communication systems. In order to maintain CSEL as a resource for communication system testing, additional equipment should be procured which will permit the simulation of new systems as they are considered. In this context we have, in the present study, defined some of the hardware and software requirements for the GPS system, which will be of importance in the near future. Multiple access systems will also be developed in the near future. Among the modes of operation which are possible, are FDMA, TDMA, and hybrid FDMA/ TDMA. CSEL, as presently configured, will not simulate these systems. Additional equipment should be procured which will permit their simulation. The procurement should be preceded by a system definition phase, in which both the hardware and the software of the system to be fabricated are defined.

262

APPENDIX A
DIFFERENTIAL DOPPLER SHIFT DUE TO THE IONOSPHERE

It is well known that the ionosphere introduces an additional delay of signals transmitted from a satellite to the ground. This is also accompanied by a differential Doppler shift, which is often ignored. In this memo we compute this Doppler shift and discuss the conditions under which it can be ignored.

Figure A-1 shows the geometry of the problem. R_o is the radius of the earth and R_s the distance from the satellite to the center of the earth. The Doppler shift is dependent on the receiver angle $\theta_o - \theta_1$ between the actual path and the straight line between receiver and transmitter. To determine this angle we use Snell's law for a spherically layered medium,

$$K_1 \triangleq n_o R_o \sin \theta_1 = n(R) R \sin \theta(R), \qquad (A-1)$$

where n_o is the refractive index at the surface of the earth, and $n(R)$, $\theta(R)$ is the refractive index and zenith angle on the signal path, at the distance R from the center of the earth (we assume a spherical earth).

If the refractive index is constant (say 1) the signal will follow the straight line, and we will have the equation

$$K_o \triangleq R_o \sin \theta_o = R \sin \theta(R). \qquad (A-2)$$

On a small section of the path, we have (see Fig. A-1)

$$R \, d\alpha = \tan \theta \, dR \qquad (A-3)$$

where α is again the angle the path makes with zenith. Using this on both the actual and the geometric path, we find using Eqs. (A-1)
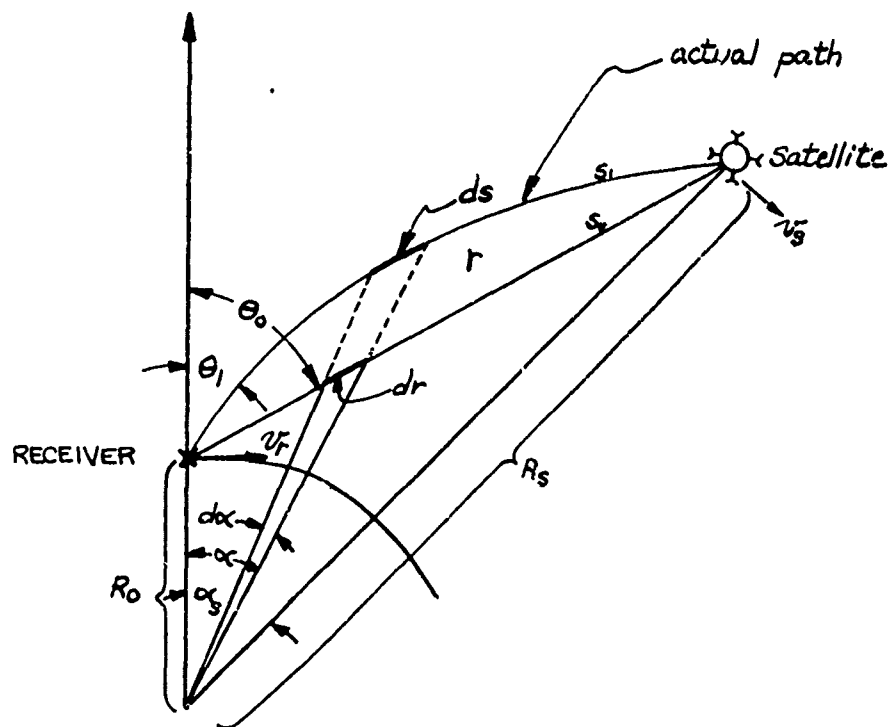
Figure A-1.   Path Geometry for Ionospheric Doppler
             Shift Calculation.

and (A-2),

$$\alpha_s = \int_0^{R_s} d\alpha = \int_{R_0}^{R_s} \frac{dR}{R\sqrt{\dfrac{n^2 R^2}{K_1^2} - 1}} = \int_{R_0}^{R_s} \frac{dR}{R\sqrt{\dfrac{R^2}{K_0^2} - 1}}. \qquad (A-4)$$

This equation determines implicitly $K_1 = n_0 R_0 \sin \theta_1$. Since $n(R) \sim 1$ everywhere, we can write

$$n^2 = 1 - v_0 \quad , \quad |v_0| \ll 1 \qquad\qquad (A-5)$$

and

$$K_1 = K_0 (1-\delta), \qquad\qquad (A-6)$$

defining v_0 and δ.

Introducing Eqs. (A-5) and (A-6) in Eq. (A-4) we get to the first order in v_0,

$$\delta \int_{R_0}^{R_s} \frac{R\,dR}{K_0^2} \left(\frac{R^2}{K_0^2} - 1\right)^{-3/2} = \frac{1}{2} \int_{R_0}^{R_s} \frac{R\,dR}{K_0^2} v_0(R) \left(\frac{R^2}{K_0^2} - 1\right)^{-3/2}.$$

$$(A-7)$$

The coefficient to δ above is

$$K_0 \left[\frac{1}{R_0 \cos\theta_0} - \frac{1}{\sqrt{R_s^2 - R_0^2 \sin^2\theta_0}} \right] \sim \mathrm{tg}\,\theta_0 \qquad (A-8)$$

since

$$R_s \gg R_0.$$

If the ionospheric layer is thin, the right hand side of Eq. (A-7) can be approximated by

$$\frac{1}{2} \frac{R_i}{K_0^2} \left(\frac{R_i^2}{K_0^2} - 1\right)^{-3/2} \int_{R_0}^{R_s} v_0(R)\,dR$$

$$= \frac{1}{2} \frac{R_i}{K_0^2} \left(\frac{R_i^2}{K_0^2} - 1\right)^{-3/2} \times \frac{80.7}{f^2} \times TEC, \qquad (A-9)$$

265

where the usual formula for the refractive index in the ionosphere has been used (neglecting the magnetic field and electron collisions), TEC is the total electron content and R_i is the location of the layer. More exact expressions can be found using an empirical model for the electron density in Eq. (A-7), and the expression

$$v_o(R) = \frac{1}{f^2} \cdot 80.7 \, N(R) \tag{A-10}$$

(MKSA units).

We now determine the difference in phase length along the actual path (s_1) and along the geometric path (s_o) in Fig. A-1.

$$ds_1 = \frac{dR}{\cos\theta} = \left(1 - \frac{K_1^2}{n^2 R^2}\right)^{-1/2} dR \tag{A-11}$$

$$ds_o = \frac{dR}{\cos\theta} = \left(1 - \frac{K_o^2}{R^2}\right)^{-1/2} dR \tag{A-12}$$

The phase difference is

$$\Delta L = \int_{R_o}^{R_s} 2\pi \, \frac{n(R) f}{c} \left\{ \left(1 - \frac{K_1^2}{n^2 R^2}\right)^{-1/2} - \frac{1}{n}\left(1 - \frac{K_o^2}{K^2}\right)^{-1/2} \right\} dR \tag{A-13}$$

We wish to determine the angular frequency. To simplify the problem, assume that the satellite path is circular (i.e., $\dot{R}_s = 0$) and passing directly over the receiver. Then the angular frequency is

$$\dot{\Delta L} = \int_{R_o}^{R_s} 2\pi \, \frac{n(R) f}{c} \left\{ \left(1 - \frac{K_1^2}{n^2 R^2}\right)^{-3/2} \frac{K_1 \dot{K}_1}{n^2 R^2} - \left(1 - \frac{K_o^2}{R^2}\right)^{-3/2} \frac{K_o \dot{K}_o}{R^2 n(R)} \right\} dR \tag{A-14}$$

266

$\dot{K}_1$ is determined by differentiating Eq. (A-4),

$$\dot{\alpha}_s = \int_{R_o}^{R_s} \frac{dR}{R} \left(\frac{n^2 R^2}{K_1^2} - 1 \right)^{3/2} \frac{n^2 R^2}{K_1^3} \dot{K}_1$$

$$= \int_{R_o}^{R_s} \frac{d\lambda}{R} \left(\frac{R^2}{K_o^2} - 1 \right)^{-3/2} \frac{R^2}{K_o^3} \dot{K}_o,$$

or,

$$\dot{\alpha}_s = \dot{K}_1 \int_{R_o}^{R_s} n^2 R \left(n^2 R^2 - K_1^2 \right)^{-3/2} dR \tag{A-15a}$$

$$= \dot{K}_o \int_{K_o}^{R_s} R \left(R^2 - K_o^2 \right)^{-3/2} dR \triangleq \dot{K}_o X, \tag{A-15b}$$

where

$$X = \frac{1}{R_c \cos^3 \theta_o} \tag{A-16}$$

(same approximation as in Eq. (A-8)). Using this in Eq. (A-14), we get

$$\Delta\dot{L} = \int_{R_o}^{R_s} 2\pi \frac{n^2 fR}{c} K_1 \dot{K}_1 \left(n^2 R^2 - K_1^2 \right)^{-3/2} dR - \int_{\lambda_o}^{R_s} 2\pi \frac{f}{c} R K_o \dot{K}_o \left(R^2 - K_o^2 \right)^{-3/2} dR$$

$$= \frac{2\pi f}{c} K_1 \dot{K}_o X - \frac{2\pi f}{c} K_o \dot{K}_o X$$

$$= \frac{2\pi f}{c} \dot{\alpha}_s \left(K_1 - K_o \right). \tag{A-17}$$

This is exact with the assumptions made above (circular orbit, etc.).

A first order approximation to $K_1 - K_o$ is given by Eqs. (A-6) - (A-9), giving (valid for $\cos \theta_o \approx 1-n$)

267

$$K_1 - K_0 = - K_0 \delta$$

$$\sim -\frac{1}{2} R_c \cos \theta_0 \frac{R_i}{K_0^2} \left(\frac{R_i^2}{K_0^2} - 1\right)^{-3/2} \times 80.7 \times TEC/d^2$$

$$= -\frac{1}{2} R_0^2 R_i \cos \theta_0 \sin \theta_0 \left(R_i^2 - R_0^2 \sin^2\theta_0\right)^{-3/2} \times 80.7 \times TEC/f^2.$$

$$(A-18)$$

$\dot{\alpha}_s$ in Eq.(17) is determined by the satellite and receiver motions. We have, using velocities in the orbit plane only,

$$\dot{\alpha}_s = +\frac{v_s}{R_s} - \frac{v_r}{R_0},$$

so,

$$\dot{\Delta L} \simeq -\frac{2\pi f}{c}\left(\frac{v_s}{R_s} - \frac{v_r}{R_0}\right) \frac{1}{2} R_0^2 R_i \cos\theta_0 \sin\theta_0 \left(R_i^2 - R_0^2 \sin^2\theta_0\right)^{-3/2} \times \frac{80.7 \ TEC}{f^2}$$

This frequency shift ($\dot{\Delta L}/2\pi$) is much smaller than one Hertz. Table 1 shows the Doppler shift for a 12 hour circular orbit, using TEC = $2 \cdot 10^{17}$ el./m^2, $R_i = R_0 + 300$ km. The shift is smaller than the accuracy required (~ 0.3 Hz).

TABLE A-1. IONOSPHERIC DOPPLER SHIFT FOR GPS LINK AS FUNCTION
OF SATELLITE ELEVATION ANGLE – TEC EQUALS $2.10^{17} e\ell/m^2$

θ_o	f=1.2 GHz v_r=0	f=1.6 HGz v_r=680m/s
	$\Delta f[Hz]$	$\Delta f[Hz]$
0°	0	0
20°	1.7×10^{-3}	1.9×10^{-3}
40°	4.5×10^{-3}	5.0×10^{-3}
60°	1.7×10^{-2}	1.2×10^{-2}
75°	1.97×10^{-2}	2.2×10^{-2}
80°	1.98×10^{-2}	2.20×10^{-2}
85°	2.15×10^{-2}	1.50×10^{-2}
86°	1.12×10^{-2}	----

APPENDIX B

A BOUND ON RECEIVER ACCURACY

The accuracy of the delay measurement can be bounded by evaluating the Cramér-Rao bound. If we ignore the Doppler measurement, the bound gives a lower bound on the rms error in an unbiased estimate of delay τ,

$$\overline{(\delta\tau)^2} \geq \frac{1}{(2\pi B_2)^2 \dfrac{2E_s}{N_o}},$$

where E_s is the signal energy, N_o the (two-sided) spectral density of the noise, and B_2 is the signal rms bandwidth.

$$B_2^2 = \left[\int_{-\infty}^{\infty} (f - \bar{f})^2 |S(f)|^2 df\right] \Big/ E_s$$

$$\bar{f} = \frac{2}{E_s} \int_{o}^{\infty} f |S(f)|^2 df$$

$$E_s = \int_{-\infty}^{\infty} |S(f)|^2 df .$$

We consider the case of a rectangular signal filtered ideally outside the first null in the spectrum,

$$|S(f-\bar{f})|^2 = \begin{cases} \left(\dfrac{\sin \pi(f-\bar{f})T}{\pi(f-\bar{f})T}\right)^2 & |f-\bar{f}| \leq \dfrac{1}{T} \\ \\ 0 & |f-\bar{f}| > \dfrac{1}{T} \end{cases}$$

We find that

$$E_s = \frac{2 \, Si(2\pi)}{\pi T}$$

and

$$E_s B_2^{\,2} = \frac{1}{\pi^2 T^3}$$

and hence

$$B_2 = \frac{1}{T} \left(2\pi \, Si(2\pi) \right)^{-\frac{1}{2}} \sim \frac{1}{3T} \, .$$

If we assume a noise temperature of $300^{\circ}K$, a transmitted signal power of 450W, a distance of 12,000 km, we can determine the ranging error as a function of antenna and processing gains.

Gains [dB]	Ranging Error [feet]
20	26
25	14.6
30	8.2
35	4.6
40	2.6
45	1.46
50	.82

REFERENCES

[1] Abramowitz, M., Stegun, L.A., 1964, Handbook of Mathematical Functions, National Bureau of Standards, Applied Mathematics Series No. 55.

[2] TRW Systems, Second Interim Technical Report Spread Spectrum Modem/Processor, Vol. 3, 10 May 1974, Contract F33615-73-C-4141.

[3] Erdelyi, A., Editor, Tables of Integral Transforms, McGraw-Hill Book Co., New York, 1954.

[4] Lindsey, W.C., Simon, M.K., (1973), Telecommunication Systems Engineering, Prentice-Hall, Inc., New Jersey, 1973.

[5] Altschuler, E.E., and P.M. Kalaghan (1974), Tropospheric Range Error Corrections for the NAVSTAR System, Air Force Cambridge Research Laboratories, Bedford, Mass. AFCRL 74-0198 TR, DDC AD-786928/2GA.

[6] Bent, R.B., S.K. Llewellyn, and M.K.Walloch (1972), Description and Evaluation of the Bent Ionospheric Model, DBA System, Inc. SAMSO TR-72-239, DDC-AD75 3081.

[7] Klobuchar, J.A. and R.S. Allen (1970), A First Order Prediction Model of Total Electron Content for a Midlatitude Ionosphere AFCRL-70-0403, Air Force Cambridge Research Laboratories, Bedford, Mass., July 1970.

[8] Pisacane, V.L., M.M.Feen, and M. Sturmanis (1972), Prediction Technique for the Effect of the Ionosphere on Pseudo-Ranging From Synchronous Altitude Satellites. Johns Hopkins University, Applied Physics Laboratory, November 1972, SAMSO-TR-72-22, DDC AD749 486.

[9] Waldman, H., and A.V. da Rosa (1971) Prognostication of Ionospheric Electron Content, Vol. I, II   Radio Science Laboratory, Stanford University, California, SAMSO-TR-71-82, DDC AD731 095, AD 731 096.

[10] Rao, N.N., M.Y.Youkim and K.C.Yeh (1971), Feasibility Study of Correcting for the Excess Time Delay of Transionospheric Navigational Ranging Signals, Ionospheric Radio Laboratory, Dept. of Electr. Eng., University of Illinois, SAMSO TR 71-163, DDC AD729 797.

[11] Al'pert, Ya. L. (1963), <u>Radio Wave Propagation and the Iono-</u>
      <u>sphere</u>,Consultants Bureau, N.Y. (Translated from Russian
      edition published 1960).

[12] Davies, K. (1969), <u>Ionospheric Radio Waves</u>, Blaisdell Pub-
      lishing Co., Waltham, Mass.

[13] Misyura, V.A., N.P.Svetlitchny, Yu. K. Chasovitin, S.S.Shluser,
      L.V.Bezrodnaya, N.D.Gerasimova, L.A.Piven, and L.F.Chernoger
      (1974), "Statistical Characteristics and Dynamics of Iono-
      spheric Irregularities as Investigated Using Satellite Sig-
      nal Records and Ground-Based Methods at Middle and High
      Latitudes". J. Atmos. Terr. Phys., Vol. 36, pp.2037-2045.

[14] Cretcher, C.K. (1975) "Ionospheric Effects in NAVSTAR-GPS",
      In Proc. of the 1975 Symposium on the Effect of the Iono-
      sphere on Space Systems and Communications, Arlington, Va.,
      January 20-22, 1975.

[15] Booker,H.G.(1975),"The Role of the Magnetosphere in Satel-
      lite and Radio-Star Scintillation," in Proc.of the 1975
      Symposium on the Effect of the Ionosphere on Space Systems
      and Communications, Arlington, Va., January 20-22,1975.

[16] Aarons, J., Whitney, H.E.Allen,R.S., 1971, "Global Morpho-
      logy of Ionospheric Scintillations," Proc. IEEE, Vol. 59,
      No. 2, February 1971, pp 159-172.

[17] Briggs, B.H., Parkin, I.A., 1963, "On the Variation of Radio
      Star and Satellite Scintillations with Zenith Angle," J.Atms.
      Terr. Phys., Vol. 25, pp 339-366.

[18] Whitney, H.E., Aarons, J., Allen, R.S., Seeman,D.R., 1972,
      "Estimation of the Cumulative Amplitude Probability Distribu-
      tion Function of Ionospheric Scintillations," Radio Science,
      Vol. 7, No.12, December 1972, pp 1095-1104.

[19] Whitney,H.E., 1974,"Notes on the Relationship of Scintilla-
      tion Index to Probability Distributions and their Uses for
      System Design," AFCRL-TR-74-0004, Air Force Cambridge Re-
      search Laboratories, L.G.Hanscom Field, Bedford, Mass., 3
      January 1974.

[20] Nakagami, M., 1960, "The m-Distribution — A General Formula
      of Intensity Distribution of Rapid Fading," printed in W.C.
      Hoffman, ed., <u>Statistical Methods in Radio Wave Propagation</u>,
      Pergamon Press, 1960, pp 3-36.

[21] Rino, C.L., Fremouw, E.J., 1972, "Statistics for Ionospher-
      ically Diffracted VHF/UHF Signals," Radio Science, Vol. 8,
      No.3, March 1973, pp 223-233.

[22] Aarons,J., Whitney,H.E.,Allen,R.S., Seeman,D.R., 1973, "High
      Latitude Models, Observations, and Analysis of Ionospheric
      Scintillations," AFCRL TR-73-0048, Air Force Cambridge Re-
      search Laboratories, L.G.Hanscom Field, Bedford, Mass.,
      12 Jan. 1973.

[23] Rino, C.L., Livingston,R.C., Whitney,H.E., 1974, "Some New
      Results on the Statistics of Radio Wave Scintillation," to
      be submitted for Publication in Journal of Geophysical Re-
      search.

[24] Paulson,M.R., Hopkins,R.V.F., 1973, "Effects of Equatorial
      Scintillation Fading in SATCOM Signals, "NELC/TR 1875,
      Naval Electronics Laboratory Center, San Diego, Cal.,92152,
      8 May 1973.

[25] Taur, R.R., "Ionospheric Scintillation at 4 and 6 GHz,"
      COMSAT Technical Review, Vol. 3, No.1, Spring 1973, pp
      145-163.

[26] Altshuler,E.E., Falcone,V.H.,Wulfsberg,K.N., 1968,"Atmospheric
      Effects on Propagation at Millimeter Wavelengths," IEEE Spec-
      trum, Vol. 5, No.7, July 1968, pp 83-90.

[27] Brookner,E., 1969, "Characterization of Millimeter Wave Earth-
      Space Link Communications Channels," 1969 IEEE International
      Conf. on Communications, Boulder, Colorado, June 9-11, 1969,
      pp 7-7 to 7-14.

[28] Omura, J., and T.Kailath,1965, "Some Useful Probability Dis-
      tributions", Stanford Electronics Laboratories Rpt. No. SU-
      SEL-65-079, September 1965.